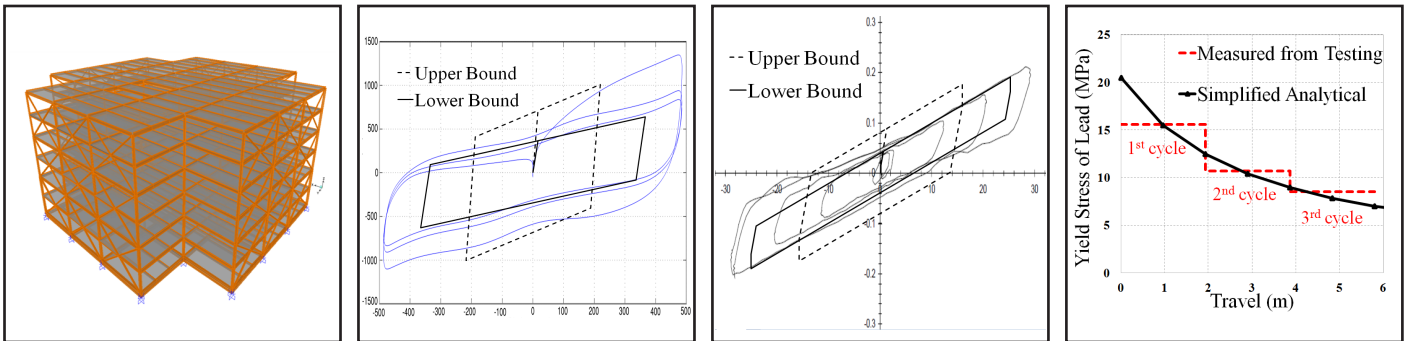# Property Modification Factors for Seismic Isolators: Design Guidance for Buildings

by

William J. McVitty and Michael C. Constantinou

NOTICE

Property Modification Factors for Seismic Isolators:
Design Guidance for Buildings

by

William J. McVitty[1] and Michael C. Constantinou[2]

MCEER Thrust Area 3: Innovative Technologies

1   Structural Design Engineer, KPFF Consulting Engineers, Seattle, WA: former graduate student, Department of Civil, Structural and Environmental Engineering, University at Buffalo, State University of New York
2   SUNY Distinguished Professor, Department of Civil, Structural and Environmental Engineering, University at Buffalo, State University of New York

PREFACE

MCEER is a national center of excellence dedicated to the discovery and development of new knowledge, tools and technologies that equip communities to become more disaster resilient in the face of earthquakes and other extreme events. MCEER accomplishes this through a system of multidisciplinary, multi-hazard research, in tandem with complimentary education and outreach initiatives.

Headquartered at the University at Buffalo, The State University of New York, MCEER was originally established by the National Science Foundation in 1986, as the first National Center for Earthquake Engineering Research (NCEER). In 1998, it became known as the Multidisciplinary Center for Earthquake Engineering Research (MCEER), from which the current name, MCEER, evolved.

Comprising a consortium of researchers and industry partners from numerous disciplines and institutions throughout the United States, MCEER's mission has expanded from its original focus on earthquake engineering to one which addresses the technical and socio-economic impacts of a variety of hazards, both natural and man-made, on critical infrastructure, facilities, and society.

The Center derives support from several Federal agencies, including the National Science Foundation, Federal Highway Administration, National Institute of Standards and Technology, Department of Homeland Security/Federal Emergency Management Agency, and the State of New York, other state governments, academic institutions, foreign governments and private industry.

This report provides guidance on the application of the provisions of the 2016 ASCE 7 Standard for the analysis and design of seismically isolated buildings. These new provisions introduced a systematic approach for the determination of the bounding values of the mechanical properties of the isolators on the basis of experimental data of prototype isolators and considerations for the effects of the environment, aging and uncertainty. The report presents an overview of the concept of system property modification factors that is used in the establishment of the bounding values and proceeds with two systematic examples, one for an elastomeric and one for a sliding isolation system. Moreover, the new provisions are critically reviewed for consistency between the requirements for establishing bounding values and the prescribed acceptance criteria in the testing of prototype isolators. Changes are proposed to the standard to avoid inconsistencies.

ABSTRACT

The application of seismic isolation in the United States is regulated by building codes which invariably refer to the ASCE 7 Standard for analysis and design requirements. The Standard has evolved over the years to reflect the state of the art and practice in the field. The latest evolution, ASCE 7-2016, now includes a systematic procedure for establishing upper and lower bound values of isolator properties with due consideration for three categories of effects, namely: a) aging effects and environmental conditions, b) hysteretic heating and history of loading effects, and c) manufacturing variations.

This report provides commentary to practicing engineers on the basis and implementation of ASCE 7-2016 (the Standard), with respect to the property modification (lambda or λ) factors. These factors are used to define the upper and lower bound properties for analysis and design. It is emphasized, however, that this report does not strictly follow all provisions of ASCE 7-2016. Rather, it includes an evaluation and a critique of the provisions on the procedures of obtaining data on the bounding values of mechanical properties, and recommendations for changes. The report starts with discussion on the mechanical properties of isolators, their force-displacement models and the concept of property modification factors. Next there is clarification on the types of property modifications mentioned in the Standard with guidance on the magnitude of various effects. An interpretation of the Standards testing requirements is presented, with direction given on how to decide on the lower bound values of mechanical properties for analysis.

The determination of property modification factors is illustrated for a elastomeric and a sliding isolation system which are made up of lead-rubber and low-damping natural rubber isolators and triple Friction Pendulum^{TM} isolators, respectively. For each system, the following design scenarios are reported: (a) assuming there is no qualification test data available, and (b) using prototype test data of two isolators. A third option (c) of having complete production test data available for the analysis and design is also discussed. These factors are project-specific, manufacturer-specific and also dependent on the material used, therefore cannot be simply adopted for other designs. Finally, nonlinear response history analyses are undertaken for each design scenario (i.e. each range of isolation system properties) to show the effects of bounding.

This Page is Intentionally Left Blank

ACKNOWLEDGEMENTS

This Page is Intentionally Left Blank

TABLE OF CONTENTS

This Page is Intentionally Left Blank

LIST OF FIGURES

LIST OF TABLES

SECTION 1

INTRODUCTION

1.1   Scope of Report

Seismically isolated buildings in the United States are designed in accordance with the requirements of Chapter 17 of the American Society of Civil Engineers Standard ASCE-7. Currently the 2010 edition of the Standard (ASCE 7, 2010) is being revised with a number of alterations proposed for Chapter 17 of the 2016 edition (ASCE 7, 2016). Appendices D and E at the end of this report present the revised Chapter 17 during the balloting period that started in late 2014 and was still ongoing at the conclusion of the writing of this report in February 2015. One major amendment, which is the focus of this report, is the addition of a new section titled "Isolation System Properties". This section consolidates and clarifies previous provisions and provides new provisions for the explicit development of property modification (lambda or λ) factors. These lambda factors are used to determine the upper and lower bound force-displacement behavior of isolation system components on a project-specific and product-specific basis.

The aim of this report is to provide guidance to practicing engineers on the basis and implementation of the Standard ASCE 7-2016, with respect to the lambda factors. This is first developed through discussion on the mechanical properties of isolators, their force-displacement models and how different factors affect behavior. Next there is clarification of parameters mentioned in ASCE 7-2016 and an interpretation on the testing requirements, which is complemented with design examples. For each system, the following design scenarios are investigated: (a) assuming there is no qualification test data available, and (b) using prototype test data of two isolators. A third option (c) of having complete production test data available for the analysis and design is also discussed. The lambda factors are calculated for lead-rubber, low-damping natural rubber and sliding isolators. Finally, nonlinear response history analyses are undertaken for each design scenario (i.e. each range of isolation system properties) to show the effects of bounding.

The building used in the examples presented in this report is taken from the Structural Engineers Association of California 2012 Seismic Design Manual, Volume 5 ("SEAOC Manual"). The SEAOC Manual is specific to the ASCE 7-10 provisions. This report gives insight on how the latest ASCE 7-2016 provisions may affect the design and gives commentary on meeting the intent of ASCE 7-2016 with regard to bounding analysis. It is noted that an author of this report was a member of the Standards committee, and therefore has first-hand accounts of how the ASCE 7-2016 revisions came to fruition.

1.2 Intent of Seismic Isolation Provisions

Seismic isolation is arguably the most effective way to protect a building, its occupants and its contents from the damaging effects of major earthquakes. The application of the technology in the United States is regulated by building codes which invariably refer to the ASCE 7 ("the Standard") for requirements for the analysis and design of structures with seismic isolation. The Standard has evolved over the years to reflect the state of the art and practice in the field. The latest evolution (ASCE 7-2016) includes a systematic procedure of establishing upper and lower bound values of isolator properties with due consideration for uncertainties, testing tolerances, aging, environmental effects and history of loading. The following paragraphs give a perspective of the intent as well as rationale for the Standard's provisions.

The ASCE Standard describes the **minimum** requirements to provide reasonable assurance of a seismic performance for buildings and other structures that will:

1. Avoid serious injury and loss of life due to:
   a. Structural collapse
   b. Failure of nonstructural components or systems
   c. Release of hazardous materials
2. Preserve means of egress
3. Avoid loss of function in critical facilities, and
4. Reduce structural and nonstructural repair costs where practicable to do so.

These performance objectives do not have the same likelihood of being achieved and depend on a number of factors. These include structural framing type, building configuration, structural and nonstructural materials and details, and the overall quality of design and construction. In addition, there are large uncertainties in the intensity and duration of shaking, which will affect performance.

The key point to note is that seismic isolation is a high-performance system which is not on a level playing field to other systems. That is, a seismically isolated building and a conventional fixed-base building, designed to their respective minimum requirements of ASCE 7 will not perform the same in a major earthquake. A seismically isolated building is expected to have a considerably better performance, with no significant damage or downtime whereas a conventional building may be damaged to the point where it is uneconomical to rehabilitate. This is due to the inherent nature of isolation (i.e. reduces both displacements and accelerations in the superstructure) as well as the minimum requirements of the Standard. The minimum requirements of ASCE 7-2016 (Chapter 17), although not explicitly seeking

damage control as an objective, indirectly will give limited damage as a consequence of ensuring that proper isolation is achieved. For example, the Standard limits the amount of inelastic action and drift that may occur in the superstructure in order to avoid detrimental coupling with the isolation system. Moreover, the Standard requires that the isolators be designed and tested for the effects of the Maximum Considered Earthquake (MCE).

Seismic isolation can be likened to introducing an engineered soft-story in the structure. All inelastic action and displacement is concentrated in a single level of the building. Therefore the global response of the building hinges on the performance of the isolation system, and special care must be taken to ensure it is reliable. The materials used for isolator units differ somewhat from conventional construction materials, in that their properties may vary considerably due to temperature, aging, contamination, history of loading, among other factors (see Section 3). There are no standards which govern how an isolator must be produced and assembled. These details vary by manufacturer and are usually proprietary. Furthermore there is no official certification required of manufacturers before they can start supplying isolators. Consequently, there can be a considerable difference in the quality and performance of isolators, even for identical isolator types produced by different manufacturers.

Given the importance of the isolation system, and considerable uncertainty in the quality of different manufacturers, ASCE 7-2016 has taken the approach of requiring the Registered Design Professional (RDP) to determine (in consultation with the manufacturer) the nominal isolator properties and to account for the likely variation in those properties on a project-specific and product-specific basis. This is achieved through a combination of test data and engineering judgment and is now explicitly required in the Standard through the use of upper bound and lower bound analysis. The intent is that this will give reasonable assurance of the isolation systems performance throughout the life of the building.

1.3   Analysis Procedures for Seismically Isolated Structures

There are three methods used to analyze and design seismically isolated buildings. These are the Equivalent Lateral Force (ELF) method, which is a static procedure, the Response Spectrum method and Response History Analysis, both of which are dynamic procedures. The practice in the United States has evolved such that most isolated buildings are designed using Nonlinear Response History Analysis (NLRHA) with an ELF analysis used to evaluate the results of the dynamic analysis and obtain minima for response quantities. NLRHA gives the most realistic prediction of response and can be used for all building types. Conversely, ASCE 7 puts limitations on when the ELF and Response Spectrum methods

can be used. Also, ASCE 7-2016 expanded the range of applicability of the ELF procedure relative to earlier versions of the Standard in an attempt to simplify the application of seismic isolation.

All structural analyses require a mathematical model of the isolator's lateral force-displacement behavior. The adopted nonlinear model can be implemented directly for NLRHA, or it can be linearized using an effective stiffness and effective damping for the ELF and Response Spectrum procedures. Section 2 gives common models used for elastomeric and sliding seismic isolators, with detail on which properties govern the force-displacement behavior. These simple models assume that the mechanical properties of the isolator remain constant during the earthquake motion as well as during the entire design life. In reality the properties will vary, perhaps significantly, from the adopted nominal values due to a number of different effects as discussed in Section 3.

To account for this variation, ASCE 7-2016 takes the approach of performing parallel analyses, one using the isolation system's upper bound force-displacement properties and one using the lower bound force-displacement properties. The upper and lower bound values of mechanical properties are determined from nominal values of properties and the use of property modification (lambda) factors. Even with the most complex models, which can explicitly account for some property variations (i.e. instantaneous temperature, velocity, axial load, etc.), there will likely always be a need to perform bounding analysis in order to account for the effects of aging and specification tolerance, since these factors are not captured by mathematical models.

The governing case for each response parameter, whether from the upper or lower bound analysis, is then used for design. Typically the maximum structural forces are from the upper bound analysis and the maximum isolator displacements are from the lower bound analysis. This approach is similar to capacity-design, whereby the probable properties of the ductile mechanism are used to design and detail structural elements. This ensures that (1) a majority of the inelastic deformation and energy dissipation is confined to the isolation system, and (2) the design can sustain and accommodate the maximum displacement.

SECTION 2

FORCE-DISPLACEMENT MODELS OF ISOLATORS

2.1 Introduction

The analysis of seismically isolated buildings requires a mathematical model of the isolator's lateral force-displacement behavior. The true behavior of an isolator is nonlinear and complex, therefore different analysis models exist with varying sophistication. This section gives examples of simple models used to characterize the force-displacement behavior of elastomeric and sliding isolators, and specifically, what properties/parameters govern the force-displacement behavior. The concept of using property modification (lambda) factors to envelope the likely isolator's behavior is introduced in Section 2.4.

The low-damping natural rubber and lead-rubber *elastomeric* isolators and the Friction Pendulum^{TM} *sliding* isolators are the predominant types of seismic isolators used in practice. The desirable features of these isolators is that laterally they have low stiffness, with good energy dissipation and re-centering ability, and vertically they remain stable under the weight of the building and large displacements. The force-displacement behavior is nonlinear, hysteretic and can be idealized by either a rigid-linear, bilinear or tri-linear model as identified in this section. These types of isolators have been extensively tested and implemented in practice for the past 30 years, with design based on the models that follow.

It is noted that new isolator concepts cannot be used unless they have verified and validated models. This involves two parts, (1) the isolators behavior must be verified by dynamic qualification testing in a rig, and (2) the mathematical model of the isolator used for structural analysis must be validated by experimental testing (e.g. shake table testing) by showing stability and generation of comparable analytical and experimental results (i.e. displacements, shear forces, etc.).

2.2 Modeling Elastomeric Isolator Units

The lateral force-displacement behavior of a lead-rubber isolator can be idealized by the bilinear hysteretic loop shown in Figure 2-1 (Constantinou et al. 2011).
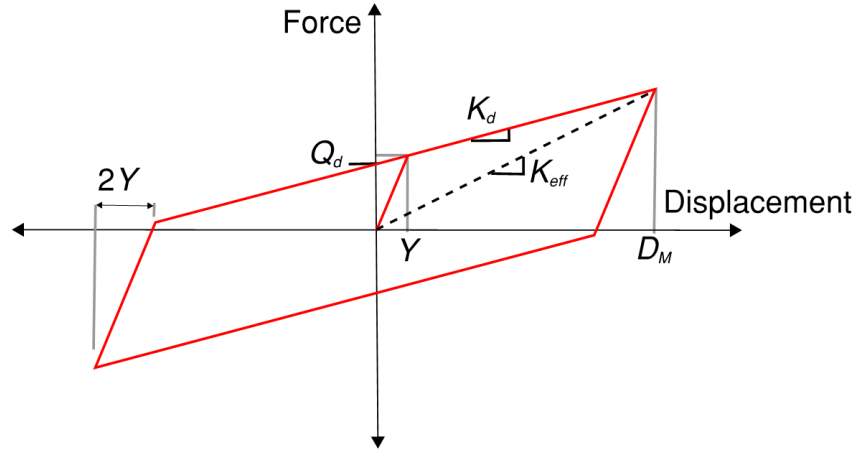
Figure 2-1 Idealized Bilinear Force-Displacement Relation of a Lead-Rubber Isolator

For this basic nonlinear model, the mechanical behavior of the lead-rubber isolator is characterized by the following three parameters:

a) **Characteristic strength, Q_d.** The characteristic strength is the strength of the isolator at zero displacement. It is related to the area of lead A_L and the effective yield stress of lead σ_L as follows:

$$Q_d = A_L \sigma_L \qquad (2 \text{-} 1)$$

Note that equation (2-1) implies any contribution to the strength from rubber is included in the effective yield strength of lead. This is a simplification as rubber has a small quantifiable contribution to strength. The reader is referred to Kalpakidis et al (2008) for a procedure to account for the contribution of rubber, although the procedure is mostly of academic interest in advanced modeling of the behavior of lead-rubber isolators.

b) **Post-elastic stiffness, K_d.** The stiffness is related to the shear modulus of rubber G, the bonded rubber area A_r and the total thickness of rubber layers T_r as follows:

$$K_d = f_L \frac{GA_r}{T_r} \qquad (2 \text{-} 2)$$

The parameter f_L accounts for the effect of the lead core on the post-elastic stiffness and ranges in value from 1.0 to about 1.2. Only after repeated cycling is the value of f_L close to unity. Within the context of bounding analysis, factor f_L is set equal to unity and any uncertainty is incorporated in the value of G (and by relation in stiffness K_d) by use of the testing lambda factor λ_{test}.

c) **Yield displacement, Y.** This parameter dictates the unloading elastic stiffness of the isolator, and is used in calculating the effective damping. Typically it is in the range of 6 to 25mm (0.25 to 1 inch) and is either assumed or estimated based on a visual fit of test data. Although the in-

structure accelerations and the isolator residual displacements can be sensitive to the value of Y, it is not an important parameter in calculating the global response. Typically only Q_d and K_d are subject to property modification factors.

The bilinear hysteretic model can be linearized by calculating the effective stiffness K_{eff} and the effective damping β_{eff}. K_{eff} is calculated by dividing the maximum force by the maximum displacement D_M and β_{eff} is calculated as:

$$\beta_{eff} = \frac{2Q_d\left(D_M - Y\right)}{\pi K_{eff} D_M^2} \qquad (2\text{-}3)$$

Low-damping natural rubber isolators are defined as having an effective damping of less than 5%. The mechanical behavior of the isolator can be characterized simply as a linear-elastic element with a stiffness obtained using equation (2-2) with f_L set to unity. A single linear viscous damping element may be added in each principal direction (and in torsion) to represent the damping capability of all isolators. Alternatively, each isolator may be modeled as a hysteretic element with post-elastic stiffness given by equation (2-2) with f_L set to unity, yield displacement determined by the procedures for lead-rubber isolators and strength Q_d approximately given by:

$$Q_d = \frac{\pi \beta_{eff} K_d D_M}{2} \approx 0.065 K_d D_M \qquad (2\text{-}4)$$

where D_M is the displacement in the maximum earthquake and β_{eff} is the effective damping. Note that the simplification in equation (2-4), $0.065K_d D_M$, is based on arbitrarily taking the effective damping as 0.04. Also, the value of Q_d may be deduced from the test loops.

2.3   Modeling Sliding Isolator Units

Spherically shaped sliding isolators come in a variety of configurations, with behavior dictated by the different combinations of surfaces upon which sliding occurs. The formulation, implementation and validation of models for multi-spherical sliding isolators can be found in Fenz and Constantinou (2008). Double and triple Friction Pendulum^{TM} (FP) configurations offer many benefits over the single FP configuration. For example, more compact isolators, increased displacement capacity, decreased sliding velocities (approximately halved) and therefore reduced frictional heating and associated problems with wear and variability in friction. This report focuses on a "special" type of triple FP isolator (defined in this section), which is commonly used in practice.

The rigid-linear model (Figure 2-2), is a simple but valuable model that can be used for all types of FP isolators. The two parameters that govern performance are the characteristic strength at zero displacement

7

Q_d and the post-elastic stiffness K_d. Q_d is a function of the friction coefficient μ and the weight W, whereas K_d is a function of the effective radius of curvature of the concave plates R_{eff} and the weight W. It is an accurate representation for a single FP isolator and for a double FP isolator where the upper and lower concave plates have the same radius of curvature and same coefficient of friction. For a triple FP isolator it slightly under-predicts the friction coefficient at zero displacement, however the effect is minor on the structures global response. K_d is equal to $W/(2R_{1,eff})$ for double and triple FP isolators when the upper and lower concave surfaces have an identical radius of curvature.

For this model only the strength needs to be determined from testing, since the stiffness is calculated from theory. The friction coefficient at zero displacement, μ, is determined directly from the measured energy dissipated per cycle (normalized by the weight) divided by the distance travelled. Therefore there is no interpretation/fitting of test data required. This model was used for the preliminary design of the triple FP isolation system and also when comparing the nominal properties from production isolators.
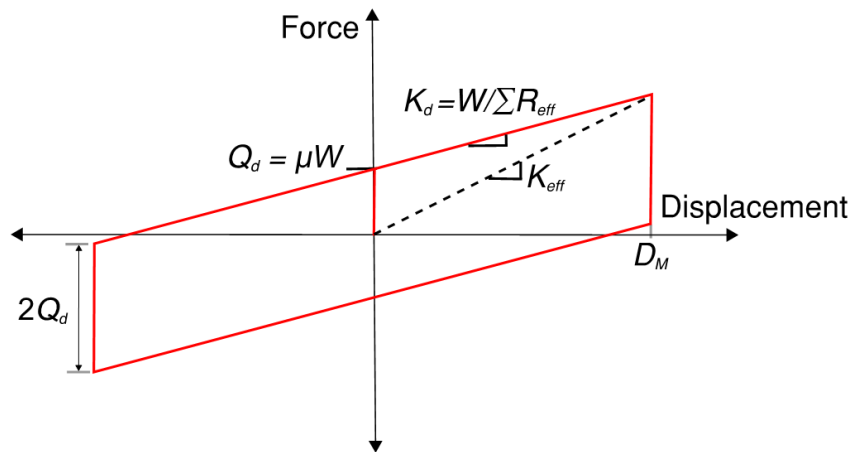
Figure 2-2 Rigid-Linear Force-Displacement Behavior of FP Isolators

The rigid-linear model, or use of a bilinear model in Figure 2-1, will give a reasonable estimate of the global response of the structure. If in-structure accelerations and residual displacement are of interest to the Registered Design Professional (RDP) then it is appropriate to adopt a more sophisticated model of the triple FP isolator, such as the tri-linear model described in the following.

The triple FP isolator has a complex behavior with various force-displacement regimes. As the displacement increases, there are multiple changes in stiffness and strength. Typically at low levels of force/displacement the system is very stiff, compared to a design level event where there is a lower stiffness and increased damping, and then different behavior again at the maximum considered event

8

where there is a higher stiffness to control displacements. This gives rise to an adaptive system which can be optimized for various performance levels.

There are 12 geometric parameters and 4 frictional parameters which define the force-displacement behavior of the triple friction pendulum isolator, outlined in Figure 2-3. Here the parameters are numbered from 1 to 4 from the bottom up.
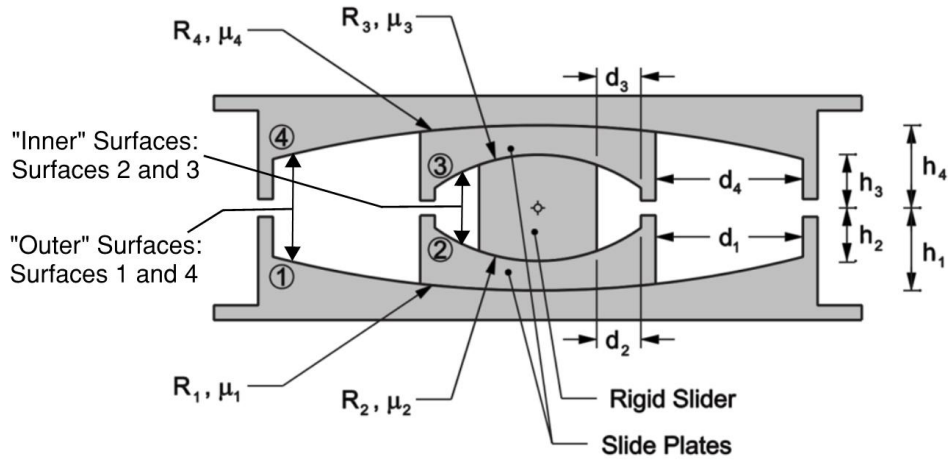
Figure 2-3 Triple Friction Pendulum Cross Section, Definition of Parameters

The three types of geometric parameters are the radius of the concave surface/plate R_i, the height of various components h_i and the distance d_i which is related to the displacement capacity. The stiffness of friction pendulum isolators is entirely dependent on the weight and some combination of the effective radius of curvature of the concave plates. The effective radius for each surface is the distance to the pivot point which, for a double and triple friction pendulum isolator, is always less than the geometric radius and calculated as:

$$R_{i,eff} = R_i - h_i, \; for \; i = 1, \, 2, \, 3, \, 4 \tag{2 - 5}$$

This is then used to calculate the actual displacement capacity of each sliding surface, given by:

$$d_i^* = \frac{R_{i,eff}}{R_i} d_i, \; for \; i = 1, \, 2, \, 3, \, 4 \tag{2 - 6}$$

The characteristics of the "special" type of friction pendulum isolator, used in this report and commonly used in practice, are as follows:
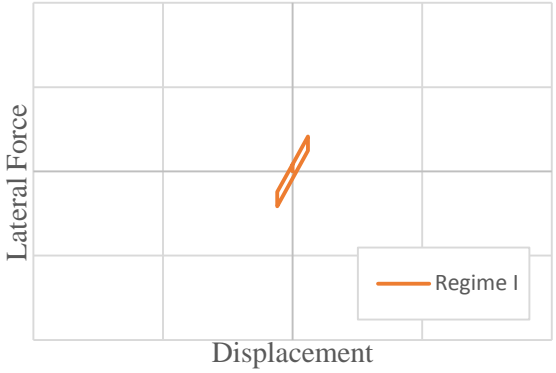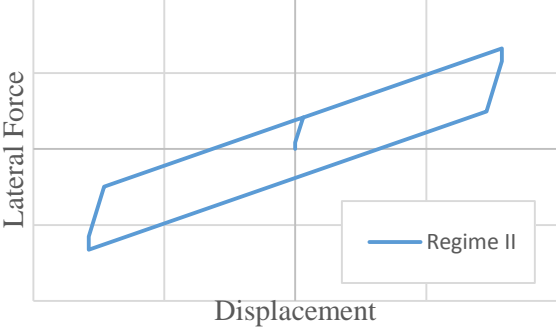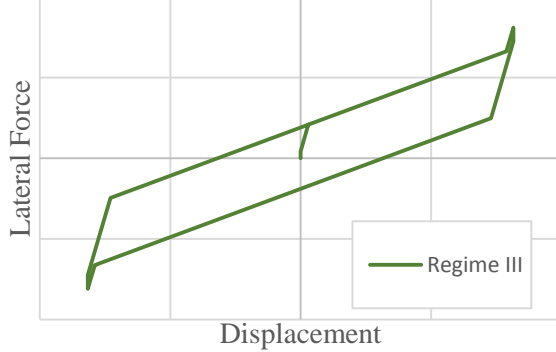
- $R_1 = R_4 \gg R_2 = R_3$
- $\mu_2 = \mu_3 < \mu_1 = \mu_4$
- $d_1 = d_4$ and $d_2 = d_3$
- $h_1 = h_4$ and $h_2 = h_3$

9

Essentially the properties of the isolator are a mirror image about the mid-height of the isolator. This reduces the number of variables from 16 to 6 geometric parameters and 2 frictional parameters. By adopting these parameters the force-displacement behavior is reduced to three regimes. A description of these regimes and force-displacement relationships is given in Table 2-1 and 2-2.

Table 2-1 Force-Displacement Behavior for a "Special" Triple FPR Isolator

Regime	Description	Force-Displacement Relationship
I	Sliding on surfaces 2 and 3 only	$$F = \frac{W}{2R_{2,eff}}u + \mu_2 W$$ *Valid for displacement, u:* $0 \le u \le u^*$ *Where:* $u^* = 2\left(\mu_1 - \mu_2\right)R_{2,eff}$
II	Motion stopped on surfaces 2 and 3; Sliding on surfaces 1 and 4	$$F = \frac{W}{2R_{eff,1}}\left(u - u^*\right) + \mu_1 W$$ *Valid for displacement, u:* $u^* \le u \le u^{**}$ *Where:* $u^{**} = u^* + 2d_1^*$
III	Slider bears on restrainer of surfaces 1 and 4; Sliding on surfaces 2 and 3	$$F = \frac{W}{2R_{2,eff}}\left(u - u^{**}\right) + \frac{W}{2R_{1,eff}}(u^{**} - u^*) + \mu_1 W$$ *Valid for displacement, u:* $u^{**} \le u \le u_{cap}$ *Where:* $u_{cap} = 2d_1^* + 2d_2^*$

Table 2-2 Schematics of Force-Displacement Behavior for "Special" Triple FP Isolator

Regime	Schematic of Isolator	Force-Displacement Behavior
I		
II		
III		

Assuming that the isolator does not reach Regime III for MCE displacements, the force-displacement can be modeled by that shown in Figure 2-4. The force at zero displacement is given by:

$$\mu W = \left[\mu_1 - (\mu_1 - \mu_2) \frac{R_{2,eff}}{R_{1,eff}} \right] W \qquad (2\text{-}7)$$
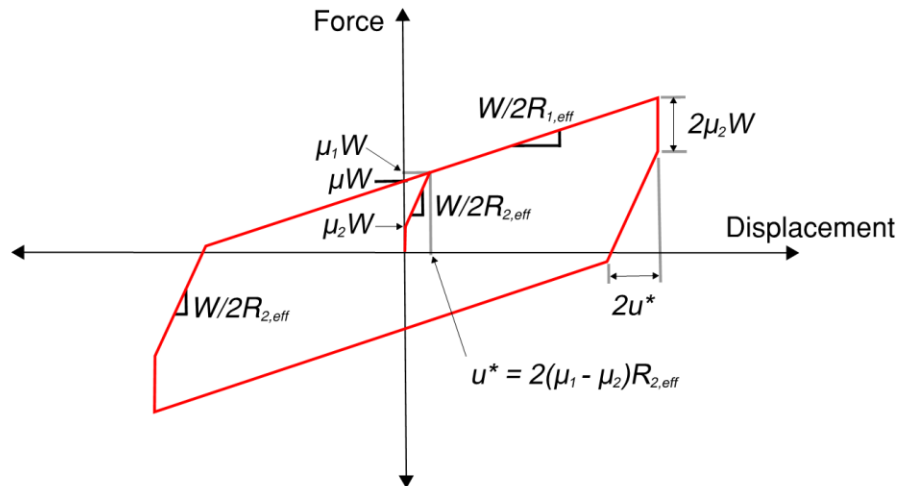
Figure 2-4 Tri-linear Force-Displacement Behavior of Special Triple FP up to Regime II

This model requires two friction coefficients to be determined from testing. As shown in Section 7, these parameters should be used with care given the uncertainty in predicting them. The stiffness can be determined based on theory.

Sarlis and Constantinou (2010) present guidelines on how to model triple friction pendulum isolators in the program SAP2000. For this report the simpler, parallel model is adopted for analysis as it can accurately capture the behavior as illustrated in Figure 2-4. This model is described in more detail in Section 9. It is based on the use of two single FP elements. Program SAP2000 also has a new triple FP element which is not used in this report.

2.4   Property Modification Factors

The concept of using property modification (lambda) factors to bound the likely isolator response was originally presented in by Constantinou et al (1999) together with information on the lifetime behavior of isolators and recommended lambda factors. Shortly after Thompson et al (2000) presented additional data to better understand the behavior of elastomeric isolators and the related lambda factors. The concept was first implemented in the AASHTO Guide Specification for Seismic Isolation Design (1999) and later in the European Standard (2005). It is noted that both of these Standards are for bridges, and that ASCE 41-2013 and ASCE 7-2016 are the first formal application to existing and new buildings, respectively. This is because bridge isolators are typically exposed to much more severe environmental and loading conditions (i.e. cumulative movement) than building isolators, and therefore have a larger variation from the tested nominal properties. The latest knowledge on lambda factors is now presented in Constantinou et al (2007), which is a revision of the original 1999 document.

The actual mechanical properties of an isolation system during an earthquake will be different to the nominal values assumed in analysis. Some reasons for this difference may be because:

1) The exact time of an earthquake is unknown and so too is the exact state of the isolator and the effects of aging, contamination, ambient temperature, and the like.

2) The force-displacement model adopted for analysis may assume that the nominal values remain constant during seismic motion (as in this report), whereas in reality the properties are changing instantaneously due to the effects of heating, rate of loading, scragging, etc.

3) The nominal values used for analysis may be based on testing of two prototype isolators, which will have a different average nominal value to that of all production isolators due to the effects of manufacturing variation.

Section 3 gives an overview of the effects that have an impact on the isolator properties. To account for these effects, a rational procedure is to form probable maximum and minimum values of the isolator's mechanical properties which envelope the likely response. One approach is to conduct a statistical analysis of the distribution of the properties and consideration of the likelihood of occurrence of relevant events, including the design seismic event. However, a simpler and more practical approach is to assess the impact of a particular effect (i.e. heating, aging, velocity of loading, vertical load, etc.) on the isolators properties through testing, rational analysis and engineering judgment (Constantinou et al 2007). If these effects are appreciable at influencing an isolators force-displacement behavior (i.e. properties K_d and/or Q_d), then it is then quantified in the form of a property modification (lambda, λ) factor.

The product of the lambda factors and the nominal properties of the isolator give the upper or lower bound of what is expected over the isolator's design life (including during earthquake excitation). ASCE 7-2016 defines the nominal design properties as the average properties over three cycles of motion and categorizes the lambda factors into three types (see Section 3), which are:

- λ_{ae} which accounts for aging and environmental effects.
- λ_{test} which accounts for heating, rate of loading, and scragging.
- λ_{spec} which accounts for permissible manufacturing variations.

The three categories above are then divided into the maximum and minimum values, which may be made up of one or a series of lambda factors. For the aging and environmental lambda factor, this is shown indicatively as follows:

$$\lambda_{ae,\max} = \lambda_{max,1} \times \lambda_{max,2} \times \ldots \times \lambda_{max,n} \qquad (2\text{ - }8)$$

$$\lambda_{ae,\min} = \lambda_{min,1} \times \lambda_{min,2} \times \ldots \times \lambda_{min,n} \qquad (2\text{ - }9)$$

Each of the individual values of $\lambda_{\max,i}$ (i = 1 to n) is greater than or equal to 1.0, whereas each of the individual values of $\lambda_{\min,i}$ (i = 1 to n) is less than or equal to 1.0.

A set of six lambda factors $\lambda_{ae,\max}$, $\lambda_{ae,\min}$, $\lambda_{test,\max}$, $\lambda_{test,\min}$, $\lambda_{spec,\max}$ and $\lambda_{spec,\min}$ are determined for each parameter which defines the force-displacement behavior of the isolator. For example, two sets for a lead-rubber isolator bilinear model are needed: one set of six for the post-elastic stiffness K_d and one set of six for the characteristic strength Q_d. The three "max" lambda factors are then combined to obtain the maximum system factor $\lambda_{\max}$, whereas the three "min" lambda factors are combined to obtain the minimum system factor $\lambda_{\min}$. The simple multiplication of the respective three lambda factors might result in a system factor that is overly conservative. That is, the probability that several additive effects (i.e. lowest temperature, maximum aging, etc.) occur simultaneously with the maximum considered earthquake is considered very small. Therefore the system factor should be adjusted based on a statistical analysis of the variations in mechanical properties with time, the probability of occurrence of joint events and the significance of the structure. Constantinou et al 1999 proposed a simple procedure for routine implementation which uses an adjustment factor f_a which is adopted in ASCE 7 as follows:

$$\lambda_{\max} = (1 + f_a(\lambda_{ae,\max} - 1)) \times \lambda_{test,\max} \times \lambda_{spec,\max} \qquad (2\text{ - }10)$$

$$\lambda_{\min} = (1 - f_a(1 - \lambda_{ae,\min})) \times \lambda_{test,\min} \times \lambda_{spec,\min} \qquad (2\text{ - }11)$$

The value of f_a is based on the significance of the project and engineering judgment. Values range from 0.66 for a typical structure to 1.0 for a critical facility. ASCE 7-2016 uses a default value of 0.75 which is only applied to the aging lambda factor, λ_{ae}. The rationale for use of the adjustment factor is that the full aging and contamination effects over the lifetime of the structure will likely not be realized when the structure is subjected to the controlling earthquake event. However, the RDP may choose to adjust the value, say to 1.0 for significant structures.

The upper and lower bound is then the product of the system lambda factor and its respective nominal property. For the post-elastic stiffness K_d that is:

$$K_{d,\max} = \lambda_{\max,K_d} \times K_{d,nominal} \qquad (2\text{ - }12)$$

$$K_{d,\min} = \lambda_{\min,K_d} \times K_{d,nominal} \qquad (2\text{ - }13)$$

14

The same process is followed for the characteristic strength Q_d. This process may be applied to other parameters of the model used in response history analysis when that model is more complex than the rigid-linear or bilinear hysteretic model. The upper and lower bound force-displacement characteristics using a bilinear analysis model are illustrated indicatively in Figure 2-5. The effective stiffness is denoted by K_M.
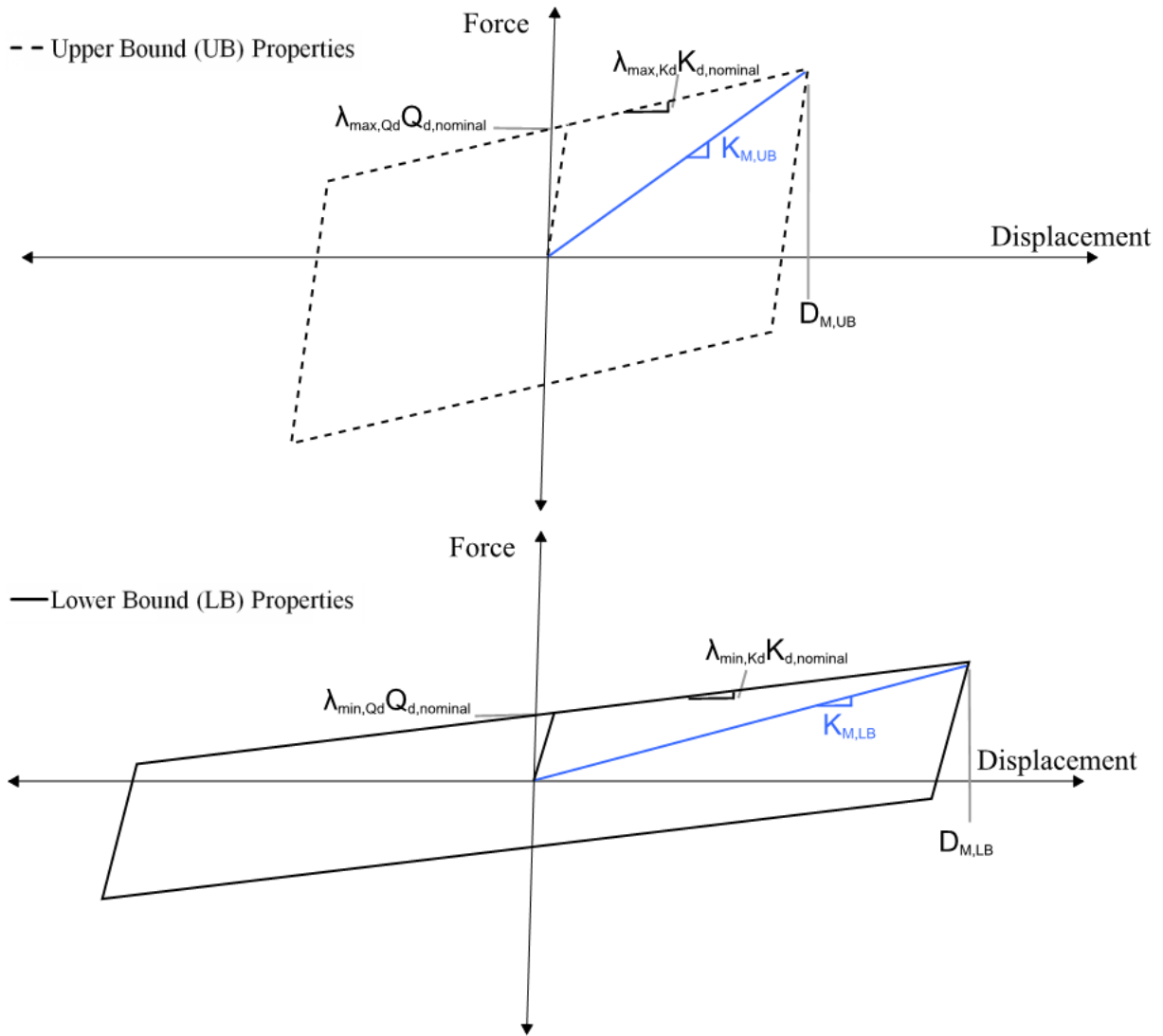
Figure 2-5: Upper and Lower Bound Isolator Force-Displacement Properties

This Page is Intentionally Left Blank

SECTION 3

TYPES OF PROPERTY MODIFICATIONS

3.1 Introduction

The properties of seismic isolators will vary over the design life due to the effects of aging and contamination; will vary during seismic motion due to the effects of heating, history of loading, and scragging; and will vary between isolator units due to manufacturing differences. Some of these effects will increase the isolators stiffness and strength (or by relation, the effecting period and effective damping), whereas others will decrease these parameters. This section presents the procedure to calculate nominal properties (Section 3.3.1) and gives an overview of how the mechanical properties of low-damping rubber and lead-rubber *elastomeric* isolators and Friction Pendulum^{TM} *sliding* isolators are influenced by different effects.

The Standard ASCE 7-2016 has categorized the varieties of property modifications (lambda, λ factors) into three types: aging and environmental, testing and the specification lambda factors- $\lambda_{ae.}$, λ_{test} and λ_{spec}, respectively. The sections that follow are titled according to these three categories of lambda factors, specifically:

- Aging and Environmental Effects- $\lambda_{ae.max}$ and $\lambda_{ae.min}$ (Section 3.2)
- Hysteretic Heating and History of Loading Effects- $\lambda_{test,max}$ and $\lambda_{test,min}$ (Section 3.3)
- Permissible Manufacturing Variation- $\lambda_{spec,max}$ and $\lambda_{spec,min}$ (Section 3.4)

These lambda factors are determined from a combination of qualification, prototype and production test data, where the description of each of these testing regimes is given in Section 4.

3.2 Aging and Environmental Effects: $\lambda_{ae,max}$ and $\lambda_{ae,min}$

The aging and environmental lambda factors $\lambda_{ae.max}$ and $\lambda_{ae.min}$ account for the change in properties that occur over the isolator's design life. The effects cannot be quantified by prototype or production testing, but are developed by a combination of qualification testing, theory and analysis. The aging and environmental lambda factors account for, but are not limited to, aging, creep, contamination, fatigue, effects of ambient temperature and cumulative travel. For buildings (and only the types of isolator used in this report), aging and contamination are the relevant considerations. This is assuming there is little/no movement in the isolators due to service loads (i.e. wind) and that the isolators are not exposed to extreme temperatures or damaging substances, which is generally the case. The effects of aging and contamination are typically always greater than unity (that is $\lambda_{ae.max} > 1.0$ and $\lambda_{ae.min} = 1.0$). Cumulative travel, fatigue

and low temperatures are an issue for bridges and are not considered further. Creep may be an issue for improperly designed isolators - an issue not addressed in this report. The interested reader may see Constantinou et al (2007) for a discussion.

3.2.1 Elastomeric Isolator Considerations

Aging in elastomeric isolators depends on the rubber compound and the quality of vulcanization and curing of the rubber, therefore it is manufacturer specific. Over time the elastomers harden due to continued vulcanization of the rubber matrix, causing both an increase in the post-elastic stiffness K_d and in the characteristic strength Q_d (i.e. both the effective stiffness and effective damping increase). The increase is expected to be of the order of 10 to 20% over a 30 year period for low-damping, high shear modulus rubber compounds (0.5-1.0MPa or 72-145psi) according to Buckle et al (2006). For both natural rubber and lead-rubber isolators, which have low-damping rubber (i.e. $\leq 5\%$ damping), the increase in strength (or damping) of the rubber due to aging, in proportion to the isolation systems strength (i.e. from lead), is minor. However the effects of strength may warrant consideration if the isolation system has a large number of natural rubber isolators compared to lead-rubber isolators.

For lower shear modulus rubbers (≤ 0.5MPa or ≤ 72psi) and for inexperienced manufacturers, the aging can be significant since low shear modulus rubber can be produced by incomplete curing. This can perhaps be detected in prototype and/or production testing by observing large scragging effects. This is because scragging is believed to also be a result of incomplete curing and hence is associated with aging and continuing chemical processes in the rubber. In the ASCE 7-2016 commentary, a default aging lambda factor $\lambda_{a,max}$ of 1.3 is applied to the post-elastic stiffness of low-damping elastomeric and lead-rubber isolators over the life of the structure. As discussed, this may not be conservative in some cases. Conversely, some experienced manufacturers are able to produce low-damping, low shear modulus rubbers with an aging factor as little as 10%, i.e. $\lambda_{a,max}=1.1$ (Constantinou et al, 2007).

Lead in quality isolators is specified with 99.99% purity and does not experience aging over the design life of the structure, therefore the aging lambda factors associated with the characteristic strength Q_d are set to unity. Furthermore, contamination is not a concern for elastomeric isolators and the contamination lambda factors are taken as $\lambda_{c,max}= \lambda_{c,min}=1.0$.

Table 3-1 gives the maximum and minimum aging and environmental lambda factors used for the three design scenarios described in this report (Section 5.4). The lambda factors for Case B and C are based on the isolators being supplied by a reputable manufacturer. The prototype and production test data is not

required to determine the λ_{ae} factors, however is noted in Table 3-1 for consistency with the "design scenarios/cases" listed in Section 5.4.

Table 3-1 Aging and Environmental Lambda Factors for Elastomeric Isolators

Case	Description	Lambda Factor	Low-Damping Elastomeric Isolator	Lead-Rubber Isolator	
			K_d	K_d	Q_d
A	No Qualification Test Data – Default Values	$\lambda_{ae,max}$	1.3	1.3	1.0
		$\lambda_{ae,min}$	1.0	1.0	1.0
B	Qualification Data and Prototype Test Data Available	$\lambda_{ae,max}$	1.1	1.1	1.0
		$\lambda_{ae,min}$	1.0	1.0	1.0
C	Qualification Data and Production Test Data Available	$\lambda_{ae,max}$	1.1	1.1	1.0
		$\lambda_{ae,min}$	1.0	1.0	1.0

Note: $\lambda_{ae,max} = \lambda_{a,max} \times \lambda_{c,max}$ and $\lambda_{ae,min} = \lambda_{a,min} \times \lambda_{c,min}$

Later, when multiplying all the lambda factors it is noted that λ_{ae} is adjusted by a factor (see equations 2-10, 2-11) to account for the conservative assumption of having full aging and environmental effects when the governing earthquake occurs. For example, the adjusted $\lambda_{ae,max}$ for the K_d of both the elastomeric and lead-rubber isolators, using an adjustment factor of 0.75, is **1.23** for default values and **1.08** for the case where qualification data are available.

3.2.2 Sliding Isolator Considerations

The aging and environmental lambda factors listed herein are determined for a particular type of sliding interface. Specifically, a sliding interface with unlubricated highly polished austenitic stainless steel in contact with PTFE (polytetrafluoroethylene) or similar composite materials, which is sealed and placed in a normal environment (refer to Constantinou et al, 2007 for details).

The lambda factors for other sliding interfaces (lubricated, bimetallic), installation methods (unsealed) and environments (severe) will generally be greater, sometimes significantly. The reader is referred to Constantinou et al (2007) for guidance. In ASCE 7-2016 commentary, the default lambda factors are given for two types of interfaces, unlubricated and lubricated. Bimetallic interfaces are discouraged. Given that there is considerable uncertainty in the lifetime behavior of generic sliding surfaces, the default lambda factors result in a large range of property modification values.

Aging results in increases in the characteristic strength/coefficient of friction. It is a complicated phenomenon, but primarily is due to corrosion of the stainless steel surface in properly designed isolators. Here the maximum aging lambda factor $\lambda_{a,max}$ is taken as 1.1 with $\lambda_{a,min}$ equal to unity. This is for an exposure time of 30 years and for Type 304 austenitic stainless steel, where a lower value might be justified if Type 316 is used since it has a higher resistance to corrosion. The ASCE 7-2016 commentary specifies a default value for $\lambda_{a,max}$ of 1.3 for unlubricated interfaces.

Contamination also gives an increase in characteristic strength /coefficient of friction. It is complex and apparently caused by third body effects and abrasion of the stainless steel (see Constantinou et al, 2007). The maximum contamination lambda factor $\lambda_{c,max}$ also depends on whether the concave sliding plate is positioned so it is facing down (i.e. on the top) or facing up (i.e. on the bottom). For a single friction pendulum (FP) isolator the contamination lambda factor $\lambda_{c,max}$ is taken as 1.0 if facing down, and 1.1 if configured to face up. For double and triple FP isolators there are multiple sliding interfaces facing up and down. Fenz and Constantinou (2006) give an equation to calculate the composite factor when there are two sliding interfaces. When the radius of curvature and coefficient of friction are equal on the top and bottom concave surface, the equation reduces to $\lambda_{c,max} = (\lambda_{c,upper} + \lambda_{c,lower})/2 = 1.05$. ASCE 7-2016 commentary gives a default $\lambda_{c,max}$ of 1.2 and is not specific on whether the sliding surface is facing up or down. For all cases $\lambda_{a,min}$ is equal to unity.

For the triple FP it is also assumed that the same stainless steel overlay is used for the inner and outer surfaces (i.e. surfaces 1 and 4, and surfaces 2 and 3, respectively-see Figure 2-3) and therefore the lambda factors above are applicable for both the inner and outer surfaces friction coefficients. Since the majority of the motion occurs on the outer surfaces, a different material may be used on the inner surfaces for ease in manufacturing which could affect the aging and contamination lambda factors.

Table 3-2 gives the maximum aging and environmental lambda factors associated with the isolator characteristic strength Q_d (or by relation, the friction coefficient). The post-elastic stiffness K_d of sliding isolators is based on the geometry of the isolator and is not effected by aging and environmental factors, hence the $\lambda_{ae,max} = \lambda_{ae,min} = 1.0$. The prototype and production test data is not required to determine the λ_{ae} factors, however is noted in Table 3-2 for consistency with the design scenarios in Section 5.4.

Table 3-2 Aging and Environmental Lambda Factors for Sliding Isolators with Unlubricated Stainless Steel-PTFE Interfaces

Case	Description	Lambda Factor	Single FP		Double and Triple FP (Composite)
			Face Up	Face Down	
			Q_d or μ		Q_d or μ
A	No Qualification Test Data Available – Default Values	$\lambda_{a.max}$	1.3	1.3	1.3
		$\lambda_{c.max}$	1.2	1.2	1.2
		$\lambda_{ae,max}$	**1.56**	**1.56**	**1.56**
		$\lambda_{ae,min}$	**1.0**	**1.0**	**1.0**
B	Qualification and Prototype Test Data Available	$\lambda_{a.max}$	1.1	1.1	1.1
		$\lambda_{c.max}$	1.1	1.0	1.05
		$\lambda_{ae,max}$	**1.21**	**1.1**	**1.16**
		$\lambda_{ae,min}$	**1.0**	**1.0**	**1.0**
C	Qualification and Production Test Data Available	$\lambda_{a.max}$	1.1	1.1	1.1
		$\lambda_{c.max}$	1.1	1.0	1.05
		$\lambda_{ae,max}$	**1.21**	**1.1**	**1.16**
		$\lambda_{ae,min}$	**1.0**	**1.0**	**1.0**

Note: For brevity, the minimum lambda factors for aging $\lambda_{a,min}$ and contamination $\lambda_{c.min}$ are not shown as they are all equal to 1.0.

As before, when multiplying all the lambda factors it is noted that λ_{ae} is adjusted by a factor (see equations 2-10, 2-11) to account for the conservative assumption of having full aging and environmental effects when the governing earthquake occurs. For example the adjusted $\lambda_{ae,max}$ for the triple FP isolator, using an adjustment factor of 0.75, is **1.42** and **1.12** based on the default and qualification data, respectively.

3.3 Hysteretic Heating and History of Loading Effects: $\lambda_{test,max}$ and $\lambda_{test,min}$

The testing lambda factors $\lambda_{test,max}$ and $\lambda_{test,min}$ are specific to the adopted nominal properties and account for the instantaneous change in properties that occur during an earthquake. The effects are best determined based on dynamic testing at relevant high velocity conditions. If quasi-static testing is undertaken, then a correction shall be applied for the testing velocity, in which qualification test data may be used to quantify the difference between quasi-static and true dynamic properties. However, the correction for dynamics effects may be too complex and with uncertainties and so dynamic testing is

preferred. The testing lambda factor accounts for, but is not limited to, heating produced during motion, velocity and strain effects, scragging of virgin rubber and variation in vertical load.

Before discussing how elastomeric and sliding isolators are affected by hysteretic heating and history of loading effects, it is important to address the issue of bounding.

3.3.1 Nominal Properties and Bounding

The nominal properties are not used for analysis directly- it is the nominal property multiplied by λ_{max} or λ_{min} factor which is used for analysis. An important part of factors λ_{max} and λ_{min} are the components $\lambda_{test,max}$ and $\lambda_{test,min}$ which are determined in the testing of prototype isolators. These two factors intend to capture scragging, and variability and degradation in properties due to the effects of heating and speed of motion.

The bounding is required because the typical models used for analysis (described in Section 2) assume that the properties are constant, whereas in reality the properties instantaneously change as shown by the test data in Figure 3-1(a). The change in properties depend on the earthquake and isolation systems characteristics. For a near-fault, pulse-like earthquake there may be only a small reduction in properties when the isolation system and/or superstructure experience its peak response. In contrast, for a large magnitude soft-site scenario there may be a substantial reduction in the isolation system properties when peak responses occur. Simply adopting the nominal properties for analysis may be a conservative lower bound (and not conservative for the upper bound) in the former case, whereas in the latter case the nominal properties may not be conservative for the lower bound. Hence bounding is required through the use of lambda-test factors to adjust the (somewhat arbitrarily defined) nominal properties to a representative upper and lower bound.

An interpretation on ASCE 7-2016 is as follows:
1) The nominal properties are defined as the average of three cycles of motion at the maximum displacement D_M.
2) The $\lambda_{test,max}$ value is defined as the ratio of the first cycle value of the property to the nominal value. Thus, effectively the first cycle value is utilized in the upper bound analysis.
3) It is implied that the $\lambda_{test,min}$ value is the ratio of the third cycle value of the property to the nominal value. Thus, effectively the third cycle value is utilized in the lower bound analysis. The authors of this report believe this to be unduly conservative for most cases and that the number of cycles considered for determining $\lambda_{test,min}$ should be based on rational analysis with due

22

consideration for the properties of the isolation system, the site conditions and the ground motion characteristics, including information on proximity to the fault.

Further to bullet point 3) above, ASCE 7-2016 gives test specimen adequacy criteria which may arbitrarily dictate the selection of the $\lambda_{test,max}$ or $\lambda_{test,min}$ used for analysis. These requirements are discussed in Sections 6.5 and 7.4 where they are compared to actual test data from two reputable manufacturers.

Figure 3-1 illustrates the concept of bounding the hysteretic heating and history of loading effects for a lead-rubber isolator. The philosophy is the same for Friction Pendulum (FP) isolators. Figure 3-1(a) gives prototype test data where there are three cycles of motion under relevant high-speed conditions and amplitude corresponding to the MCE displacement D_M. Using the procedures described in Section 6, the measured properties per cycle can be used to plot a bilinear representation (per Section 2.2) for each cycle, as shown in Figure 3-1(b). This data can then be used to calculate the nominal properties, defined as the average among the three cycles, and can be used as a basis to determine the bounds for analysis. Figure 3-1(b) also shows schematically the upper and lower bounds for analysis (i.e. range in properties during seismic motion) set as the 1st cycle and 2nd cycle properties, respectively. A rational approach to determine these bounds is explained in the following.
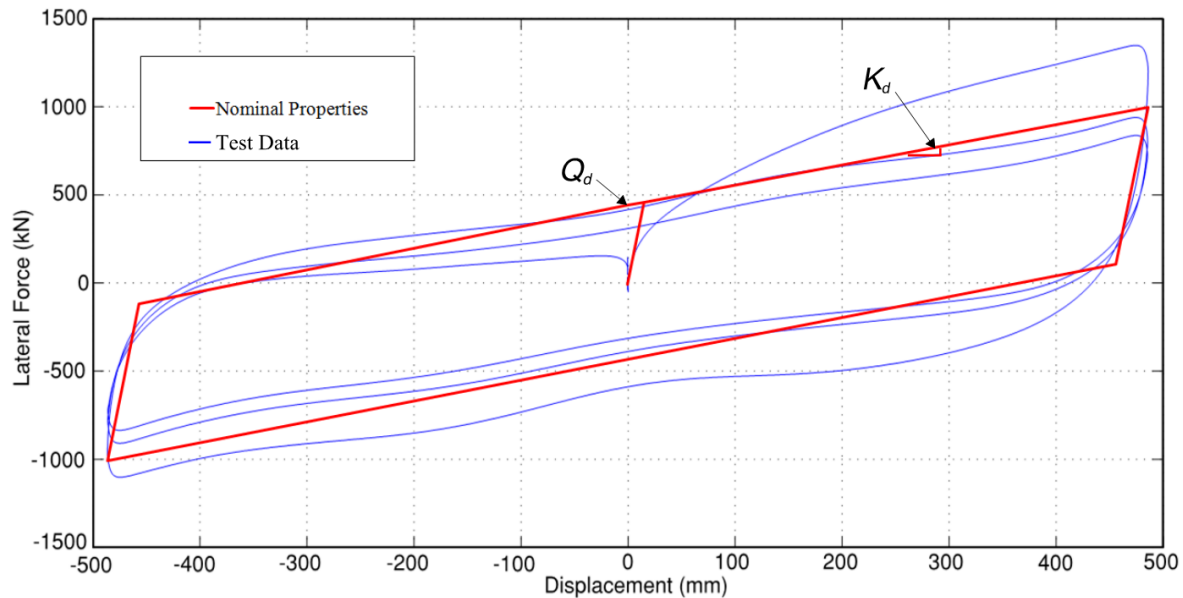
(a) **Prototype Test Data and Bilinear Model of Nominal Properties**

23
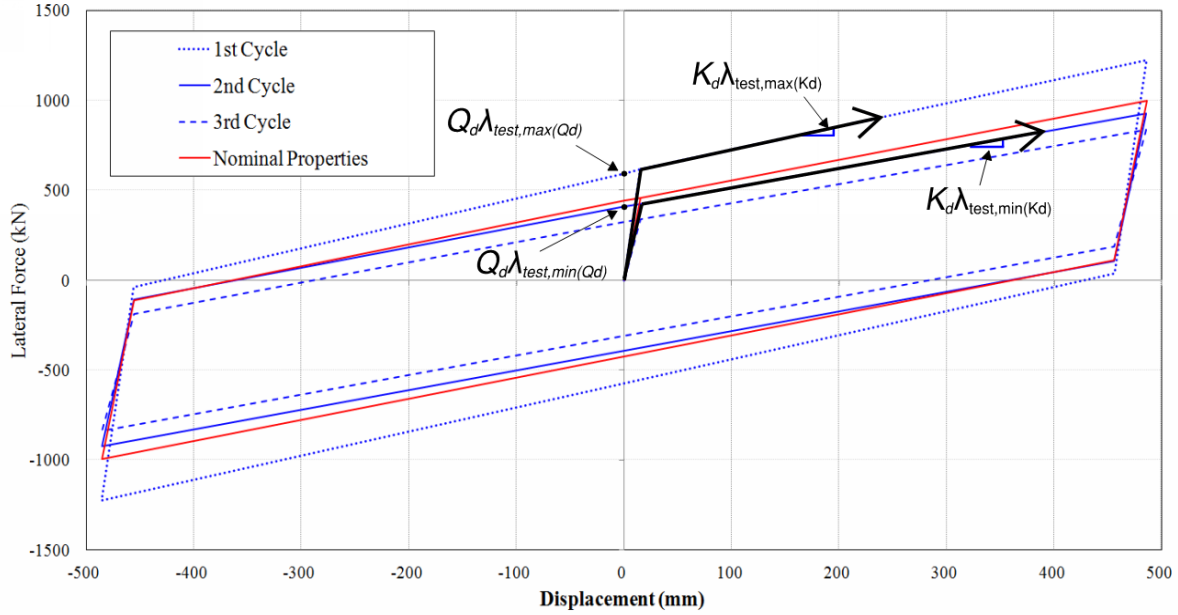
(b) Bilinear Model of Each Cycle of Motion with Representative Bounds

Figure 3-1 Concept of Bounding the Hysteretic Heating and History of Loading Effects

The $\lambda_{test,max}$ value intends to capture effects during the first cycle of motion (i.e. the upper bound) which will certainly be experienced during an earthquake and is thus defined as the ratio of the first cycle value of the property divided by the nominal value. The $\lambda_{test,min}$ value is meant to provide a lower bound value of the property related to the expected number of cycles. Typically the expected number of cycles is small and is dependent on the properties of the isolation system and the seismic excitation. Representative results are provided in Warn and Whittaker (2004, 2007) from where the Figures 3-2 (a), (b) and (c) are adopted. The three figures are for three types of ground motion: (a) near-fault, (b) large-magnitude, small distance and (c) large magnitude, soft-site.

Figure 3-2 shows the average number of equivalent cycles (or normalized energy dissipated- NED) at the maximum displacement to have the same energy dissipated as in the actual history of bi-directional motion determined in response history analysis. It is calculated as follows:

$$NED = \frac{\int Fdu}{EDC} \tag{3 - 1}$$

where EDC is the energy dissipated from one fully reversed cycle at the maximum displacement and F is the isolator lateral force corresponding to an increment of displacement du. Integration of $F.du$ over the duration of motion gives the cumulative energy dissipated by the seismic isolation system as obtained

from the nonlinear response history analysis. Quantity Q_d/W is the characteristic strength divided by the weight and quantity T_d is the period calculated on the basis of the post-elastic stiffness K_d:

$$T_d = 2\pi \sqrt{\frac{W}{K_d g}} \qquad (3\text{-}2)$$

Consider for example the case of the analyzed friction pendulum isolation system in this report. The nominal values of Q_d/W and T_d are 0.055 (weighted average of coefficient μ_B, Tables 7-3 and 7-4) and 4.1sec, respectively. Note that these are the nominal properties, not the lower bound values of Q_d/W and T_d which are stated in the preliminary design (Section 5). Considering that for the site of the structure the motions will be near-fault or large magnitude, short distance, the expected number of cycles is two (see Figure 3-2 a) and b)). Therefore at the conclusion of the event, the isolation system is expected to have undergone the equivalent of two fully reversed cycles at the MCE displacement amplitude, and the second-cycle properties are appropriate (and somehow conservative-to be demonstrated in the sequel) for the lower bound. For this case, the $\lambda_{test,min}$ should be defined as equal to the second-cycle value divided by the nominal value for each property of interest. If the site is such that soft soil conditions prevail, the expected number of cycles is about three (see Figure 3-2 c)), thus the RDP may choose to set $\lambda_{test,min}$ equal to the third-cycle value divided by the nominal value.

For the analyzed elastomeric isolation system, the nominal values of Q_d/W and T_d are 0.10 and 2.6sec, respectively. Considering again that for the site of the structure the motions will be near-fault or large magnitude, short distance, the expected number of cycles is again two. In this case the expected number of cycles is also two for the soft-site case.
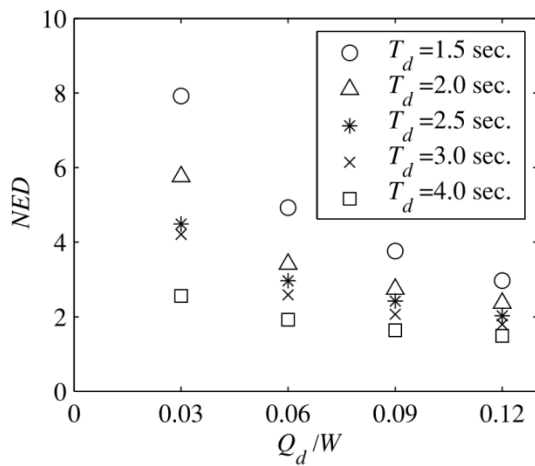
(a) Near-Fault Ground Motions (Bin 1)   **(b) Large Magnitude, Small Distance Motions (Bin 2M)**
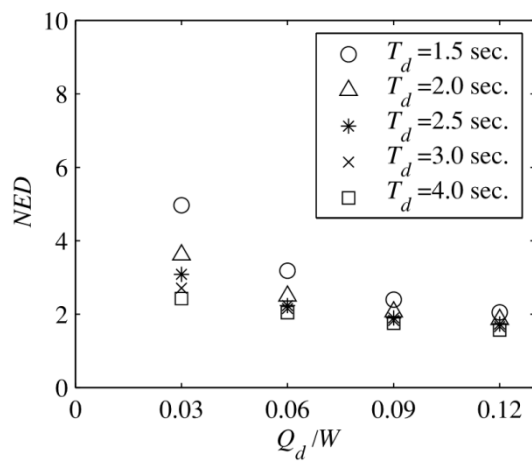
25
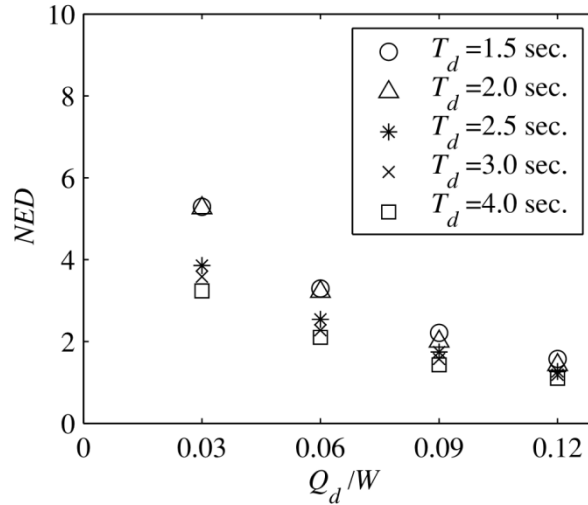
(c) Large Magnitude Soft-Site Motions (Bin 7)

Note: Bin numbers refer to the set of ground motions used in response history analysis

Figure 3-2 Number of Equivalent Cycles at Maximum Displacement for Various Isolation System Properties based on Bi-Directional Response History Analysis (Warn and Whittaker 2004)

It is noted that Constantinou et al (2011) recommend adopting the nominal values, which are the average of three cycles, as the lower bound (i.e. $\lambda_{test,min}$ set equal to 1.0). This is considered a reasonable approach because:

a) The expected number of cycles for typical isolation systems is about two and therefore the three-cycle average is representative of the lower bound (i.e. second cycle values). Two cycles appears to be a reasonable single value for all isolation systems cases based on Figure 3-2 and considering that typical building isolation systems have a Q_d/W of around 0.06 or larger and T_d of 2.5 seconds or greater.

b) The second-cycle values and nominal values are similar as shown in Figure 3-1(a). From test data in this report the difference was 9% or less.

c) Studies by Kalpakidis et al (2010) which show that adopting the three-cycle average value as the lower bound provides conservative estimates of demands. This last point is explained in summary below.

To illustrate the conservatism of the bounding analysis when accounting for the properties of lead-rubber isolators over three cycles of motion at the MCE displacement, Kalpakidis et al (2010) utilized a validated mathematical model which accounts for the instantaneous heating effects on the lead core strength to compute the response of seismically isolated structures. They were then compared to results obtained by

using bilinear hysteretic modeling of the isolators and performing bounding analysis with due consideration to only the heating effects. The upper bound value of the strength was based on the first cycle results and the lower bound value was based on the three-cycle average of tests results of actual isolators at the amplitude of 500mm. Thus, effectively $\lambda_{test,min}=1.0$. The results of the study demonstrated that bounding analysis produces conservative results for the prediction of isolation system displacement demand, isolation system peak shear force and peak structural responses. The conservatism was particularly pronounced for ground motions with strong near-fault pulses.

Table 3-3 presents a summary of the results as assembled from Kalpakidis et al (2010). In this table, W is the weight of the analyzed structure supported by the isolation system and W_s is the weight of the superstructure (W minus the basemat weight). The analyzed structure was a simplified model of an actual isolated structure - the Erzurum Hospital in Turkey. The period, based on the post-elastic stiffness, and strength to weight ratio of the isolated structure in the lower bound condition and at amplitude of 500mm are 4.54sec and 0.07, respectively.

Table 3-3 Peak Response of Analyzed Isolated Structure

Motion		Model	Resultant Isolator Displ. (mm)	Resultant Isolation Shear/W	Resultant Structural Shear/W_s	Drift (mm)		Accel. (g)		Lead Core Temp. Increase (°C)
X	Y					X	Y	X	Y	
NF17 Kobe, Japan 1995	-	Upper	466	0.21	0.26	16	-	0.27	-	-
		Lower	553	0.18	0.20	12	-	0.20	-	-
		Heating effects	539	0.19	0.23	15	-	0.24	-	87
BOL000 Ducze, Turkey 1999	BOL090 Ducze, Turkey 1999	Upper	177	0.15	0.19	10	12	0.16	0.19	-
		Lower	210	0.10	0.12	6	7	0.10	0.11	-
		Heating effects	180	0.14	0.16	9	10	0.15	0.16	59
NF02 Tabas, Iran 1978	-	Upper	355	0.19	0.20	12	-	0.20	-	-
		Lower	455	0.16	0.16	10	-	0.16	-	-
		Heating effects	399	0.17	0.17	11	-	0.17	-	66
NF13 North-ridge 1994	-	Upper	376	0.20	0.20	13	-	0.20	-	-
		Lower	484	0.17	0.17	11	-	0.17	-	-
		Heating effects	381	0.19	0.19	12	-	0.19	-	54
TCU065 N Chi-Chi, Taiwan 1999	TCU065 W Chi-Chi, Taiwan 1999	Upper	707	0.24	0.25	10	15	0.17	0.23	-
		Lower	1048	0.25	0.25	9	15	0.15	0.24	-
		Heating effects	1017	0.24	0.25	9	14	0.14	0.23	207

Of interest in Table 3-3 is the case of the Chi-Chi motion for which the amplitude of motion is much larger (twice) than the amplitude of motion in the testing of the isolators and the resulting heating of the isolators causes a lead core temperature increase of 207 °C (this is a hypothetical case as the actual isolators would have experienced instability at this displacement). At the end of the motion, the effective yield stress of lead has dropped to 25% of its initial value (from a starting value of 16.9MPa to 4.2MPa), which is much less than the value in the lower bound analysis (10MPa). Intuitively in such conditions it may be thought that bounding analysis will not provide a conservative estimate of the response and importantly, the isolator displacement demands may be underestimated due to the use of an incorrectly high value for the characteristic strength. However interestingly, this does not happen because the maximum displacement demand of the isolation system occurs early in the history of excitation when the

isolators still have high characteristic strength. Effectively, the number of cycles at 500mm amplitude was about 2 so that the average three-cycle characteristic strength of the isolation system was a representative lower bound value. This example demonstrates the complexity in selecting the bounding values. Nevertheless, the use of the three-cycle average for the lower bound value provides systematically conservative estimates of displacement demands and is consistent with the results of Warn and Whittaker (2004) on the equivalent number of cycles. Accordingly, the value of $\lambda_{test,min}$=1.0 is an appropriate single value for building isolation systems, with lower than unity values typically reserved for cases of uncertainty in the test results (e.g. cases of similar isolators per ASCE 7-2016 §17.8.2.7).

Although adopting the nominal value ($\lambda_{test,min}$=1.0) would be appropriate for the examples in this report, it was decided to use the second cycle properties instead. This is to be consistent with the intent of basing the lower bound on the expected number of cycles, which can be determined on a case by case basis. Furthermore the second cycle properties were slightly less than the nominal properties. This is typical because the first cycle has a greater weighting for strength and stiffness than the second and third cycles due to heating effects and scragging of rubber. Later calculations show that the $\lambda_{test,min}$ values for the sliding and elastomeric isolation systems were between 0.93-1.0, so are slightly more conservative than taking the nominal value as the lower bound.

3.3.2 Elastomeric Isolator Considerations

Within the context of bounding of properties of isolators made of low damping rubber in building applications, there are two major considerations for the history of loading effects. These are the scragging of virgin rubber and the heating during cyclic motion. Scragging is applicable for both low-damping natural rubber (NR) isolators and lead-rubber (LR) isolators, whereas heating effects are only significant in lead-rubber isolators.

In NR isolators (i.e. without a lead core), heat is produced throughout the entire volume of rubber. Constantinou et al (2007) have shown that the temperature rise is less than 1°C per cycle in large shear strain motion, and therefore too small to have any effects to warrant consideration in design. For lead-rubber isolators the lead core has substantial heating during cyclic motion which causes a reduction in the effective strength of lead (and to effective damping). A validated theory exists to predict this reduction in strength and is described in this section with examples of its application in Section 6.2.

The rubber shear modulus (or equivalently the post-elastic stiffness) of elastomeric isolators is not significantly affected by changes in axial compression load (that is the average axial load on isolators of

the same type and not the load on an individual isolator under conditions approaching instability). Nevertheless, testing at a range of axial load is required by ASCE 7-2016 to corroborate this assumption.

a) Scragging of Virgin Rubber

When rubber isolators are tested for the first time, they typically exhibit a higher stiffness and strength in the initial cycle which tends to stabilize after subsequent cycling (see Figure 3-3). This phenomenon is termed scragging of the virgin rubber. During the initial cycles of deformation the elastomer molecules stretch and fracture to give a scragged state with stable properties. In the past it was believed that the rubber cannot recover its virgin state, and therefore the isolators were routinely scragged before testing/installation, with this initial higher stiffness and strength being disregarded in analysis. However, more recent understanding of the behavior of elastomers (Thompson et al 2000, Constantinou et al 2007) claims that it is highly likely that full recovery of virgin properties occur with time, since chemical processes continue in the rubber following (incomplete) vulcanization. Therefore it is essential that isolators be tested in their virgin state so that both the unscragged and the scragged properties can be determined for use in the analysis and design of the isolation system.
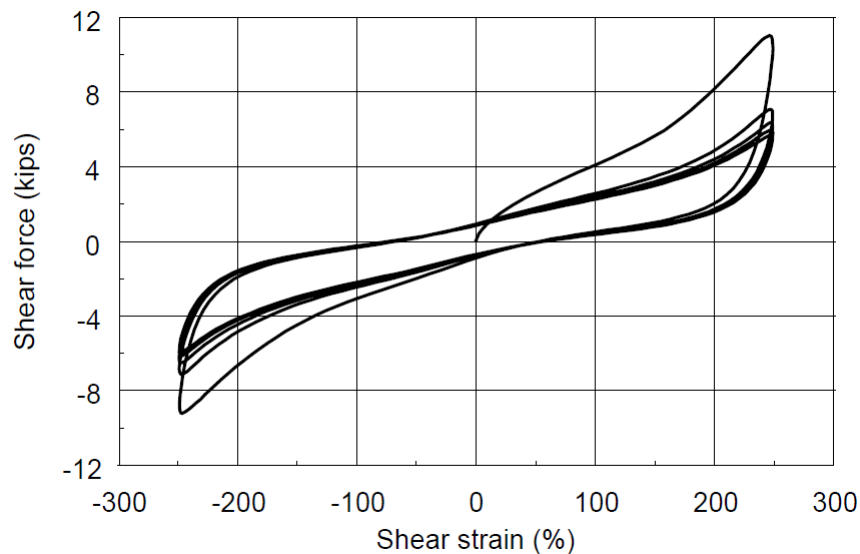
Figure 3-3 Effects of Scragging in a Rubber Isolator (Thompson et al, 2000)

Thompson et al (2000) found that scragging effects are typically greatest for high-damping and low shear modulus isolators, which often have a greater volume of filler materials (i.e. carbon black, synthetic elastomers, oils and resins). This is of particular interest as it is known that some unscrupulous manufacturers have been using increased proportions of filler materials to replace natural rubber in order to reduce the cost of elastomeric bearings/isolators.

As shown in Figure 3-4, the scragging factor varied between about 1.4 and 2.1 for a range of rubber compounds. The scragging factor in Figure 3-4 is defined as the ratio of effective stiffness in the 1st cycle (virgin or unscragged conditions) to the effective stiffness in the 3rd cycle (scragged condition), whereas bounding in this report is taken as the ratio of the first cycle post-elastic stiffness to the *average* post-elastic stiffness over three cycles of motion. Hence the value of the scragging lambda factor per ASCE 7 definition is less than that of Figure 3-4. The default lambda factor for scragging λ_{scrag} in low-damping rubber isolators is stated as 1.3 in the ASCE 7-2016 commentary, which is roughly equivalent to a 1.5 scragging factor in Figure 3-4. This factor is applied to the post-elastic stiffness K_d for low-damping natural rubber isolators and for lead-rubber isolators.
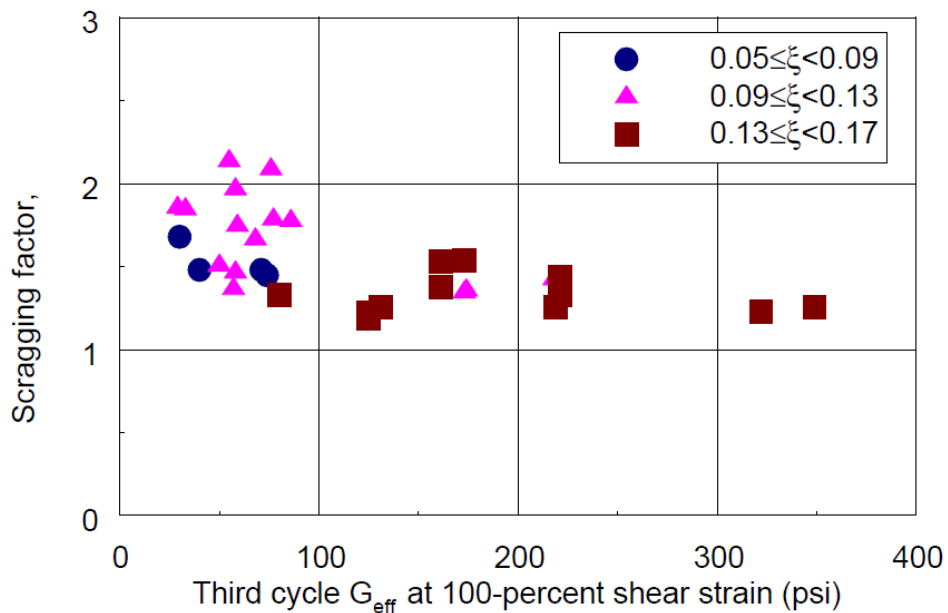
Figure 3-4 Scragging Effects for a Range of Elastomeric Isolator Types, 1000psi=6.9MPa
(Thompson et al, 2000)

It is noted that test data in Figure 3-4 is primarily for high-damping rubbers (damping > 9%). Although low-damping, low modulus rubbers contain fillers, there is a reduced percentage of carbon black (added to increase damping) compared to high-damping rubber isolators, therefore the scragging effects are likely to be smaller. Nevertheless, the scragging effects need to be determined explicitly from prototype or similar isolator test data.

For lead-rubber isolators, the scragging effects cannot be determined directly from prototype test data. This is because of the effects of heating of the lead core which completely masks the scragging behavior. The proper procedure is to request additional data from the manufacturer. It is preferable to test additional

31

isolators without the lead core. Pushing out the lead core and testing after the completion of the lead-rubber isolator prototype testing program is not recommended as the rubber has been scragged and therefore it will not be possible to observe the behavior the test seeks to reveal.

Data may also be obtained from testing of coupons of the actual rubber used, although this test data should be viewed with great caution. This is because there may be differences in the behavior obtained from testing of coupons (typically of dimensions 25mm by 25mm by 6mm) and the actual isolator (e.g. in this report an isolator of 850mm diameter is considered). The difference is due to differences in the curing of the rubber, with the small specimen typically completely cured and the isolator (depending on size) not fully cured, particularly in the interior and depending on the processes used and the experience of the manufacturer. Therefore the results from coupon testing should be viewed and used with extreme caution and with conservative adjustments due to the inevitable differences in the curing of small specimens of rubber and of large rubber isolators.

Moreover, it is noted that coupon tests should not be used for measuring the shear modulus of rubber. This is because the coupon tests usually have a very low shape factor (typically 1.0) and when they are displaced laterally there is both shear and bending deformations. In contrast, a building's isolators have a shape factor typically larger than 10 and often larger than 20 so that they deform purely in shear. Hence the coupon tests will underestimate the rubber shear modulus. In contrast, the scragging factor can be quantified from these coupon tests (but for the uncertainty due to the curing process) because it is the ratio of the stiffness in the first and subsequent cycles and it is presumed that scragging affects equally the shear and bending behavior of rubber.

b) Effective Yield Stress of Lead and Heating Effects

The characteristic strength Q_d and damping of a lead-rubber isolator is primarily due to the lead core. Using equation 2-1, the effective yield stress of lead σ_L can be calculated as Q_d divided by the area of lead A_L. This is a common simplification which implies that the small contribution to strength from rubber is included in the effective yield stress of lead.

An important concept is that the effective yield stress of lead at the initiation of motion varies from isolator to isolator, even within a single building. This is because the effective yield stress depends on a variety of parameters, including the compression axial load (i.e. confinement of lead), size of lead core, velocity of loading and manufacturer details. Therefore only dynamic testing of the actual isolator can provide the exact initial value of the effective yield stress of lead.

32

Furthermore there is a reduction in the effective yield stress of lead from cycle to cycle due to hysteretic heating effects. While testing of actual isolators will capture these effects, a validated theory from Kalpakidis et al (2008) can be used to quantify these heating effects, thus reducing the need for extensive testing. The effects of heating on a lead-rubber isolator (bearing) are illustrated in Figure 3-5. The data in this figure show a significant reduction in the effective yield stress of lead (expressed in the figure by the energy dissipated per cycle) in the first few cycles of high-velocity motion which tends to stabilize when the number of cycles is large. This is because the lead core tends to reach a constant temperature when the heat generation is equal to the heat lost by conduction through the isolator steel components. A brief interruption in testing resulted in nearly a full recovery of the effective yield stress of lead, which shows that (a) the reduction in energy dissipated per cycle is a result of the heating of the lead core, and (b) the heat conduction is significant.
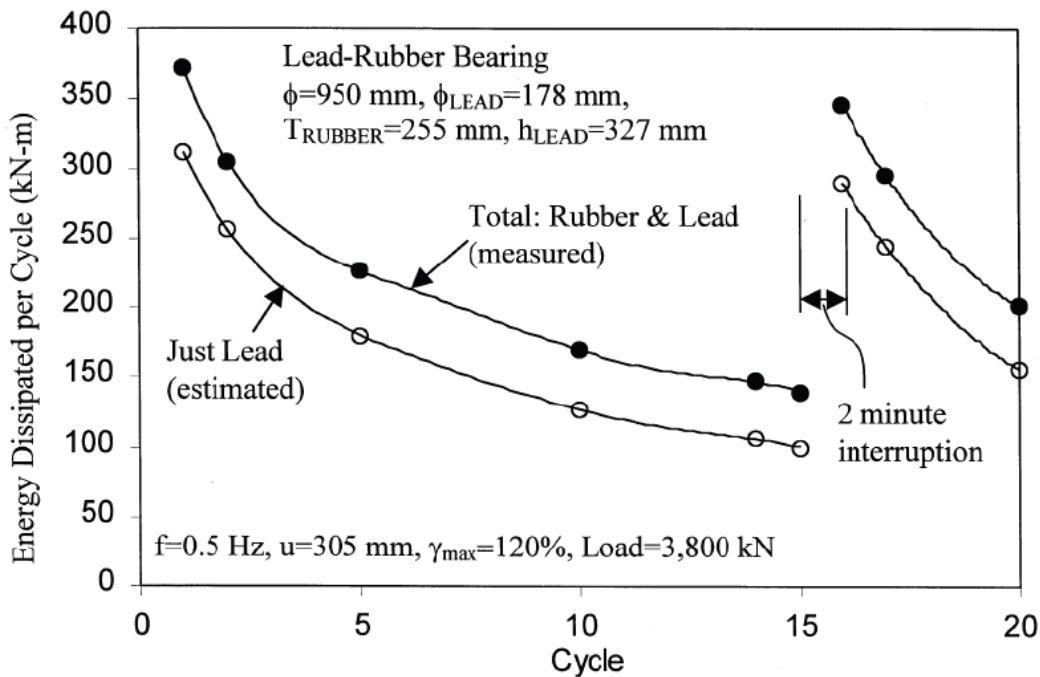
Figure 3-5 Effect of Hysteretic Heating on the Energy Dissipated per Cycle for Lead-Rubber Isolators (Constantinou et al, 2007)

The heating theory by Kalpakidis et al (2008) can be used to calculate the instantaneous reduction in the effective yield stress of lead σ_L. Performing heating calculations is complex and requires the solution of a differential equation. However if heat conduction through the shim and end steel plates are neglected (valid for the first few cycles of high-speed motion), the temperature rise in the lead core T_L and corresponding effective yield stress can be obtained by:

$$T_L = \frac{1}{E_2} ln\left(1 + \frac{E_2 \sigma_{L0} S}{\rho_L c_L h_L}\right)$$ (3 - 3)

$$\sigma_L = \sigma_{L0} \exp\left(-E_2 T_L\right)$$ (3 - 4)

The above equations, when combined, give:

$$\sigma_L = \frac{\sigma_{L0}}{1 + \dfrac{E_2 \sigma_{L0} S}{\rho_L c_L h_L}}$$ (3 - 5)

In equation (3-5), σ_{L0} is the effective yield stress at initiation of motion (at time t = 0), S is the distance travelled, ρ_L is the density of lead (11,300 kg/m^3), c_L is the specific heat of lead (130 Joule/(kg °C)), h_L is the height of the lead core, and E_2 is a material property of lead (0.0069/°C). Equation 3-5 shows that the instantaneous yield stress of lead is related to the ratio of the distance travelled to height of lead core and the initial value σ_{L0} in a complex nonlinear relationship. This relationship may be used to adjust results obtained from testing of similar isolators to results valid for the actual isolators based on rational considerations. Specifically, the lower bound value of σ_L can be determined for different ground motion characteristics (i.e. amplitude of motion and number of cycles). The only constraint is that both the similar and actual isolators shall have a similar axial compression load/confinement so that the effective yield stress of lead at the initiation of motion σ_{L0} is the same. Actually it may be different and hence some uncertainty in its value has to be considered. The utility of this theory is shown in examples that follow in Section 6.2.

The default lambda factors from ASCE 7-2016 commentary are presented in Case A in Table 3-4 together with information on other cases. Constantinou et al (2011) recommend taking an upper bound of the yield stress of lead σ_L (or by relation Q_d) as 1.35 times the nominal 3-cycle value, whereas ASCE 7-2016 adopts further conservatism by using a factor of 1.6 given the uncertainty in products that lack qualification data.

Table 3-4 Testing Lambda Factors for Elastomeric Isolators

Case	Description	Lambda Factor	Low-Damping Elastomeric Isolator K_d	Lead-Rubber Isolator K_d	Lead-Rubber Isolator Q_d
A	No Qualification Test Data Available- Default Values	λ_{scrag}	1.3	1.3	-
		λ_{lead}	-	-	1.6
		$\lambda_{test,max}$	1.3	1.3	1.6
		$\lambda_{test,min}$	0.9	0.9	0.9
B	Qualification and Prototype Test Data Available	$\lambda_{test,max}$	Section 6.3	Section 6.2	Section 6.2
		$\lambda_{test,min}$	Section 6.3	Section 6.2	Section 6.2
C	Qualification and Production Test Data Available	$\lambda_{test,max}$	Section 6.3	Section 6.2	Section 6.2
		$\lambda_{test,min}$	Section 6.3	Section 6.2	Section 6.2

3.3.3 Sliding Isolator Considerations

The stiffness of sliding isolators is dictated by the geometry, whereas the strength and damping is dictated by the coefficient of friction (friction force divided by normal load). Typically sliding isolators, whether flat or spherically shaped, can be manufactured with a high degree of geometric precision leaving only the coefficient of friction as the parameter that varies during seismic excitation. Friction is an extremely complex phenomenon of which the exact mechanism is not known. Rather, several mechanisms are believed to contribute in the generation of friction. The current state of knowledge is provided in Constantinou et al (2007). Some key concepts are provided here for an interface of PTFE or similarly behaving composites in contact with highly polished stainless steel, which are used in Friction Pendulum^{TM} isolators.

The coefficient of friction for PTFE-stainless steel interfaces is affected by a number of factors, of which sliding velocity, bearing pressure and temperature are the most important.

Sliding velocity influences the friction coefficient due to a) the friction coefficient being dependent on velocity and b) frictional heating during motion. At the initiation of motion, there is a higher value for the friction coefficient (termed the breakaway or static friction μ_B) which then reduces to a minimum value f_{min} at very low velocities, as shown in Figure 3-6. At high velocity the friction coefficient increases to attain a maximum value f_{max}, at velocities above 25 to 100 mm/s. The friction coefficient tends to be invariable once f_{max} is reached but for the effect of heating which is dependent on the duration of motion.
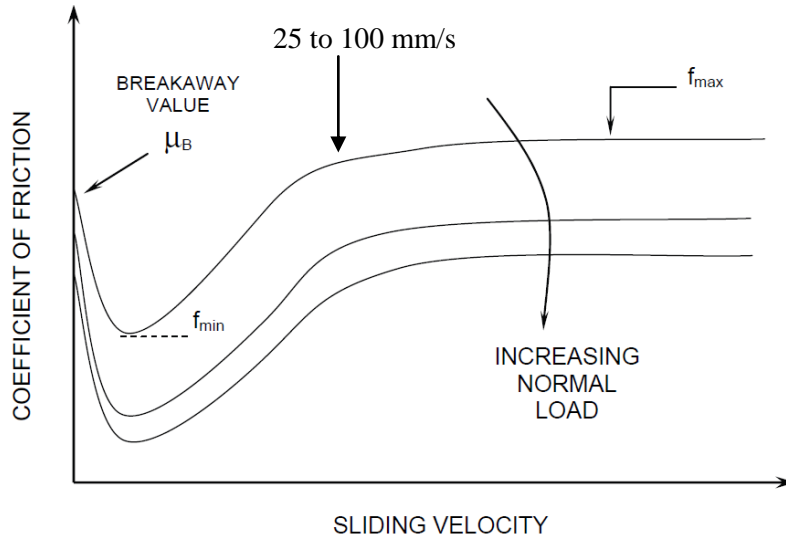
Figure 3-6 Effect of Sliding Velocity and Axial Compression Load on the Coefficient of Friction for PTFE-Stainless Steel Interfaces

Increases in the bearing pressure, or equivalently, increases in the axial compression/normal load result in decreases in the friction coefficient as shown schematically in Figure 3-6, or more explicitly in Figure 3-7. Figure 3-7 includes a measure of the breakaway friction μ_B and maximum and minimum friction coefficients, f_{min} and f_{max} (defined in Figure 3-6) from FP isolators in four different test programs. Under high bearing pressures the value of friction tends to reach a constant value as shown in Figure 3-7. The mechanism by which this occurs is discussed in Constantinou et al (2007).
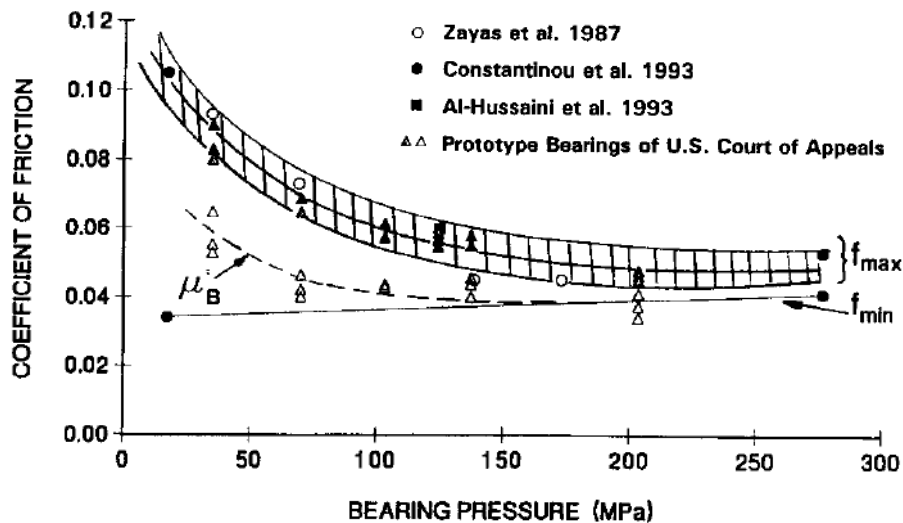
Figure 3-7 Effect of Axial Compression Load on the Coefficient of Friction in Friction Pendulum Isolators (Mokha et al, 1996)

Low ambient temperature can have a significant effect on the breakaway and minimum friction coefficients, but only a mild effect on the friction coefficient at high velocity (f_{max}). This is due to the significant frictional heating occurring at the interface which moderates the effects of low temperature. This along with the assumption that building isolators are located in normal environments, mean that ambient temperature is not considered herein.

The increase in temperature through frictional heating is of importance as it causes wear and a reduction in the friction coefficient. Since frictional heating occurs at the contact surface, which is very small in volume, the temperature increase is substantial, however diffuses quickly into the surrounding medium. The temperature increase at the interface is proportional to the heat flux. The heat flux (energy per unit of area per unit of time) at the interface is proportional to the coefficient of friction, the average pressure and the velocity of sliding. Therefore the similar unit requirements in ASCE 7-2016 require that the isolators be tested at a velocity and bearing pressure no less than that required in design to capture the hysteretic heating effects. Moreover the heating generated during high-velocity motion may also affect the bond strength of the material sliding against the stainless steel surface (typically proprietary materials in several layers glued to form a 1mm to 2mm thick liner), thus real time testing of production isolators is important.

The above effects justify why it is necessary to carry out high-velocity dynamic testing under design specific conditions to get an accurate estimate of the friction coefficient, as well as to validate workmanship. Ideally this is at full-scale as the size (of the slider) can also affect behavior. When this is not possible, complicated scaling and similarity principles must be satisfied for testing (see Constantinou et al 2007 for an example of application of principles of similarity in the testing of reduced size bearings).

Table 3-5 lists the default values recommended in ASCE 7-2016 commentary for cases where qualification data are unavailable and for other cases. Given the uncertainty of the sliding interface and mechanism of friction, the range of $\lambda_{test,max}$ and $\lambda_{test,min}$ is large. Theory predicts the stiffness of isolators based on geometry, which is invariable with the hysteretic heating and history of loading hence the $\lambda_{test,max}$ and $\lambda_{test,min}$ factors on K_d are 1.0.

Table 3-5 Testing Lambda Factors for Sliding Isolators with Unlubricated PTFE-Stainless Steel Sliding Interfaces

Case	Description	Lambda Factor	Friction Pendulum Isolators	
			K_d	Q_d
A	**No Qualification Test Data – Default Values**	$\lambda_{test,max}$	1.0	1.3
		$\lambda_{test,min}$	1.0	0.7
B	**Qualification Data and Prototype Test Data Available**	$\lambda_{test,max}$	1.0	Section 7.2
		$\lambda_{test,min}$	1.0	Section 7.2
C	**Qualification Data and Production Test Data Available**	$\lambda_{test,max}$	1.0	Section 7.2
		$\lambda_{test,min}$	1.0	Section 7.2

3.4   Permissible Manufacturing Variations: $\lambda_{spec,max}$ and $\lambda_{spec,min}$

The specification lambda factors $\lambda_{spec,max}$ and $\lambda_{spec,min}$ are a manufacturing tolerance assumed for design and written into specifications. These factors are determined by the RDP, in consultation with the manufacturer. The specification lambda factors account for, but are not limited to, the natural variability in properties, manufacturing variations and other uncertainties or contingencies.

The nominal properties of each and every prototype and production isolator unit will be different from the average properties of all production isolators of a common type, with the extent of this variation depending on the quality and reliability of a supplier's manufacturing methods. Since the Standard requires testing of every isolator that is used in construction, the data can be used to determine the mean isolation system properties and ensure that the as-built average nominal properties are consistent with the design assumptions. However, this is not the main reason for carrying out production testing on 100% of the production isolators. Other important concerns are discussed in Section 4.4.

Typically the nominal property values used for analysis are based on test data from only two prototype isolators (instead of production data) and the design accounts for manufacturing variations by incorporating a range of values defined by $\lambda_{spec,max}$ and $\lambda_{spec,min}$. These lambda factors therefore set a range that the average values from production testing must fall within. In the unusual case where production test data is available for use in the analysis, then the exact nominal properties for the isolation system are known and $\lambda_{spec,max}$ and $\lambda_{spec,min}$ are both set to unity.

The specification tolerance is explained in Figure 3-8 for a hypothetical sliding isolation system which requires 12 isolators. Two prototype isolators are assembled at the beginning of the project to determine nominal properties for analysis. Here the prototype isolators are not used in construction, however this is up to the RDP's discretion. The nominal coefficient of friction for analysis is taken as the average nominal value of the prototype isolators, numbered 1 and 2 in Figure 3-8, which is (0.063 + 0.062)/2 = 0.0625. The RDP then assumes a $\lambda_{spec,max}$ and $\lambda_{spec,min}$ of 1.15 and 0.85, respectively, for analysis and design and specifies a ±15% tolerance for manufacturing variations. This gives a range (see grey solid line) of 0.053 to 0.072 which the average nominal value of all production isolators must fall within. As shown in Figure 3-8, the average of the nominal values for production isolators is 0.057, therefore the manufacturer has met the specification requirement. It is noted that this is an imaginary scenario. If a project required only 12 isolators then there may be savings in constructing and testing all isolators so that $\lambda_{spec,max}$ and $\lambda_{spec,min}$ can be set equal to unity.

Individual isolators may be permitted to have a wider variation from the nominal properties used in design. This second tolerance may have been specified as ±20% as shown in Figure 3-8. Here two isolators fall slightly outside this range, yet the average of all production isolators is within the ±15% tolerance. The RDP has the option to reject or accept these two isolators. Given that the average behavior of the isolators is important and not that of the individual isolators, the tolerance for individual isolators could be larger than the ±15% in ASCE 7 or the ±20% mentioned above. However, it is noted that the maximum individual isolator properties are typically used for local design of connections and the supporting structure.
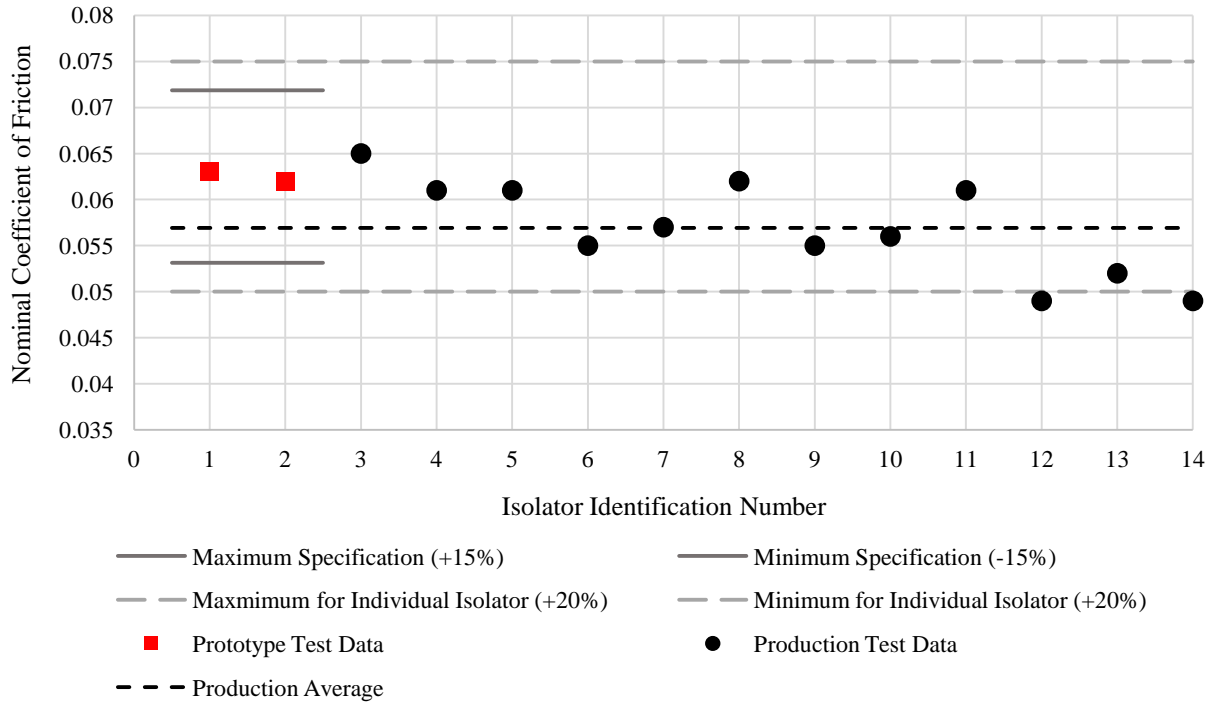
Figure 3-8 Hypothetical Illustration of Specification Tolerances

It is assumed that the production test data in Figure 3-8 is from dynamic testing at relevant loading conditions, so is identical to the prototype testing conditions and the nominal values can be compared directly. If quasi-static production testing is undertaken, assumed to be common practice for most manufacturers at present, then there has to be a relationship established between quasi-static and dynamic conditions in order to check the manufacturing tolerance. This is discussed further in Section 4.4.

The most common condition for calculating nominal properties is expected to be as follows: *Test data for two prototype isolators (or similar units per ASCE 7-2016 criteria) per type are available under relevant conditions of load, amplitude of motion, velocity and number of cycles. Production test data are available from other projects to use in verifying property modification factors for specifications.* In this case the RDP may adopt a ±15% tolerance, as recommended in the ASCE 7-2016 commentary. Specifying a smaller tolerance is acceptable however overly tight tolerances have the potential to delay projects. An uncommon but ideal situation is having all production isolators tested and using the actual nominal properties for design. The three design scenarios for this report are given in Table 3-6. The lambda-test factors are applied to both Q_d and K_d for lead-rubber isolators and to Q_d for sliding isolators.

Table 3-6 Specification Lambda Factors

Case	Description	Lambda Factor	Any Nominal Property
A	**No Qualification Test Data – Default Values**	$\lambda_{spec,max}$	≥1.15
		$\lambda_{spec,min}$	≤0.85
B	**Qualification Data and Prototype Test Data Available**	$\lambda_{spec,max}$	1.15
		$\lambda_{spec,min}$	0.85
C	**Production Test Data Available**	$\lambda_{spec,max}$	1.0
		$\lambda_{spec,min}$	1.0

Exception: The post-elastic stiffness K_d of sliding isolators is based on the geometry of the isolator which can be manufactured with a high degree of accuracy, hence $\lambda_{spec,max} = \lambda_{spec,min} = 1.0$ for all cases.

This Page is Intentionally Left Blank

SECTION 4
TESTING REQUIREMENTS

4.1 Introduction

The testing requirements in ASCE 7-2016 are extensive and, in the authors view, complex. This section describes the key requirements of testing which is based on recommendations by Constantinou et al (2007) and Buckle et al (2006).

The Standard ASCE 7-2016 mandates qualification, prototype and production testing of the isolation systems hardware. This testing has multiple objectives, such as validating the stability and robustness of isolator components and as a means to establish and validate properties used in analysis and design. Such testing is necessary due to:

a) The importance of the isolation system, since it is the chief mechanism that reduces the structural seismic response.

b) Most isolators being custom designed and constructed.

c) Isolators being manufactured using non-traditional civil engineering materials (i.e. composites, lead and elastomers).

d) Some isolators being mechanical systems which involve moving parts.

The sections that follow elaborate on the three types of tests mentioned in ASCE 7-2016, namely qualification, prototype and production testing. Within the context of property modification (lambda) factors, the former two are used in establishing the force-displacement properties and property modification factors for analysis, with production testing usually used for validation of these properties and to reveal any problems with individual production isolators.

4.2 Qualification Testing

Qualification testing is a new clause in ASCE 7-2016, which complements the formal requirement to undertake bounding analysis of the isolator's force-displacement behavior. Clause 17.8.1.1 states:

Isolation device manufacturers shall submit for approval by the Registered Design Professional the results of qualification tests, analysis of test data and supporting scientific studies that are permitted to be used to quantify the effects of heating due to cyclic dynamic motion, loading rate, scragging, variability and uncertainty in production bearing properties, temperature, aging, environmental exposure, and contamination. The qualification testing shall be applicable to the component types, models, materials and sizes to be used in the construction. The qualification testing shall have been

performed on components manufactured by the same manufacturer supplying the components to be used in the construction. When scaled specimens are used in the qualification testing, principles of scaling and similarity shall be used in the interpretation of the data.

The RDP has flexibility and authority to determine what data qualifies as qualification test data. However it is generally the responsibility of the manufacturer to conduct qualification testing. These tests may be used to aid in the establishment of nominal properties and lambda factors, to characterize the longevity of the isolator, and to develop models of the isolators for analysis.

In practice it is assumed that manufacturers have comprehensive databases of properties, based on research projects and past prototype and production testing. This is already the case for two suppliers in the United States which have compiled large databases. With regard to the nominal properties and lambda factors, the following comments are made:

a) The aging and environmental lambda factors $\lambda_{ae,max}$ and $\lambda_{ae,min}$ generally can only be determined with the use of qualification test data and theoretical considerations.

b) It is expected that the practice will evolve such that similar units test data (per ASCE 7-2016 criteria) will be the common basis for determining nominal properties and lambda-test factors $\lambda_{test,max}$ and $\lambda_{test,min}$. This is instead of performing prototype testing on every project. In this case, production testing may be used to corroborate analysis and design assumptions.

c) Past production test data is useful in determining the specification tolerance, $\lambda_{spec,max}$ and $\lambda_{spec,min}$, for manufacturing variations.

4.3 Prototype Testing

The testing protocols (sequence and cycles) outlined in ASCE 7-2016 can be traced back to historical documents where testing was performed quasi-statically. Nowadays it is recognized that the dynamic force-displacement behavior of isolators can be significantly different to the quasi-static behavior. Therefore dynamic testing is necessary to quantify the velocity and strain-rate effects.

The different tests in ASCE 7-2016 §17.8.2.2 are seeking multiple objectives. The opinion of the authors is that only one characterization test is required to determine the isolation systems properties for analysis. This is the test with three fully reversed cycles of loading at the maximum (MCE) displacement D_M performed dynamically at high speed. This test is item 3 of §17.8.2.2. The procedure for this prototype testing is described in Constantinou et al (2007) as follows:

- Supply a virgin (unscragged) isolator to the test facility and install it in the test machine. Apply an axial compressive load equal to 100% of the gravity load plus 50% of live load (load combination 1 of ASCE 7-2016 §17.2.7.1, take the average for all isolators of a common type). Test at an ambient and bearing temperature of 20 ±8 °C. Apply three cycles of sinusoidal loading to a lateral displacement amplitude D_M, at a loading frequency (or velocity) which is calculated from the effective frequency (inverse of effective period T_M) of the isolated building. The displacement amplitude should be the calculated displacement in the maximum earthquake D_M without the effect of torsion. Continuously record and report the vertical and lateral force and displacement histories for the duration of the test. Plot the lateral-force-versus lateral displacement relationship for the test. Record and report the ambient temperature at the start of the test.

Constantinou et al (2007) states that this test provides benchmark data on the force-displacement response of the virgin seismic isolator. The test isolator unit must not have been tested previously by the manufacturer regardless of whether it is the practice of the manufacturer to conduct such tests as part of a quality control program. Three cycles of displacement are specified based on the studies of Warn and Whittaker (2004), who demonstrated that less than three fully-reversed cycles at the maximum displacement are expected for isolation systems with strength-to-supported weight ratio (Q_d/W) of 0.06 or larger and period based on a post-elastic stiffness associated with a period of 2.5 seconds or greater (see Section 3.3.1).

The Standard ASCE 7-2016 §17.2.8.2 requires that the isolator properties are determined using three axial/vertical load combinations consisting of:

1. Average vertical load: $D + 0.5L$
2. Maximum vertical load: $(1.2 + 0.2S_{MS})D + \rho Q_E + L + 0.2S$
3. Minimum vertical load: $(0.9 - 0.2S_{MS})D + \rho Q_E$

where D = dead load, L = live load, S= snow load (if applicable), $0.2S_{MS}$=vertical seismic effects, and ρQ_E=horizontal seismic effects with a redundancy factor. The Standard allows the properties determined from each load combination to be averaged to give a single representative deformation cycle at each displacement level of the test regime. If the properties (i.e. effective stiffness and effective damping) from load combination 1 differ by less than 15% than the average of the properties from the three load combinations, then the properties are permitted to be computed for load combination 1 only. For this report it is declared (but should be corroborated on an actual project) that the lead-rubber, low-damping rubber and triple Friction Pendulum isolators meet this requirement. Therefore the range of lambda-test values is not further increased to incorporate a variation in properties from lower and higher axial loads

than D + 0.5L (see Section 6 and 7). This requirement acknowledges that the mechanical properties of the isolation system are not (materially) affected by fluctuations in the axial load on individual isolators. Rather, the behavior is determined by the average load on the isolators, which is D+0.5L. However, the effect of varying axial load on the properties of individual isolators is of interest as it affects the design of the isolator and of the structure in the vicinity of the isolator.

The purpose of other testing may be to check that the measured force or displacement are within specified limits (i.e. wind test), to verify the stability of isolators in the maximum considered event, or to verify the isolator performance following several design earthquake events. These other tests are not intended for calculating properties, and may underestimate the upper bound and overestimate the lower bound. This is because the isolator has been scragged and perhaps there is not sufficient idle time between test sequences to let the heating effects dissipate.

For large aftershocks, such as those experienced in Christchurch New Zealand in 2010/2011, although the isolator may be scragged, it is expected to have its characteristic strength restored and therefore the lower bound properties used in analysis are still appropriate. This is because heating effects take in the order of minutes to dissipate as shown in Figure 3-4 and in Constantinou et al (1999).

ASCE 7-2016 also specifies "test specimen adequacy" criteria, which may dictate the bounds, particularly the lower bound, of the properties used for analysis if the testing is performed dynamically. These requirements are checked in Section 6.5 for actual prototype test data of lead-rubber isolators and Section 7.4 for sliding isolators. It is the opinion of the authors that the requirements (specific to the lambda-test factors) are arbitrary since they do not take into account the project-specific isolation systems characteristics (i.e. Q_d and T_d) or the earthquake excitation. Furthermore as described in Section 3.3.1, bounding analysis using simplified bilinear hysteretic models, where the lower bound heating effects are based on the nominal 3-cycle values, have been shown to give a conservative estimate of response compared to more realistic validated models which account for the instantaneous heating effects (Kalpakidis et al 2010).

It is essential that prototype testing is undertaken using full-scale specimens. If testing of reduced scale specimens is the only option (based on capacity of testing equipment) then application of principles of scaling and similarity is required. This requires the development and verification of theories to predict the degrading behavior of the isolation hardware. Often complete similarity cannot be achieved with the available testing equipment and therefore incomplete similarity may be employed, however its limitations

need to be understood (Constantinou et al, 2007, Kalpakidis and Constantinou, 2010). Finally it is noted that as displacement, velocity and force demands increase for seismic isolation applications in demanding environments, dynamic testing at full scale becomes increasingly difficult, time consuming and expensive, and occasionally impossible.

4.4 Production Testing

Production testing intends to verify the quality of the individual production isolators and is commonly referred to as quality control testing. Furthermore it is used to check that the isolation system properties are within the tolerance (specification lambda factor, λ_{spec}) assumed for analysis and design. Buckle et al (2006) state that under certain circumstances it may be acceptable to test only a portion of the isolators (say 50%) and implement a rigorous inspection program. However, ASCE 7-2016 mandates that 100% of the project's isolators are tested, and gives the RDP flexibility to determine the acceptance criteria and manufacturing quality control test program. The requirement for production testing of all isolation hardware has been the result of recent observation of failures or unacceptable behavior of hardware that has not been tested with two notable examples being:

1) Elastomeric isolators for the Kunming Airport in China were installed in 2011 without testing. As construction progressed and loads increased on the isolators, several showed signs of delamination. Hundreds of isolators were removed and replaced.

2) The California State Buildings 8 and 9 in Oakland, CA were fitted in 2007 with viscous damping devices of which 75% were installed without testing and with the remaining 25% to be tested prior to installation. Several tested devices showed abnormal behavior that necessitated the removal, testing and re-building of the installed dampers.

Quasi-static production testing is assumed to be the common practice for most manufacturers at present. Therefore to evaluate the consistency of the nominal values measured from production testing, there must be a relationship established between properties determined under quasi-static and to behavior under dynamic conditions. Typically, this requires that the prototype isolators are tested under the same conditions as the production testing to establish the criteria for acceptance of the production isolators, and to be tested under dynamic conditions for obtaining the nominal values and related property modification factors for analysis. Nevertheless, the quality of production isolators may not be adequately demonstrated when tested quasi-statically and this may be a concern for products of inexperienced manufacturers.

This Page is Intentionally Left Blank

SECTION 5

PRELIMINARY DESIGN AND DESIGN SCENARIOS

5.1 Introduction

The building selected as a basis for the subsequent examples is the six story steel framed building used in the SEAOC Volume 5 Seismic Design Manual ("SEAOC Manual") (2014), with details reproduced in Appendix A. However, the preliminary design of the isolation systems in this report deviates from those in the SEAOC Manual. The building is located in San Francisco, California (Latitude 37.783°, Longitude -122.392°) with spectral acceleration values of S_{MS}=1.50g and S_{M1}=0.90g to ASCE 7-10 site class D. There are examples for two types of isolation systems, namely the elastomeric isolation system consisting of low-damping natural rubber and lead-rubber isolators, and a sliding isolation system consisting of triple Friction Pendulum^{TM} isolators.

The preliminary design of the elastomeric and sliding isolation systems is summarized in Section 5.2 and 5.3, respectively. These details provide a basis to systematically determine the nominal properties and lambda-test factors for detailed analysis, as illustrated in Sections 6 and 7. A detailed analysis, such as the nonlinear response history analysis (NLRHA) in Section 9, can then be used to assess the adequacy of the design and to confirm the isolator's specifications. For illustration, the lambda factors are determined for three different design scenarios/cases. These cases are described in Section 5.4

The preliminary designs in this report are based on the approach presented in the Constantinou et al. (2011) Appendix C and D examples. The method utilizes simplified calculations based on the equivalent lateral force (ELF) procedure of ASCE 7, and does not require NLRHA analysis. It is noted that preliminary design will vary, perhaps considerably between engineers, which is expected. Furthermore the preliminary design is an iterative process, and is based on the test data available as shown in Appendix B and C of this report. The analysis only considers the lower bound isolation properties, which is critical in assessing adequacy related to stability and displacement capacity. The upper bound analysis is typically also conducted in preliminary design as it may result in the maximum forces for the assessment of adequacy of the structure. This is not done in this report as the work concentrates on the isolation system.

The seismic weight of the building is 53090kN (11930kip) which consists of the dead load of 47795kN (10740kip) including the weight of the isolators, plus a partition live load of 5295kN (1190kip). The reduced live load is about 20196kN (4538kip). Further information on the buildings weights is given in

Appendix A.2. The live load does not contribute to seismic weight in this example (but for the partitions) but are needed for isolator stability checks, and for the load combinations in ASCE 7-2016 §17.2.7.1. It is noted that the seismic weight of 53090kN used for analysis is slightly different from the ASCE 7-2016 load combination of D+0.5L = 57893kN. A mathematical model was used to calculate the distribution of axial compression loads, which are given in Tables 5-2 and 5-3 for the elastomeric and sliding isolation systems, respectively.

5.2   Preliminary Design for Elastomeric Isolation System

A description of the preliminary design procedure is presented in Appendix B. The design incorporates data from the tested isolators presented in Section 6. The nominal properties (average over three cycles of motion) were:

- Lead-rubber (LR) isolator rubber shear modulus, G = 0.40MPa (58 psi)
- Natural rubber (NR) isolator rubber shear modulus, G = 0.49MPa (71 psi)
- Effective yield stress of lead, σ_L = 11.6MPa (1.68 ksi)

A different type of rubber was used for the LR and NR isolators, and this is to be kept consistent for the final design. The details of the elastomeric isolation system are given in Table 5-1. The required isolator dimensions determined in the preliminary design are smaller than the tested isolators and are checked to see if they meet the similar unit requirements of ASCE 7-2106 in Section 6.4.

Table 5-1 Rubber and Natural Rubber Isolator Dimensions obtained from Appendix B

Isolator Type	Number of Isolators	Bonded Diameter, D_B, mm (in)	Total Rubber Thickness, T_r, mm (in)	Lead Plug Diameter D_L, mm (in)	Center Hole D_{hole}, mm (in)
Lead-rubber (LR) Isolator	12	800 (31.5)	203 (8.0)	220 (8.66)	N/A
Low-damping Natural Rubber (NR) Isolators	20	750 (29.5)	203 (8.0)	N/A	70 (2.76)

The lower bound properties, which are taken as the nominal properties multiplied by a factor of 0.85, were used to determine the maximum displacement using the ELF procedure. The isolation systems key parameters from preliminary analysis are:

- MCE Displacement D_M = 350mm   (13.7inch)
- Effective Stiffness K_M = 40.2kN/mm   (229kip/in)
- Effective Period T_M = 2.3 seconds

- Effective Damping β_M = 20%
- Total Post-Elastic Stiffness $K_{d,\,total}$ = 27.2kN/mm (155kip/in)
- Total Characteristic Strength $Q_{d,\,total}$ = 4497 kN (1011kip)

As explained in Appendix B, the elastomeric isolators were sized based on the minimum required rubber thickness to maintain stability. For the lower bound isolation system properties, the characteristic strength is 8.5% of the seismic weight, and structural shear at the maximum displacement is 26% of the seismic weight. The design velocity based on the effective period and the calculated maximum displacement is about 950 mm/s (37.4 in/s). Note that the design velocity was calculated as the pseudo-velocity (effective frequency times amplitude of displacement $= 2\pi D_M/T_M$), which is known to be a rough approximation to the peak velocity. The latter may be better estimated by multiplying the pseudo-velocity by a correction factor based on the values of effective period (2.3sec) and effective damping (0.20) per procedures in Ramirez et al (2000) to calculate a peak velocity of about 1050 mm/sec (41.3in/sec).

Preliminary design revealed that the corner isolators (i.e. Grid 1/E) experience large tension loads due to the isolator having the lightest gravity loading combined with the maximum overturning effects from the structure above. Tension stresses in elastomeric isolators are discouraged as the capacity in tension is very limited and is dependent on the manufacturing quality. Furthermore, the necessary production testing of the isolator in tension (to verify the behavior) may result in damage to the isolator and therefore it will not be fit for use. Various options to address this issue are discussed in Appendix B. Herein it is assumed the isolators are bolted at the bottom and slotted at the top, therefore allowing uplift to occur but checking that displacements (calculated using NLRHA) are within acceptable limits. This uplift is not modeled in the NLRHA in Section 9 as it is outside the scope of this report and is expected to have minimal effect on the lateral behavior of the isolators. However, uplift will have some effect on the distribution of vertical load on the isolators.

The configuration of the isolation system is illustrated in Figure 5-1. This configuration parallels the one in SEAOC Design Manual but the lead-rubber isolators have been re-located from the corners to the perimeter so as to increase the compression load on them and thus achieve better confinement of the lead core and improve their expected behavior. The configuration is still resistant to torsional motion. Four additional lead-rubber isolators have been placed at the reentrant corners to further improve performance of the isolation system.
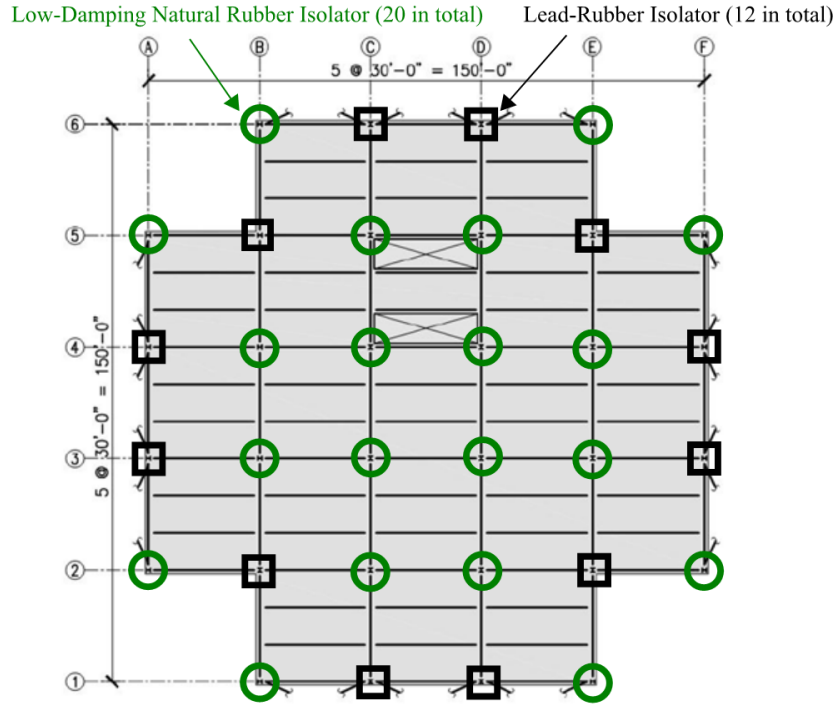
Figure 5-1: Schematic of Isolator Layout for Lead-Rubber Isolation System

The isolation system is divided into two components of a common type, namely LR and NR isolators. The average compression load for these two categories for ASCE 7-2016 §17.2.7.1 load combination 1, is given in Table 5.2.

Table 5-2: Elastomeric Isolation System Compression Loads

Load Combination	Combination	Lead-Rubber Isolator		Natural-Rubber Isolator	
1. Average vertical load kN (kip)	D + 0.5L	1724	kN	1860	kN
		387	kip	418	kip

5.3 Preliminary Design for Sliding Isolation System

The preliminary design of the special triple Friction Pendulum (FP) isolator is presented in Appendix C and follows the procedure of Constantinou et al. Appendix C (2011). Of the 8 parameters used to define the force-displacement behavior of a "special" triple FP isolator (defined in Section 2.3), typically only the outer surfaces friction μ_1 (or μ, the friction at zero displacement) and outer surfaces radius R_1 are determined by the Registered Design Professional (RDP) since they govern the structures global seismic response. Other details of the triple FP isolator can be determined based on recommendations from the manufacturer. The best strategy is to contact the manufacturer of triple FP isolators and request proposals for isolator configurations that are most suitable for the application (i.e. trial designs) that can then be

evaluated by the RDP. By using standard isolator components and configurations the design will be more economical and have a more reliable performance compared to theoretical optimization studies.

For this report, it is assumed the manufacturer recommended an isolator used on a past project with the dimensions given in Figure 7-1 and prototype test data presented in Section 7.2. The preliminary design in Appendix C also explores other scenarios, namely:

a) The scope for altering the recommended isolator geometry (i.e. the isolator's post-elastic stiffness parameter R_1 and the displacement capacity d_1).

b) Calculating the friction coefficients based on qualification test data, in the case where the prototype test data does not meet the similarity requirements of ASCE 7-2016.

Scenario b) is a hypothetical and involved process which gives insight into how the friction coefficient varies due to isolator pressure, velocity and frictional heating. Sometimes the RDP simply specifies a friction coefficient, with a range, and then the manufacturer uses their proprietary construction methods and/or alters the isolator's dimensions to actually achieve this friction value. Alternatively, the manufacturer provides information on what friction properties can be achieved in standardized isolator designs, which results in reduced manufacturing costs and expedited delivery of the isolators.

For the preliminary analysis (See Section C.3 in Appendix C), the nominal coefficient of friction at zero displacement μ is taken as 0.048. This value is based on the test data available (Table 7-3). The maximum displacement is calculated using the ELF procedure using the rigid-linear and assuming lower bound properties of $\mu = 0.85 \times 0.048 = 0.040$ for all isolators. The isolation systems key parameters from preliminary analysis are:

- MCE Displacement D_M = 627mm   (24.7inch)
- Effective Stiffness K_M = 15.9kN/mm   (91kip/in)
- Effective Period T_M = 3.7 seconds
- Effective Damping β_M = 14%
- Total Post-Elastic Stiffness $K_{d, \, total}$ = 12.5kN/mm   (71kip/in)
- Total Characteristic Strength $Q_{d, \, total}$ = 2134 kN   (480kip)

The total maximum displacement is taken as $1.2 \times D_M$ to account for torsion and bi-directional effects, or D_{TM}=752mm (29.6inch). The isolators displacement capacity is 828mm (32.6 inch) with stiffening (i.e. force-displacement response enters regime III as specified in Tables 2-1 and 2-2) at around 762mm (30 inch). Therefore the prototype isolator is adequate and the tri-linear model in Figure 2-4 is applicable.

The required design velocity for testing, based on this preliminary design, can then be determined. Assuming a sinusoidal displacement and a period of oscillation using the stiffness of the outer concave plates radius R_1 = 2235mm (88inch), not the effective stiffness as would be the case for an elastomeric system, the design velocity is calculated as $2\pi D_M/T_d = 2\pi \times 627mm/4.14sec$ = 950mm/sec (37.5 inch/sec). Note that the design velocity was calculated as the pseudo-velocity (frequency times amplitude of displacement = $2\pi D/T_d$), which is known to be a rough approximation to the peak velocity. The latter may be better estimated by multiplying the pseudo-velocity by a correction factor based on the values of the effective period (about 3.7sec which is less than the post-elastic period of 4.14sec) and effective damping (0.14) per procedures in Ramirez et al (2000) to calculate a peak velocity of about 1025mm/sec (40.4in/sec).
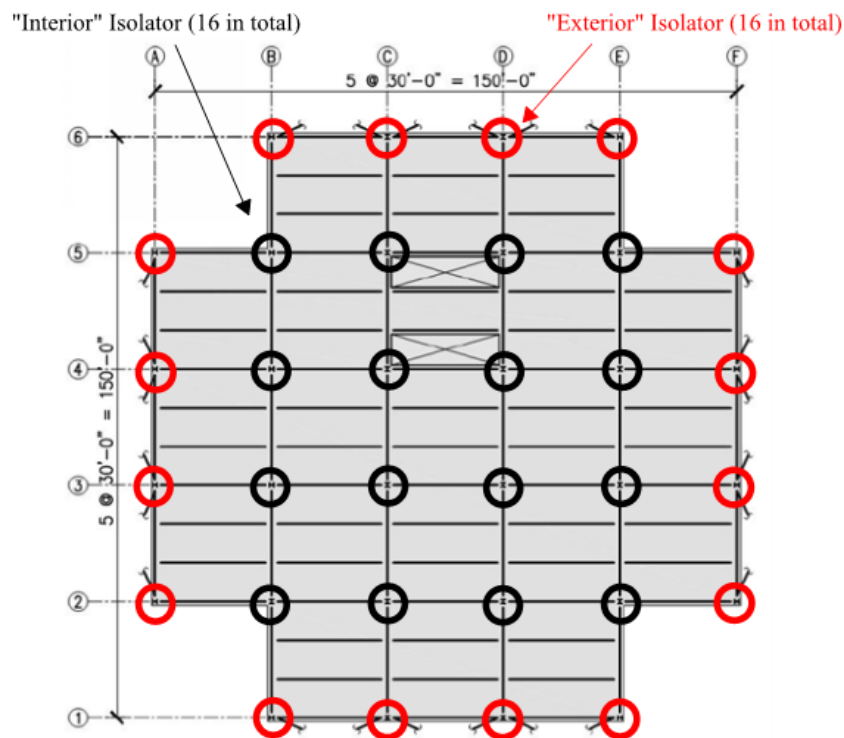
Figure 5-2: Schematic of Isolator Terminology for Sliding Isolation System

The friction coefficient and frictional heating are dependent on the compression load (or bearing pressure) and therefore the FP isolators are categorized in two types for design, namely "interior" isolators and "exterior" isolators. These two types of isolators will have different sets of nominal values and/or lambda test factors as illustrated in Section 7. The average compression load on the interior and exterior isolators, for ASCE 7-2016 §17.2.7.1 load combination 1, is given in Table 5.3.

Table 5-3: Sliding Isolation System Compression Loads

Load Combination	Combination	Interior Isolator		Exterior Isolator	
1. Average vertical load kN (kip)	D + 0.5L	2351	kN	1267	kN
		528	kip	285	kip

5.4 Design Scenarios for Detailed Analysis

There are three main design scenarios investigated in this report, these are:

- **Case A: No Qualification Test Data/Manufacturer Unknown (Default Lambda Factors)**

  It is assumed that there is no qualification test data from a reputable manufacturer to review and establish lambda factors. The default values of ASCE 7-2016 are used, as discussed in Section 3 and summarized in Section 8. Nominal values are assumed based on generic information. The assumed nominal values must be verified in prototype testing (as required by ASCE 7-2016 §17.8.2), however detailed design commences before this testing. This is an undesirable situation and will result in the largest difference between response computed based on upper and lower bound properties, which will have an influence on maximum displacements (and hence isolator size) and maximum forces.

- **Case B: Prototype or Similar Unit Test Data Available**

  It is assumed that there is qualification data from a reputable manufacturer to review and establish lambda factors. The establishment of the nominal values and lambda factors is based on recommendations of the manufacturer, analysis by the Registered Design Professional (RDP) and review by the Peer Review Panel (PRP). In this report, the nominal values and associated testing lambda factors are established from past prototype testing of similar isolators (assumed to meet the similarity requirements of ASCE 7-2016 §17.8.2.7). No further prototype testing is conducted. This is expected to be a common case as manufacturers develop large databases of test results in past projects. Since the analysis is based on test data from similar but not the actual isolators, still some uncertainty exists and some adjustment of data may be needed. This is illustrated in the examples that follow. Herein, the approach is taken to establish the nominal values of properties on the basis of the available data from the similar isolators and then adjusting the system property modification factors to reflect the uncertainty. Moreover, the examples that follow show how data obtained in the testing of one isolator may be adjusted on the basis of

validated theory to apply to different conditions of motion that are relevant to the application for which the isolators are considered.

- **Case C: Production Test Data Available**

  In the case where there is comprehensive qualification data from a reputable manufacturer to review and establish lambda factors. Also, it is assumed that the isolators have been manufactured and tested so that the nominal values are available based on the production test data. This is an ideal scenario as there is no uncertainty on manufacturing variation (i.e. $\lambda_{spec,max} = \lambda_{spec,min} = 1.0$), therefore it will have the smallest difference between response computed based on upper and lower bound properties. This case is uncommon at present because it requires all isolators to be constructed and tested prior to the analysis.

The quantity and quality of test information available to determine an isolation system's nominal properties and associated lambda factors has been categorized as specific cases above, yet it is better described by the continuum in Figure 5-3 below. At one end of the range there is limited test data, with the most uncertainty in the isolator system performance, compared to full production data from dynamic testing which is the ideal but uncommon scenario. The three cases considered above fall somewhere between these district cases along the continuum of possibilities.

Figure 5-3 Indicative Continuum of Quantity and Quality of Test Data vs. Range in Isolation System Properties

SECTION 6

COMPUTING PROPERTIES FOR ELASTOMERIC ISOLATORS

6.1   Introduction

This section presents examples of how to calculate nominal properties and the associated testing lambda factors $\lambda_{test,max}$ and $\lambda_{test,min}$. Dynamic test data is presented for two lead-rubber isolators and two low-damping natural rubber isolators (i.e. Case B: Prototype or Similar Unit Test Data of Section 5.4). The rubber shear modulus G and the effective yield stress of lead σ_L nominal values are calculated for the bilinear analysis model discussed in Section 2.2. These are the material parameters which are used to calculate the post-elastic stiffness K_d and the characteristic strength Q_d, respectively.

In this report the axial compression load used to calculate the nominal properties and associated lambda-test values only considers the average vertical load (§17.2.7.1 load combination 1), for reasons discussed in Section 4.3.

6.2   Lead-Rubber Isolators

6.2.1   Prototype Isolators

Two full scale lead-rubber prototype isolators of a past project were subjected to high speed testing with three fully reversed cycles. The details of the two isolators are illustrated in Figure 6-1. The isolator has a total rubber thickness T_r = 203 mm (8.0 in), a bonded rubber area including half the rubber cover thickness A_r = 505528 mm² (822 in²), a lead core area A_L = 38013 mm² (59 in²), and a shape factor (loaded area divided by the area free to bulge) of S = 28.4.

SEE TOP PLATE
FOR PLATE SIZE
AND HOLE LAYOUT

850.9mm ISOLATOR ⌀
[33.5"]
(DIMENSION A)
812.8mm INT. PL. ⌀
[32"]

220mm LEAD ⌀
[8.661"]
(DIMENSION C)
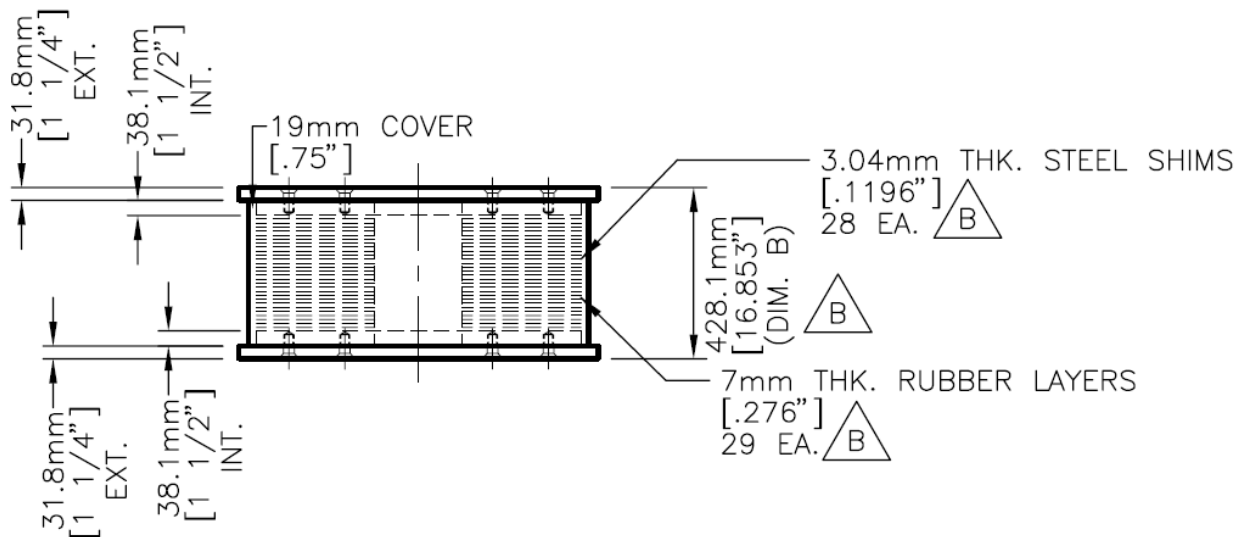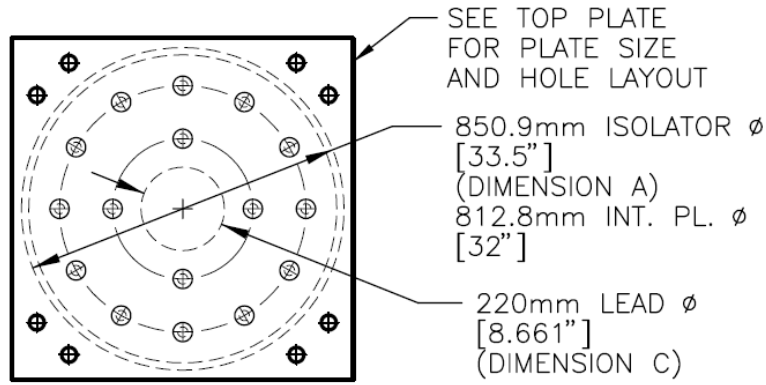
BOTTOM VIEW

Figure 6-1 Tested Lead-Rubber Isolator Unit Details

The identical isolators were tested at an average axial load of 3683 kN (828 kip) with a sinusoidal displacement of 483mm (19.0 in) amplitude, corresponding to a peak shear strain of 238 %. The tests were conducted dynamically at high speed with a peak velocity of 1012 mm/s (39.8 in/s). This corresponds to a frequency of 0.33Hz or period of oscillation of 3.0 seconds. Figures 6-2 and 6-3 give the lateral force-displacement loops for Isolator No. 1 and Isolator No. 2, respectively, which fortuitously have nearly identical behavior.
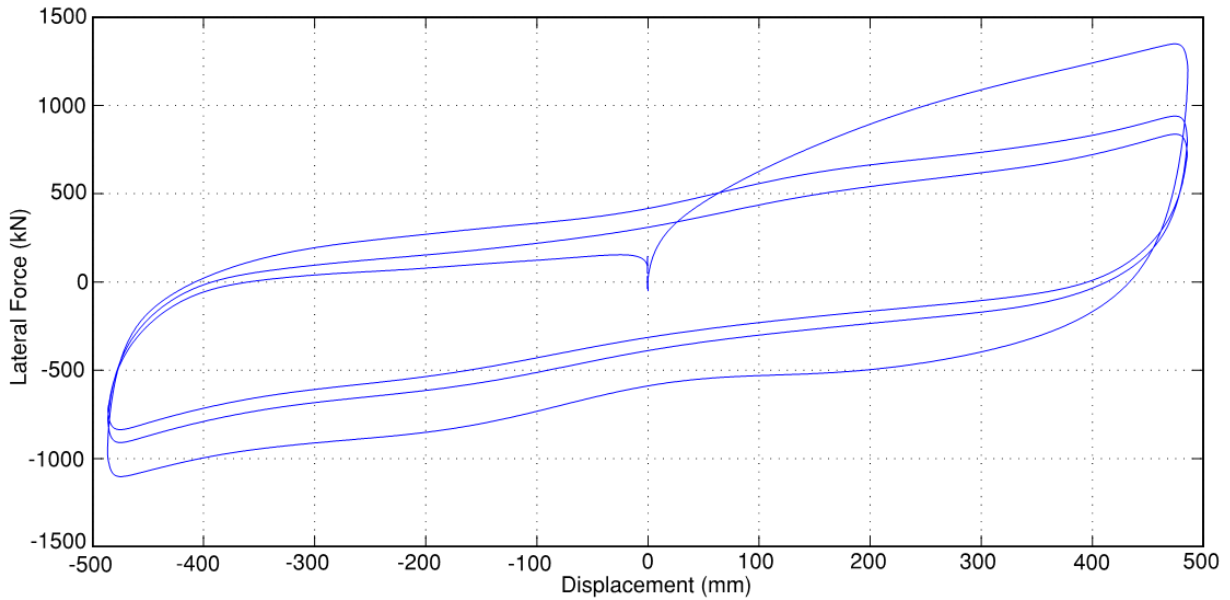
Figure 6-2 Lateral Force-Displacement Loops of Isolator No. 1
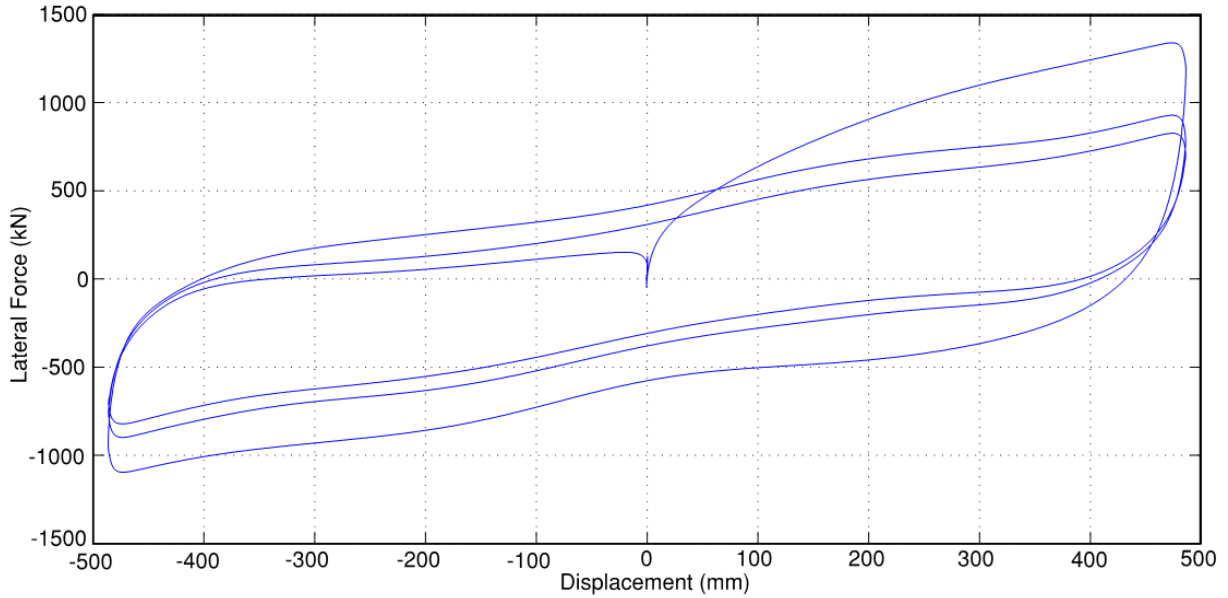
Figure 6-3 Lateral Force-Displacement Loops of Isolator No. 2

An initial comparison of the tested isolators to the preliminary design requirements shows a peak displacement of 483mm compared to 350mm, a peak velocity of 1012mm/s compared to 1050mm/s, and a compression load of 3683kN compared to 1724kN. Therefore the tested isolators above appear appropriate but the properties may require adjustment, as discussed later.

There are three fundamental properties for the lead-rubber isolator bilinear model. These are the shear modulus of rubber G, the effective yield stress of lead σ_L and the yield displacement Y. The mechanical properties of the two tested isolators are given in Table 6-1.

Table 6-1 Mechanical Properties of Two Prototype Lead-Rubber Isolators

Cycle/Loop	Shear Modulus of Rubber, G MPa	Energy Dissipated per Cycle, E_{loop} kN-mm	Characteristic Strength of Lead, Q_d kN	Effective Yield Stress of Lead, σ_L MPa
Isolator No. 1				
1	Discard	1120677	599	15.7
2	0.41	768538	411	10.8
3	0.37	610929	326	8.6
Average	0.39	833381	445	11.7
Isolator No. 2				
1	Discard	1109697	593	15.6
2	0.43	761081	407	10.7
3	0.40	606266	324	8.5
Average	0.41	825681	441	11.6
Average of two isolators	**0.40 MPa** (58 psi)	**829531 kN-mm** (7339 kip-in)	**443 kN** (100 kip)	**11.65 MPa** (1688 psi)

The calculation of each of these parameters is outlined as follows:

1. Shear Modulus of Rubber, G

The shear modulus of rubber is calculated from the post-elastic stiffness K_d using equation (2-2). This equation includes a factor (greater than unity) which is used to account for the stiffening effect of the lead core. This factor is assumed to be equal to unity in cycles 2 and beyond owing to the heating effects of the lead core that diminish its contribution to the stiffness. For this reason the first cycle is discarded for the calculation of the post-elastic stiffness. The higher stiffness seen in the ascending branch of the first cycle is accounted for in the model for analysis by using a combined upper bound value of stiffness (accounting for uncertainty in properties and scragging effects) and upper bound value of strength (accounting for heating effects).

The value of K_d is calculated graphically by finding the slope of the loops as shown in Figure 6-4. This is an example for the second loop of Isolator No. 1. The slopes are fitted to the data up to a displacement of around 75% of the maximum displacement in each direction (corresponding to 180% shear strain). Care is

taken to determine slopes that have equal values for the ascending and the descending branches of the loop. This results in the calculation of stiffness K_d, which is taken as 1.03 kN/mm for this loop.
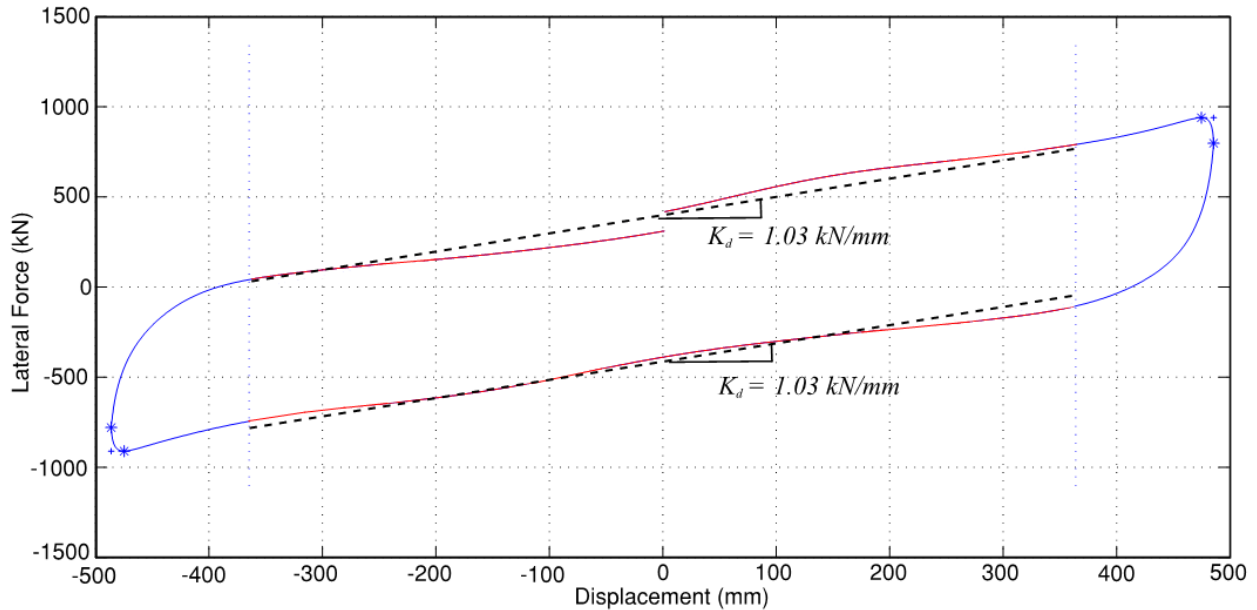
Figure 6-4 Graphical Calculation of the Post-Elastic Stiffness, Loop 2 Isolator No. 1

The shear modulus or rubber is then calculated by rearranging equation 2-2. Assuming after one loop that there is a negligible stiffening effect from the lead core and rubber scragging, the shear modulus of rubber for the second loop of Isolator No. 1 is calculated as follows:

$$G = \frac{K_d T_r}{f_L A_r} = \frac{(1.03 \times 1000) \times 203}{1.0 \times 505,528} = 0.41 MPa \, (59 \, psi)$$

The nominal value of the shear modulus of rubber is the average over three cycles. Herein, only two cycles are available but as seen in Table 6-1 there is small difference in post-elastic stiffness after the first cycle, part of which is real and part the result of the method of processing of the data by selecting a "best fit" straight line to represent the stiffness. Accordingly, the average value of the two cycles is used as the nominal value for the shear modulus. Any presumed uncertainty related to the effect of a third cycle motion will have to be incorporated in the property modification factors. Taking the average for the two prototype isolators gives a nominal shear modulus of rubber of 0.40MPa.

Based on an expected number of cycles of two (determined in Section 3.3.1) the minimum lambda-test factor $\lambda_{test,min}$ is taken as 1.0. The corresponding maximum lambda-test factor $\lambda_{test,max}$, which is accounting for the effect of scragging, cannot be calculated accurately from the available test data on

lead-rubber isolators. This is because of the effects of heating on the lead core, which completely masks the scragging behavior. If the same rubber has been used for both the lead-rubber and the low-damping natural rubber isolators, the scragging factor may be obtained from the low-damping natural rubber isolator test data. However in the scenario where all the project's isolators are lead-rubber or a different rubber is used (as is the case here), then the proper process is to request additional information from the manufacturer. Further discussion on this matter is provided in Section 3.3.2.

Based on actual prototype data, the nominal value and associated testing lambda factors for the calculation of the lead-rubber isolator's post-elastic stiffness is:

- Nominal shear modulus of rubber, **$G_{nominal}$ = 0.40 MPa (58 psi)**
- Maximum testing lambda factor, $\lambda_{test,max}$ = more data required
- Minimum testing lambda factor, $\lambda_{test,min}$ = **1.0**

2. **Effective Yield Stress of Lead, σ_L**

The characteristic strength Q_d (force at the zero displacement) for each cycle can be calculated from test data using:

$$Q_d = \frac{E_{loop}}{4(D-Y)}$$

(6 - 1)

In equation 6-1, E_{loop} is the measured energy dissipated per cycle, D is the displacement and Y is the yield displacement. The energy dissipated per cycle is the area within the loop and can be measured by numerical methods using the recorded test data of force and displacement. The yield displacement is taken as 15mm (0.6inch) based on a visual fit of data, and the displacement D is the maximum displacement, assumed to be the same in each direction. The effective yield stress of lead σ_L is then calculated using equation (2-1) by dividing the characteristic strength by the area of the lead core (A_L=38013mm^2). It is noted that the rubber also contributes a small amount to this characteristic strength, however for simplicity it is assumed that all the strength is contributed by the lead core. The effective yield stress of lead for each cycle of the tested isolators is provided in Table 6-1.

The nominal effective yield stress of lead is taken as the average over three cycles of motion, and then averaged for the two prototype isolators, which is equal to 11.65 MPa, and rounded to 11.6 MPa for use in calculations. Note that velocity effects are directly accounted for in the test which is dynamic, so that only heating effects are reflected in the values of λ_{test}. For the calculation of the upper bound properties, the average of the σ_L in the first cycle from the two prototype isolators is needed, which is 15.65 MPa.

Therefore the $\lambda_{test,\ max}$ value is the ratio of the first cycle σ_L to the average of three cycles, giving 15.65/11.6 = 1.35. Based on the isolation systems properties and site ground motions, the expected number of cycles is two cycles (see Section 3.3.1 for details). Since the second cycle properties are less than three-cycle average (nominal properties), the lower bound is set to the second cycle properties with $\lambda_{test,min}$ equal to ½(10.7+10.8)/11.6 = 0.93. Therefore the nominal value and associated lambda factors for these prototype isolators is:

- Nominal yield strength of lead, $\boldsymbol{\sigma_{L,nominal}} = \boldsymbol{11.6\ MPa}$

- Maximum testing lambda factor, $\boldsymbol{\lambda_{test,max}} = \boldsymbol{1.35}$

- Minimum testing lambda factor, $\boldsymbol{\lambda_{test,min}} = \boldsymbol{0.93}$

6.2.2 Adjustments for Heating Effects

The two lambda-test factors $\lambda_{test,max}$ and $\lambda_{test,min}$ above assume that the testing conditions are identical to what is required in design, which they are not. The "similar" isolators above are tested to a displacement of 483mm with a compression load of 3683kN, whereas the preliminary design resulted in a maximum displacement (without torsion) of 350mm and compression load of 1724kN (D + 0.5L). Therefore some adjustment is necessary. As introduced in Section 3.3.2, a validated theory from Kalpakidis et al (2008) can be used to calculate the heating effects in lead-rubber isolators. The general theory is first discussed below before undertaking adjustments of the lambda-test factors for the design conditions.

Depending on the nature of the earthquake source and proximity to faults, the RDP may decide to utilize a number of cycles less or more than two, which will result in different values of $\lambda_{test,}$. The established nominal value of the effective yield stress of lead and of $\lambda_{test,}$ only apply for the tested pair of isolators and for the conditions of load and motion in the test. In the following we describe how the data obtained in the testing of these two isolators may be adjusted to apply to different conditions.

The effective yield stress of lead at initiation of motion varies from isolator to isolator. This is because it depends on a variety of parameters, including axial compression load on the isolator (i.e. confinement of lead), amplitude of motion, size of lead core, and isolator manufacturer details. Furthermore there is a reduction in the strength of lead from cycle to cycle due to heating effects, which can be significant in the first few cycles of high-speed motion. A problem with using data from the testing of similar (but not the actual) isolators is that the value of the effective yield strength of lead needs to be adjusted for the conditions of testing of the actual isolators, which are related to the expected response of the actual isolators (amplitude of motion and number of cycles).

Simplified heating calculations (Kalpakidis et al, 2008) can be used to calculate the reduction in the effective yield stress of lead, which are presented in Section 3.3.2. This theory is applicable for the first few cycles of high speed motion as it neglects heat conduction through the shim and end steel plates.

The implementation of this theory is illustrated as follows:

1. Calculate the effective yield stress of lead for each cycle, as shown in Table 6-1. This effective yield of lead is an "average" over the full cycle, i.e. if the characteristic strength was held constant at this value over the full loop then the energy dissipated per cycle will be equal to that obtained from the test data. In reality the yield stress of lead is continually reducing during motion due to heating effects.

2. Plot the data for the effective yield stress of lead measured from testing for each loop, as shown in Figure 6-5. For a displacement D of 483mm, the travel S completed for one full loop is 4 × 0.483 =1.932m. As discussed earlier, the effective yield stress calculated in Step 1 is an "average" value representative of a full cycle, hence is plotted as a stepped line (see grey dotted line Figure 6-5).

3. Extrapolate the data points back to the vertical axis to obtain the reference effective yield stress of lead at zero time σ_{L0}, before motion begins. Using the simplified heating calculations (Kalpakidis 2008), with an estimate of σ_{L0} (may require iteration) and travel S (based on the calculated D_M), one can plot the reduction in the effective yield stress of lead as a function of travel or number of cycles (see Simplified Analytical line in Figure 6-5). The fitting of the "simplified analytical" curve to the measured data should be made at mid-cycle.

For the first cycle, the temperature increase and corresponding reduced effective yield stress for each cycle is calculated using equations (3-3) and (3-4) as follows using a height of lead $h_L = 428 - 2$ x (31.8 + 38.1) = 0.288 m, an estimate of σ_{L0}=20.5 MPa and the travel at mid-cycle for the first cycle is S = 0.966m, giving:

$$T_L = \frac{1}{0.0069} \ln\left(1 + \frac{0.0069 \times 20.5 \times 10^6 \times 0.966}{11,300 \times 130 \times 0.288}\right) = 40.6°C$$

$$\sigma_L = 20.5 \times \exp\left(-0.0069 \times 40.6\right) = 15.5\,MPa$$

It is important to note that the temperature increase is calculated based on travel at mid-cycle (i.e. 0.966m, 2.898m, and 4.83m for the 1st, 2nd and 3rd cycles, respectively).
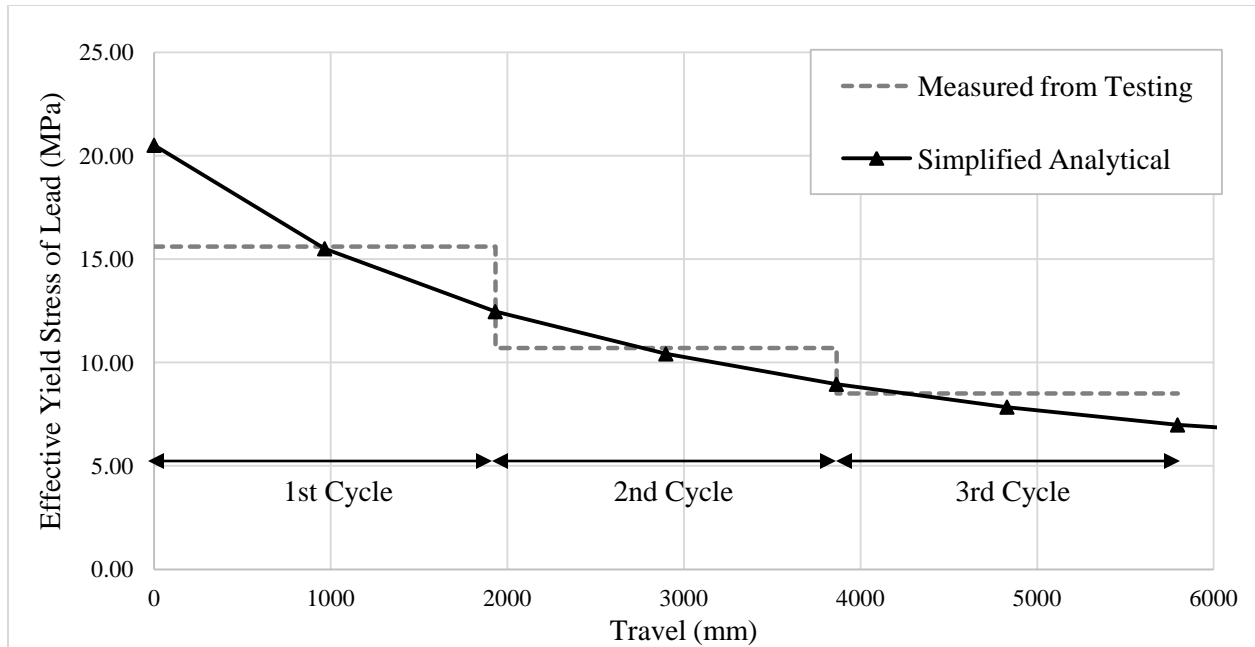
Figure 6-5 Measured and Calculated Effective Yield Stress of Lead

In Figure 6-5 the analytical calculation slightly over-predicts the temperature increase (and thus under-predicts the yield stress for the third cycle). This is because the simplified theory ignores heat conduction through the steel shims and steel end plates, which is a conservative assumption as it over-predicts the temperature increase. The theory explains and quantifies the substantial reduction in energy dissipated per cycle in the initial cycles. More accurate calculation is possible (Kalpakidis et al, 2008) but the numerical solution of a differential equation will then be needed.

This theory may be applied for this design, where the maximum displacement required by preliminary design is 350mm, whereas for the tested isolators the amplitude is 483mm. The initial value of the effective yield stress of lead σ_{L0} is 20.5 MPa, obtained as shown above. Calculations using equation 3-5 give the following: σ_{L1}=16.6MPa (at S=0.7m), σ_{L2}=12.05MPa (at S=2.1m) and σ_{L3}=9.45MPa (at S=3.4m). The average of the three cycles is the nominal value $\sigma_{L,nominal}$ = 12.7 MPa, and the ratio of σ_{L1} to $\sigma_{L,nominal}$ is $\lambda_{test,max}$ = 16.6/12.7=1.30, whereas $\lambda_{test,min}$ = 1.0, or 0.95 based on the second cycle properties.

Conversely, if the nominal value calculated from the prototype isolators above (11.6MPa) is maintained, the corresponding lambda-test factors would be adjusted to $\lambda_{test,max}$ = 16.6/11.6=1.4 whereas, unusually, $\lambda_{test,min}$ = 12.05/11.6 = 1.04. However since the tested compression load is 3683kN, which is more than twice the average design load, there is uncertainty in the initial value σ_{L0} and some adjustment is

necessary. The compression load provides confinement to the lead core, and therefore the lower compression load will correspond to a lower effective yield stress of lead. Therefore the lower bound is reduced by 10% (i.e. $\lambda_{test,min} = 1.04 - 0.1 \approx 0.95$) and the upper bound value is maintained conservatively. Hence the nominal value with the adjusted lambda factors, specific for the preliminary design case, based on similar isolators is:

- Nominal yield strength of lead, $\boldsymbol{\sigma_{L,nominal} = \textbf{11.6 MPa}}$
- Maximum testing lambda factor, $\boldsymbol{\lambda_{test,max} = \textbf{1.40}}$
- Minimum testing lambda factor, $\boldsymbol{\lambda_{test,min} = \textbf{0.95}}$

This range (1.4/0.95=1.47) in the lambda-test factors is slightly more than the range based on prototype isolators (1.35/0.93=1.45), even though the heating effects are greater for the prototype isolators since they have greater travel. This is because of the uncertainty in the initial value of the effective yield stress of lead, which was accounted for by increasing the range of the λ_{test} values.

To further illustrate the utility of the theory consider a lead-rubber isolator having a lead core height h_L=0.2 m and calculated amplitude of motion in the maximum earthquake (excluding torsion) equal to 0.24m (this will be the amplitude of motion for which the prototype isolators should have been tested). Let us assume the initial value of the effective yield stress of lead σ_{L0} is 20.5 MPa, as obtained in the testing of the similar isolators. (In reality it will not be the same so some adjustment will be needed). Calculations using equation (3-5) give the following: σ_{L1}=16.7MPa (at S=0.48m), σ_{L2}=12.1MPa (at S=1.44m) and σ_{L3}=9.5MPa (at S=2.4m). The average of the three cycles is the nominal value $\sigma_{L,nominal} =$ 12.8 MPa and the ratio of σ_{L1} to $\sigma_{L,nominal}$ is $\lambda_{test,max} = 16.7/12.8=1.30$, whereas $\lambda_{test,min} = 1.0$ (this is a representative value as explained in Section 3.3.1). However, due to uncertainty in the initial value of the yield strength of lead it is appropriate to further adjust the lambda factors to say $\lambda_{test,max} = 1.35$ and $\lambda_{test,min} = 0.95$.

In another example, consider the case in which the RDP has determined (and the Peer Review Panel approved) that for the same isolator with lead core height h_L=0.2 m the amplitude of motion is 0.5m and only two cycles at this amplitude are expected due to the nature of the fault and the proximity of the structure to the fault. Assuming a value of σ_{L0}=20.5 MPa, calculations using equation (3-5) give the following: σ_{L1}=13.8MPa (at S=1m) and σ_{L2}=8.4MPa (at S=3m). The average of the two cycles is now defined as the nominal value $\sigma_{L,nominal} = 11.1$ MPa and the ratio of σ_{L1} to $\sigma_{L,nominal}$ is $\lambda_{test,max} =$ 13.8/11.1=1.24, whereas $\lambda_{test,min} = 1.0$. However, due to uncertainty in the initial value of the yield

strength of lead it is appropriate to further adjust the lambda factors to say $\lambda_{test,max} = 1.30$ and $\lambda_{test,min} = 0.95$.

6.3 Low-Damping Rubber Isolators

Two low-damping natural rubber prototype isolators of a past project were subjected to high speed testing with three fully reversed cycles. The details of the two isolators are illustrated in Figure 6-6. The isolator has a total rubber thickness $T_r = 203$ mm (8.0 in), a bonded rubber area including half the rubber cover thickness $A_r = 539692$mm^2 (875 in^2), a hole/mandrel diameter of 70mm (2.756 in), and a shape factor of S $= 27$. The isolators were made using the same manufacturing methods used for the two lead-rubber isolators but the rubber was different as its shear modulus was slightly higher.
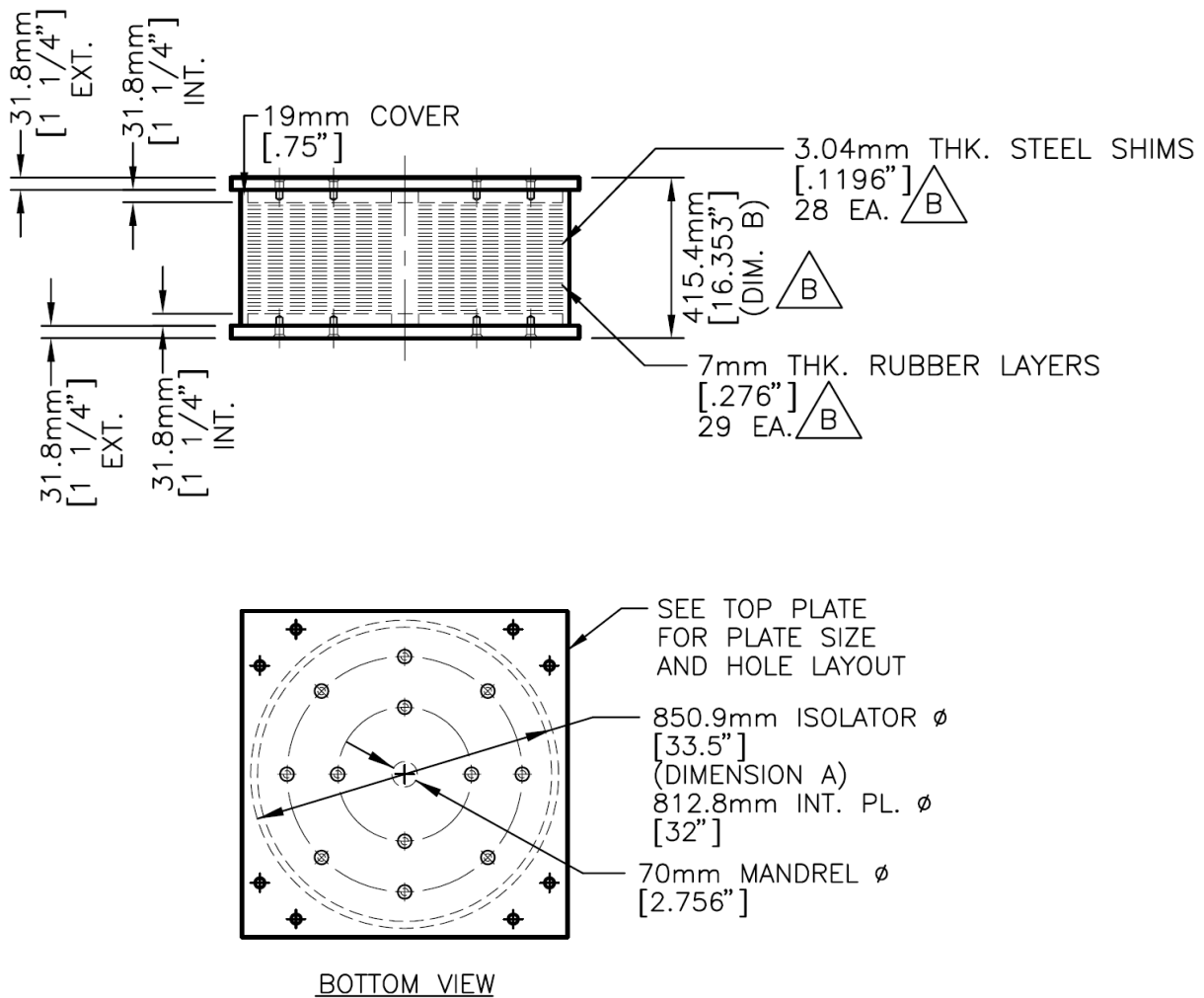
Figure 6-6 Tested Low-Damping Natural Rubber Isolator Details

The identical isolators were tested at an average axial compression load of 1779 kN (400 kip) with a sinusoidal displacement of 483mm (19.0 in) amplitude and peak shear strain of 238 %. The tests were conducted dynamically at high speed with a peak velocity of 1012 mm/s (39.8 in/s). This corresponds to a frequency of 0.33Hz or period of oscillation of 3.0 seconds. Figures 6-7 and 6-8 present the recorded lateral force-displacement loops for Isolator No. 3 and Isolator No. 4, respectively.
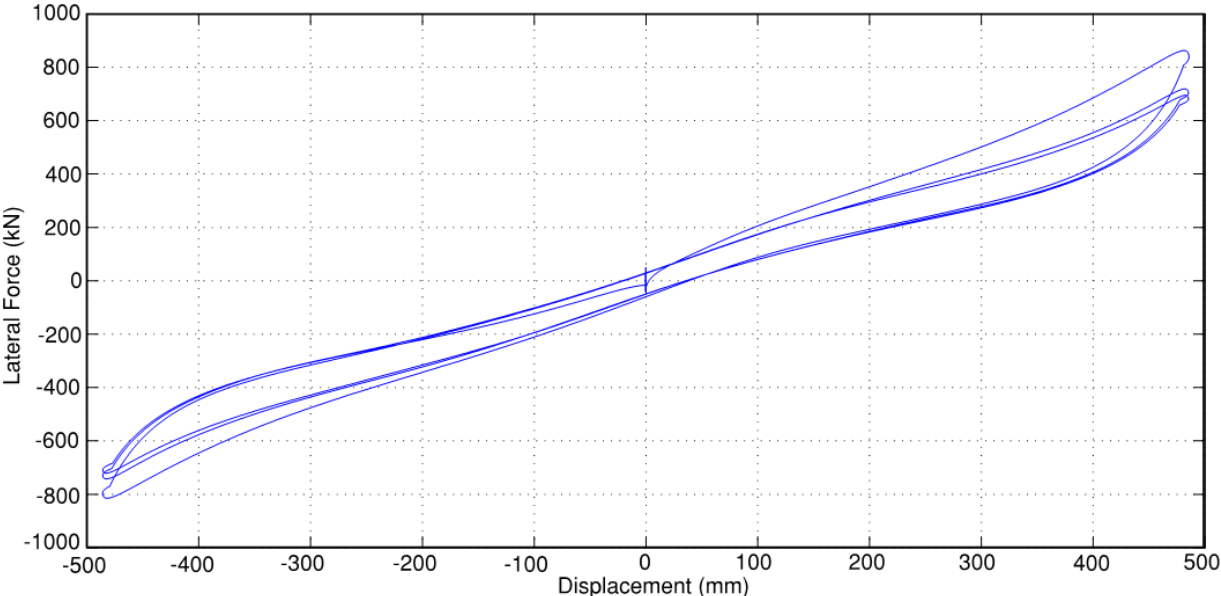
Figure 6-7 Lateral Force-Displacement Loops of Isolator No. 3
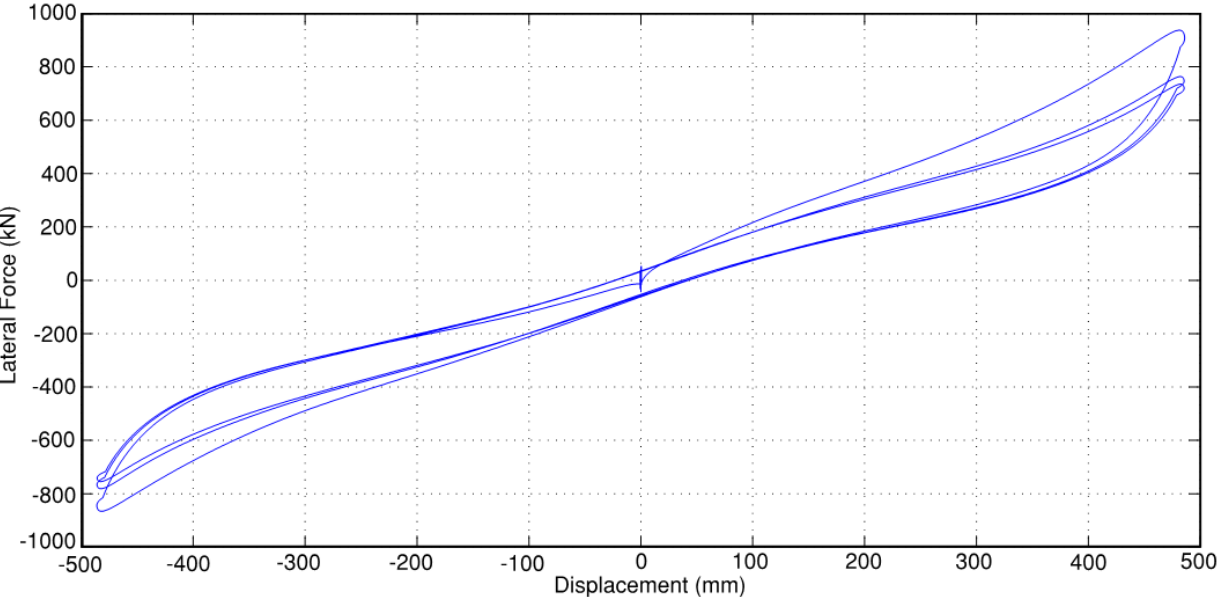
Figure 6-8 Lateral Force-Displacement Loops of Isolator No. 4

An initial comparison of the tested isolators to the preliminary design requirements shows a peak test displacement of 483mm compared to 350mm, a test peak velocity of 1012mm/s compared to 1050mm/s, and a test compression load of 1779kN compared to 1860kN. Therefore the tested isolators may be judged as not meeting the similarity requirements based on the observation that the actual load is higher than the test load and size the preliminary design size of the isolator is smaller. This is checked in Section 6.4.

Figures 6-7 and 6-8 both show the first cycle having a higher stiffness than the second and third cycles. This is due to scragging of the virgin rubber. The post-elastic stiffness for each loop is calculated graphically as illustrated in Figures 6-9 and 6-10. Note that the calculation of the scragging factor is based on the post-elastic stiffness as that is the quantity used in the analysis. In this case, however, the use of the effective stiffness (which is easier to obtain) would provide a very close result to the calculated value of the scragging factor due to the low-damping in the isolator.
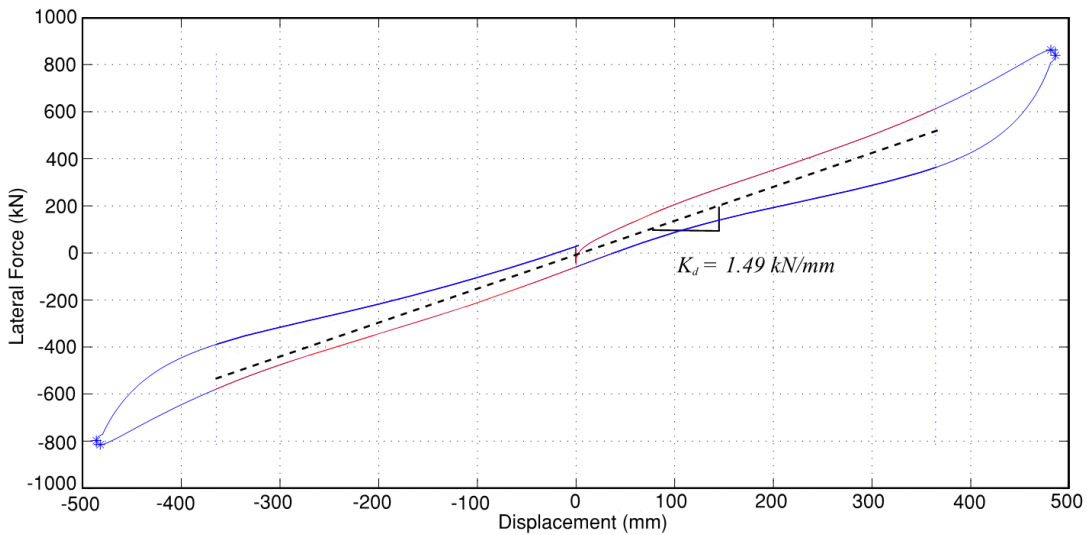
Figure 6-9 Graphical Calculation of the Post-Elastic Stiffness, Loop 1 Isolator No. 3
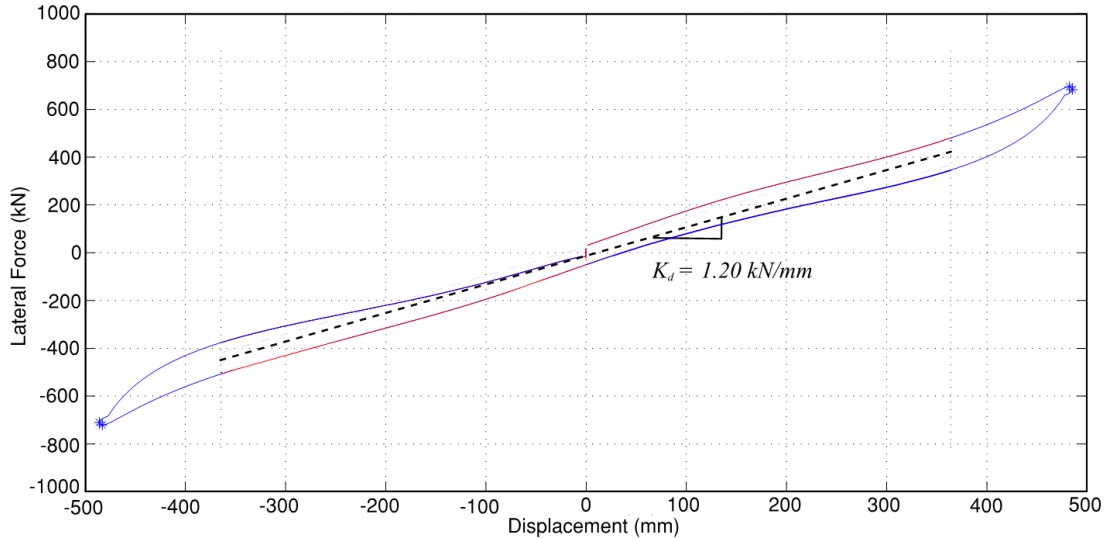
Figure 6-10 Graphical Calculation of the Post-Elastic Stiffness, Loop 3 Isolator No. 3

The slope is calculated by carefully drawing a line that best fits the slope to the loading branches (in the positive and negative displacement directions) over a strain from around +180% shear strain to -180% shear strain. From the illustrations in Figures 6-9 and 6-10, the scragging factor for Isolator No. 3 is as follows:

$$Scragging\ Factor = \frac{K_{d\ loop\ 1}}{K_{d\ loop\ 3}} = \frac{1.49}{1.20} = 1.24 \tag{6 - 2}$$

However, the scragging factor as calculated above is not directly used per ASCE 7-2016 procedures. Rather, the scragging effects are included in the property modification factor $\lambda_{test,max}$ defined as the ratio of the property in the first cycle to the average 3-cycle value of the property in a test under dynamic conditions so that heating and rate of loading effects are also accounted for. The value is calculated herein to provide the reader a better insight into the behavior of the isolators. This would allow the RDP to make decisions on the adjustments of factors for uncertainties.

The same process is carried out for Isolator No. 4 with the same scragging factor calculated. This low scragging factor corroborates the selection of a low aging lambda factor, since both effects are thought to be related to chemical processes occurring in the rubber. The mechanical properties for the two prototype isolators are summarized in Table 6-2.

70

Table 6-2 Mechanical Properties of Two Prototype Low-Damping Rubber Isolators

Cycle	Post-Elastic Stiffness, K_d kN/mm	Effective Stiffness, K_{eff} kN/mm	Shear Modulus of Rubber, G MPa	Energy Dissipated per Cycle, E_{loop} kN-mm	Effective Damping, β_{eff} %
Isolator No. 3					
1	1.49	1.73	0.56	150312	5.9
2	1.22	1.50	0.46	109348	4.9
3	1.20	1.46	0.45	98549	4.6
Average	1.30	1.56	0.49	119403	5.1
Isolator No. 4					
1	1.48	1.85	0.56	173705	6.3
2	1.20	1.59	0.45	122993	5.2
3	1.19	1.53	0.45	112508	4.9
Average	1.29	1.66	0.49	136402	5.5
Average of two isolators	**1.30** (7.4 kip/in)	**1.61** (9.2 kip/in)	**0.49** (71 psi)	**127903** (1132 kip-in)	**5.3**

The nominal shear modulus of rubber is calculated from the average post-elastic stiffness over the three cycles of motion. The $\lambda_{test,max}$ is not equal to the scragging factor of 1.24, since the scragging factor is the ratio of the first cycle to the third cycle post-elastic stiffness. The value of $\lambda_{test,max}$ is the ratio of the first cycle to the nominal post-elastic stiffness, giving a value of 0.56/0.49 = 1.15. The $\lambda_{test,min}$ value calculated as 0.455/0.49 = 0.93 based on two cycles, as determined in Section 3.3.1.

In summary, the nominal value for the shear modulus and associated lambda factors to account for scragging effects are:

- Nominal shear modulus of rubber, **$G_{nominal}$ = 0.49 MPa (71 psi)**
- Maximum testing lambda factor, **$\lambda_{test,max}$ = 1.15**
- Minimum testing lambda factor, **$\lambda_{test,min}$ = 0.93**

These values of properties apply for the particular rubber compound used in the tested isolators. They do not apply for the rubber used in the lead-rubber isolators discussed earlier. The proper procedure is to request additional data from the supplier of the isolators. As discussed in Section 3.3.2, coupon test data should be viewed with great caution.

An option available to the RDP is to use the data obtained from the testing of the natural rubber (NR) isolators, even when the material is not exactly the same, on the assumption that the behavior cannot be very different between the tested material of G=0.49MPa and the material in the lead-rubber isolators of G=0.40MPa. However, some adjustment of properties will be needed. It is appropriate to utilize generic results like those in Thompson et al (2000) (see Section 3.3.2) on the rubber scragging factor which demonstrate a general increase in the scragging factor with reduction of the shear modulus.

It is important to recognize that the nominal value of the shear modulus calculated for the lead-rubber (LR) isolators is the average over the last two cycles and does not include the first cycle which would have scragging effects, and hence result in an increase in the 3-cycle nominal value. Therefore $\lambda_{test,max}$ should be increased accordingly. For the LR isolator, the average rubber shear modulus G for the two isolators is 0.42MPa for the 2nd cycle and 0.385MPa for the 3rd cycle (i.e. the nominal value was based on 2 cycles, calculated as 0.40MPa). If the scragging factor was the same for the NR and LR isolators (i.e. 1.24), then back-calculating will give a 3-cycle nominal value of the LR isolator of $(1.24 \times 0.385 + 0.42 + 0.385)/3 = 0.43MPa$, with $\lambda_{test,max} = 1.15$ as above. However since the nominal value for the LR isolators is stated as G=0.40MPa, then $\lambda_{test,max}$ would have to be increased to $(0.43/0.40) \times 1.15 = 1.24$ to give the same upper bound value. But the rubber for the LR and NR isolators is not the same, therefore some further adjustment is needed. Based on Thompson et al (2000) the lambda factors are adjusted as follows given that for the lead-rubber isolators the shear modulus is slightly less than the NR isolators. That is, for the lead-rubber isolators:

- $\lambda_{test,max} = 1.3$ and $\lambda_{test,min} = 1.0$

Both the isolators are of low-damping type since the effective damping is about 5%. The modeling of these types of isolators is discussed in Section 2.2.

6.4 Similar Unit Criteria

There are two parts to the similarity criteria in ASCE 7-2016 Section 17.8.2.7:

1. Items 1 to 6 need to be met in order to avoid conducting project-specific prototype testing. In this case, production testing may be used to corroborate nominal properties and bounding values used in analysis. The prior prototype testing may have been conducted quasi-statically (slow-speed) or dynamically at high-speed.

2. Only Items 2, 4, 7 and 8 need to be satisfied when the prior prototype testing, which is conducted dynamically, is used to establish $\lambda_{test,max}$ and $\lambda_{test,min}$ factors. This gives greater flexibility on the

size of the previously tested bearings, however the RDP must use "principles of scaling and similarity" to interpret the test data.

Differences between the prototype test data and the parameters obtained in preliminary design (as per Table 5-1 and 5-2) result in further uncertainties which must be taken into account. This is dealt with by using further adjustment factors when computing the final $\lambda_{test,max}$ and $\lambda_{test,min}$.

In order to avoid project-specific prototype testing and to be able to use past prototype test data as a basis for developing nominal properties and lambda factors, the new project's isolators must be of the same type and material and manufactured by the same manufacturer using the same processes and quality as the past prototype isolator. Furthermore, the following criteria must be satisfied according to ASCE 7-2016 §17.8.2.7 Testing Similar Units:

1. The isolator design is not more than 15% larger nor more than 30% smaller than the previously tested prototype, in terms of governing device dimensions; and

The governing isolator dimensions are outlined in Table 6-4. The prototype isolators are within the specified limits for all governing dimensions.

Table 6-3 Comparison of Governing Dimensions

Parameter	Tested Prototype Isolator	Preliminary Design Isolator Table 5-1	Difference to Design
Lead-rubber Isolators			
Diameter of rubber (mm)	851	800	-6%
Total rubber thickness (mm)	203	203	0%
Lead core diameter (mm)	220	220	0%
Low-damping Natural Rubber Isolators			
Diameter of rubber (mm)	851	750	-13%
Total rubber thickness (mm)	203	203	0%

2. Is of the same type and materials; and

It is assumed that the same type and materials as the prototype isolators will be used for the actual isolators. While not stated in ASCE 7-2016, it is presumed that the RDP may accept small variations in materials with assumptions for a larger tolerance on the λ_{spec} factors.

The energy dissipated per cycle in the "Preliminary Design" column of Table 6-5 is calculated using the tested isolator's displacement, 483mm (19in), and the nominal yield stress of lead. It is noted that the calculated displacement from preliminary design is 350mm (13.7 in) at the center of mass.

The average energy dissipated over three cycles of motion for the prototype isolator is 93762 kN-mm (829.5 kip-in), which is only 6 % larger than the preliminary design nominal value. This is not surprising since the effective yield stress of lead used in the preliminary design is based on the prototype isolator test data, and the lead core diameters were identical. Evidently, the similarity criteria on E_{loop} are satisfied.

Table 6-4 Comparison of Energy Dissipated per Cycle (kN-mm)

Cycle	Tested Prototype Isolators			Preliminary Design Isolator Table 5-1	Ratio of Design/Test Values
	Isolator 1	Isolator 2	Average		
1	1120677	1109697	1115187	825466[1]	0.74
2	768538	761081	764810	825466	1.08
3	610929	606266	608598	825466	1.36
Average of 3	**833381**	**825681**	**829531**	**825466**	**1.06**

1. Based on nominal yield stress of lead, 11.6 MPa (1,681 psi), same displacement as tested isolator-483mm (19 in), and 15 mm (0.6 in) yield displacement.

It is assumed that identical processes will be followed to that used in the production of the prototype isolator. This is an issue of particular concern as it is known that some manufacturers utilize different processes and even different manufacturing facilities for the production isolators. In general, any deviation should be rejected.

5. For elastomeric type isolators, the design shall not be subject to a greater shear strain nor greater vertical stress than that of the previously tested prototype.

Based on the preliminary design displacement of 350mm (13.7in), the design shear strain is less than that achieved in testing for both the lead-rubber and the natural rubber isolator (see Table 6-6).

The vertical stress, however, is less for the tested natural rubber isolator than the actual isolator. Table 6-6 presents the vertical stress for the tested and actual isolators, where for the latter it is based on load combination 1 of Section 17.2.7.1- the average vertical load D + 0.5L. Other vertical load combinations are not considered, for reasons discussed in Section 4.3.

For the lead-rubber isolators, the tested compression stress is about 88% less than the preliminary design compression stress, therefore acceptable. Adjustments for uncertainties are incorporated as discussed in Section 6.2.2.

The tested low-damping natural rubber (NR) isolators have a compression stress 23% less than that in design, hence the design NR isolators (as per Table 5-1) are subjected to a greater (average) compression stress and do not meet the similarity requirements of ASCE 7-2016. Nevertheless, the compression stress has small effect on the stiffness and damping of low damping natural rubber bearings (Constantinou et al, 2007) and the RDP may choose to use the data together with an adjustment factor in order to progress with analysis, which can later be verified by prototype (or production) testing. Herein an adjustment of ±5% to the upper and lower bounds of the NR isolator's rubber shear modulus is used. The term "similar" isolators is still used for illustration purposes for the NR isolators, however it is noted that the similarity requirements of ASCE 7-2016 are not met in every respect and prototype testing, or other similar units, are required.

Adjustment factors to natural rubber isolator's G (or K_d) based on uncertainty due to higher vertical stress are:

- **Maximum adjustment = 1.05 and Minimum adjustment = 0.95**

Table 6-5 Comparison of Shear Strain and Compression Stress

Parameter	Tested Prototype Isolator	Preliminary Design Isolator (Table 5-2)	Difference to Preliminary Design
Lead-Rubber Isolators			
Rubber shear strain	238%	172%[1]	-38%
Compression stress (MPa)[3]	7.7	4.1[2]	-88%
Low-Damping Natural Rubber Isolators			
Rubber shear strain	238%	172%[1]	-38%
Compression stress (MPa)	3.5	4.5[2]	23%

1. Based on preliminary design value of displacement D_M for lower bound properties

2. Based on a vertical load of D + 0.5L and average of all NR or LR isolator locations.

3. Calculated as the vertical load divided by the bonded rubber area (the rubber cover and lead core area were excluded).

6.5　Test Specimen Adequacy Criteria

The discussion that follows relates to the adequacy criteria for the prototype isolators. It does not directly relate to the work in this report as a complete set of prototype test results per Section 17.8.2 of ASCE 7-2016 does not exist. Rather, this report presents procedures of how to obtain the data on bounding values of mechanical properties for use in analysis and design. Nevertheless, this section of the report attempts to provide some commentary on the ASCE 7-2016 adequacy criteria based on the limited available results used in obtaining the nominal and lambda values.

Section 17.8.4 of ASCE 7-2016 lists the test specimen adequacy criteria for the prototype isolators. It is not clear whether the requirements are specific for quasi-static or dynamic testing. Since the requirements may influence the bounds of the lambda factors, particularly the lambda-test factor, the testing is assumed to be dynamic. Furthermore the requirements are checked for the lambda factors of individual prototype isolators of each type, and not a composite for the overall isolation system. The parameters K_d and E_{loop} (referenced in the checks) are a function of the size of the isolator, that is- the bonded rubber area of the isolator and the area of lead (and travel), respectively, whereas the rubber shear modulus G and effective yield stress of lead σ_L are material parameters and allow direct comparison. The requirements are checked in the following:

> The performance of the test specimens shall be deemed adequate if all of the following conditions are satisfied:
> 1.　The force-deflection plots for all tests specified in Section 17.8.2 have a positive incremental force-resisting capacity.

The isolators have positive incremental force-resisting capacity.

> 2. The average post-yield stiffness, k_d, and energy dissipated per cycle, E_{loop} , for the three cycles of test specified in Section 17.8.2.2, item 3 for the vertical load equal to the average dead load plus one-half the effects due to live load, including the effects of heating and rate of loading in accordance with Section 17.2.8.3, shall fall within the range of the nominal design values defined by the permissible individual isolator range which are typically +/-5% greater than the $\lambda_{(spec, min)}$ and $\lambda_{(spec, max)}$ range for the average of all isolators.

The item 3 test is the characterization test used to determined nominal properties as discussed in Section 4.3. It consists of 3 cycles at the maximum displacement D_M.

For the lead-rubber isolators:

$G_{nominal}$=0.40MPa, $\lambda_{spec,min}$=0.85 and $\lambda_{spec, max}$=1.15 giving a required range of 0.34 to 0.46MPa (or 0.32 to 0.48MPa when adding the +/-5% allowance). The average from prototype isolator 1 and 2 is 0.39MPa and 0.42MPa, respectively (although ignoring the first cycle for reasons described in this report), therefore meeting the ASCE 7-2016 criteria.

$\sigma_{L,nominal}$=11.6MPa, $\lambda_{spec,min}$=0.85 and $\lambda_{spec, max}$=1.15 giving a required range of 9.9 to 13.3MPa (or 9.4 to 14MPa when adding the +/-5% allowance). The average from prototype isolator 1 and 2 is 11.6MPa and 11.7MPa, respectively, therefore meeting the ASCE 7-2016 criteria.

For the natural rubber isolators:

$G_{nominal}$=0.49MPa, $\lambda_{spec,min}$=0.85 and $\lambda_{spec, max}$=1.15 giving a required range of 0.42 to 0.56MPa (or 0.48 to 0.59MPa when adding the +/-5% allowance). The average from prototype isolator 3 and 4 is 0.49MPa and 0.49MPa, respectively, therefore meeting the ASCE criteria.

The prototype isolators meet the ASCE 7-2016 acceptance criteria of Section 17.8.4, item 2. Furthermore there is no major variation in behavior between the individual isolators.

3. For each increment of test displacement specified in item 2 and item 3 of Section 17.8.2.2 and for each vertical load case specified in Section 17.8.2.2,

a. For each test specimen the value of the post-yield stiffness, k_d, at each of the cycles of test at a common displacement shall fall within the range defined by $\lambda_{(test, min)}$ and $\lambda_{(test, max)}$ multiplied by the nominal value of post-yield stiffness.

The variation in vertical load is not considered in these checks, for reasons described in Section 4.3, where it is declared the isolators meet the exception of the Standard. This exception permits the computation of nominal properties using only load combination 1 (if the conditions of the exception are meet), and therefore the lambda-test values should not be arbitrarily influenced by this acceptance criteria.

Of these tests, it is the 3-cycle dynamic test at the maximum displacement D_M which is assumed to give the greatest heating effects and variation of properties from the nominal value (compared to the other smaller displacement tests in item 2).

For the lead-rubber isolators:

$G_{nominal}$=0.40MPa, $\lambda_{test,min}$=1.0 and $\lambda_{test, max}$=1.3 giving a required range of 0.40 to 0.52MPa

For the natural rubber isolators:

$G_{nominal}$=0.49MPa, $\lambda_{test,min}$=0.93 and $\lambda_{test, max}$=1.15 giving a required range of 0.46 to 0.56MPa.

Table 6-6 presents data on the tested and the required values of the shear modulus, where the cases that do not meet the ASCE 7-2016 acceptance criteria are highlighted in bold red. Since the stiffness of rubber stabilizes after the first cycle (rubber is scragged), along with the stiffness of rubber not being significantly affected by heating, the result may be accepted, even though there is minor noncompliance.

Table 6-6 Tested Prototype Elastomeric Isolator Shear Moduli Criteria.

Type	Lead Rubber		Natural Rubber	
Isolator Number	**1**	**2**	**3**	**4**
Cycle	**G (MPa)**	**G (MPa)**	**G (MPa)**	**G (MPa)**
1	Discarded	Discarded	0.56 (0.46-0.56)	0.56 (0.46-0.56)
2	0.41 (0.40-0.52)	0.43 (0.40-0.52)	0.46 (0.46-0.56)	**0.45** (0.46-0.56)
3	**0.37** (0.40-0.52)	0.40 (0.40-0.52)	**0.45** (0.46-0.56)	**0.45** (0.46-0.56)

Notes: 1) Values in parenthesis is the range required by ASCE 7-2016, Section 17.8.4, Item 3a).

2) Tested values in bold red color do not meet ASCE 7-2016 requirement.

b.   For each cycle of test, the difference between post-yield stiffness, k_d, of the two test specimens of a common type and size of the isolator unit and the average effective stiffness is no greater than 15 percent.

The two isolators of each type have nearly identical properties so that this criterion is met.

4.   For each specimen there is no greater than a 20 percent change in the initial effective stiffness over the cycles of test specified in item 4 of Section 17.8.2.2.

There is a significant difference between quasi-static and dynamic testing acceptance requirements. Since the testing is dynamic, the relevant test is that of ASCE 7-2016 Section 17.8.2.2, item 4b for which testing for five continuous cycles at amplitude of $0.75D_M$ is required. There is not test data available for five continuous cycles at $0.75D_M$, however comparison can be made based on the available test data for three cycles at the amplitude of D_M. If the isolator is scragged then there will be little change in the effective stiffness of the natural rubber isolators. For dynamic testing of the lead-rubber isolators at three cycles of amplitude D_M (item 3 test), the heating effects will be less than in five cycles at a displacement of $0.75D_M$. This is because the latter test has greater travel and therefore greater heating effects (Kalpakidis et al, 2008). The two tested isolators in the 3-cycle test have a near identical behavior with an effective stiffness in the 1st, 2nd and 3rd cycles of about 2.5, 1.9 and 1.7 kN/mm, respectively (see Figures 6-2 and 6-3). The change in initial effective stiffness is (2.5-1.7)/2.5 = 32% in this case, and expected to be more

with the larger travel in a test with 5-cycles at $0.75D_M$ due to more heating effects, although some mitigation is expected due to scragging effects that diminish with increasing number of cycles. Nevertheless, it is unlikely that the lead-rubber isolators utilized in the examples of this report would have met the criterion of item 4b of ASCE 7-2016 Section 17.8.2.2. The related criterion 4a for the case of quasi-static testing would also be unlikely to be satisfied as the test requires at least 10 **continuous** cycles for which the heating effects will be significant even when motion is slow.

The main reason for this problem is the large number of cycles specified in the prototype testing. As mentioned earlier in this report, the number of cycles should be related to the proximity to the fault, soil conditions and properties of the isolation system. Another reason is the specification of adequacy criteria that are not related to the upper and lower bound properties utilized in the analysis. Evidently, the testing adequacy criteria require modification. The implications of maintaining the current adequacy criteria is to force the RDP to utilize lead-rubber isolators with smaller lead-core diameter and effectively less characteristic strength (so that heating effects are less) and unnecessarily impede the application of these isolators in near-fault cases where displacement demands are large and the use of high characteristic strength isolators would be beneficial.

5. For each test specimen the value of the post-yield stiffness, k_d, and energy dissipated per cycle, E_{loop}, for any cycle of each set of five cycles of test 17.8.2.2.4 shall fall within the range of the nominal design values defined by $\lambda_{(test,\,min)}$ and $\lambda_{(test,\,max)}$.

Similar to the comments above, it is not clear whether this testing is dynamic, however reference to the lambda-test factors would indicate dynamic testing. Test data for five cycles of testing at amplitude of $0.75D_M$ is not available. However, the arguments made in item 4 above related to the number of cycles required in the prototype testing are still valid. The $\lambda_{(test,\,min)}$ and $\lambda_{(test,\,max)}$ values were obtained using data over three cycles of testing. Therefore, it is unnecessarily conservative to require that the measured properties over five cycles be within the bounds established using three cycles. It is also wrong if the expected number of cycles is smaller than 5 (or even 3) as discussed earlier in this report.

To illustrate the point consider the energy dissipated per cycle (EDC) for the prototype lead-rubber isolator No. 1 (Figure 6-2 and Table 6-1 of Section 6.2.1 of this report). However, instead of reporting EDC, it is more convenient to report the value of the effective yield stress of lead which has a direct relation to the EDC for constant amplitude of motion. Note that the range set by the nominal value and lambda-test factors for the prototype isolators was determined to be $\sigma_{L,nominal}=11.6\text{MPa}$, $\lambda_{test,min}=0.93$ and $\lambda_{test,\,max}=1.35$. Therefore, the range of values of σ_L is 10.8 to 15.7MPa. On the basis of adequacy criterion

item 5 of Section 17.8.4 of ASCE 7-2016, the values of σ_L over five cycles of dynamic testing at amplitude of $0.75D_M$ shall be within this range.

Table 6-7 presents values of the effective yield stress of lead and the effective damping for the tested prototype isolator No.1 (see Section 6.2.1). The calculated values at amplitude of $0.75D_M$ are based on the theory of Kalpakidis et al (2010) and following the calculations in Section 6.2.2 using the identified value of σ_{L0}=20.5MPa. The calculation is slightly conservative as it neglects heat conduction. The calculated temperature rise in the lead at the middle of the fifth cycle is 168^0C. Clearly, the effective yield stress values (equivalently EDC) over the five cycles are outside the acceptable range of 10.8 to 15.7MPa dictated by the adequacy criteria. The discrepancy is so large to require re-visiting the adequacy criteria.

Table 6-7 Tested Prototype Lead-rubber Isolator No. 1 Properties

Cycle	Measured at Amplitude D_M=483mm		Calculated at Amplitude $0.75D_M$=362mm		
	σ_L (MPa)	β_{eff}	σ_L (MPa)	G (MPa)	β_{eff}
1	15.7	0.30	16.5	0.52^1	0.35
2	10.8	0.27	11.9	0.41^2	0.34
3	8.6	0.24	9.3	0.37^2	0.31
4	NA	NA	7.6	0.37^3	0.28
5	NA	NA	6.5	0.37^3	0.26

1. Estimated test value; 2. Test value; 3. Assumed value

6.   For each specimen there is no greater than a 20 percent decrease in the initial effective damping over the cycles of test specified in item 4 of Section 17.8.2.2.

Similar to item 5 above, Table 6-8 lists the effective damping for each cycle of the tested lead-rubber isolator No. 1 and presents estimates of the effective damping of the same isolator if it were tested at amplitude of $0.75D_M$ for five cycles. The effective damping for the case of the 5-cycle motion was calculated as:

$$\beta_{eff} = \frac{EDC}{2\pi K_{eff} D^2} = \frac{4Q_d(D-Y)}{2\pi(K_d D^2 + Q_d D)}$$

(6 - 3)

in which Y is the yield displacement (=15mm) and Q_d and K_d are given by equations (2-1) and (2-3), respectively, where f_L=1, A_L=38013mm^2, A_r 505528mm^2 and T_r=203mm. Furthermore, the values of σ_L and G in Table 6-7 were used. Note that the value of σ_L was calculated on the basis of theory starting with an experimentally identified value at the start of the motion. The values of G are based on the identified nominal value G=0.4MPa and $\lambda_{(test,\ max)}$=1.3 to obtain the first cycle value of 0.4x1.3=0.52MPa,

whereas the other values were obtained from Table 6.1 for cycles 2 and 3 (experimental values). Finally the value of G for cycles 4 and 5 was assumed to remain constant at the 3rd cycle value of 0.37MPa.

The reduction of the calculated damping ratio from the initial value is 26% which fails the adequacy criteria of ASCE 7-2016. However, when heat conduction through the end and shim plates of the isolator is accounted for, the damping ratio is on the limit of acceptability. It is not difficult to understand that the adequacy criterion could not be met when the test is conducted at 10 or more cycles under quasi-static conditions. Again, the issue of the number of cycles and of the adequacy criteria being based on data from 3-cycle testing needs to be re-visited.

7.   All specimens of vertical-load-carrying elements of the isolation system remain stable where tested in accordance with Section 17.8.2.5.

All isolators in the design are vertical-load carrying elements. The force-displacement loops from item 3 testing do not show instability.

It is evident in the discussion of the ASCE 7-2016 adequacy criteria and the comparison to the properties of the prototype lead-rubber isolators that the ASCE 7-2016 adequacy criteria have two deficiencies:

1) The number of cycles required in some of the prototype tests appears as arbitrary whereas it should be related to the properties of the isolation system, and type of earthquake excitation as distinguished by proximity to fault and soil properties. The number of cycles, whether sets of 5 or at least 10 depending whether the testing is dynamic or quasi-static, is generally much larger than would be expected during an MCE_R event.

2) The adequacy criteria appear as inconsistent and unrelated to the data utilized in extracting the nominal values of properties and the λ_{test} values. For example, the nominal and λ_{test} values are based on testing for 3 cycles at one amplitude of motion (D_M), whereas the adequacy criteria are based on testing for 5 or more cycles at different amplitude ($0.75D_M$) of motion.

Appendix D presents suggested simple changes and clarifications in Chapter 17 of the ASCE 7-2016 revision that will eliminate these problems.

SECTION 7

COMPUTING PROPERTIES FOR SLIDING ISOLATORS

7.1 Introduction

These section gives examples of how to calculate nominal properties and the associated testing lambda factors $\lambda_{test,max}$ and $\lambda_{test,min}$ for sliding isolators. Dynamic test data from two testing regimes is presented for two triple Friction Pendulum[TM] isolators (i.e. Case B: Prototype or Similar Unit test data available of Section 5.4). The coefficient of friction for the inner and outer surfaces is calculated for use in the tri-linear analysis model discussed in Section 2.3, Figure 2-4. The coefficient of friction is a material parameter which is used to calculate and the characteristic strength Q_d.

In this report the axial compression load used to calculate the nominal properties and associated lambda-test values only considers the average vertical load (§17.2.7.1 load combination 1), for reasons discussed in Section 4.3

7.2 Prototype Isolators

For a triple friction pendulum (FP) isolator the stiffness in different regimes is characterized by the isolator's axial load and the geometric parameters described in Figure 2-3. It is assumed herein that we have a reputable manufacturer and that these geometric parameters are known with confidence, hence the post-elastic stiffness K_d lambda factors are set to unity and the stiffnesses are determined based on theory.

The only parameter to determine is the friction coefficient(s). The friction is used to define the isolator lateral strength (along with the axial load) as well as the displacements at which there is a change in force-displacement behavior (along with the effective radii). It can be a complicated task to determine the friction coefficients since there are multiple surfaces with different values of friction. Furthermore the friction coefficient depends on the isolator pressure (different for surfaces 1 and 4 versus 2 and 3), condition of the sliding surface, velocity of loading, and is affected by heating produced during motion. This makes it a complex task to obtain friction coefficients from dynamic test data. Even for the *special* triple FP, where there are only two friction values to determine, there is some uncertainty in measuring the friction coefficients. Also, the processing and interpretation of test data are sensitive to engineering judgment.

Some common representations of the force-displacement behavior of a sliding isolator are the rigid-linear, bi-linear or tri-linear models. The latter of these models (see Figure 2-4) gives a more accurate

representation of the special triple FP behavior. The focus of this section is the determination of properties for the tri-linear model, however there is also discussion on the use of other models.

Data on two triple FP isolators, which were tested on a past project at high speed, will be used to determine the nominal properties and the testing lambda factors for analysis. The isolators are declared similar to the isolators required for the SEAOC example building of this report as they meet the similarity criteria of ASCE 7-2016 (See Section 7.3). The geometry of the isolators is given in Figure 7-1. It is noted that if the displacement capacity is too small/large, the dimension d_1 (see Figures 2-3 or 7-1), which is 16 inches in Figure 7-1, can be adjusted as required with no significant effect on the force-displacement behavior (and particularly the friction properties), as it only influences the displacement at which the behavior enters the force-displacement Regime III.
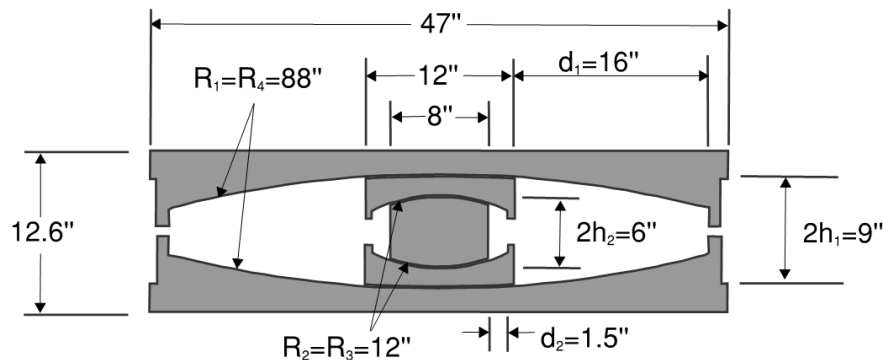
Figure 7-1 Cross-Section and Details of Tested Triple Friction Pendulum Isolator (1in=25.4mm)

The two prototype isolators were subjected to two types of tests with different axial loads and displacements, of which the force-displacement loops are shown in Figures 7-2 to 7-5. The vertical axis in Figures 7-2 to 7-5 is the instantaneous lateral force divided by the instantaneous vertical load, and therefore suitable to obtain the friction coefficient. In the first test, "Test 1" (Figures 7-2 and 7-4), the isolators have an average axial load of 2710 kN (609 kip) and are subjected to a displacement of about 740mm (29 inches) in the first cycle, then around two-thirds of that displacement in the second cycle, and then around one-third displacement in the third cycle. The fourth cycle is at very low amplitude and is not used herein for calculating properties. The frequency of testing is 0.25Hz, leading to the recorded peak velocity values shown in the figures. The preliminary design indicates an MCE maximum displacement (without torsion) D_M of 627mm (24.7 inches) with an average axial load (D + 0.5L) for an interior isolator of 2351 kN (528 kip). Test 1 contains valuable information that can be used for design even though it is not strictly in accordance with ASCE 7-2016 provisions (i.e. three fully reversed cycles at the MCE displacement or the alternative protocol of 17.8.2.2 item 2b). The average displacement for the three

cycles in Test 1 is about equal to 510 mm (20.4 inches), which is less than the preliminary design MCE displacement D_M. However, for similarity requirements it is the velocity which is the important parameter. As discussed in Section 7.3, the intent of the ASCE 7-2016 similarity requirements as well as testing provisions are believed to be meet, since the testing is at high velocity and frictional heating effects are properly captured.

For the second test, termed the quality control "Test 2" (Figures 7-3 and 7-5), the isolator has an average axial load of 1348 kN (303 kip) and is cycled three times at a displacement of 380mm (15inch) which is only 60% of the MCE calculated displacement of 627mm. Therefore, while the vertical load is appropriate for the exterior isolator, the test sliding velocity is less than that required for similar isolators per the definition of ASCE 7-2016. That is, Test 2 does not qualify as a "similar" tested isolator unit. The data from Test 2 are useful, however, to support the selection of the inner surfaces friction coefficient from Test 1. Also, the data from this test, in combination with the data in Test 1, will be used to obtain conservative estimates of the bounds of the friction coefficient for the exterior isolators which have a vertical load (D + 0.5L) of 1267 kN (285kip).

The testing regime used in Test 1 represents a practical scenario which some manufacturers are recommending and something close to this regime is defined in 17.8.2.2 item 2b. The testing regimes specified in ASCE 7-2016 may come across as convoluted, and it is the opinion of the authors that only a few tests (as illustrated in this report) are needed to determine an isolator's force-displacement behavior for analysis (see Section 4.3).

Tables 7-1 and 7-2 present the conditions of testing and the normalized measured energy dissipated per cycle (instantaneous lateral load is divided by instantaneous normal load). Table 7-1 presents results obtained from Test 1 where there was an average axial load of 2710 kN (609 kip) (Figures 7-2 and 7-4 for Isolators 1 and 2, respectively) and Table 7-2 presents results obtained from Test 2 where there was an average axial load of 1348 kN (303 kip) (Figures 7-3 and 7-5 for Isolators 1 and 2, respectively).
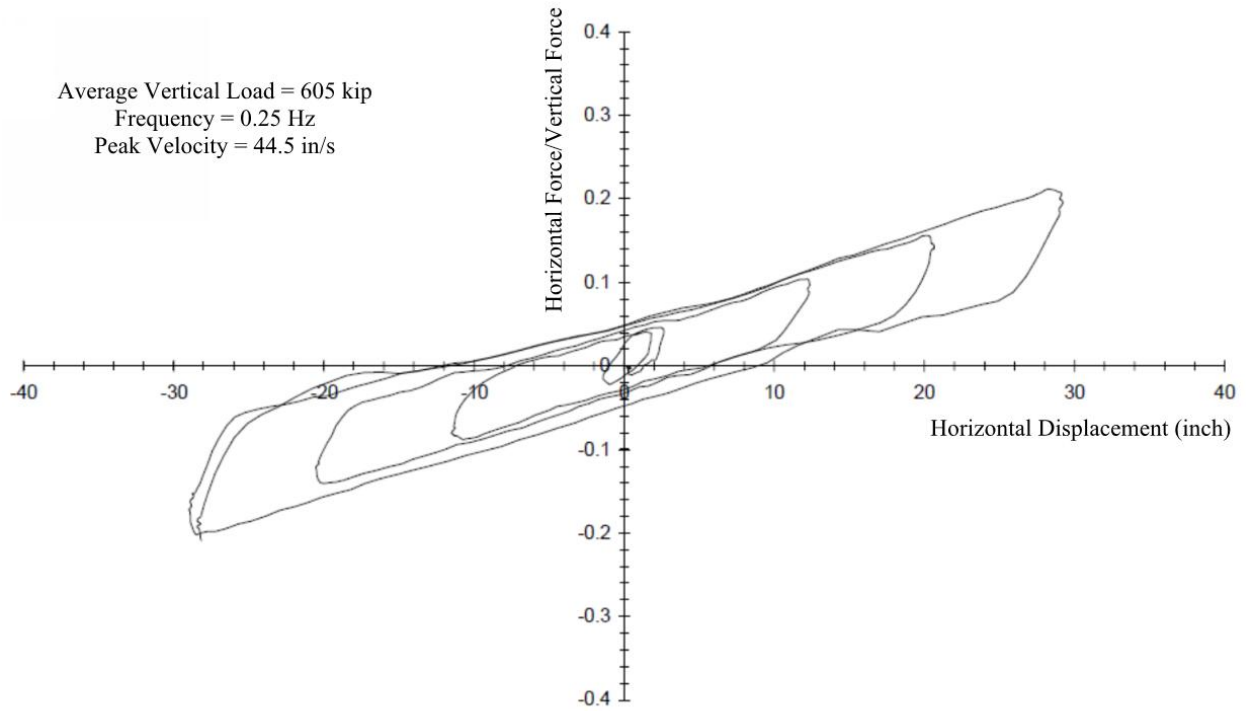
Figure 7-2 Dynamic Force-Displacement Behavior of Prototype Isolator 1: Test 1

(1kip = 4.45kN, 1inch = 25.4mm)
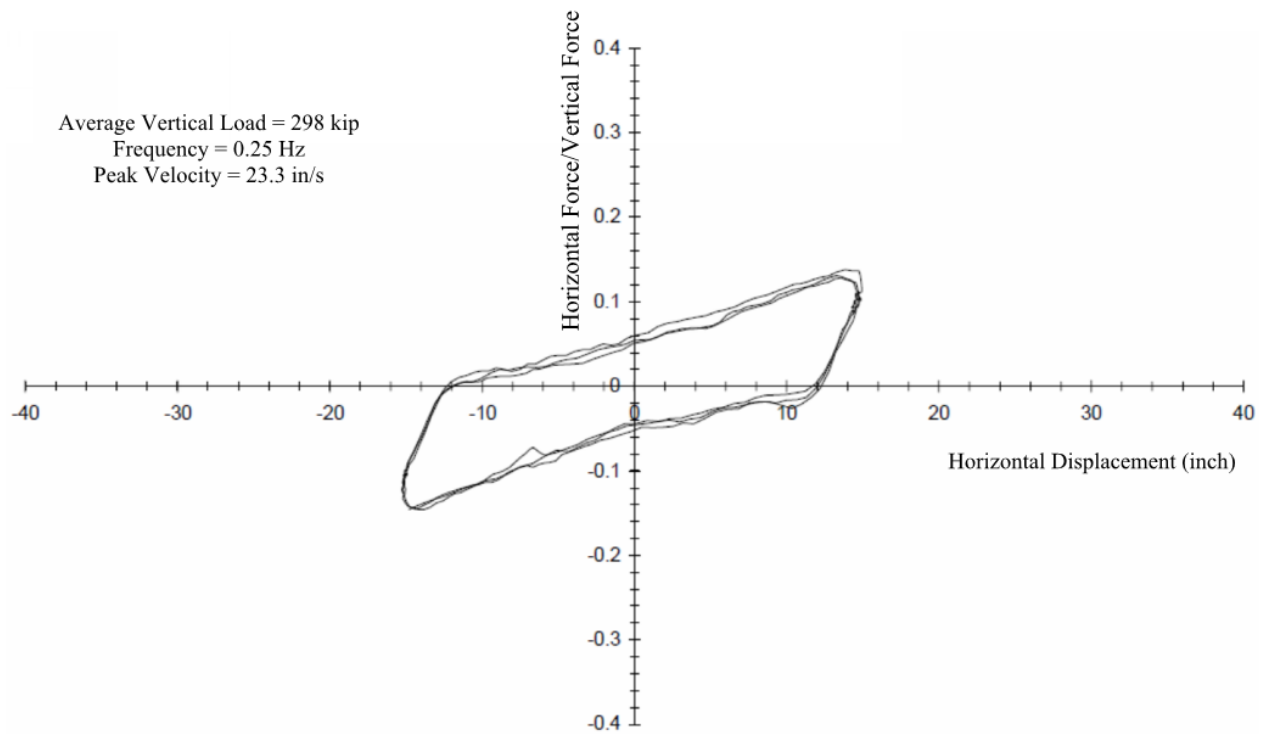
Figure 7-3 Dynamic Force-Displacement Behavior of Prototype Isolator 1: Test 2

86
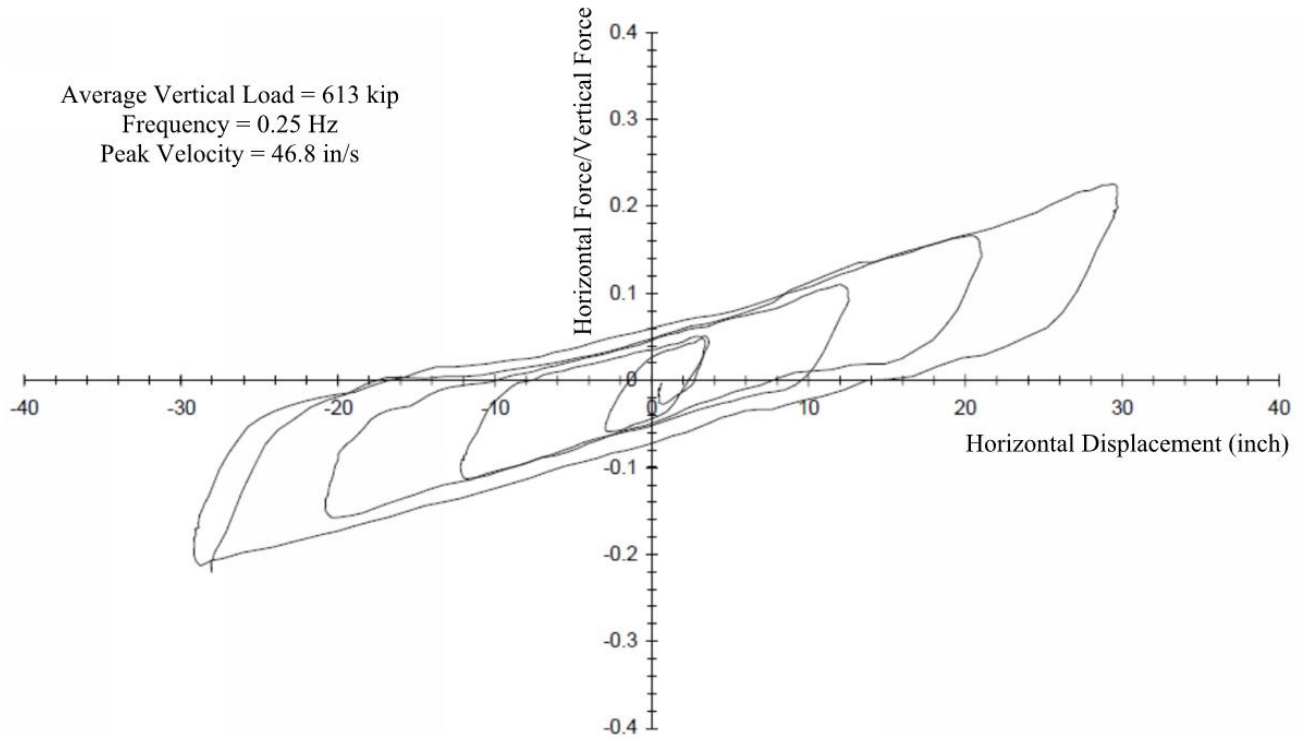
Figure 7-4 Dynamic Force-Displacement Behavior of Prototype Isolator 2: Test 1

(1kip = 4.45kN, 1inch = 25.4mm)
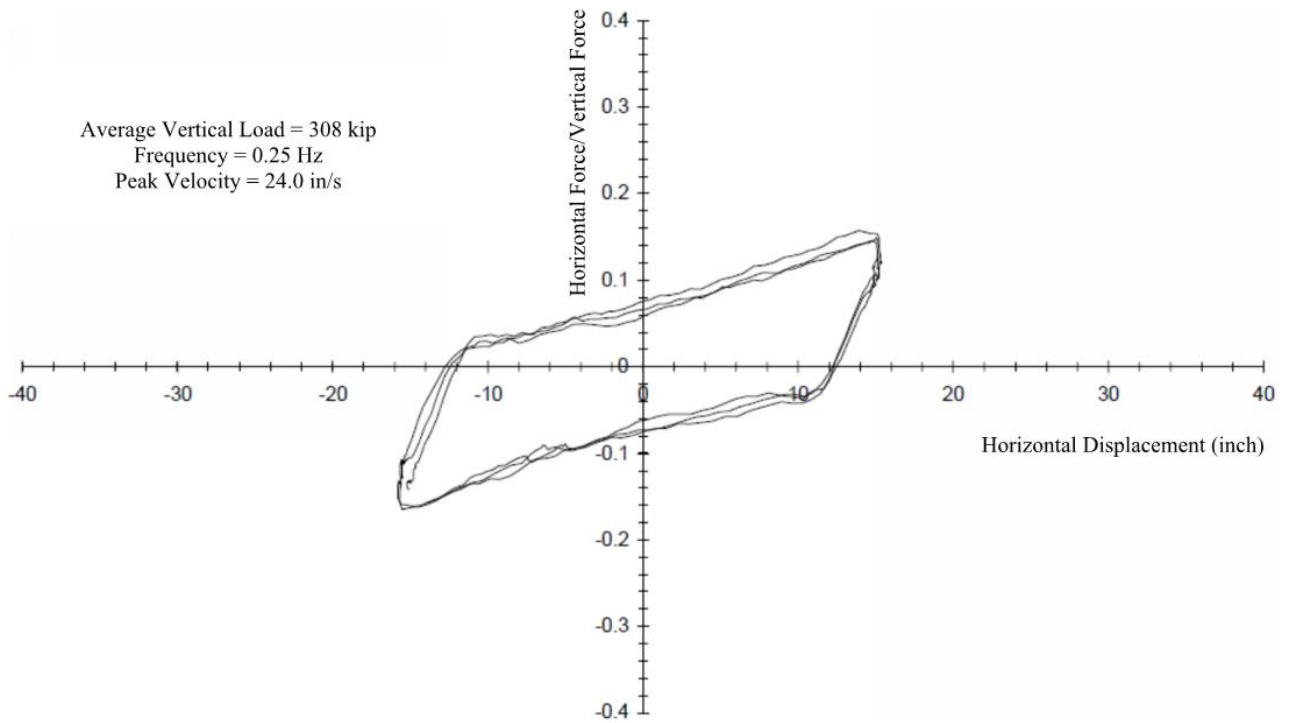
Figure 7-5 Dynamic Force-Displacement Behavior of Prototype Isolator 2: Test 2

87

Table 7-1 Test 1 Data for Prototype Triple FP Isolators

Cycle/Loop	Maximum Displacement, D mm (in)	Peak Velocity mm/s (in/s)	Normalized Energy Dissipated per Cycle, E^*_{loop} kN-mm/kN (kip-in/kip)
Isolator No. 1			
1	737 (29.0)	1130 (44.5)	158.4 (6.24)
2	521 (20.5)	864 (34.0)	82.6 (3.25)
3	300 (11.8)	648 (25.5)	35.7 (1.41)
Average	519 (20.4)	-	92.2 (3.63)
Isolator No. 2			
1	744 (29.3)	1189 (46.8)	200.4 (7.89)
2	518 (20.8)	937 (36.9)	106.1 (4.18)
3	310 (12.2)	577 (22.7)	53.4 (2.10)
Average	524 (20.6)	-	120.0 (4.72)

Table 7-2 Test 2 Data for Prototype Triple FP Isolators

Cycle/Loop	Displacement D mm (in)	Peak Velocity mm/s (in/s)	Normalized Energy Dissipated per Cycle, E^*_{loop} kN-mm/kN (kip-in/kip)
Isolator No. 1			
1			88.8 (3.49)
2	381 (15.0)	592 (23.3)	81.3 (3.20)
3			78.9 (3.10)
Average	-	-	82.9 (3.26)
Isolator No. 2			
1			114.4 (4.50)
2	381 (15.0)	610 (24.0)	103.9 (4.09)
3			103.6 (4.08)
Average	-	-	107.3 (4.22)

The interest is to use the available test data in Figures 7-2 to 7-5 and Tables 7-1 and 7-2 (and information on aging and contamination, and assumptions on data variability) to determine appropriate upper and lower bound friction values for use in the tri-linear representation of the *special* triple FP model. Two friction values are needed for each bound. The process to calculate these friction values is approximate as it is based on a graphical interpretation of the data. Since the testing is dynamic, at high-speed, it is difficult to see the transition points in the force-displacement behavior as illustrated theoretically in Figure 2-4 (which is based on constant values of friction, whereas in reality friction is velocity dependent).

The first step involves estimating a value for the friction on the internal surfaces, μ_2. This can be estimated graphically based on the vertical amplitude upon unloading in the first cycle of Test 1, which is theoretically equal to $2\mu_2$. For Isolator 1 the value of μ_2 was measured as 0.017 from taking the average of both sides of the force-displacement loop in the first cycle as shown in Figure 7-6. The data from Test 2 can be interpreted in the same way to validate the selection of μ_2 from Test 1 as shown in Figure 7-7. It should be noted that quantity μ_2 is of secondary importance and has insignificant effect on the displacement demand. Therefore, great accuracy in establishing this value is not warranted.
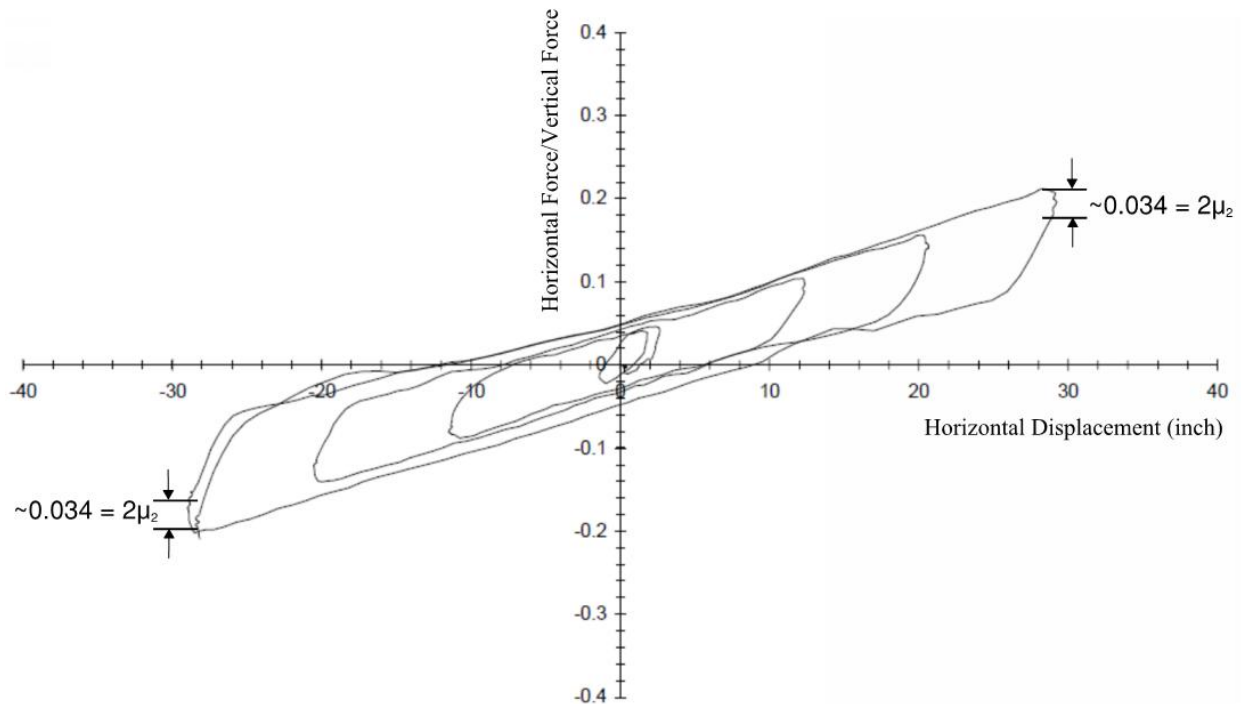
Figure 7-6 Graphical Measure of Properties of Prototype Isolator 1 for Test 1
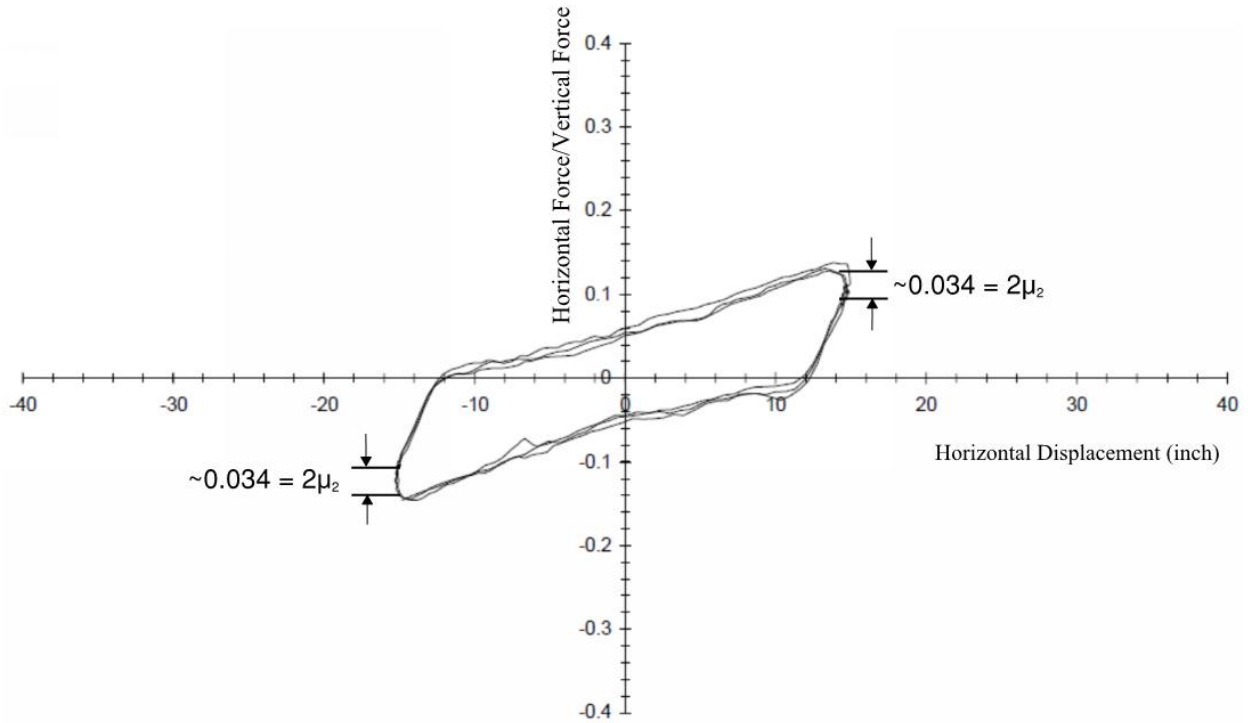
Figure 7-7 Graphical Measure of Properties of Prototype Isolator 1 for Test 2

The inner friction μ_2 is not measured for cycles 2 and 3, as it is assumed to remain constant. This is based on the fact that a majority of the displacement and high velocities are occurring on the outer surfaces 1 and 4 and therefore this is where the heating effects are greatest and the friction coefficient varies. In reality there will be some reduction of μ_2 over the cycles, but all variability is lumped into μ_1 since this friction coefficient is the important parameter controlling the triple FP global behavior.

Following the selection of μ_2, the values of μ_1, the coefficient of friction on the outer surfaces 1 and 4, and u*, the displacement at which sliding initiates on the outer surfaces, can be determined based on theory and the measured value of the energy dissipated per cycle. The energy dissipated per cycle E_{loop} can be approximated by equation (7-1) in which D is the constant amplitude of motion in one cycle:

$$E_{loop}^{*} = \frac{E_{loop}}{W} = 4\mu_B \left(D - u^* \right) \qquad (7-1)$$

The friction coefficient μ_B is the normalized force at zero displacement (y-intercept). Also, quantity u* resembles a "yield displacement, Y" in a bilinear hysteretic representation of the force-displacement loop as shown in Figure 7-8, with the theoretical tri-linear loop given in Figure 2-4. There is only a small difference in the shape (or area) of Figure 7-8 compared to Figure 2-4. The dashed line in Figure 7-8 is the bilinear hysteretic loop with characteristic strength equal to $\mu_B W$ (W = the vertical load), post-elastic

90

stiffness equal to the theoretical stiffness W/(2R$_{1,\text{eff}}$) and yield displacement Y simply taken as u* given in Table 7-3.

The calculation of the friction coefficient μ$_B$ is somehow complex given the fact that quantity u* needs to be determined first. If quantity u* is set equal to zero, equation (7-1) provides a simple equation to obtain another estimate of the friction coefficient, say μ$_A$, from the measured energy dissipated per cycle. This friction coefficient can be used for a rigid-linear model as shown in the preliminary design. Note that coefficient μ$_A$ is smaller than μ$_B$. Analysis with μ$_A$ will result in only slightly larger displacements and therefore is slightly conservative.
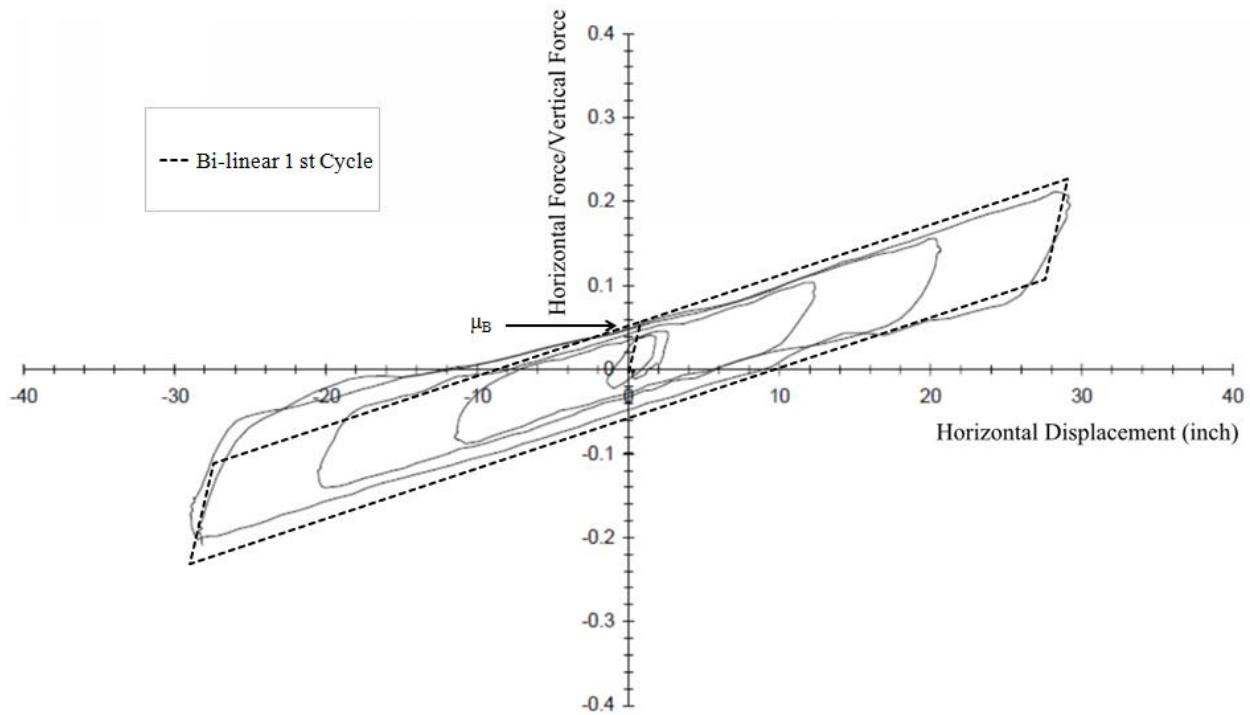
Figure 7-8 Estimate of Area for Calculating Friction μ$_B$, Isolator 1, Test 1, Cycle 1

The procedure for calculating μ$_1$ is based on the theory discussed in Section 2.3. The friction at zero displacement μ$_B$ is based on the energy dissipated per cycle in equation (7-1) and can also be related to the inner and outer surface friction coefficients and isolator geometry as given in equation (7-2). From the theoretical force-displacement behavior (Figure 2-4), the displacement u* can be calculated using equation (7-3).

$$\mu_B = \mu_1 - (\mu_1 - \mu_2)\frac{R_{eff,2}}{R_{eff,1}} \qquad (7\text{-}2)$$

$$u^* = 2(\mu_1 - \mu_2)R_{eff,2} \qquad (7\text{-}3)$$

91

Combining and rearranging equations (7-2) and (7-3) gives:

$$\mu_1 = \mu_B + \frac{u^*}{2R_{eff,1}} \qquad (7\text{ - }4)$$

where μ_B is obtained by use of equation (7-1), the measured value of E^*_{loop} and using some estimate on u^*. Graphical means need to be used, however judgment is needed to avoid excessive rigor and inconsistencies. Fundamental is that theory predicts the behavior of this isolator very accurately and the only unknowns are the values of the friction coefficients. Iteration is required on u^* to confirm that equation (7-3) is valid based on the value used for μ_2 and the value of μ_1 calculated from equation (7-4).

Table 7-3 summarizes the key parameters for Isolators 1 and 2 determined using Test 1. The inner friction μ_2 is based on test results, determined graphically from the first cycle and assumed to be constant over all cycles. The outer friction μ_1 and displacement u^* are determined based on theory which is stated in equations (7-4) and (7-3), respectively. The theoretical force-displacement loops for Isolator 1 using the parameters in Table 7-3 are illustrated in Figure 7-9. This shows reasonable agreement between theoretically derived stiffness (based on geometry) and experimental results. Table 7-4 illustrates the results from Test 2. Note that the two tables also include data on another parameter, the fiction coefficient μ_A which is obtained by use of equation (7-1) with $u^*=0$ (i.e. rigid-linear model Figure 2-1). The utility of this parameter is that it can be readily obtained from the measured energy dissipated per cycle without any other determination of parameters. This parameter is often used in practice instead of μ_B. The difference between the two values is small when the amplitude of motion D is large. The use of parameter μ_A will be illustrated later in this section when looking at production test data.

Table 7-3 Frictional Properties of Isolator at Load of 2710kN (609kip) from Test 1

Cycle/ Loop	Inner Friction μ_2	Outer Friction μ_1	Displacement, u* mm (in)	$\mu_B = \dfrac{E^*_{loop}}{4(D - u^*)}$	$\mu_A = \dfrac{E^*_{loop}}{4D}$
Isolator No. 1					
1	0.017	0.060	19.6 (0.77)	0.055	0.054
2	0.017	0.043	12.1 (0.48)	0.041	0.040
3	0.017	0.032	6.9 (0.27)	0.030	0.030
Average	-	0.045	-	0.042	0.041
Isolator No. 2					
1	0.017	0.076	26.8 (1.06)	0.070	0.067
2	0.017	0.056	17.7 (0.70)	0.052	0.050
3	0.017	0.048	14.2 (0.56)	0.045	0.043
Average	-	0.060	-	0.056	0.054
Average of two isolators	**-**	**0.052**	**-**	**0.049**	**0.048**
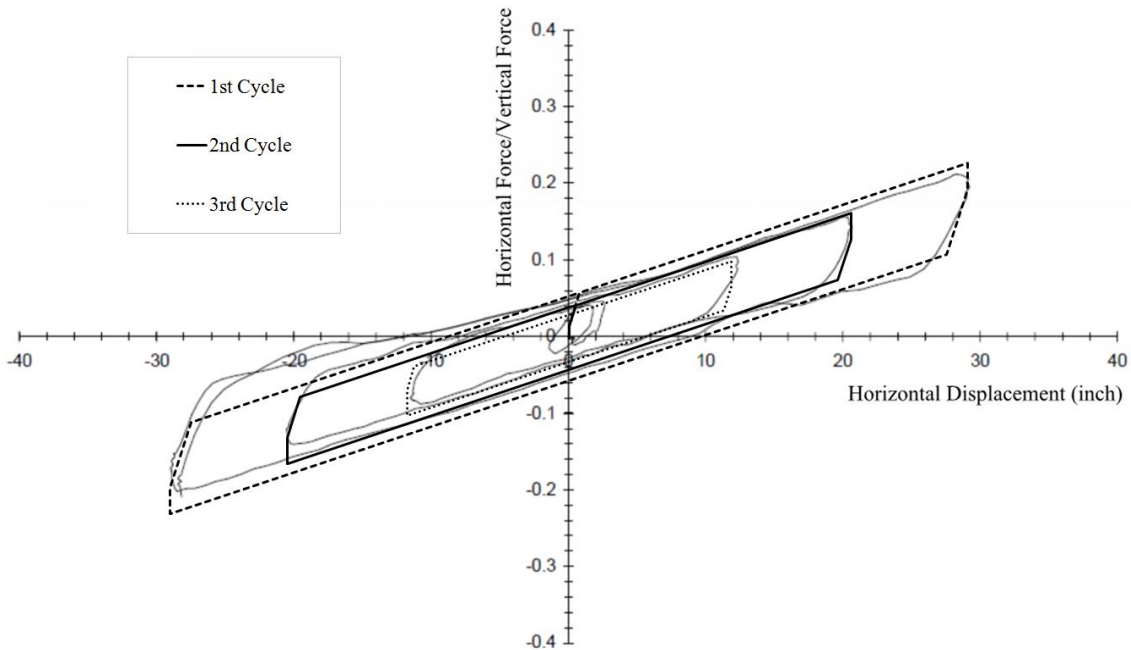
Figure 7-9 Theoretical and Actual Force-Displacement Behavior: Prototype Isolator 1, Test 1

93

Table 7-4 Frictional Properties of Isolator at Load of 1348kN (303kip) from Test 2

Cycle/ Loop	Inner Friction μ_2	Outer Friction μ_1	Displacement, u* mm (in)	$\mu_B = \dfrac{E^*_{loop}}{4(D - u^*)}$	$\mu_A = \dfrac{E^*_{loop}}{4D}$
Isolator No. 1					
1	0.017	0.067	23.1 (0.91)	0.062	0.058
2	0.017	0.061	20.2 (0.79)	0.056	0.053
3	0.017	0.059	19.2 (0.76)	0.054	0.052
Average	-	0.063	-	0.058	0.054
Isolator No. 2					
1	0.017	0.090	33.2 (1.31)	0.082	0.075
2	0.017	0.081	28.8 (1.14)	0.074	0.068
3	0.017	0.080	28.7 (1.13)	0.074	0.068
Average	-	0.084	-	0.076	0.070
Average of two isolators	**-**	**0.0735**	**-**	**0.067**	**0.062**

The data on friction in Tables 7-3 and 7-4 reveal some important observations:

1) The two isolators differ in frictional properties. Particularly, the average, three-cycle value of friction coefficient μ_1 at the load of 1348kN (Test 2) is 0.063 and 0.084 in the two isolators. At the load of 2710kN (Test 1) the values are 0.045 and 0.060, respectively. The nominal value for μ_1 will be the average of the two prototype isolators, that is, 0.0735 at the load of 1348kN and 0.0525 at the load of 2710kN. Note that each of the values of μ_1 is within about ±14% of the nominal value, which is very close to the range of ±15% to be allowed in the production isolators (λ_{spec}). This brings up the question on what would be the variability in properties from isolator to isolator in a large group of isolators and the relation of the average properties of the large group to the average properties of the two prototype isolators. An example is provided to illustrate the property variation over a large group of isolators. Among the several production data sets available, data exist for a group of 43 production isolators of the type tested under load of 1348kN (303kip) and three cycles of motion at amplitude of about 380mm (15in) , which is Test 2. The average three-cycle value of the friction coefficient μ_A of each test is available and shown in Figure 7-10. The average value of μ_A in the 43 production isolators is 0.0573 and the values of

μ_A for the two prototype isolators are 0.054 and 0.070 (Table 7-4). The nominal value is the average of the two prototype isolators or 0.062, which is within 8% of the tested average value of the production isolators. Thus, the production isolators are comfortably within the ±15% production allowance (λ_{spec} values of 1.15 and 0.85), which was based on the friction values obtained from the two prototype isolators.
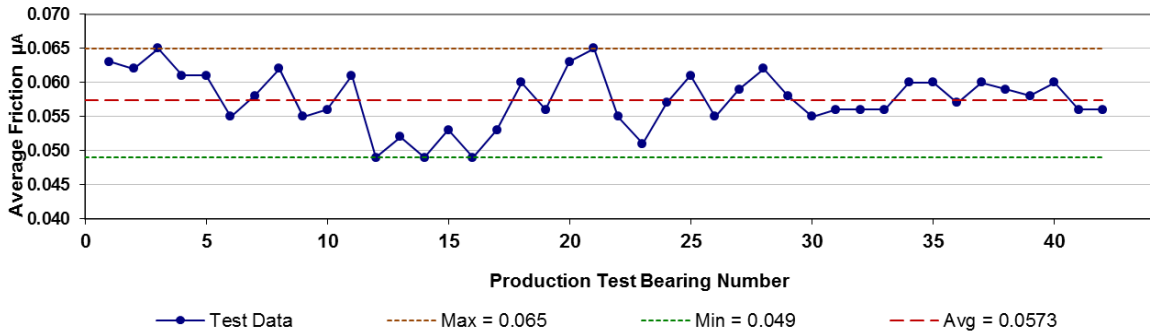
Figure 7-10 Three-cycle Average Coefficient of Friction μ_A of 43 Production Isolators under Load of 1348kN (Test 2)

2) The values of friction coefficient μ_2 are assumed to be constant and independent of cycling (hence heating) and load in the range of 1348 to 2710kN. This requires justification. This coefficient of friction is that of the inner sliding interface which experiences smaller amplitude and peak velocity of motion. Specifically, in Test 1, Isolator 2 at the cycle of amplitude of 745mm and peak velocity of 1189mm/sec, the advanced theory by Sarlis et al (2013) predicts that the inner sliding interface experiences sliding twice, each at amplitude equal to 16mm and peak velocity equal to 200mm/sec, whereas the outer sliding interface experiences sliding twice, each at amplitude equal to 380mm and peak velocity equal to 610mm/sec. Accordingly, there is significantly less heating of the inner interface than the outer one. Moreover, the lower velocity of sliding at the inner interface supports the constant value of friction independently of the load. Specifically, data in Constantinou et al. (2007) and Mokha et al. (1996) show that at low velocities the coefficient of friction of materials of the type used in the tested isolators is essentially independent of pressure over a wide range of values (similar to composite 1 in Constantinou et al. 2007).

There are two separate sets of properties determined for the interior and the exterior/perimeter isolators. Friction coefficient μ_1 is an essential parameter controlling both the force and displacement behavior of the isolator. The inner interface friction coefficient μ_2 is of secondary importance and of some

95

significance when considering residual displacements and the response of nonstructural components and contents, which is not the focus of this report. For these reasons, and the assumption that there will be little heating effects on the inner sliding surfaces due to lower velocities, the lambda-test factors $\lambda_{test,max}$ and $\lambda_{test,min}$ associated with the inner friction is taken as a constant value for both the upper and lower bound analysis and the variability in properties (i.e. change in energy dissipated per cycle) is taken into account in the bounding of the outer surface friction coefficient μ_1. The inner friction coefficient μ_2 adopts the same property modification factors as the outer surfaces μ_1 for the specification and environmental and aging factors with the lambda-test factors are set to unity

The interior isolators have a nominal value of μ_1 taken as the average over three cycles from Test 1 (~2710kN), averaged for the two prototype isolators. That is, the nominal value of μ_1 is the average of 0.045 and 0.060 (see Table 7-3), or 0.0525, rounded to 0.052. The upper bound for the internal isolators is taken as the friction in the first cycle of Test 1 divided by the nominal value. The $\lambda_{test,max}$ is the ratio of the average first cycle value of the friction coefficient μ_1 (average of 0.060 and 0.076 per Table 7-3, or 0.068) to 0.052, or 1.3. Taking the lower bound as the second-cycle properties (see reasoning Section 3.1.1) results in a minimum lambda-test factor of $\lambda_{test,min} = \frac{1}{2}(0.043+0.056)/0.052 = 0.95$.

For the exterior isolators, there are various options to consider since Test 2 (1348kN) does not meet the similarity requirements of ASCE 7-2016. It is left to the RDP's discretion when deciding on the nominal properties and associated lambda-test factors. One approach is to use the same process as for the internal isolators utilizing the data from Test 2 (Table 7-4). This leads to a nominal value of μ_1 as the average of 0.063 and 0.084, giving 0.0735, rounded to 0.073 and a $\lambda_{test,max}$ value equal to the average of 0.067 and 0.090 divided by 0.073, giving $\lambda_{test,max}$=1.08. This low value of $\lambda_{test,max}$, compared to 1.3 in Test 1, denotes the lower heating effects due to the reduced pressure (half of that in Test 1 used for the interior isolators) and the fact that the amplitude of motion (hence also velocity and heating effects) was less than in Test 1. These values are based on a peak velocity of about 600mm/s (24 in/s) whereas the design requires a velocity of around 1025mm/s (40.4 in/s). Therefore the similarity requirements of ASCE 7-2016 would not allow the Test 2 data to be used directly. This is because the test underestimates the heating effects. Hence based on some rational theory the RDP may adjust the nominal value of μ_1 to a lower value (while increasing $\lambda_{test,max}$) and/or the minimum lambda factor $\lambda_{test,min}$ could be reduced further.

The approach applied herein, which is conservative for the lower bound, is to reduce the lower bound to that measured in the second-cycle of Test 1. This is done by altering the $\lambda_{test,min}$ value accordingly. Test 1 has an appropriate velocity but twice the isolator pressure, therefore although it is conservative for heating effects and meets the similarity requirements of ASCE 7-16, it may under-predict the upper bound. Therefore the $\lambda_{test,max}$ is maintained and the $\lambda_{test,min}$ is calculated to be ½(0.043+0.056)/0.073 = 0.68. This low value reflects the lack of adequate information for the exterior isolators. A more favorable value would require additional testing data.

A summary of the nominal values and associated lambda-test factors is:

- **Interior Isolators:**
  - Nominal Value **μ_2 = 0.017** with associated lambda-test factors: **$\lambda_{test,max}$ = 1.0, $\lambda_{test,min}$ = 1.0**
  - Nominal Value **μ_1 = 0.052** with associated lambda-test factors: **$\lambda_{test,max}$ = 1.3, $\lambda_{test,min}$ = 0.95**
- **Exterior Isolators:**
  - Nominal Value **μ_2 = 0.017** with associated lambda-test factors: **$\lambda_{test,max}$ = 1.0, $\lambda_{test,min}$ = 1.0**
  - Nominal Value **μ_1 = 0.073** with associated lambda-test factors: **$\lambda_{test,max}$ = 1.08, $\lambda_{test,min}$ = 0.68**

Since the interior isolators have higher axial compression load, it is expected that they will have greater heating effects and hence generally a wider range of friction coefficients than that calculated for the exterior isolators. This is not the case here due to the uncertainty on the selection of the lower bound value for the exterior isolators (i.e. Test 2 did not meet similarity requirements), which led to conservative adjustments. This wider range in friction values for the exterior isolators reflects a lack of adequate information, which is consistent with the Standards approach.

7.3   Similar Unit Criteria

Throughout Section 7.2 there is discussion on meeting the similar unit requirements of ASCE 7-2016. As stated in ASCE 7-2016 §17.8.2.7, project-specific prototype tests need not be performed if the following criteria are satisfied:

1. The isolator design is not more than 15% larger nor more than 30% smaller than the previously tested prototype, in terms of governing device dimensions; and

The dimensions of the prototype isolator are adopted directly for the design. Therefore, the similarity criterion is satisfied.

2. Is of the same type and materials; and

The materials can have a considerable effect on the coefficient of friction. It is important that the materials used and the production methods utilized (covered in item 4 below) for the production isolators are the same as those used in the prototype isolators. To ensure this, production isolator testing is needed with acceptance criteria related to the properties obtained from the prototype isolators.

3. Has an energy dissipated per cycle, E_{loop}, that is not less than 85% of the previously tested unit, and

Since the design nominal friction coefficient was derived from the tested energy dissipated per cycle, this requirement is satisfied.

4. Is fabricated by the same manufacturer using the same or more stringent documented manufacturing and quality control procedures.

Similar to the materials, the manufacturing process can have a measurable effect on the friction coefficient. Since the FP isolators manufacturing involves manual labor (i.e. attaching the stainless steel overlay to the concave plate), tight quality control on the workmanship is required to ensure consistency. To ensure this, production isolator testing is needed with acceptance criteria related to the properties obtained from the prototype isolators.

6. For sliding type isolators, the design shall not be subject to a greater vertical stress or sliding velocity than that of the previously tested prototype using the same sliding material.

The prototype isolators were subject to a greater vertical stress than that required in design. The design interior and exterior isolators have an average axial load (D +0.5L) of 2351kN (528kip) and 1267kN (285kip), respectively. This is comparable to the Test 1 and Test 2 axial loads of about 2710kN (609kip) and 1348kN (303kip). Although a lower vertical stress meets this criterion, the vertical stress of the tested isolator should not be significantly more as then it may underestimate the friction coefficient.

Sliding velocity influences the friction coefficient due to a) the friction coefficient being dependent on velocity and b) frictional heating during motion. High-speed testing, say above velocities of 50mm/s, is sufficient to obtain the dynamic coefficient of friction, which tends to be invariable at these high velocities except for the effect of heating which is dependent on the duration of the motion. The design velocity was calculated as 1025mm/s (40.4in/s) in the preliminary design (Section 5.3).

The peak velocity in Test 1 varies between cycles, with it being about 1160mm/s (45.6in/s) in the first cycle and less than that required in design for the second and third cycles. The average peak velocity over the three cycles was 890mm/s (35in/s), which is less than the preliminary design calculated peak velocity. However it is noted that the tested isolator has a greater pressure than that required for design, and therefore increased heating effects (i.e. heat flux is a multiple of the friction coefficient, velocity and isolator pressure). Furthermore the nominal properties and lambda factors are conservatively determined assuming that all the heating effects occur on the outer surfaces 1 and 4. Therefore the intent of the clause is met since the frictional heating is comparable to that required in design.

The peak velocity in Test 2 does not meet similarity requirements, however the data along with Test 1 data have been used to rationally and conservatively attain upper and lower bound values for the exterior isolators, as discussed in Section 7.2. Therefore the intent of the clause, which is to capture the heating, axial load and history of loading effects, has been met. Furthermore, a RDP may also choose to have prototype tests performed on the exterior isolators for the appropriate velocity.

7.4 Test Specimen Adequacy Criteria

This section provides a discussion on the test specimen adequacy criteria of ASCE 7-2016 when applied to Friction Pendulum (FP) isolators. It does not directly relate to the work in this report as a complete set of prototype test results per Section 17.8.2 of ASCE 7-2016 does not exist. The reader is referred to Section 6.5 for a critique of the requirements when assessed for lead-rubber isolators, as some of the comments are applicable to FP isolators as well.

The adequacy criteria mention the post elastic stiffness, K_d and the energy dissipated per cycle, E_{loop}. The stiffness K_d for the FP isolators was not measured from test data in this report. Instead the stiffness was calculated as a function of the load on the isolator and the geometry of the isolator (i.e. effective concave plate(s) radius of curvature). This is because theory predicts the behavior well (Fenz and Constantinou 2008) and manufacturers typically can construct isolators with a high degree of geometric precision. Also, the stiffness of these isolators does not change from cycle to cycle, and accordingly and in consistency with ASCE 7-2016, the corresponding lambda factors $\lambda_{test,min}$ and $\lambda_{test, max}$ are set to unity. This is discussed further in the following.

Furthermore, the checks that follow use the friction coefficient instead of E_{loop} to allow for direct comparison. The friction coefficient is a mechanical property of the isolator whereas the E_{loop} is a function of the weight, friction coefficient and test regime (i.e. travel). The friction coefficient μ_A is used (for

definition and values see Tables 7-3 and 7-4), which is directly related to the normalized (by vertical load) E_{loop}.

There is a significant difference between quasi-static and dynamic testing acceptance requirements, since the friction coefficient is velocity dependent. The requirements below are checked for high-speed testing, as follows:

> The performance of the test specimens shall be deemed adequate if all of the following conditions are satisfied:
>
> 2.   The force-deflection plots for all tests specified in Section 17.8.2 have a positive incremental force-resisting capacity.

The isolators have positive incremental force-resisting capacity.

> 2. The average post-yield stiffness, k_d, and energy dissipated per cycle, E_{loop} , for the three cycles of test specified in Section 17.8.2.2, item 3 for the vertical load equal to the average dead load plus one-half the effects due to live load, including the effects of heating and rate of loading in accordance with Section 17.2.8.3, shall fall within the range of the nominal design values defined by the permissible individual isolator range which are typically +/-5% greater than the $\lambda_{(spec, min)}$ and $\lambda_{(spec, max)}$ range for the average of all isolators.

The item 3 test is the characterization test used to determined nominal properties as discussed in Section 4.3. It consists of 3 cycles at the maximum displacement D_M. As noted in Section 7, the test data ("Test 1") does not exactly match the test regime of item 3, however it is believed that the test data was applicable to meet the similar unit requirements and is used for discussion herein.

For the interior isolators:

$\mu_{A,nominal}$=0.048 (Table 7-3), $\lambda_{spec,min}$=0.85 and $\lambda_{spec, max}$=1.15 giving a required range of 0.041 to 0.055 (or 0.039 to 0.058 when adding the +/-5% allowance). The average from prototype isolator 1 and 2 is 0.041 and 0.054, respectively.

For the exterior isolators:

$\mu_{A,nominal}$=0.062 (Table 7-4), $\lambda_{spec,min}$=0.85 and $\lambda_{spec, max}$=1.15 giving a required range of 0.053 to 0.071 055 (or 0.050 to 0.075 when adding the +/-5% allowance). The average from prototype isolator 1 and 2 is 0.054 and 0.070, respectively.

The prototype isolators meet the ASCE 7-2016 acceptance criteria of Section 17.8.4, item 2.

3.   For each increment of test displacement specified in item 2 and item 3 of Section 17.8.2.2 and for each vertical load case specified in Section 17.8.2.2,

a.   For each test specimen the value of the post-yield stiffness, k_d, at each of the cycles of test at a common displacement shall fall within the range defined by $\lambda_{(test,\ min)}$ and $\lambda_{(test,\ max)}$ multiplied by the nominal value of post-yield stiffness.

Figure 7-9 for FP isolator 1, and below in Figure 7-11 for Isolator 2, give the theoretical force-displacement model for each cycle overlaid the actual test data. In the figure the tri-linear model is based on the measured energy dissipated per cycle (i.e. friction coefficient) whereas the post-elastic stiffness is calculated based on the geometry of the isolator. The figures show that recorded normalized (by instantaneous vertical load) loops do not exactly match the theoretical loops, however the agreement is satisfactory. The reasons for the differences are (a) fluctuation of the vertical load during the tests (294 to 897kip for isolator 1 and 282 to 920kip in isolator 2) which affects the instantaneous value of the friction coefficient, and (b) heating effects on the friction coefficient which are more pronounced in the highest velocity-largest amplitude cycle. The differences seen in Figures 7-9 and 7-11 are due to changes in friction and not due to changes in stiffness. Thus the approached followed in this report is to accept that the post-elastic stiffness does not vary and any variability from cycle to cycle is assigned to the frictional properties. Accordingly,   the prototype isolators meet the ASCE 7-2016 acceptance criteria of Section 17.8.4, Item 3a.
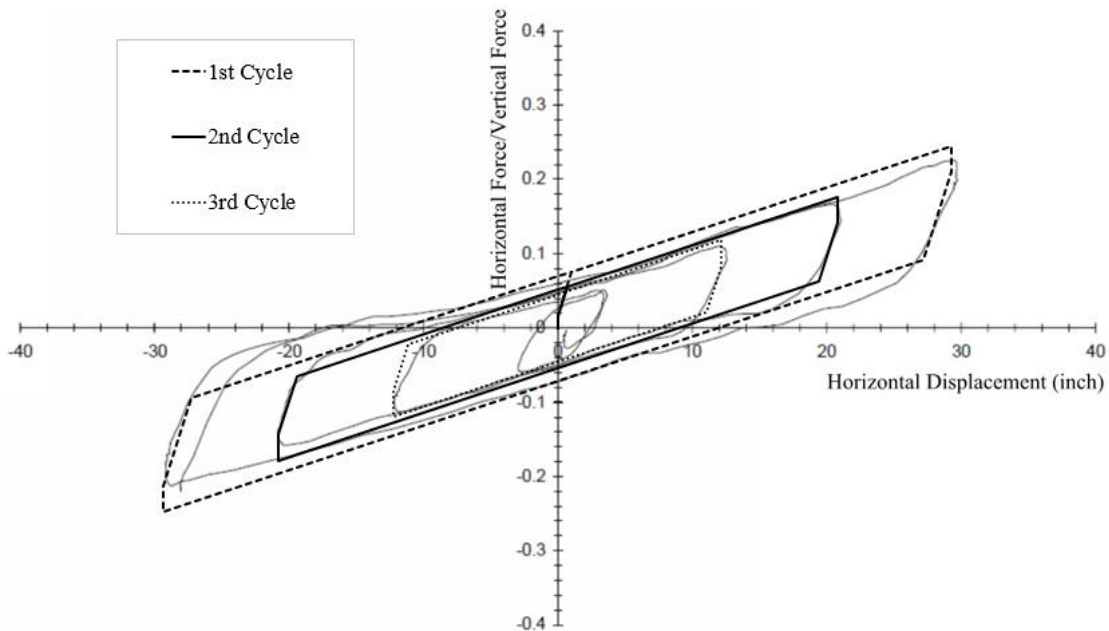
Figure 7-11 Theoretical and Actual Force-Displacement Behavior for Isolator 2, Test 1

101

For the reasons stated above, the post-elastic stiffness of the isolators does not vary and any variability from cycle to cycle is assigned to the frictional properties. Accordingly, the prototype isolators meet the ASCE 7-2016 acceptance criteria of Section 17.8.4, Item 3b.

There is not test data available for five continuous cycles at $0.75D_M$, however comparison can be made based on the available test data for three cycles of loading. As explained in Section 7, Test 1 the isolator was subjected to varying amplitude with one cycle having amplitude larger than $0.75D_M$. Test 2 was conducted for three cycles at a constant amplitude (approximately $2/3D_M$). Data are presented in Table 7-5 (note that the effective stiffness is based on the normalized-by vertical load-loops). It is not possible to check in the case of Test 1 as the amplitude is variable but for Test 2 there is a 5% reduction of the third cycle effective stiffness from the initial effective stiffness.

Table 7-5 Effective Stiffness of FP Isolators (kip/inch/kip)

Cycle	Test 1 Isolator 1	Test 1 Isolator 2	Test 2 Isolator 1	Test 2 Isolator 2
1	0.0078	0.0083	0.0099	0.0109
2	0.0079	0.0084	0.0095	0.0105
3	0.0085	0.0095	0.0094	0.0105

Similar to requirement 5, comparison can be made based on the test data available using the effective stiffness in Table 7-5 and equation (6-3) to calculate the effective damping. However, it should be noted that requirement 6 is based on having cycles of the same amplitude. Results are presented in Table 7-6. For Test 1 there is an increase in the effective damping due to the decreasing amplitude of displacement. Test 2 shows a slight decrease in the effective damping in the first three cycles, which amounts to about or less than 8% of the initial value.

Table 7-6 Effective Damping of FP Isolators

Cycle	Test 1 Isolator 1	Test 1 Isolator 2	Test 2 Isolator 1	Test 2 Isolator 2
1	15%	18%	25%	29%
2	16%	18%	24%	27%
3	19%	24%	23%	27%

The reader is referred to Section 6.5 where two deficiencies of the ASCE 7-16 adequacy criteria are discussed, and these comments are also applicable to FP isolators. It is noted that these requirements are not as arduous to achieve for FP isolators compared to lead-rubber isolators.

This Page is Intentionally Left Blank

SECTION 8

SUMMARY OF ISOLATION SYSTEM PROPERTIES

8.1 Elastomeric Isolation System

This section provides a summary of the elastomeric isolator lambda factors and of the upper and lower bound values of properties for three main design scenarios discussed in Section 5.4. These are:

- Case A: No qualification data/manufacturer unknown (Table 8-2)
- Case B: Prototype or similar unit test data available (Tables 8-3 and 8-4)
- Case C: Production test data available for all isolators (Table 8-5)

The adopted aging and environmental lambda factors λ_{ae} and the specification lambda factors λ_{spec} are discussed in Section 3.2 and 3.4, respectively. The calculation of the nominal values and testing lambda factors is presented in Section 6.

For all cases the nominal property values in Table 8-1 are adopted. This assumes that the nominal values are the same for all cases, which need not be true. For example, in the case where data exist for only two prototype isolators as in this report, the nominal values would be as in the Table 8-1. But if the data for all production isolators exist, the average of this data would be used to obtain the nominal value.

Table 8-1: Nominal Properties from Prototype Test Data used for all Examples

Isolator Type:	Lead-Rubber Isolators	Natural Rubber Isolators
Nominal Rubber Shear Modulus, G (MPa)	0.40	0.49
Nominal Effective Yield Stress of Lead, σ_L (MPa)	11.6	N/A

8.1.1 No Qualification Data/Unknown Manufacturer (Default)

The Standard ASCE 7-2016 states that if prototype isolator testing is not conducted on full-scale specimens utilizing relevant dynamic test data conditions, then the upper and lower limits of equations 17.2-1 and 17.2-2 apply. These limits are 1.8 and 0.60 respectively. Yet when referring to the commentary of ASCE 7-2016 the default values for elastomeric low damping and lead-rubber isolators are calculated as 1.83 and 0.77, with the composition of these lambda factors given in Table 8-2. The commentary lists the default values as 1.8 and 0.8, not 1.8 and 0.6. Since the commentary is not mandatory, the limit of 0.6 shall apply, as shown in the final calculation of the default properties in Table 8-2.

The lambda factors and nominal properties need to be considered in unison. ASCE 7-2016 Section 17.2.8.2 defines the nominal properties as the average properties over three cycles of motion using testing which can be performed dynamically or at slow velocity. The velocity of testing has a significant effect on the calculated nominal properties due primarily to heating effects and secondarily to rate effects, and therefore applying the default testing lambda factors arbitrarily to account for these effects may underestimate the upper and/or lower bounds. Fundamental is to obtain the nominal properties and the $\lambda_{test,}$ values in dynamic testing of prototype isolators. This approached is followed in this report.

Table 8-2: Default Lambda Factors and Upper and Lower Bound Property Values in Absence of Qualification Data for Elastomeric Isolation System in Examples of this Report

Isolator Type:	Lead-Rubber Isolators		Natural Rubber Isolators
Parameter Adjusted:	G	σ_L	G
Testing Lambda Factors – λ_{test}			
Maximum Testing Lambda Factors			
Heating - $\lambda_{heating}$	-	-	-
Scragging - $\lambda_{scragging}$	-	-	-
Similarity Adjustment	-	-	-
$\lambda_{test,max}$	**1.3**	**1.6**	**1.3**
Minimum Testing Lambda Factors			
Heating - $\lambda_{heating}$	-	-	-
Scragging - $\lambda_{scragging}$	-	-	-
Similarity Adjustment	-	-	-
$\lambda_{test,min}$	**0.9**	**0.9**	**0.9**
Aging and Environmental Lambda Factors – λ_{ae}			
Maximum Aging & Environmental Lambda Factors			
Aging - λ_{aging}	1.3	1.0	1.3
$\lambda_{ae,max}$	1.3	1.0	1.3
$\lambda_{ae,max}$ after adjustment-0.75	**1.23**	**1.0**	**1.23**
Minimum Aging & Environmental Lambda Factors			
Aging - λ_{aging}	1.0	1.0	1.0
$\lambda_{ae,min}$	**1.0**	**1.0**	**1.0**
Specification Lambda Factors – λ_{spec}			
Maximum Specification Lambda Factor			
$\lambda_{spec,max}$	**1.15**	**1.15**	**1.15**
Minimum Specification Lambda Factor			
$\lambda_{spec,min}$	**0.85**	**0.85**	**0.85**
System Lambda Factors			
λ_{max}	**1.83**	**1.84**	**1.83**
λ_{min} as per Section 17.2.8.4	**0.60**	**0.60**	**0.60**
Upper Bound Nominal Value	0.73 MPa	21.3 MPa	0.90 MPa
Lower Bound Nominal Value	0.24 MPa	7.0 MPa	0.29 MPa
Ratio Upper/Lower	**3.1**	**3.1**	**3.1**

8.1.2 Prototype or Similar Unit Test Data

Since there are differences between the tested isolators and isolators required in preliminary design, there are further adjustments applied to the lambda-test factors to account for uncertainties as shown in Table 8-3. It is noted that the tested isolators do not strictly meet the similarity requirements of ASCE 7-2016, and

prototype testing (or further test data) will be required. However the isolators are labeled as "similar", with further adjustments for uncertainty, in order to continue with design.

Table 8-3: Lambda Factors and Upper and Lower Bound Property Values Based on Data from "Similar" Units for Elastomeric Isolation System used in Examples of this Report

Isolator Type:	Lead-Rubber Isolators		Natural Rubber Isolators
Parameter Adjusted:	G	σ_L	G
Testing Lambda Factors – λ_{test}			
Maximum Testing Lambda Factors			
Heating - $\lambda_{heating}$	1.0	1.40[1]	1.0
Scragging - $\lambda_{scragging}$	1.3	1.0	1.15
Similarity Adjustment	1.0	-	1.05
$\lambda_{test,max}$	**1.3**	**1.40**	**1.21**
Minimum Testing Lambda Factors			
Heating - $\lambda_{heating}$	1.0	0.95[1]	1.0
Scragging - $\lambda_{scragging}$	1.0	1.0	0.93
Similarity Adjustment	1.0	-	0.95
$\lambda_{test,min}$	**1.0**	**0.95**	**0.88**
Aging and Environmental Lambda Factors – λ_{ae}			
Maximum Aging & Environmental Lambda Factors			
Aging - λ_{aging}	1.1	1.0	1.1
$\lambda_{ae,max}$	1.1	1.0	1.1
$\lambda_{ae,max}$ after adjustment-0.75	**1.08**	**1.0**	**1.08**
Minimum Aging & Environmental Lambda Factors			
Aging - λ_{aging}	1.0	1.0	1.0
$\lambda_{ae,min}$	**1.0**	**1.0**	**1.0**
Specification Lambda Factors – λ_{spec}			
Maximum Specification Lambda Factor			
$\lambda_{spec,max}$	**1.15**	**1.15**	**1.15**
Minimum Specification Lambda Factor			
$\lambda_{spec,min}$	**0.85**	**0.85**	**0.85**
System Lambda Factors			
λ_{max}	**1.61**	**1.61**	**1.50**
λ_{min}	**0.85**	**0.81**	**0.75**
Upper Bound Nominal Value	0.64 MPa	18.7 MPa	0.74 MPa
Lower Bound Nominal Value	0.34 MPa	9.4 MPa	0.37 MPa
Ratio Upper/Lower	1.9	2.0	2.0

1. Adjustment for uncertainty already included, see Section 6.2.2, with similarity calculations based on Kalpakidis et al (2008) heating calculations.

Table 8-4 presents the lambda factors and the upper and lower property values when assuming that the tested isolators were in fact the prototype isolators. Section 6.2 explains how the similar isolator and prototype lambda test factors were determined.

Table 8-4: Lambda Factors and Upper and Lower Bound Property Values Based on Data from Actual Prototype Isolators for Elastomeric Isolation System used in Examples of this Report

Isolator Type:	Lead-Rubber Isolators		Natural Rubber Isolators
Parameter Adjusted:	G	σ_L	G
Testing Lambda Factors – λ_{test}			
Maximum Testing Lambda Factors			
Heating - $\lambda_{heating}$	1.0	1.35	1.0
Scragging - $\lambda_{scragging}$	1.3	1.0	1.15
Similarity Adjustment	-	-	-
$\lambda_{test,max}$	**1.3**	**1.35**	**1.15**
Minimum Testing Lambda Factors			
Heating - $\lambda_{heating}$	1.0	0.93	1.0
Scragging - $\lambda_{scragging}$	1.0	1.0	0.93
Similarity Adjustment	-	-	-
$\lambda_{test,min}$	**1.0**	**0.93**	**0.93**
Aging and Environmental Lambda Factors – λ_{ae}			
Maximum Aging & Environmental Lambda Factors			
Aging - λ_{aging}	1.1	1.0	1.1
$\lambda_{ae,max}$	1.1	1.0	1.1
$\lambda_{ae,max}$ after adjustment-0.75	**1.08**	**1.0**	**1.08**
Minimum Aging & Environmental Lambda Factors			
Aging - λ_{aging}	1.0	1.0	1.0
$\lambda_{ae,min}$	**1.0**	**1.0**	**1.0**
Specification Lambda Factors – λ_{spec}			
Maximum Specification Lambda Factor			
$\lambda_{spec,max}$	**1.15**	**1.15**	**1.15**
Minimum Specification Lambda Factor			
$\lambda_{spec,min}$	**0.85**	**0.85**	**0.85**
System Lambda Factors			
λ_{max}	**1.61**	**1.55**	**1.43**
λ_{min}	**0.85**	**0.79**	**0.79**
Upper Bound Nominal Value	0.64 MPa	18.0 MPa	0.70 MPa
Lower Bound Nominal Value	0.34 MPa	9.2 MPa	0.39 MPa
Ratio Upper/Lower	1.9	2.0	1.8

8.1.3 Production Test Data

Table 8-5 adopts the values and assumptions from Table 8-4 directly, but now full production test data is assumed to be available to determine the actual nominal values. Hence the specification lambda factors are set to unity. It is assumed that the nominal values calculated from production test data are equal to the nominal values calculated from the two prototype isolators just for the purpose of presentation of the differences to other cases. This need not be true, as the average nominal value of the two prototype isolators is likely to be different than the average nominal value of all production isolators.

Table 8-5: Lambda Factors and Upper and Lower Bound Property Values Based on Data from All Production Isolators for Elastomeric Isolation System used in Examples of this Report

Isolator Type:	Lead-Rubber Isolators		Natural Rubber Isolators
Parameter Adjusted:	G	σ_L	G
Testing Lambda Factors – λ_{test}			
Maximum Testing Lambda Factors			
Heating - $\lambda_{heating}$	1.0	1.35	1.0
Scragging - $\lambda_{scragging}$	1.3	1.0	1.15
Similarity Adjustment	-	-	-
$\lambda_{test,max}$	**1.3**	**1.35**	**1.15**
Minimum Testing Lambda Factors			
Heating - $\lambda_{heating}$	1.0	0.93	1.0
Scragging - $\lambda_{scragging}$	1.0	1.0	0.93
Similarity Adjustment	-	-	-
$\lambda_{test,min}$	**1.0**	**0.93**	**0.93**
Aging and Environmental Lambda Factors – λ_{ae}			
Maximum Aging & Environmental Lambda Factors			
Aging - λ_{aging}	1.1	1.0	1.1
$\lambda_{ae,max}$	1.1	1.0	1.1
$\lambda_{ae,max}$ after adjustment-0.75	**1.08**	**1.0**	**1.08**
Minimum Aging & Environmental Lambda Factors			
Aging - λ_{aging}	1.0	1.0	1.0
$\lambda_{ae,min}$	**1.0**	**1.0**	**1.0**
Specification Lambda Factors – λ_{spec}			
Maximum Specification Lambda Factor			
$\lambda_{spec,max}$	**1.0**	**1.0**	**1.0**
Minimum Specification Lambda Factor			
$\lambda_{spec,min}$	**1.0**	**1.0**	**1.0**
System Lambda Factors			
λ_{max}	**1.40**	**1.35**	**1.24**
λ_{min}	**1.0**	**0.93**	**0.93**
Upper Bound Nominal Value	**0.56 MPa**	**15.7 MPa**	**0.61 MPa**
Lower Bound Nominal Value	**0.40 MPa**	**10.8 MPa**	**0.46 MPa**
Ratio Upper/Lower	**1.4**	**1.5**	**1.3**

8.1.4 Comparison of Elastomeric Lambda Factors

The force-displacement loops of the lead-rubber isolator using the nominal, lower and upper bound properties for the case of default values are presented in Figure 8-1. Similarly, Figures 8-2 and 8-3 present the loops when the lower and upper bound properties are based on prototype and production test

data, respectively. The idealized bilinear model loops are overlaid on the actual prototype test data of isolator 1 (isolator 2 has a similar behavior) in order to better appreciate the range of properties considered in the analysis of each case. Note that the amplitude of displacement in each of the loops has been calculated using the ELF procedure utilizing the MCE response spectrum for the site of the example, the isolation system details in Table 5-1, the nominal properties in Table 8-1 and the system lambda factors presented in Tables 8-2, 8-4 and 8-5 for the default, prototype and production values, respectively.
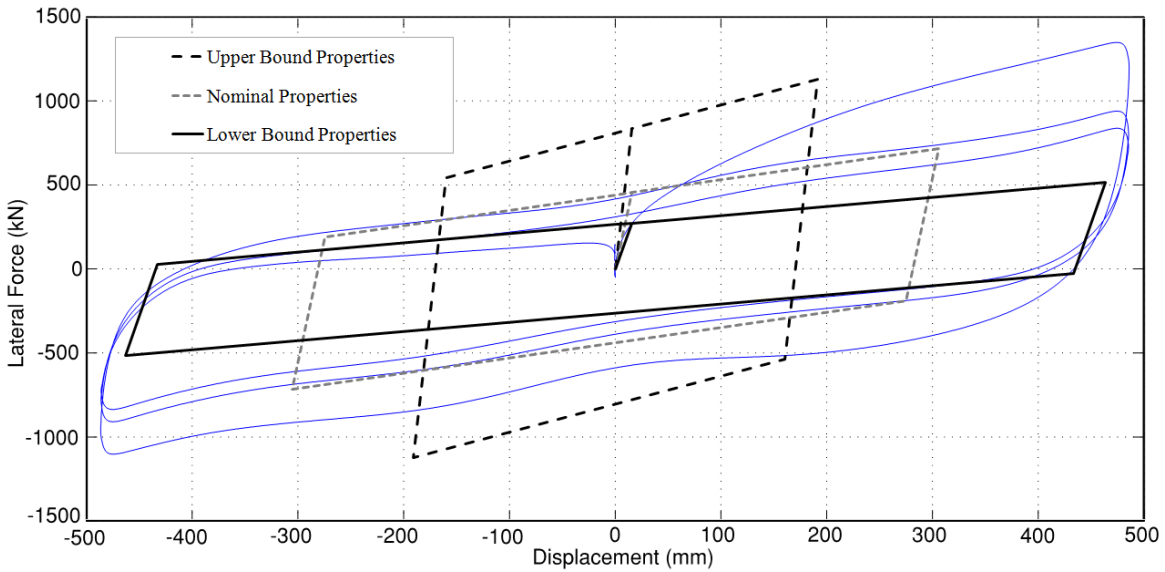
Figure 8-1: Idealized Force-Displacement of Lead-Rubber Isolator using Default Properties
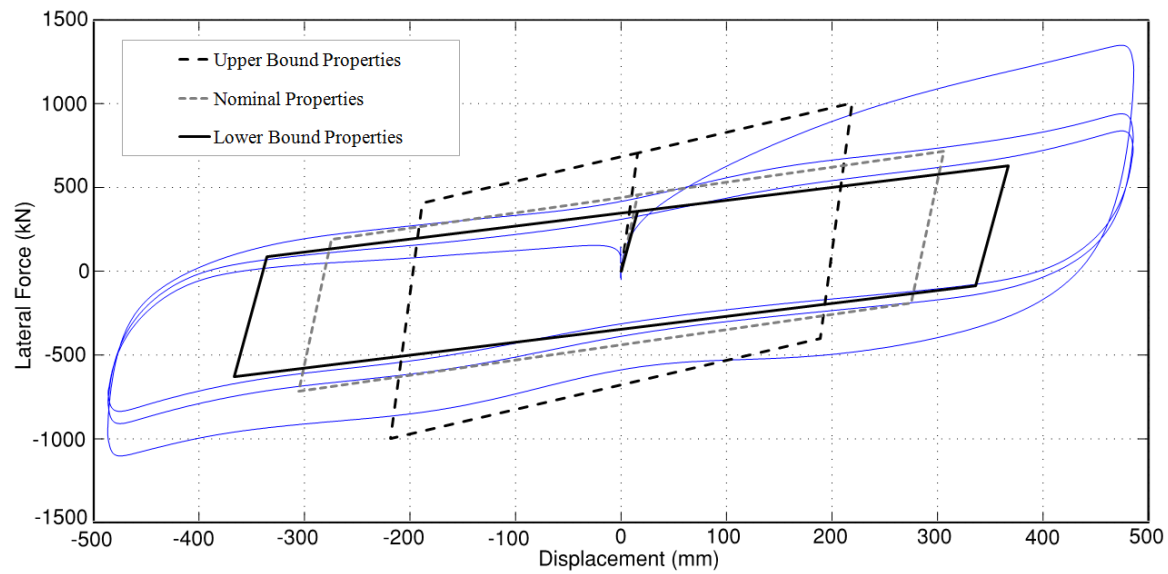
Figure 8-2: Idealized Force-Displacement of Lead-Rubber Isolator using Prototype Properties

112
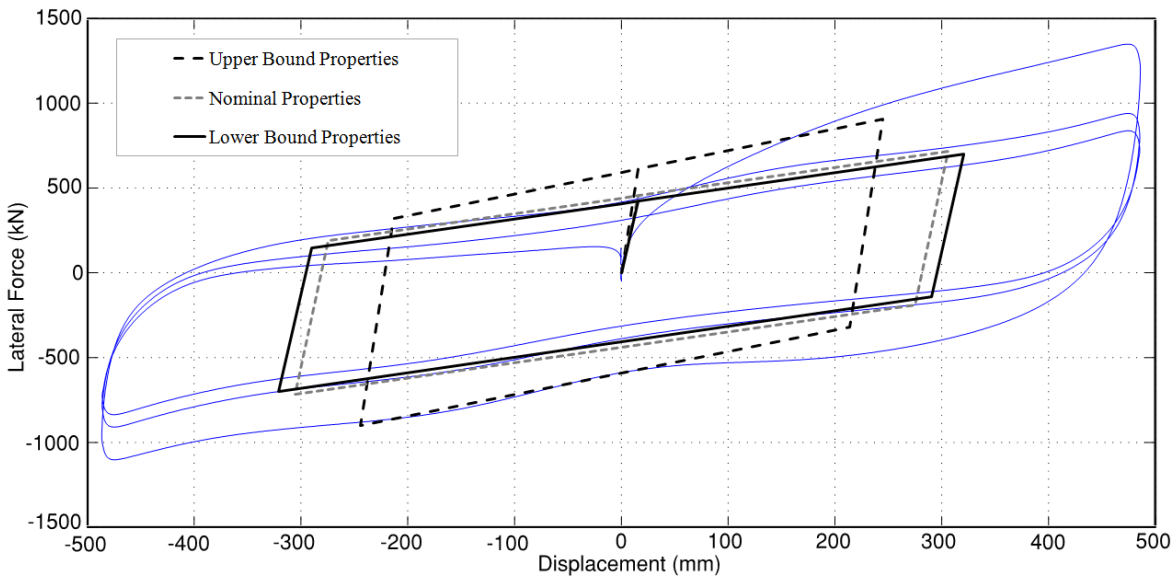
Figure 8-3: Idealized Force-Displacement of Lead-Rubber Isolator using Production Isolator Properties

It should be noted that the tested isolators are similar isolators and were tested to a greater displacement than that required by preliminary design (350mm), which is why the test loops have a greater displacement than the lower bound loops in Figure 8-2.

The NLRHA in Section 9 illustrates the effects on important design parameters by comparing the response using default force-displacement bounds (Figure 8-1) against the response using the bounds developed from prototype test data (Figure 8-2) and production test data (Figure 8-3).

8.2   Sliding Isolation System

This section provides a summary of the friction pendulum isolator lambda factors and of the upper and lower bound values of properties for three main design scenarios discussed in Section 5.4. These are:

- Case A: No qualification data/manufacturer unknown (Table 8-7)
- Case B: Prototype or similar unit test data available (Tables 8-8 and 8-9)
- Case C: Production test data available for all isolators (Table 8-10)

The adopted aging and environmental lambda factors λ_{ae} and the specification lambda factors λ_{spec} are discussed in Section 3.2 and 3.4, respectively. The calculation of the nominal values and testing lambda factors is presented in Section 7.

113

For all cases the nominal property values in Table 8-6 are adopted. This need not be true. For example, in the cases where data exist for only two prototype isolators as in this report, the nominal values would be as in the tables. But if the actual data for all production isolators exist, the average of those data would be used to obtain the nominal value. In the data for the 43 production isolators presented earlier (Section 6.2), the nominal value of friction μ_A (average of 43 isolators) was 1.082 times larger than the nominal value obtained from the two prototype isolators (see Section 6.2). Accordingly, the value of μ_1 would have been 1.082x0.052=0.056 instead of 0.052. The difference in this case is too small to be of significance in analysis and design as it is somehow accounted for in the conservatism exercised in the establishment of λ_{test} values.

Table 8-6: Nominal Properties from Prototype Test Data used for all Examples

Parameter	Interior Isolators (~2710kN)	Exterior Isolators (~1348kN)
Outer Surface Friction Coefficient μ_1	0.052	0.073
Inner Surface Friction Coefficient μ_2	0.017	0.017

The lambda factors for the inner surface friction coefficient μ_2 have not been included in the Tables that follow. This is because the related lambda-test factors have been set to unity and since it is a parameter which does not significantly affect the global response (see Section 7.2 for explanation). The aging and environmental lambda factors $\lambda_{ae,max}$, and the specification lambda factors $\lambda_{spec,max}$ are taken the same as those of the outer surface values μ_1.

8.2.1 No Qualification Data- Default Lambda Factors

The Standard ASCE 7-2016 states that if prototype isolator testing is not conducted on full-scale specimens utilizing relevant dynamic test data conditions, then the upper and lower limits of equations 17.2-1 and 17.2-2 apply. These limits are 1.8 and 0.60 respectively.

It is noted that typical values of aging and contamination lambda factors utilized for reputable manufacturers with available qualification data are $\lambda_a = 1.1$ and $\lambda_c = 1.05$, leading to $\lambda_{ae,max}=1.16$ and, after adjustment, to a value of 1.12 (see Section 6.4). When this is implemented in equation (2-10) with default lambda factors $\lambda_{test,max}=1.3$ and $\lambda_{spec,max}=1.15$, the resulting maximum system lambda factor is calculated to be $\lambda_{max,Qd}= 1.67$. Although Section 17.2.8.4 of ASCE 7-2016 states an upper and lower limit for the system lambda factor of 1.8 and 0.6, respectively, the RDP has some flexibility in accepting data

and deciding on lambda factors. Ultimately ASCE 7-2016 requires testing, therefore the lambda factors will be based on prototype test data (or using similar unit test data) in conjunction with qualification test data and the limits need not apply.

The default lambda factors (Table 8-7) and nominal properties need to be considered in unison. ASCE 7-2016 Section 17.2.8.2 defines the nominal properties as the average properties over three cycles of motion using testing as specified by Item 2 of ASCE 7-2016 §17.8.2.2, where Item 2 (a) can be performed dynamically or at slow velocity. The velocity of testing has a significant effect on the calculated nominal properties due primarily to heating effects and secondarily to rate effects, and therefore applying the default testing lambda factors arbitrarily to account for these effects may underestimate the upper and/or lower bounds. Fundamental is to obtain the nominal properties and the $\lambda_{test,}$ values in dynamic testing of prototype isolators. This approached is followed in this report.

Table 8-7: Nominal Coefficient of Outer Surfaces Friction μ_1 and Lambda Factors- Default Values in Absence of Qualification Data

Isolator Location:	Interior	Exterior
Parameter Adjusted:	μ_1	μ_1
Testing Lambda Factors – λ_{test}		
Maximum Testing Lambda Factors		
All cyclic effects	1.3	1.3
$\lambda_{test,max}$	**1.3**	**1.3**
Minimum Testing Lambda Factors		
All cyclic effects	0.7	0.7
$\lambda_{test,min}$	**0.7**	**0.7**
Aging and Environmental Lambda Factors – λ_{ae}		
Maximum Aging & Environmental Lambda Factors		
Aging - λ_{aging}	1.3	1.3
Contamination - λ_c	1.2	1.2
$\lambda_{ae,max}$	**1.56**	**1.56**
$\lambda_{ae,max}$ after adjustment-0.75	**1.42**	**1.42**
Minimum Aging & Environmental Lambda Factors		
Aging - λ_{aging}	1	1
Contamination - λ_c	1	1
$\lambda_{ae,min}$	**1**	**1**
Specification Lambda Factors – λ_{spec}		
Maximum Specification Lambda Factor		
$\lambda_{spec,max}$	**1.15**	**1.15**
Minimum Specification Lambda Factor		
$\lambda_{spec,min}$	**0.85**	**0.85**
System Lambda Factors		
λ_{max}	**2.12**	**2.12**
λ_{min}	**0.60**	**0.60**
Upper Bound Outer Friction μ_1	**0.110**	**0.155**
Lower Bound Outer Friction μ_1	**0.031**	**0.044**
Ratio Upper/Lower	**3.5**	**3.5**

8.2.2 Prototype/Similar Unit Test Data

The configuration of the tested isolators is directly adopted for the preliminary design. Strictly speaking, Table 8-8 is for similar isolators. Since the determination of lambda values met the intent of the similar unit requirements of ASCE 7-2016, which would mean prototype testing is not required, the Table 8-8 values are reasonable to expect for prototype isolators, but for the fact that the data for the exterior isolators were incomplete so that the isolator parameters were conservatively adjusted.

Table 8-8: Coefficient of Outer Surfaces Friction μ₁ and Lambda Factors- Prototype/Similar Test Data Available

Isolator Location:	Interior	Exterior
Parameter Adjusted:	**μ₁**	**μ₁**
Testing Lambda Factors – λ_test		
Maximum Testing Lambda Factors		
All cyclic effects	1.3	1.08
λ_test,max	**1.3**	**1.08**
Minimum Testing Lambda Factors		
All cyclic effects	0.95	0.68[1]
λ_test,min	**0.95**	**0.68**
Aging and Environmental Lambda Factors – λ_ae		
Maximum Aging & Environmental Lambda Factors		
Aging - λ_aging	1.1	1.1
Contamination - λ_c	1.05	1.05
λ_ae,max	**1.16**	**1.16**
λ_ae,max after adjustment-0.75	**1.12**	**1.12**
Minimum Aging & Environmental Lambda Factors		
Aging - λ_aging	1.0	1.0
Contamination - λ_c	1.0	1.0
λ_ae,min	**1.0**	**1.0**
Specification Lambda Factors – λ_spec		
Maximum Specification Lambda Factor		
λ_spec,max	**1.15**	**1.15**
Minimum Specification Lambda Factor		
λ_spec,min	**0.85**	**0.85**
System Lambda Factors		
λ_max	**1.67**	**1.39**
λ_min	**0.81**	**0.58**
Upper Bound Outer Friction μ₁	**0.087**	**0.101**
Lower Bound Outer Friction μ₁	**0.042**	**0.042**
Ratio Upper/Lower	**2.1**	**2.4**

1. Includes an adjustment for uncertainty, see Section 7.2 for discussion.

8.2.3 Production Test Data

Table 8-9 adopts the values and assumptions from Table 8-4 directly, but now full production test data is assumed to be available to determine the actual nominal values (with the exception of the exterior isolators for which the conservatively adjusted values are still used). Hence the specification lambda factors are set to unity. The reader is referred to the introduction of Section 8.2 on the selection of the nominal values.

Table 8-9: Coefficient of Outer Surfaces Friction μ₁ and Lambda Factors- Production Test Data Available

Isolator Location:	Interior	Exterior
Parameter Adjusted:	μ_1	μ_1
Testing Lambda Factors – λ_{test}		
Maximum Testing Lambda Factors		
All cyclic effects	1.3	1.08
$\lambda_{test,max}$	**1.3**	**1.08**
Minimum Testing Lambda Factors		
All cyclic effects	0.95	0.68
$\lambda_{test,min}$	**0.95**	**0.68**
Aging and Environmental Lambda Factors – λ_{ae}		
Maximum Aging & Environmental Lambda Factors		
Aging - λ_{aging}	1.1	1.1
Contamination - λ_c	1.05	1.05
$\lambda_{ae,max}$	**1.16**	**1.16**
$\lambda_{ae,max}$ after adjustment-0.75	**1.12**	**1.12**
Minimum Aging & Environmental Lambda Factors		
Aging - λ_{aging}	1	1
Contamination - λ_c	1	1
$\lambda_{ae,min}$	**1**	**1**
Specification Lambda Factors – λ_{spec}		
Maximum Specification Lambda Factor		
$\lambda_{spec,max}$	**1.0**	**1.0**
Minimum Specification Lambda Factor		
$\lambda_{spec,min}$	**1.0**	**1.0**
System Lambda Factors		
λ_{max}	**1.46**	**1.21**
λ_{min}	**0.95**	**0.68**
Upper Bound Outer Friction μ_1	**0.076**	**0.087**
Lower Bound Outer Friction μ_1	**0.049**	**0.049**
Ratio Upper/Lower	**1.5**	**1.8**

8.2.4 Comparison of Friction Pendulum Lambda Factors

The idealized tri-linear force-displacement model of an "interior" Friction Pendulum isolator for the case of default, prototype and production lambda values are presented in Figures 8-4, 8-5 and 8-6, respectively. Each figure presents the nominal, lower and upper bound properties for the interior isolator. An exterior isolator has different nominal and lambda values. These tri-linear loops, which are the mathematical representations used for analysis, are compared in the figures to the actual prototype test data of isolator 1 for illustration purposes. It is noted that the test data from isolator 2 (Figure 7-4) was also used to determine the model loop properties, and had slightly different behavior (i.e. a higher strength). The amplitude of displacement in each of the tri-linear model loops has been calculated using the ELF procedure utilizing the MCE response spectrum for the site of the example, the isolator dimensions in Figure 7-1 (16 exterior and 16 interior isolators make up the isolation system), the nominal properties in Table 8-6 and the system lambda factors presented in Tables 8-7, 8-8 and 8-9 for the default, prototype and production values, respectively.
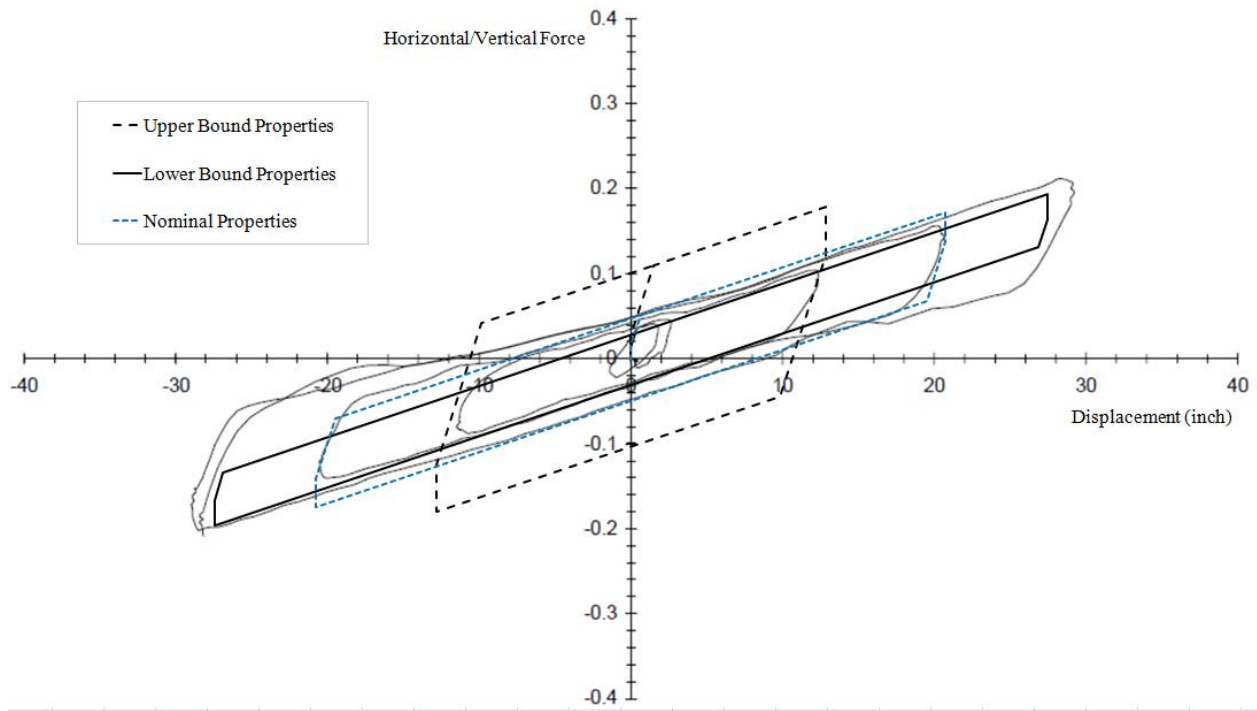
Figure 8-4: Tri-linear Model for Interior Isolator using Default Properties
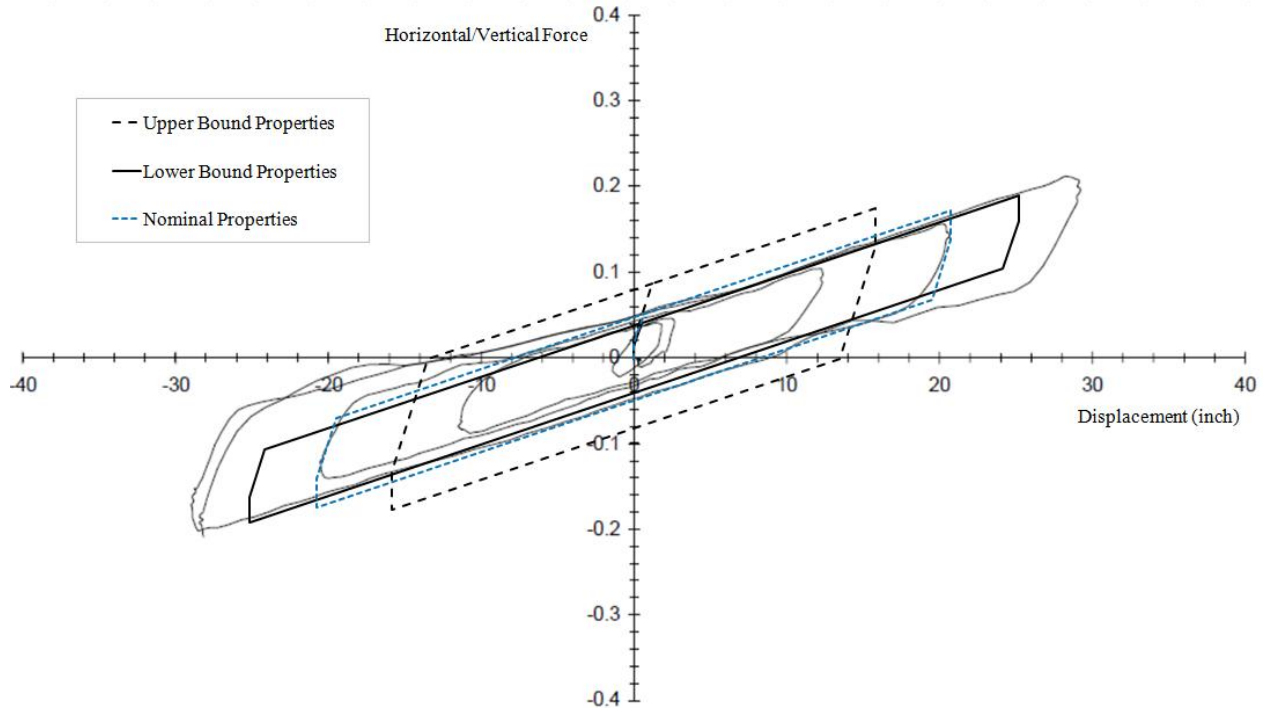
Figure 8-5: Tri-linear Model for Interior Isolator using Prototype Properties
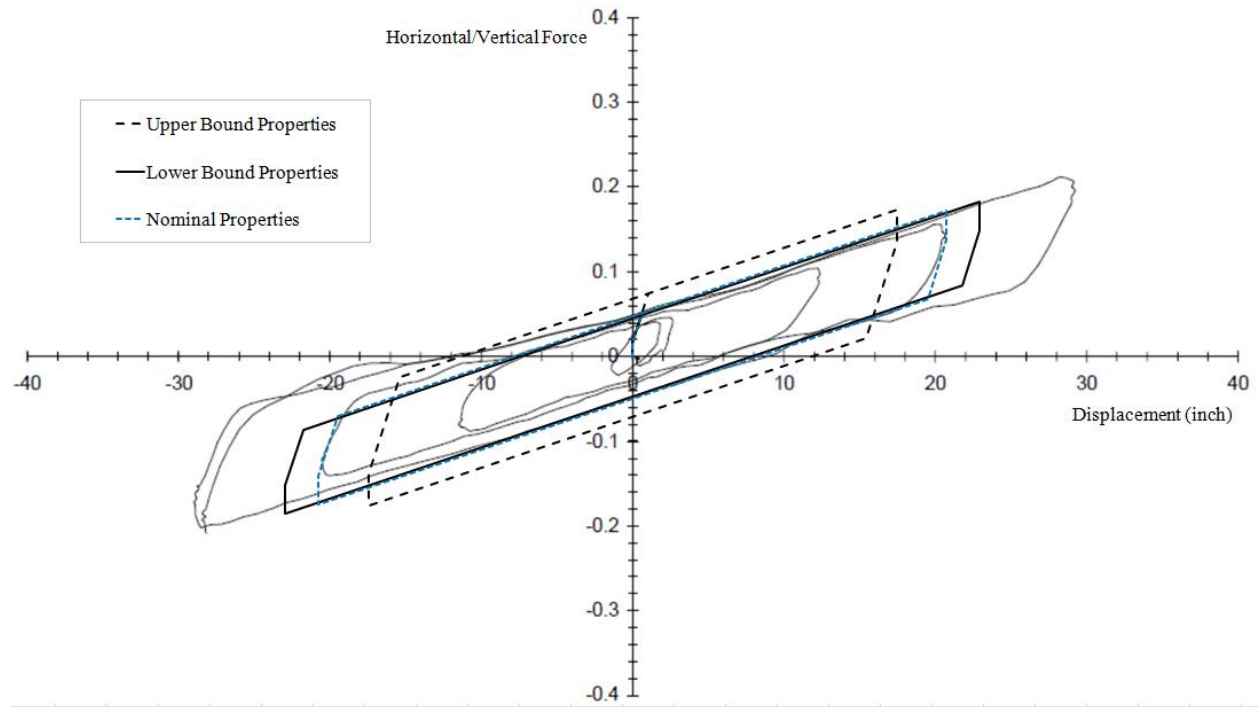
Figure 8-6: Tri-linear Model for Interior Isolator using Production Properties

120

SECTION 9
NONLINEAR RESPONSE HISTORY ANALYSIS

9.1 Introduction

Nonlinear Response History Analysis (NLRHA) was used to compare the isolation system maximum displacement and maximum base shear force obtained in different design scenarios. Three cases were considered a) no qualification data available so default values are used, case b) prototype test data are available, and case c) full production test data are available. The mathematical models in Section 2 along with the nominal properties and lambda factors summarized in Section 8 were used to calculate the upper and lower bound force-displacement behavior of the isolators for the analysis.

The NLRHA was undertaken in the program SAP2000 using the Fast Nonlinear Analysis procedure. For this analysis the nonlinear forces from the isolator elements are treated as loads on the right hand side of the equations of motions. Inherent damping was specified as 2% in each mode of vibration with override such that the damping in the first six (isolated) modes was specified as zero per procedures described in Sarlis and Constantinou (2010).

The vertical earthquake effects were not considered and, although uplift has been identified as an issue in preliminary design, this is not addressed in the NLRHA as it is not the focus of this report.

The ground motion histories and scaling were directly adopted from the SEAOC Manual (2014) and are given in Appendix A. There are seven ground motion histories hence ASCE 7 allows the average of the seven responses to be used for design. The square root sum of the squares (SRSS) at each time step is used to calculate the resultant maximum isolator displacement and shear force. Since the building is symmetrical in both directions, the earthquake records (available in fault normal and fault parallel directions) were not rotated and additional analyses were avoided.

For torsion effects, only the actual eccentricities (none in this case since the superstructure and isolation system are symmetric) were modeled. The calculated displacements and forces presented in this section do not include accidental eccentricity effects, and will need to be increased to account for torsion. For displacements, D_M can simply be multiplied by the amplification factor given in equation 17.5-3 of ASCE 7-2016. This equation is based on work by Wolff et al (2014) which rewards isolation systems configured to resist torsion. This procedure of amplifying D_M by a factor is the recommended method to account for accidental torsion in NLRHA. This is because it is problematic to artificially alter the mass and/or center

of stiffness of the model because it changes the dynamic characteristics of the model and may unintentionally improve performance. For shear and axial forces, the effects of accidental eccentricities can be accounted for by using the ELF procedure, applying the torsion to a 3D model, and superimposing the results on the NLRHA results.

For the elastomeric isolation system, the isolators are configured to resist torsion by placing the lead-rubber isolator around the exterior. The use of equation 17.5-3 of ASCE 7-2016 with e=0.05×45.72m=2.29m, b=d=45.7m, y=22.9m and P_T=2.42/2.11=1.15 results in a ratio of the total maximum displacement D_{TM} to D_M equal to 1.11, which is less than the minimum limit of 1.15. The calculation of period ratio P_T was based on eigenvalue analysis of the isolated structure using each isolator's effective stiffness calculated at the amplitude of 366mm for the lower bound properties in the case of the prototype test data (i.e. Table 8-4 lambda factors).

9.2 Elastomeric Isolation System

The SRSS maximum displacement and base shear for each design scenario and for each of the seven earthquakes are given in Tables 9-1, 9-2 and 9-3. The bilinear model used in NLRHA is based on default properties in Table 9-1, prototype properties for Table 9-2 and is based on production properties in Table 9-3. For comparison, the tables also include the ELF calculated values of the displacement and shear force. Note the acceptable accuracy of prediction of the ELF procedure, which over-predicts the displacement for the lower bound properties by about 18%, 6% and 4% in the three cases, and under-predicts the displacement for the upper bound properties by about 4%, 4% and 1% in the three cases: default, prototype and production lambda factors, respectively.

Table 9-1: NLRHA Results of Elastomeric Isolation System using Properties based on Default Lambda Factors

Ground Motion	Lower Bound		Upper Bound	
	SRSS Max Displacement (mm)	SRSS Max Base Shear (kN)	SRSS Max Displacement (mm)	SRSS Max Base Shear (kN)
GM 1	381	10448	111	16277
GM 2	413	11467	237	22623
GM 3	430	10869	224	22831
GM 4	670	16314	434	35067
GM 5	363	9333	78	14025
GM 6	299	7906	131	16672
GM 7	200	7394	180	20343
NLRHA Average	**394**	**10533 (20%[1])**	**199**	**21120 (40%[1])**
ELF	**462**	**23%[1]**	**191**	**39%[1]**

1. Percentage of seismic weight (53090kN)

Table 9-2: NLRHA Results of Elastomeric Isolation System using Properties based on Prototype Lambda Factors

Ground Motion	Lower Bound		Upper Bound	
	SRSS Max Displacement (mm)	SRSS Max Base Shear (kN)	SRSS Max Displacement (mm)	SRSS Max Base Shear (kN)
GM 1	335	12944	120	14055
GM 2	426	13897	303	21106
GM 3	325	12231	259	20985
GM 4	567	18985	451	29155
GM 5	309	11857	120	13979
GM 6	259	9600	149	15061
GM 7	188	9360	178	17036
NLRHA Average	**344**	**12696 (24%)**	**226**	**18768 (35%)**
ELF	**366**	**26%**	**218**	**35%**

Table 9-3: NLRHA Results of Elastomeric Isolation System using Properties based on Production Lambda Factors

Ground Motion	Lower Bound		Upper Bound	
	SRSS Max Displacement (mm)	SRSS Max Base Shear (kN)	SRSS Max Displacement (mm)	SRSS Max Base Shear (kN)
GM 1	292	13786	158	12783
GM 2	428	16481	366	20456
GM 3	293	13508	265	18530
GM 4	472	18594	437	24451
GM 5	265	12718	155	13454
GM 6	228	11042	169	13587
GM 7	181	10680	165	14410
NLRHA Average	309	13830 (26%)	245	16810 (32%)
ELF	320	28%	244	33%

Use of the properties based on prototype testing results in lesser displacement and lesser maximum base shear than the use of properties based on the default lambda values. What is of interest is a comparison of the range between the upper bound and lower bound isolator properties and the range of response based on those properties. The ratio of results for the ELF and NLRHA analyses and the ratio of maximum and minimum lambda factors are presented in Table 9-4 for the three design scenarios.

Table 9-4: Ratio of Lambda Factors and Bounding Analysis for Elastomeric Isolation System

Case	Description	Analysis	Lower/Upper Bound Ratio Displacement	Upper/Lower Bound Ratio Base Shear	$\lambda_{max}/\lambda_{min}$ LR Isolator		$\lambda_{max}/\lambda_{min}$ NR Isolator,
					G	σ_L	G
A	No Qualification Test Data – Default Values	ELF	2.4	1.7	3.1	3.1	3.1
		NLRHA	2.0	2.0			
B	Qualification Data and Prototype Test Data Available	ELF	1.7	1.3	1.9	2.0	1.8
		NLRHA	1.5	1.5			
C	Qualification Data and Production Test Data Available	ELF	1.3	1.2	1.4	1.5	1.3
		NLRHA	1.3	1.2			

The range in isolation system properties used for analysis is typically less than the range of the calculated response. The table also gives indication of the benefits provided when not using the default values although the above numerical results are specific to the example building and its ground motion characteristics.

For illustration, representative NLRHA force-displacement loops of a lead-rubber (LR) and a low-damping natural rubber (NR) are presented in Figures 9-1, 9-2 and 9-3 for the cases of the default, prototype and production lambda factors. The results are arbitrarily presented for ground motion GM3.
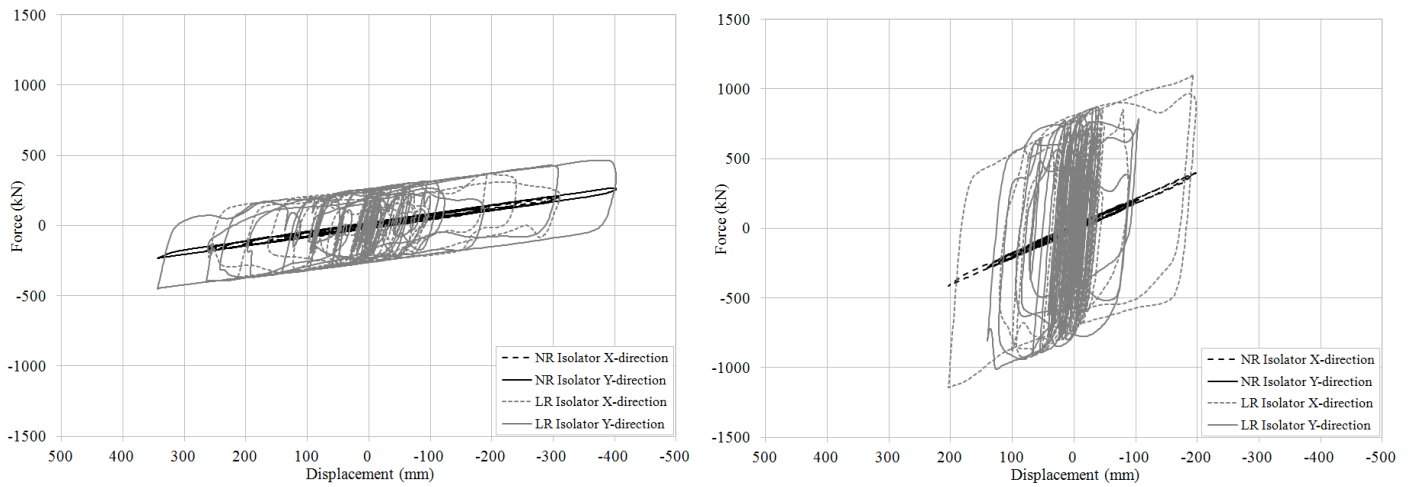
(a) Lower Bound Properties   (b) Upper Bound Properties

Figure 9-1: Force-Displacement Loops of Elastomeric Isolators for Motion GM3, Default Lambda Factors
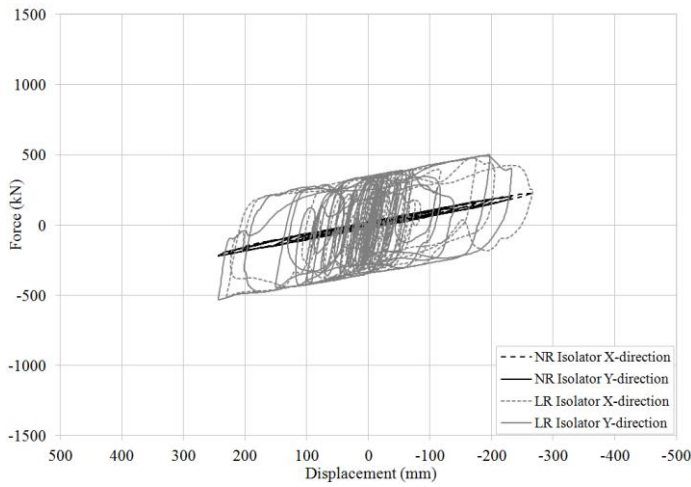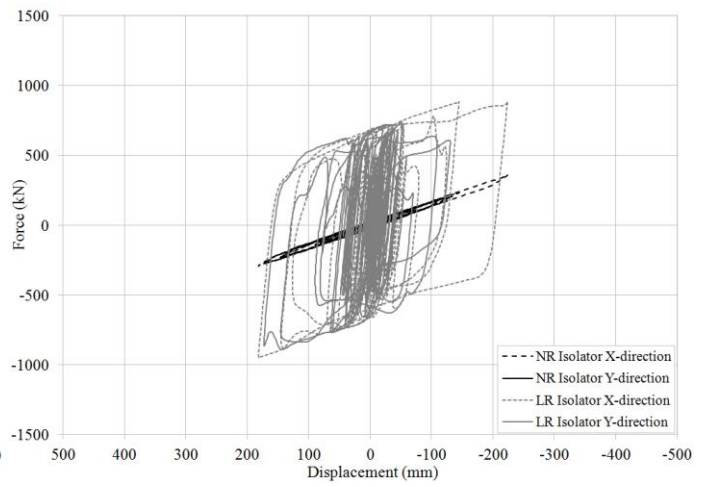
(a) Lower Bound Properties   **(b) Upper Bound Properties**

Figure 9-2: Force-Displacement Loops of Elastomeric Isolators for Motion GM3,

Prototype Lambda Factors
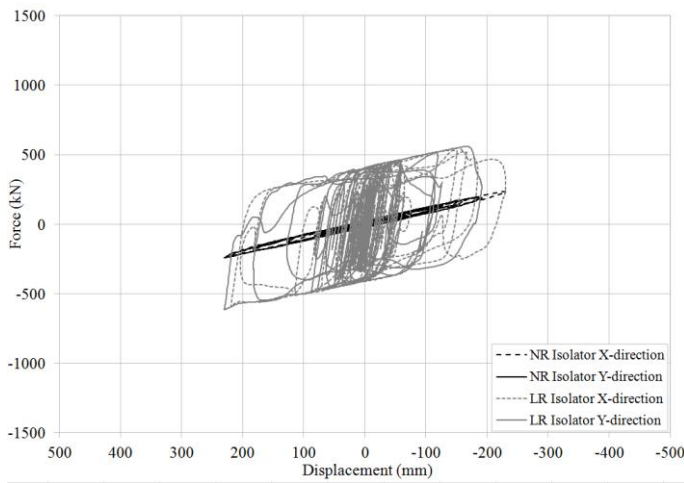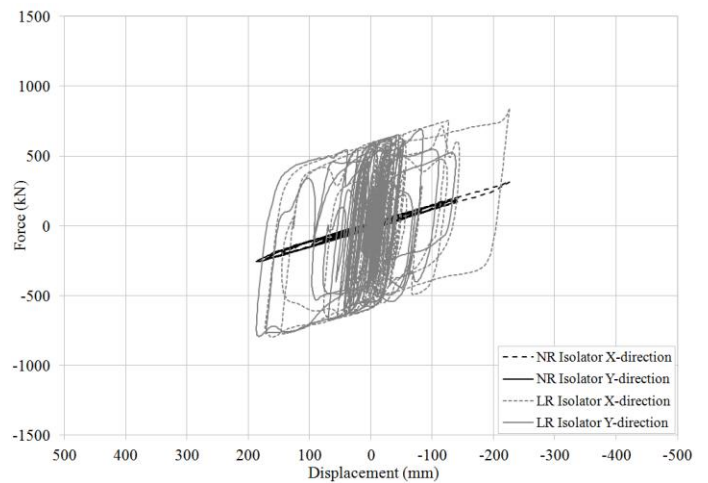
(a) Lower Bound Properties   **(b) Upper Bound Properties**

Figure 9-3: Force-Displacement Loops of Elastomeric Isolators for Motion GM3,

Production Lambda Factors

9.3   Sliding Isolation System

The NLRHA of the Friction Pendulum (FP) isolation system was undertaken in the program SAP2000 using the parallel isolator model (Sarlis and Constantinou, 2010). The behavior of the "special" triple FP isolator is accurately captured by the parallel model prior to initiation of stiffening, where the hysteretic behavior is as depicted in Figure 2-4. This model is appropriate as primarily the seismic motion is confined to the first two regimes of operation, where regime III results in stiffening to control displacements in extreme events. Sarlis and Constantinou (2010) present guidelines on how to implement the parallel and the more sophisticated series model in SAP2000 using the standard single FP element of the program. SAP2000 also has a new triple FP link element which has a resulting behavior equivalent to a series arrangement of three FP isolators, which can capture all five regimes of force-displacement behavior but is computationally more demanding than the simpler parallel model. The paper by Sarlis and Constantinou (2010) also address damping specification (i.e. control leakage), Ritz vector modes, and P-Δ analysis, which are not explicitly addressed herein.

Program SAP2000 accounts for the velocity dependence of the friction coefficient and requires "slow" and "fast" friction coefficients values and a rate parameter to be defined. The three parameters are used to calculate the friction coefficient as shown in equation (9-1), which was first proposed by Mokha and Constantinou in 1988.

$$\mu = f_{max} - (f_{max} - f_{min})e^{-aV} \tag{9-1}$$

where f_{max} is the friction coefficient at high speed ("fast"), which is calculated from prototype testing as in Section 7 and f_{min} is simply taken as half of f_{max} for this report (this is the "slow" value). The f_{max} value is specified for the analysis based on the requirements of the parallel model and the data in Tables 8-7 to 8-9. The rate parameter a controls the transition of the friction coefficient from its minimum to its maximum value and is dependent on the sliding interface. Constantinou et al (2007) recommend a rate parameter of 100mm/s (2.54in/s) for a PTFE composite. This value is used in the analysis.

Tables 9-5, 9-6 and 9-7 present the SRSS displacement and base shear force from NLRHA where the isolator models are based on default, prototype and production lambda factors. The tables also include the isolator results calculated by the ELF procedure.

127

Table 9-5: NLRHA Results of Sliding Isolation System using Properties based on Default Lambda Factors

Ground Motion	Lower Bound		Upper Bound	
	SRSS Max Displacement (mm)	SRSS Max Base Shear (kN)	SRSS Max Displacement (mm)	SRSS Max Base Shear (kN)
GM 1	537	8367	243	9735
GM 2	1020	14417	347	9997
GM 3	665	9803	313	10702
GM 4	762	10794	533	13638
GM 5	550	8111	263	9848
GM 6	526	8373	235	9628
GM 7	245	4510	177	8847
NLRHA Average	**615**	**9197 (17%[1])**	**301**	**10342 (19%[1])**
ELF	**696**	**20%[1]**	**325**	**19%[1]**

1. Percentage of seismic weight (53090kN)

Table 9-6: NLRHA Results of Sliding Isolation System using Properties based on Prototype Lambda Factors

Ground Motion	Lower Bound		Upper Bound	
	SRSS Max Displacement (mm)	SRSS Max Base Shear (kN)	SRSS Max Displacement (mm)	SRSS Max Base Shear (kN)
GM 1	457	7729	289	8457
GM 2	826	12498	325	8850
GM 3	582	9307	347	9273
GM 4	712	10612	586	12216
GM 5	467	7004	307	8268
GM 6	413	7311	265	7853
GM 7	226	4751	187	7393
NLRHA Average	**526**	**8459 (16%)**	**329**	**8901 (17%)**
ELF	**638**	**19%**	**401**	**18%**

Table 9-7: NLRHA Results of Sliding Isolation System using Properties based on Production Lambda Factors

Ground Motion	Lower Bound		Upper Bound	
	SRSS Max Displacement (mm)	SRSS Max Base Shear (kN)	SRSS Max Displacement (mm)	SRSS Max Base Shear (kN)
GM 1	429	7364	322	8043
GM 2	686	11107	367	9035
GM 3	518	8955	367	8879
GM 4	682	10694	607	11711
GM 5	433	6963	328	7704
GM 6	349	6583	277	7142
GM 7	212	4982	191	6742
NLRHA Average	**473**	**8092 (15%)**	**351**	**8465 (16%)**
ELF	**582**	**18%**	**442**	**18%**

Of interest is a comparison of the range between the upper bound and lower bound isolator properties and the range of response based on those properties. The ratio of results for the ELF and NLRHA analyses and the ratio of maximum and minimum lambda factors are presented in Table 9-8 for the three design scenarios.

Table 9-8: Ratio of Lambda Factors and Bounding Analysis for Sliding Isolation System

Case	Description	Analysis	Lower/Upper Bound Ratio Displacement	Upper/Lower Bound Ratio Base Shear	$\lambda_{max}/\lambda_{min}$ Interior Isolator μ_1	$\lambda_{max}/\lambda_{min}$ Exterior Isolator μ_1
A	No Qualification Test Data – Default Values	ELF	2.1	0.95	3.5	3.5
		NLRHA	2.0	1.1		
B	Qualification Data and Prototype Test Data Available	ELF	1.6	0.95	2.1	2.4
		NLRHA	1.6	1.1		
C	Qualification Data and Production Test Data Available	ELF	1.3	1.0	1.5	1.8
		NLRHA	1.3	1.1		

Similar to the elastomeric isolation system, there was a smaller range in the calculated response than the range of isolator properties used for analysis. These tables also present evidence of the benefits provided when not using the default values, although the above numerical results are specific to the example building and its ground motion characteristics. It is noted that for the ELF procedure the lower bound isolator properties gave a larger base shear than the upper bound isolator properties, which is why the ratio is less than 1.0. Also it so happened that the maximum base shear was not significantly affected by the bounding analysis, since the higher effective stiffness with lesser displacement (upper bound) was comparable to the lower effective stiffness with larger displacement (lower bound).

For illustration, representative NLRHA force-displacement loops of the entire isolation system are presented in Figures 9-4, 9-5 and 9-6 for the cases of the default, prototype and production lambda factors. The results are for ground motion GM3 only. The ELF calculated isolation system response is compared to the NLRHA analysis results using a bilinear hysteretic representation of the isolation system behavior, whereas, the isolators in the NLRHA are modeled as a tri-linear hysteretic representation (parallel model).
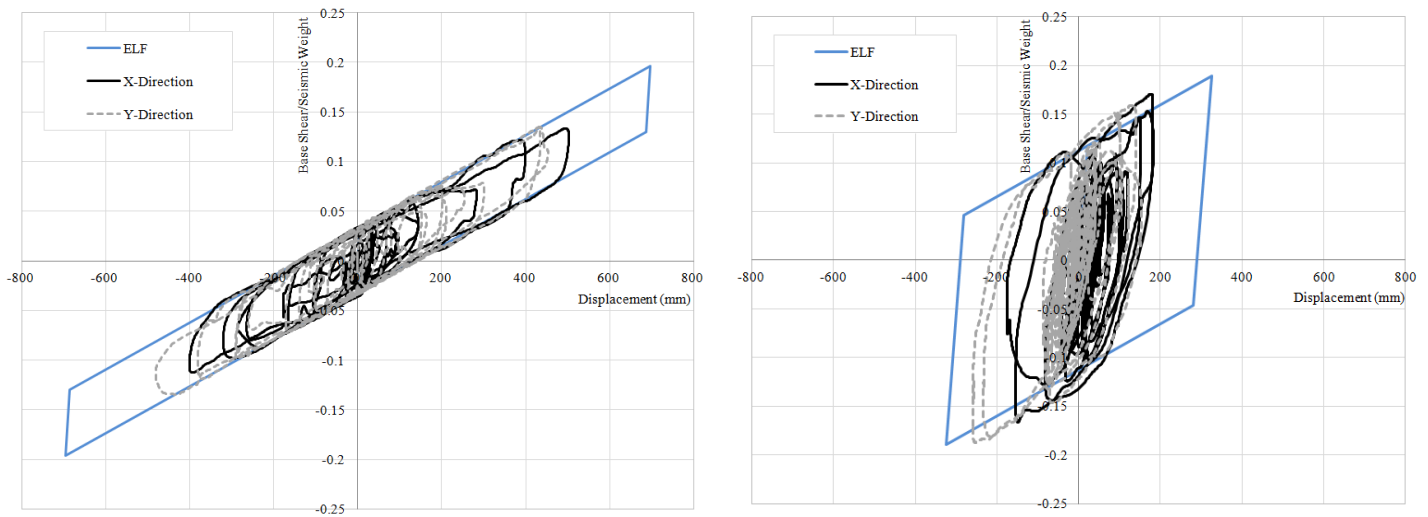
(a) Lower Bound Properties   **(b) Upper Bound Properties**

Figure 9-4: Force-Displacement Loops of Friction Pendulum Isolation System for Motion GM3, Default Lambda Factors
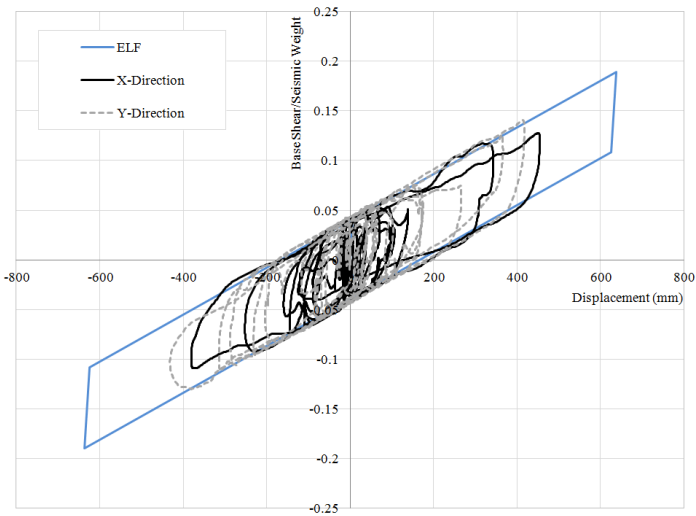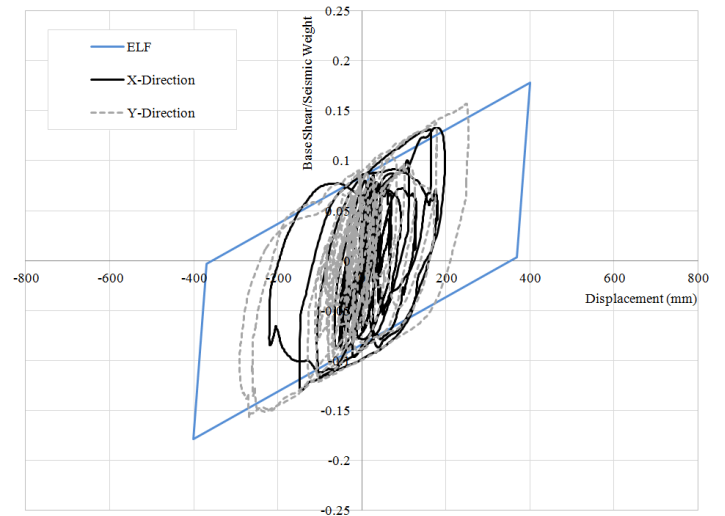
(a) Lower Bound Properties   **(b) Upper Bound Properties**

Figure 9-5: Force-Displacement Loops of Friction Pendulum Isolation System for Motion GM3, Prototype Lambda Factors
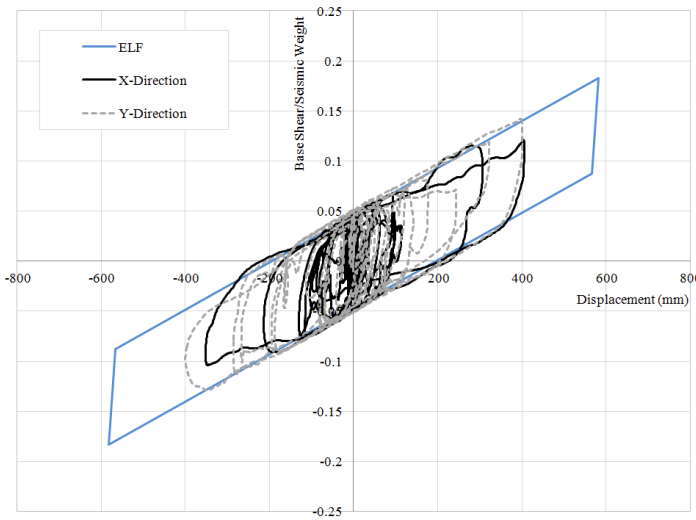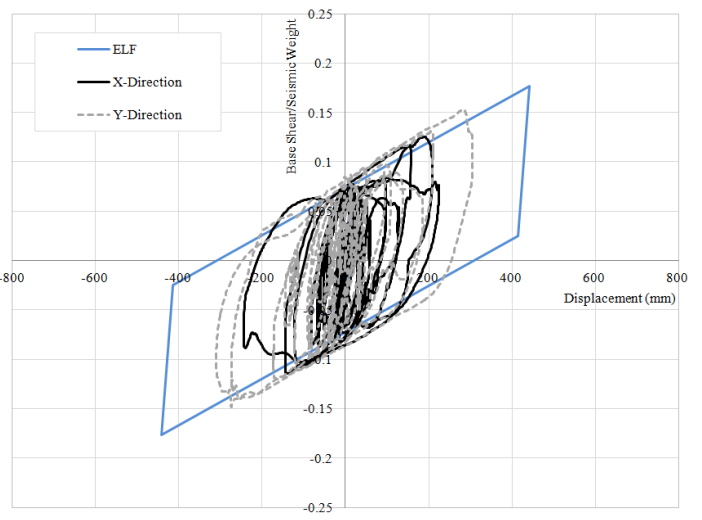
(a) Lower Bound Properties   **(b) Upper Bound Properties**

Figure 9-6: Force-Displacement Loops of Friction Pendulum Isolation System for Motion GM3, Production Lambda Factors

131

This Page is Intentionally Left Blank

SECTION 10

SUMMARY AND CONCLUSIONS

This report primarily provides guidance on how to determine the upper and lower bound properties of an isolation system for analysis and design. However, through referring to a new version of the Standard (Chapter 17 of ASCE 7-2016- see Appendix D), it was found that some requirements were inconsistent and overly conservative which prompted the need to report observations and recommendations on improvements.

The previous version of the Standard (ASCE 7-2010) simply had two clauses: §17.1.1 and §17.2.4.1 which more or less stated that "analysis shall consider variations in isolator material properties" without any further direction. Given the importance of the isolation system in reducing seismic response, along with the potential for large variations in material properties (from those assumed for design) from different manufacturers and on different projects, among other reasons, it is appropriate that ASCE 7-2016 has introduced the formal requirement of bounding analysis. The concept of using property modification factors (lambda or λ) factors originated over 15 years ago and provides a logical and practical approach to explicitly account for the variations in the nominal properties of an isolator. The Standard defines three unique categories of lambda factors. Both the aging effects and the environmental conditions lambda factors $\lambda_{ae.max}$ and $\lambda_{ae.min}$ and the manufacturing variation lambda factors $\lambda_{spec,max}$ and $\lambda_{spec,min}$ can be determined in a straightforward manner as explained in this report. However, it is the testing lambda factors $\lambda_{test,max}$ and $\lambda_{test,min}$ which can make up a significant proportion of the overall system lambda factors λ_{max} and λ_{min} and which are not clearly addressed in ASCE 7-2016.

The testing lambda factors are determined by prototype testing and intend to capture scragging, and variability and degradation in properties due to the effects of heating and speed of motion. This bounding (see Section 3.3.1 for illustration) is required because the typical models used for analysis (described in Section 2) simply assume constant properties, whereas in reality the properties instantaneously change throughout the seismic event. This is shown in the dynamic test data in Sections 6 and 7 which are tested at relevant high-speed conditions.

The opinion of the authors is that only one prototype/characterization test is required to determine the nominal properties and lambda values $\lambda_{test,max}$ and $\lambda_{test,min}$. This test is item 3 of §17.8.2.2 which consists of three fully reversed cycles of loading at the maximum (MCE) displacement D_M performed dynamically at high-speed. The $\lambda_{test,max}$ value intends to capture effects during the first cycle of motion (i.e. the upper

bound) which will certainly be experienced during an earthquake and is thus defined as the ratio of the first cycle value of the property divided by the nominal value. The $\lambda_{test,min}$ value is meant to provide a lower bound value of the property related to the expected number of cycles. Typically the expected number of cycles is small and is dependent on the properties of the isolation system and the seismic excitation. It is implied in ASCE 7-2016 that the $\lambda_{test,min}$ value is the ratio of the third cycle value of the property to the nominal value. Thus, effectively the third cycle value is utilized in the lower bound analysis. The authors of this report believe this to be unduly conservative for most cases and that the number of cycles considered for determining $\lambda_{test,min}$ should be based on rational analysis with due consideration for the properties of the isolation system, the site conditions and the ground motion characteristics, including information on proximity to the fault.

This report uses an energy equivalent approach to justify the lower bound properties (or $\lambda_{test,min}$). Representative results from Warn and Whittaker (2004) are used as a basis to determine number of cycles of prototype testing (fully reversed at the maximum displacement) that are required to give the equivalent energy as that dissipated in the actual history of bi-directional motion determined in response history analysis. As shown in Section 3.3.1, the number equivalent of cycles was calculated as two for both the elastomeric and sliding isolation system examples. As an example, prototype testing of the lead-rubber isolators gave a nominal (three-cycle average) yield strength of lead $\sigma_{L,nom}$ of 11.6MPa, $\lambda_{test,max}$=1.35 and $\lambda_{test,min}$=0.93 where the overall ratio of $\lambda_{max}/\lambda_{min}$ was 2.0. If the third cycle properties were arbitrarily set as the lower bound, as implied by ASCE 7-2016, this would give a $\lambda_{test,min}$=0.74 and corresponding $\lambda_{max}/\lambda_{min}$ ratio of 2.5. However the default values stated in ASCE 7 commentary (Appendix E) would give a smaller $\lambda_{max}/\lambda_{min}$ ratio of 1.84/0.77=2.4, which are supposed to be penalizing since no test data is available. Hence the third cycle appears overly conservative. Furthermore, studies by Kalpakidis et al (2010) show that adopting the three-cycle average value (which is representative of the second cycle) as the lower bound for bounding analysis provides conservative estimates of demands when compared to more sophisticated and realistic modeling of lead-rubber isolators which accounts for the instantaneous heating effects on the lead core strength (see Section 3.3.1 for discussion).

The lower bound for analysis may also be dictated arbitrarily by the test specimen adequacy criteria of ASCE 7-2016 §17.8.4. The checking of this criteria does not directly relate to the work in this report as a complete set of prototype test results per Section 17.8.2 does not exist. However the adequacy criteria directly refer to the lambda factors and therefore the compliance with these requirements was addressed in Sections 6.5 and 7.4 for elastomeric and sliding isolators, respectively. It is evident from discussion in

these sections, and the comparison to the properties of the prototype lead-rubber isolators in particular, that the ASCE 7-2016 adequacy criteria have two deficiencies:

1) The number of cycles required in some of the prototype tests appears as arbitrary whereas it should be related to the properties of the isolation system, and type of earthquake excitation as distinguished by proximity to fault and soil properties. The number of cycles, whether continuous sets of 5 or at least 10 depending whether the testing is dynamic or quasi-static, is generally much larger than would be expected during an MCE_R event.

2) The adequacy criteria appear as inconsistent and unrelated to the data utilized in extracting the nominal values of properties and the λ_{test} values. For example, the nominal and λ_{test} values are based on testing for 3 cycles at one amplitude of motion (D_M), whereas the adequacy criteria are based on testing for 5 or more cycles at different amplitude ($0.75D_M$) of motion.

To remedy the issues raised by this report, the authors propose the red highlighted markup of ASCE 7-2016 given in Appendix D. The key changes to the document are as follows:

- Adding language in Section 17.2.8.4 to clarify the determination of the lambda-test maximum and minimum values and leaving some room for the Registered Design Professional (RDP) to decide on a representative cycle for the lower bound.

- Editing Section 17.2.8.2 so that the Item 3 test regime of Section 17.8.2.2 can also be used to compute properties. This test is the three-cycle dynamic testing at D_M displacement amplitude which was used in this report.

- Adding clarity to the testing procedures by differentiating between quasi-static and dynamic tests.

- In the test specimen adequacy criteria, Section 17.8.4 Item 5, the language is changed to give slightly more flexibility to the RDP to determine a representative number of cycles (which is peer review approved).

- Removing Items 4 and 6 of the Section 17.8.4 Test Specimen Adequacy criteria. These criteria put limits on the allowable change in initial effective stiffness and initial effective damping which is arbitrary and inconsistent with the current test regimes. They are removed since there are already acceptance criteria for the post-elastic stiffness K_d and energy dissipated per cycle E_{loop}- which are related to the nominal values and lambda-test factors.

These changes to ASCE 7-16 would mean the procedures for bounding analysis presented in this report are in accordance with the Standard. It is noted however that the testing regimes in the Standard generally have too many cycles, since they are based on historic provisions where testing was performed quasi-statically, and therefore further changes to the testing requirements of Section 17.8.2 may be necessary in the future.

This Page is Intentionally Left Blank

SECTION 11

REFERENCES

American Association of State Highway and Transportation Officials (1999). "Guide Specification for Seismic Isolation Design", Washington, D. C.

American Society of Civil Engineers (2010). "Minimum Design Loads for Buildings and Other Structures", Standard ASCE/SEI 7-10.

American Society of Civil Engineers (2016). "Minimum Design Loads for Buildings and Other Structures", Draft Version (November 2014) of Standard ASCE/SEI 7-16.

Buckle, I., Constantinou, M. C., Dicleli, M., Ghasemi, H. (2006). "Seismic Isolation of Highway Bridges". Special Report, MCEER-06-SP07, Multidisciplinary Center for Earthquake Engineering Research, Buffalo, New York.

Constantinou, M. C., Kalpakidis, I., Filiatrault, A. and Ecker Lay, R. A. (2011). "LRFD-Based Analysis and Design Procedures for Bridge Isolators and Seismic Isolators", Technical Report MCEER-11-0004, Multidisciplinary Center for Earthquake Engineering Research, Buffalo, New York.

Constantinou, M. C., Tsopelas, P., Kasalanati, A, Wolff, E. D. (1999). "Property Modification Factors for Seismic Isolation Isolators", Technical Report MCEER-99-0012, Multidisciplinary Center for Earthquake Engineering Research, Buffalo, New York.

Constantinou, M. C., Whittaker, A. S., Kalpakidis, Y., Fenz, D. M. and Warn, G. P. (2007). "Performance of Seismic Isolation Hardware under Service and Seismic Loading", Technical Report MCEER-07-0012, Multidisciplinary Center for Earthquake Engineering Research, Buffalo, New York.

European Committee for Standardization (CEN) (2005). "Eurocode 8 – Design of structures for earthquake resistance - Part 2: Bridges", EN 1998-2:2005+A2.

Fenz, D. M., Constantinou, M. C. (2006). "Behavior of Double Concave Friction Pendulum Isolator", Earthquake Engineering and Structural Dynamics 2006, 35:1403-1421.

Fenz, D. M., Constantinou, M. C. (2008). "Development, Implementation and Verification of Dynamic Analysis Models for Multi-Spherical Sliding Isolators", Technical Report MCEER-08-0018, Multidisciplinary Center for Earthquake Engineering Research, Buffalo, New York.

Kalpakidis, I. V., Constantinou, M. C., (2008). "Effects of Heating and Load History on the Behavior of Lead-Rubber Isolators", Technical Report MCEER-08-0027, Multidisciplinary Center for Earthquake Engineering Research, Buffalo, New York.

Kalpakidis, I. V., Constantinou, M. C., Whittaker, A., W. (2010). "Modeling Strength Degradation in Lead-Rubber Bearings under Earthquake Shaking", Earthquake Engineering and Structural Dynamics, 39:1533-1549.

Kumar, M., Whittaker, A. S., Constantinou, M. C. (2014). "An Advanced Numerical Model of Elastomeric Seismic Isolation Isolators", Earthquake Engineering and Structural Dynamics, in press, published on line 2014.

Mohka, A. S., Amin, N., Constantinou, M. C., Reinhorn, A. M. (1988). "Teflon Bearings in Aseismic Base Isolation: Experimental Studies and Mathematical Modeling", Report NCEER-88-0038, National Center for Earthquake Engineering Research, Buffalo, NY.

Mohka, A. S., Amin, N., Constantinou, M. C., Zayas, V. (1996). "Seismic Isolation Retrofit of Large Historic Building", Journal of Structural Engineering, March 1996 p. 298-308.

Sarkisian, M., Lee, P., Hu, L., Doo, C. (2012). "Property Verification of Triple Pendulum Seismic Isolation Isolators", ASCE 20th Analysis & Computation Specialty Conference.

Sarlis A. A. S., Constantinou, M. C. (2010). "Modeling Triple Friction Pendulum Isolators in Program SAP2000", Technical Report released to the engineering community.

Sarlis A. A. S., Constantinou, M. C. (2013). "Model of Triple Friction Pendulum Bearing for General Geometric and Frictional Parameters and for Uplift Conditions", Technical Report MCEER-13-0010, Multidisciplinary Center for Earthquake Engineering Research, Buffalo, New York.

Structural Engineers Association of California (2014). "2012 IBC SEAOC Structural/Seismic Design Manual", Volume 5: Examples for Seismically Isolated Buildings and Buildings with Supplemental Damping, Published January 2014.

Thompson, A. C. T., Whittaker, A. S., Fenves, G. L., and Mahin, S. A. (2000). "Property modification factors for elastomeric seismic isolation isolators." Proc., 12th World Conf. on Earthquake Engineering, Auckland, New Zealand, 1–8.

Warn G. P., Whittaker, A. S. (2004). "Performance Estimates in Seismically Isolated Bridge Structures", Engineering Structures 26, 2004, 1261-1278.

Warn G. P., Whittaker, A. S. (2007). "Performance Estimates for Seismically Isolated Bridges", Technical Report MCEER-07-0024, Multidisciplinary Center for Earthquake Engineering Research, Buffalo, New York.

Wolff, E. D., Ipek, C., Constantinou, M. C., Morillas, L. (2014). "Torsional Response of Seismically Isolated Structures Revisited", Engineering Structures 59, 462-468

APPENDIX A

GENERAL BUILDING INFORMATION

A.1   General Information

- Office occupancy on all floors

- Located at a site in San Francisco, CA (site location: Latitude 37.783°, Longitude -122.392°)

- Site Class D

- Risk Category II

- The building is considered irregular per ASCE 7-2010 Table 12.3-1 item #2

- Seismic Design Category D

A.2   Building Geometry

- 45.72m by 45.72m (150ft by150ft) centerline dimension in plan with typical floor and roof framing shown in Figure A-1. The edge of deck is approximately 0.46m (1'-6") from gridline.

- Six-stories as shown in A1-2 through A1-3.

- The lateral system is a steel Special Concentrically Braced Frame (SCBF) per ASCE 7-2010 Table 12.2-1 with a frame layout of three bays on gridlines A, F, 1 and 6 per figures A-1 and A-2.
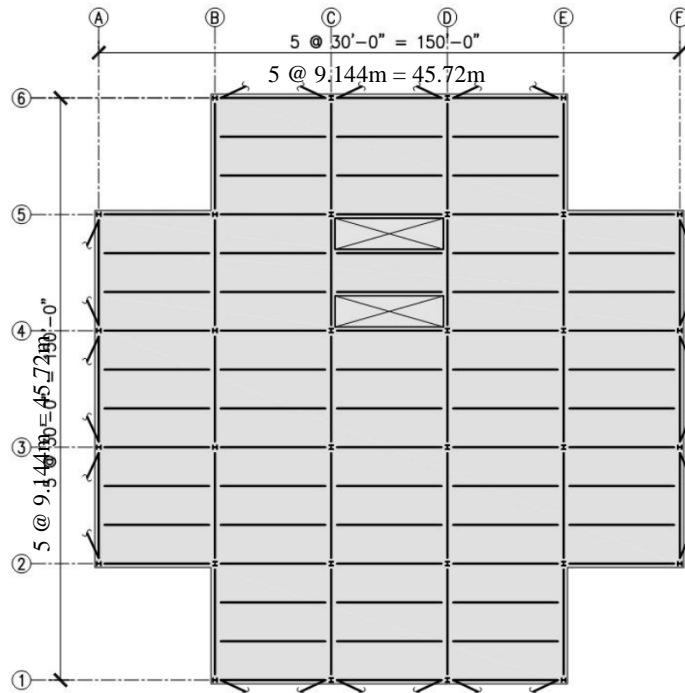
Figure A-1 Typical floor and roof framing plan
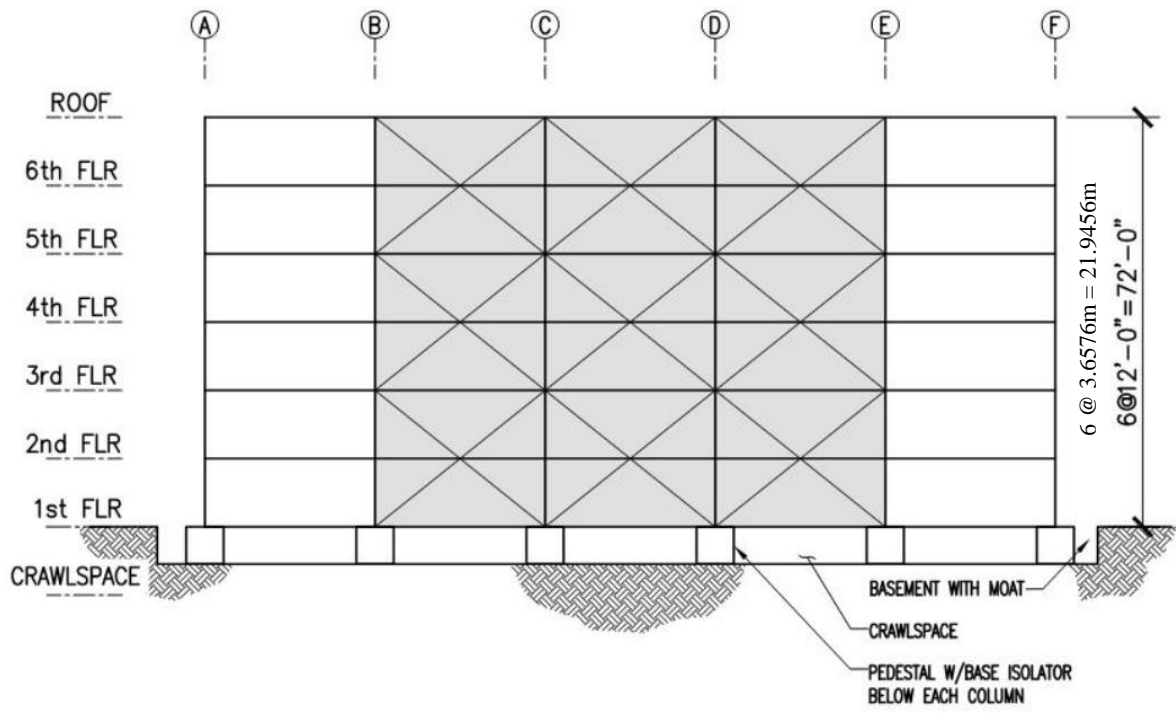
Figure A-2 Building elevation
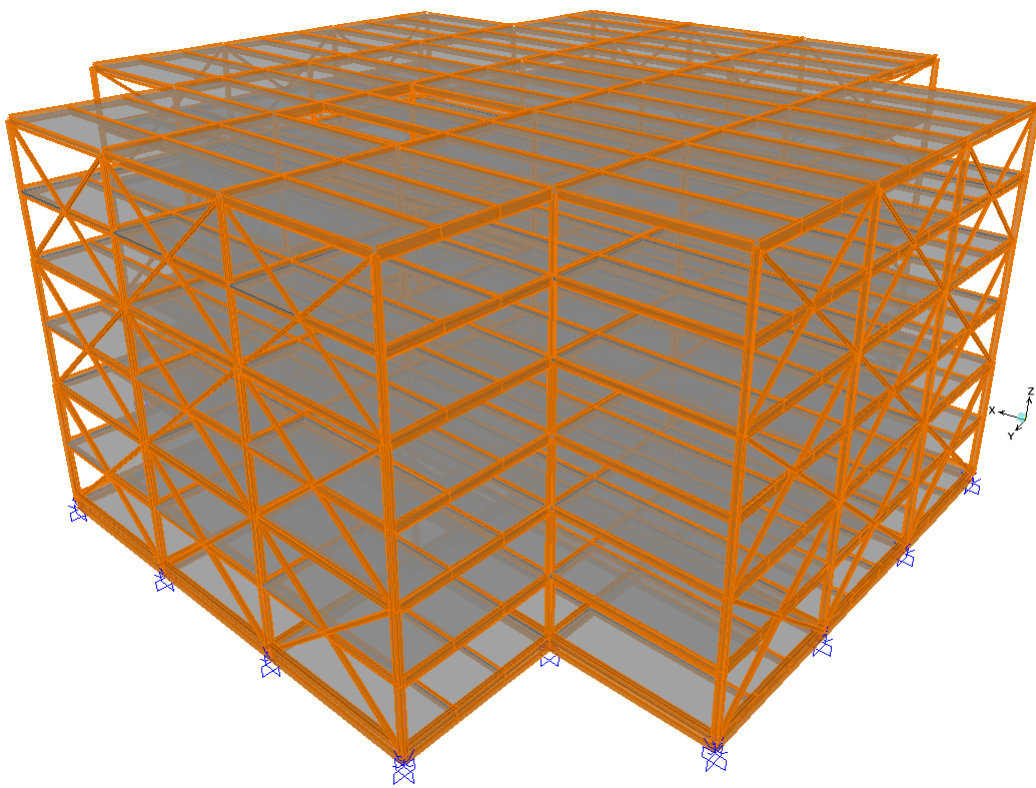
Figure A-3 Three-Dimensional Extruded Sections SAP2000 Model

A.3 Assembly Weights

The total seismic weight of the building, including the weight of the isolators (5kip) is 11,930kip or 53090kN (1kip=4.45kN and 100psf = 4.79kPa).The gravity loading comprises of:

Floor	Dead Loads	Gravity Load	Effective[3] Seismic Weight
	Floor Finish	5 psf	5 psf
	2" 18 Ga. deck	2.7 psf	2.7 psf
	3 ¼" Light-weight concrete fill	39.0 psf	39.0 psf
	Steel Framing	N/A[4]	N/A[4]
	Mechanical / Plumbing / Electrical	4 psf	4 psf
	Ceiling	4 psf	4 psf
	Partitions	Under "Live Load"	10 psf [4]
	Miscellaneous	3 psf	3 psf
	Total Dead Load	**57.7 psf**	**67.7 psf**

Office Building Live Loads [1,2]	Live Load
All Floors and Stairs = 100 psf	100 psf

Roof	Dead Loads	Gravity Load	Effective[3] Seismic Weight
	Built-Up Roof	6 psf	6 psf
	Insulation	2 psf	2 psf
	Metal Roof Deck	4 psf	4 psf
	Steel Framing	N/A[4]	N/A[4]
	Mechanical / Plumbing / Electrical	4 psf	4 psf
	Ceiling	4 psf	4 psf
	Partitions	0 psf	5 psf [4]
	Miscellaneous	3 psf	3 psf
	Total Dead Load	**23 psf**	**28 psf**

Roof Live Loads [1]	Live Load
Ordinary Flat Roof	20 psf

Exterior Wall	Dead Loads	Gravity Load	Effective[3] Seismic Weight
	Cladding	7 psf	7 psf
	Metal Studs	2 psf	2 psf
	Insulation	2 psf	2 psf
	5/8" Gypsum Board	3 psf	3 psf
	Miscellaneous	5 psf	5 psf
	Total Dead Load	**19 psf**	**19 psf**

[1] From ASCE 7 Table 4-1.
[2] ASCE 7 Section 4.3.2 specifies a 15 psf live load where partitions will be erected or rearranged. This may be omitted in this case where the live load is greater than 80psf.
[3] Per section 12.7.2, 10 psf is included for partitions where partition load is required per ASCE 7 Section 4.3.2. Only ½ of this is tributary to the roof.
[4] Explicitly accounted for in the computer model

A.4   Design Spectral Accelerations

USGS web tools can be used to determine the Risk-Targeted Maximum Considered Earthquake (MCE_R) spectral accelerations for 0.2 sec, S_S, and 1.0 sec, S_1 based on the longitude and latitude of the site. The longitude and latitude can be entered into the web application found on the USGS website at: https://geohazards.usgs.gov/secure/designmaps/us/application.php to get the S_S and S_1 values interpolated for this site. The output values are:

$S_S = 1.50g$

$S_1 = 0.60g$

The site class is D, so the factors to modify the MCE spectral accelerations are:

$F_a = 1.0$ Table 11.4-1

$F_v = 1.5$ Table 11.4-2

These values are used to modify the spectral accelerations:

$S_{MS} = F_a\, S_S = 1.0 \times 1.50 = 1.50g$ Eq 11.4-1

$S_{M1} = F_v\, S_1 = 1.5 \times 0.60 = 0.90g$ Eq 11.4-2

$T_L = 12$ seconds

A.5   Ground Motions

The seven earthquake records used for response history analysis were directly adopted from the SEAOC Design Manual (2014) and are given in Table A-1. The ground motions were amplitude scaled so that the average of the seven ground motions SRSS response spectrums was equal to or greater than the MCE_R response spectrum as illustrated in Figure A-4. The consideration for vertical earthquake effects are important, however are outside the scope of this report.

ASCE 7-2016 has specific scaling requirements which depend on the proximity to an active fault as well as whether the motions are amplitude scaled or spectrally matched. According to the Caltrans web tool (http://dap3.dot.ca.gov/shake_stable/v2/index.php) the building site is located greater than 5km from an active fault. The period range of $0.75T_M$ using upper bound default properties and $1.25T_M$ using lower bound default properties gives a range of 2.0 to 4.7 and 1.1 to 3.4 seconds for the Friction Pendulum and elastomeric isolation systems, respectively. As shown in Figure A-4, the SEAOC Manual scaled motions are greater than the MCE_R spectrum over a these period ranges and therefore the scaled ground motions are in accordance with ASCE 7-2016 requirements. It is noted that this scaling is conservative for prototype and production properties, since they would have a smaller period range.

Table A-1 SEAOC Manual Horizontal Ground Motions and Scale Factors

Ground Motion	NGA[1] Number	PEER[2] Scale Factor	SAP2000 Scale Factor (kip-inch)	Number of points in record	Time Step (second)	Event
1	175	3.9	1499	7802	0.005	Imperial Valley - 06
2	1158	1.7	641	5437	0.005	Kocaeli- Turkey
3	728	3.0	1168	8000	0.005	Superstition Hills- 02
4	864	3.2	1255	2200	0.02	Landers
5	187	3.9	1499	7866	0.005	Imperial Valley - 06
6	549	3.9	1499	7996	0.005	Chalfant Valley- 02
7	458	3.9	1499	7996	0.005	Morgan Hill

1. Next Generation Attenuation (NGA) Models for Western US (http://peer.berkeley.edu/ngawest2/)

2. Pacific Earthquake Engineering Research Centre (PEER)
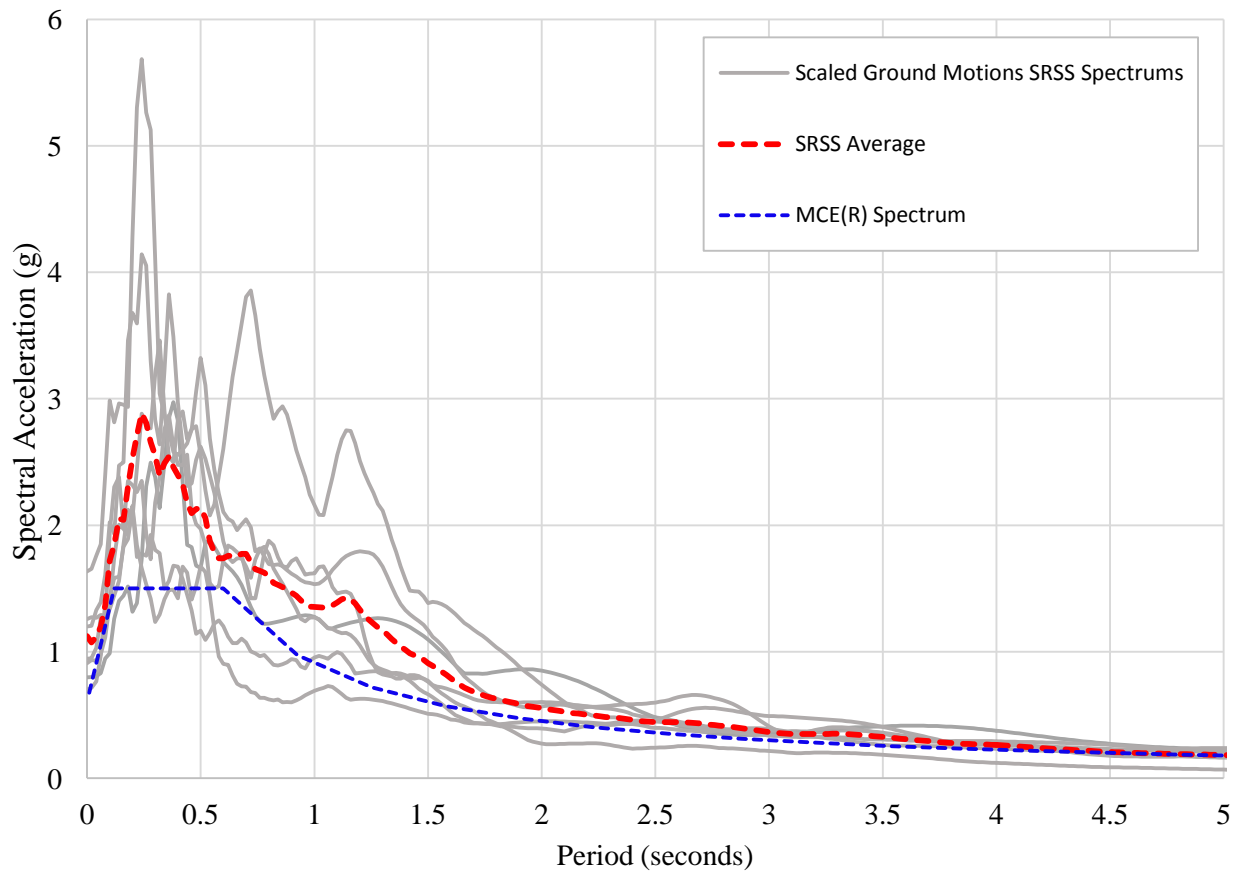
Figure A-4 Response Spectrum for Scaled Ground Motions and MCE_R

This Page is Intentionally Left Blank

APPENDIX B

PRELIMINARY DESIGN OF ELASTOMERIC ISOLATION SYSTEM

B.1   Introduction

Preliminary design is an iterative process which varies between engineers, and does not have to follow the requirements of ASCE 7-2016 necessarily. In this example there are four design iterations illustrated. The first iteration assumes there is no data available and proceeds based on a range of nominal values recommended in Constantinou et al. (2011). This gives a first estimate of the required isolator size, after which contact can be made with the manufacturer to see if similar isolators have been produced and tested. At this juncture two cases are considered. Design iteration 2 assumes that still no data is available and the isolator dimensions and layout is optimized as much as practical, which would then provide the basis for prototype testing. In the second case, test data is available (See Section 6) and the isolator dimensions and nominal properties from testing are used as a basis for the next (third) preliminary design iteration. There are no project-specific design requirements however the fourth iteration seeks to optimize the isolator dimensions and isolation system layout. This forth iteration is the "preliminary design" case stated in the body of the report under Section 5. A summary of the preliminary design calculations are provided at the end of Appendix B in Tables B-2 and B-3 in SI and Imperial units, respectively. The equations presented in the following sections use values from the first design iteration.

The analysis only considers the lower bound isolation properties, which is critical in assessing adequacy related to rubber strains, stability and displacement capacity. The upper bound analysis is typically also conducted in preliminary design as it may result in the maximum forces for the assessment of adequacy of the structure. This is not done in this report as the work concentrates on the isolation system.

A basic design procedure is outlined in Figure B-1 with note given to the relevance of each design iteration shown in Tables B-2 and B-3. The parameters D_B, D_L, T_r, are the diameter of the bonded rubber, the lead core diameter and the total thickness of rubber layers, respectively. If the manufacturer is unknown (step 3) then the Registered Design Professionals (RDP) can proceed with Case 1: No data available.

145

Step 1: Adopt Nominal Properties

The manufacturer is unknown. Select isolator nominal properties G and σ_L, based on the lower bound of the range of values recommended in Constantinou et al (2011)

Step 2: Estimate Isolator Dimensions

Determine paremters D_B, D_L and T_r and check that the isolator stability (required rubber layer thickness) is acceptable (see Design Iteration 1). The procedure and calculations are shown herein.

Step 3: Contact Manufacturer

Consult with manufacturer to obtain test data based on the inital estimate of isoaltion dimensions.

Case 1: No similar isolators have been previously manufacured and tested. Design Iteration 2 seeks to optimize bearing dimensions and the isolation system details. It may be necessary to adjust the nominal properties based on manufacturer recommendations, however no test data is assumed herein.

Case 2: Test data is available for similar isolators, produced with the same materials and manufacturing processes as that proposed for the new isolators. Adopt the nominal properties and dimensions of the similar beraings (Design Iteration 3) and refine bearing dimensions and/or isolation system details (Design Iteration 4).

Proceed with default properties and lambda factors and refine and validate later with prototype testing.

The nominal properties and associated test lambda factors are determined as shown in Section 6.

Figure B-1 Preliminary Design Procedure for Elastomeric Isolation System

B.2 Isolation Systems Characteristic Strength, $Q_{d,total}$

The strength of the isolation system $Q_{d,total}$ is a function of the lead core diameter, the effective yield stress of lead and number of isolators with a lead core. The first step involves selecting some desirable ratio of $Q_{d,total}$ to the building seismic weight W. In general, the ratio of $Q_{d,total}/W$ should be 0.05 or greater in the lower bound analysis. The effective yield stress of lead is a complex parameter as it depends on the axial load, amplitude and velocity of loading, size of lead core and manufacturer details. An approximate range of values for the average effective yield stress of lead σ_L over three cycles of high-velocity motion is 10 to 12 MPa (1.45 to 1.75 ksi) (Constantinou et al 2011). Therefore taking the lower limit of 10 MPa (1.45 ksi) and assuming 8 isolators have lead cores, the required lead core diameter is calculated as follows:

$$D_L = \sqrt{\frac{4 \times \dfrac{Q_{d,total}}{W} Ratio \times W}{\pi \times Number\ of\ lead\ cores \times \sigma_L}}$$ (B - 1)

$$D_L = \sqrt{\frac{4 \times 0.05 \times 53090 \times 10^3\ N}{\pi \times 8 \times 10 MPa}} = 206\ mm\ \ (8.1\ inch)$$

This diameter should now be rounded to a value based on isolators used in other projects. Constantinou et al (2011) states that increments in sizes of previously manufactured and tested isolators are D_L = 160 mm (6.3 in), 180 mm (7.08 in), 200 mm (7.86 in) are 220mm (8.66 in), which is to be confirmed with the specific manufacturer. Therefore a lead core diameter of $\boldsymbol{D_L}$ = **220 mm (8.66 in)** is selected here. This corresponds to a $Q_{d,total}$ of 3040 kN (683 kip) which is 5.7% of the seismic weight.

B.3   Isolation System Post-Elastic Stiffness, $\mathbf{K_{d,total}}$

The post-elastic stiffness is a function of the rubber shear modulus G, isolator diameter D_B and the total height (sum) of the individual rubber layers T_r as given in equation (2 - 2). To effectively isolate the structure, we seek the softest (lowest shear modulus) rubber to give a large period shift while maintaining compact isolators. Constantinou el al (2011) notes that the shear modulus depends on the rubber compound, conditions of loading and the amplitude and frequency of loading. A recommended average value for the shear modulus over three cycles of motion is in the range of 0.45 to 0.85 MPa (65 to 125 psi). Lower values are possible however few manufactures can reliably achieve this without experiencing significant scragging effects. Assuming we have a reputable manufacturer, a lower bound shear modulus **G = 0.45 MPa (65 psi)** is adopted. Quality manufacturers have a number of rubbers at their disposal, but the 0.45 MPa represents the soft end of the range. Very heavy structures may need stiffer rubbers.

The selection of the dimensions D_B and T_r is then based on the lead core diameter D_L calculated in Section B.2. Constantinou et al (2011) recommends (although deviation based on experience is recommended) the following rules:
   a)   The isolator diameter D_B should be in the range of 3 D_L to 6 D_L
   b) T_r should be equal to or larger than D_L

Therefore for the first design iteration the value of T_r is simply set equal to D_L, $\boldsymbol{T_r}$ = **220 mm (8.66 in)** and D_B is approximated as 4 times D_L, $\boldsymbol{D_B}$ = **880 mm (34.6 in)**.

The total post-elastic stiffness depends on the number of isolators. Typically an isolator is located beneath each column, which gives a total of 32 isolators. The first iteration assumes only 8 isolators are lead-rubber (LR) isolators (i.e. SEAOC Design Manual layout). The other 24 isolators are low-damping natural rubber (NR) isolators. For the first two iterations it is simply assumed that the NR isolators are the same dimensions as the LR isolators, but simply with the lead core removed. Therefore they have the same post-elastic stiffness. The isolation systems post-elastic stiffness is calculated as follows:

$$K_{d,total} = Number\ of\ isolators \times \frac{G\pi(D_B^{\ 2} - D_L^{\ 2})}{4T_r} \qquad \text{(B - 2)}$$

$$K_{d,total} = 32 \times \frac{0.45MPa \times \pi \times ((880mm)^2 - (220mm)^2)}{4 \times 220mm} / 1000$$

$$= 37.2kN/mm \ (212kip/inch)$$

The third and fourth iterations incorporate the information from tested isolators, which gives rise to different dimensions and a different rubber shear modulus for the NR and LR isolator (see Tables B-2 and B-3).

B.4   Lower Bound MCE Displacement

The building is approximated as a single-degree of freedom system and the maximum displacement at the isolation systems center of mass is calculated using the ELF procedure. The values for $Q_{d,total}$ and $K_{d,total}$ are based on the lower bound of properties (i.e. average over three cycles of motion). A further 0.85 adjustment is applied to these values to account for manufacturing variations. Therefore the isolation systems properties are adjusted as follows for the lower bound (LB):

$$K_{d,total\ LB} = 0.85 \times 37.2 = 31.6kN/mm \ (180kip/inch)$$

$$Q_{d,total\ LB} = 0.85 \times 3040 = 2584kN \ (581kip)$$

The equivalent lateral force procedure is an iterative process, with the calculations as follows:
   a) Assume a MCE displacement, say $D_M = 460mm$ (18inch)
   b) Calculate the effective stiffness K_M

$$K_M = K_{d,total\ LB} + \frac{Q_{d,total\ LB}}{D_M} \qquad \text{(B - 3)}$$

$$= 31.6 + \frac{2584}{460} = 37.25kN/mm \ (213kip/inch)$$

c) Calculate the effective period T_M

$$T_M = 2\pi\sqrt{\frac{W}{K_M g}} \tag{B - 4}$$

$$= 2\pi\sqrt{\frac{53090}{37.3 \times 9810}} = 2.4\,\text{sec}$$

d) Calculate the effective damping β_M. The yield displacement Y is arbitrarily assumed to be 25mm.

$$\beta_M = \frac{4Q_{d,total\,LB}(D_M - Y)}{2\pi K_M D_M^{\;2}} \tag{B - 5}$$

$$= \frac{4 \times 2584 \times (460 - 25)}{2\pi \times 37.3 \times 460^2} = 0.09$$

e) Interpolate the damping coefficient B_M from Table 17.5-1

$$B_M = 1.17$$

f) Check the displacement matches what was initially assumed

$$D_M = \frac{gS_{M1}T_M}{4\pi^2 B_M} \tag{B - 6}$$

$$= \frac{9810 \times 0.9 \times 2.4}{4 \times \pi^2 \times 1.17} = 459mm\ (18inch)\ \therefore O.K$$

B.5 Isolator Axial Loads and Uplift Potential

The axial load on each isolator depends on their relative vertical compression stiffness K_v, the rigidity of the base level diaphragm/framing and the mass distribution. This can be approximated based on a uniformly distributed mass and tributary area, or more precisely using a mathematical model. The compression stiffness of a multilayered elastomeric isolated can be approximated accordingly:

$$K_v = A\left[\sum_i t_i\left(\frac{1}{E_{ci}} + \frac{4}{3K}\right)\right]^{-1} \tag{B - 7}$$

where t_i is the individual rubber layers thickness, E_{ci} is the compression modulus for incompressible material behavior which is dependent on the rubber shear modulus, shape factor and the isolator geometry (see Constantinou et al, 2007) and K is the bulk modulus of rubber, typically assumed as 2000MPa (290ksi). The compression stiffness for the LR and NR isolators was calculated as 1805 kN/mm (10300 kip/in) and 1525 kN/mm (8700 kip/in). These stiffnesses are for the final isolator geometry (iteration 4); nevertheless the relative stiffness between the LR and NR isolators should be similar for the other design iterations to result in an appropriate distribution of axial loads.

The seismic weight less the partition weight gives a total dead load, D = 53090 − 5295 = 47795kN (10740kip). The unreduced live load is 50490kN (11346kip) which is then multiplied by a 0.4 factor based on the limit for the uniform live load reduction formula to give a live load of L = 20196kN (4538kip). It is noted that the seismic weight of 53090kN used for analysis is slightly different from the load combination of D+0.5L = 57893kN. Using a SAP2000 analysis, the axial load for various isolator locations is calculated to be:

- Interior Isolator Grid 3/C: D = 1924 kN (432 kip) L = 942 kN (212 kip)
- Re-entrant corner Isolator Grid 2/E: D = 1838 kN (413 kip) L = 756 kN (170 kip)
- Exterior Inside Isolator Grid 1/D: D = 1257 kN (282 kip) L = 443 kN (100 kip)
- Exterior Corner isolator Grid 1/E: D = 913 kN (205 kip)   L = 290 kN (65 kip)

To assess the potential for isolator uplift there must be an estimate of the seismic overturning from the superstructure. This is calculated from the ELF procedure using the lower bound properties. It is noted that the upper bound properties may give a larger lateral seismic force V_b; however the lower bound properties will give a ball-park first estimate (i.e. small effective stiffness and large displacement vs. large effective stiffness and smaller displacement). The minimum design lateral seismic force is calculated as follows:

$$V_b = K_M D_M \tag{B - 8}$$

$$= 37.25 \times 457 = 17023 kN \ (3825 kip)$$

This base shear of 17023 kN (or 17033 kN in Table B-1 without rounding error) is then distributed up the height of the building according to the revised provisions of ASCE 7-2016, Section 17.5.5. These provisions are considered to give a more accurate distribution of the shear over height considering the period of the superstructure and isolation system's effective damping. Table B-1 gives illustration of the procedure and equations in ASCE 7-2016 Section 17.5.5. Some key assumptions in these calculations are as follows:

- There is no reduction of forces. Even if the superstructure forces are reduced by an R factor, the design of the isolation systems elements for overturning loads shall be based on R = 1.0 or the unreduced lateral seismic force V_b (Section17.5.4).
- The fixed-base fundamental period T_{fb} is calculated as 0.6 seconds from a SAP2000 analysis, or could be approximated quickly using ASCE 7 Equation 12.8-7.
- There are two Concentrically Braced Frames (CBF) in each principle building direction, with the force per level F_x being evenly distributed to each CBF.

- The orthogonal earthquake effects on axial load are considered to be minor as the lateral-load resisting systems for two perpendicular directions do not share a similar column.
- Torsion is taken as the minimum required by ASCE 7-2016: accidental eccentricity of 5% times the length of the building, all in the same direction for each level.

The effects of torsion result in increases of the forces on one frame and decreases of the forces on the other. Here the most critical frame is shown in Table B-1. The force per level is then multiplied by its respective height to get the overturning moment. The uplift and compression force on the exterior columns of the CBF frame was calculated assuming a linear distribution of resistance across the four isolators.

Table B-1 Preliminary Design Structural Overturning, Iteration 1

Level	Height (m)	Weight (kN)	$w_x h^k_x$	C_{vx}	F_x (kN)	Torsion (kN-m)	CBF Force (kN)	Over-turning (kN-m)
Roof	21.9	3560	40138	0.14	1982	4530	1090	23918
6	18.3	7988	78059	0.26	3854	8809	2120	38762
5	14.6	7988	65525	0.22	3235	7395	1779	26030
4	11.0	7988	52289	0.18	2581	5901	1420	15579
3	7.3	7988	38044	0.13	1878	4294	1033	7557
2	3.7	7988	22089	0.07	1091	2493	600	2194
1 (Base)	0.0	9590	n/a	n/a	2412[1]	5515	n/a	n/a
Totals =		53089[2]	296144	1	17033		8041	114039

1. From ASCE Equation 17.5-8 with no reduction (R = 1.0). This force does not contribute to superstructure overturning.
2. Includes the isolator's weight

The resulting tension/compression axial load on the exterior isolators (i.e. corner 1/E) is 3742 kN (841 kip), whereas the factored dead load, 0.9D, for these corner isolators is only 913 kN (205 kip). The tension in the critical corner isolators is approximated from the following load combination:

$$(0.9 - 0.2 S_{MS})D + \rho Q_E$$

$$= (0.9 - 0.2 \times 1.5) \times 913 - 1.0 \times 3742 = -3194 kN \ (-718 kip)$$

In this calculation $0.2S_{MS}$ is used to account for vertical earthquake effects and the redundancy factor ρ is set to 1.0. The conservative basis of the calculation is noted in the assumption that the vertical ($0.2S_{MS}$) and lateral earthquake (Q_E) effects are assumed to be in unison.

Tension in lead-rubber isolators should be avoided. Nevertheless, Constantinou et al (2007) states that high quality isolators can sustain a tensile pressure of about 3G before cavitation occurs (where G is the shear modulus of rubber). Well-made isolators can sustain extension without resistance beyond the limit of tensile displacement at initiation of cavitation, however this cannot be known without testing of the production isolators and testing will damage the isolators. Accordingly, it is recommended to avoid tension beyond the tension capacity, $3GA_r$ which is 770 kN (175 kip) for this application and therefore well short of the uplift demand. It is noted that these are simplified conservative calculations. For example, the overturning analysis is only for a 2-dimensional frame. In reality the framing in the perpendicular direction will distribute the localized demands to other isolators. ELF forces applied to a 3D mathematical model would give a more refined estimate of uplift demands. Regardless, from this early stage we can see that uplift is a significant issue for the 8 corner isolators under the CBF exterior columns (i.e. Grids 1/B, 1/E, 2/A, 2/F, 5/A, 5/F, 6/B and 6/E). There are various options and combinations of these options to mitigate the uplift issue, as follows:

1. Change the structural system to eliminate or reduce isolator tension to an acceptable level, by:
   a. Increasing the number of bays with a CBF.
   b. Moving the CBF to a location where the end columns have a higher dead load.
   c. Adopting or incorporating a different lateral load resisting structural system.
   d. Stiffening the beams above the isolators to distribute the tension load over a larger number of isolators.
2. Change the layout of the isolation system, change the isolator connection details and allow for limited and controlled uplift. The 2012 SEAOC layout has all the lead-rubber isolator on the corners of the building, directly under the end columns of the CBF. This is the location where the axial dead load is the smallest and where the overturning forces from the structural system are the greatest. An improvement would be to place the lead-rubber isolators on the exterior (i.e. Grids A/3, A/4, C/1, C/6, D/1, D/6, F/3, and F/4) and have isolators which are not integral to the energy dissipation of the isolation system on these corners. Various options for the 8 corner isolators that are subject to uplift include:
   a. Natural rubber isolators with one end bolted and the other end recessed/slotted to allow for controlled uplift.
   b. Use of sliding isolators.

These options require explicit modelling of the uplift behavior to quantify effects of isolator uplift (see Kumar et al, 2014). Testing under these conditions will also be required.

3. Use uplift restraining systems.

The final isolation system layout is illustrated in Figure 5-2 with the corner isolators adopting approach 2a) in the recommendations above. Further commentary on modeling and testing for uplift is outside the scope of this report.

B.6 Rubber Layer Thickness Required for Isolator Stability

The isolator stability is a critical check in the selection of preliminary isolators. The process and equations that follow are sourced from the Constantinou et al (2011) report. For a hollow circular isolator, the buckling load in its un-deformed configuration P_{cr} is calculated as follows:

$$P_{cr} = 0.218 \frac{GD_o^4}{tT_r} \frac{\left(1 - D_i/D_o\right)\left(1 - D_i^2/D_o^2\right)}{1 + D_i^2/D_o^2} \tag{B - 9}$$

where t is the thickness of individual rubber layers, D_o and D_i are the outside and inside bonded diameters, respectively and T_r is the sum of individual rubber layers. The lead core is assumed not to contribute to the buckling capacity.

When a bolted isolator is subjected to combined compression and lateral deformation, the buckling load P'_{cr} is given by the following empirical expression based on the reduced area of rubber:

$$P'_{cr} = P_{cr} \frac{(\delta - \sin \delta)}{\pi} \tag{B - 10}$$

In equation (B-10) the value of quantity δ is given by:

$$\delta = 2cos^{-1}\left(\frac{\Delta}{D}\right) \tag{B - 11}$$

where Δ is the lateral deformation of the isolator. For the MCE check, the ratio of the buckling capacity under lateral deformation, P'_{cr}, divided by the factored axial compression load should be larger than 1.1.

Using the equations above and rearranging equation (B-9), one can calculate the maximum allowable rubber layer thickness to ensure stability, and of a thickness that is economical to construct. This check is critical under a combination of large displacements and large axial loads. For this preliminary stage,

153

conservatism is used by adopting the maximum axial load combination (i.e. interior or exterior location) and the displacement based on an exterior isolator with accidental torsion. The axial load is calculated for an internal and corner isolator as follows:

$$Load\ Combination = (1.2 + 0.2S_{MS})D + L + \rho Q_E$$

$$Interior\ Isolator = (1.2 + 0.2 \times 1.5) \times 1924 + 942 + 1.0 \times 0 = 3828\ kN\ (860\ kip)$$

$$Corner\ Isolator = (1.2 + 0.2 \times 1.5) \times 913 + 290 + 1.0 \times 3765 = 5424\ kN\ (1219\ kip)$$

The maximum MCE displacement D_M calculated from the ELF method is for the center of mass and does not include additional displacements due to actual and accidental torsion. Here there are no actual eccentricities and the accidental eccentricity is taken as the prescribed distance of 0.05 times the longest plan dimension of the building. In ASCE 7-2016 the total maximum displacement D_{TM} is calculated by amplifying the maximum displacement D_M by a factor given by equation 17.5-3.

A SAP200 modal analysis was used to calculate a ratio of the translation period (first mode) divided by the torsional period (third mode), P_T of 2.32/2.02 = 1.15. This is for Design Iteration 4 isolator details, as per the configuration in Figure 4-2 with effective stiffnesses (used for linear analysis) based on the displacement D_M from the ELF method. Using Equation 17.5-3, with an eccentricity of 7.5ft, gives a D_{TM} of 1.11 times D_M. The displacement is further increased to $1.2D_M$ to account for the orthogonal earthquake effects. For the first design iteration, this gives a total maximum displacement of:

$$D_{TM} = 1.2D_M = 1.2 \times 460 = 550\ mm\ (21.7\ in)$$

Based on this displacement of 550mm and compressive load of 5410 kN, the required rubber layer thickness is calculate to be, at most, 7.7mm. The rubber layer thickness should be at least 5-6mm to be economical, otherwise the isolator dimensions or isolation system properties should be revised.

The procedure described in the preceding sections of this Appendix can be incorporated into a spreadsheet to quickly iterate to an optimal solution. This was implemented and the key results are presented in Tables B-2 and B-3 for SI and Imperial units, respectively. In the tables there are three key classes of variables a) the nominal properties, b) the isolator dimensions, and c) the isolation system details (i.e. number of LR and NR isolators). With these inputs, the ELF procedure is conducted to find the convergent displacement. Then the rubber layer thickness can be check to see if it is greater than a 5-6mm limit. It is noted that this spreadsheet is specific for this building and structural layout but can be adapted for other projects.

154

Table B-2 Preliminary Design Iterations, SI Units

Property	Symbol	Iteration 1	Iteration 2	Iteration 3	Iteration 4	Units
Nominal Properties[1]						
Effective Lead Yield Stress	$\sigma_{L,nom}$	10.00	10.00	11.60	11.60	MPa
LRB Rubber Shear Modulus	$G_{nom,LR}$	0.45	0.45	0.40	0.40	MPa
NRB Rubber Shear	$G_{nom,NR}$	0.45	0.45	0.49	0.49	MPa
Isolator Dimensions						
LR Bonded Rubber	$D_{B,LR}$	880	800	850	800	mm
Lead Core Diameter	D_L	220	220	220	220	mm
NR Bonded Rubber	$D_{B,NR}$	880	800	850	750	
NR Mandrel/Hole Diameter	D_{hole}	220	220	70	70	
Total Rubber Thickness	T_r	220	220	203	203	mm
Total Post-elastic Stiffness	$K_{d,total\ LB}$	31.6	25.8	35.0	27.3	kN/mm
Total Characteristic Strength	$Q_{d,total\ LB}$	2584	3877	2998	4497	kN
Isolation System Details						
Number of LR Isolators	LRB #	8	12	8	12	
Number of NR Isolators	NR #	24	20	24	20	
ELF Procedure						
MCE Displacement	D_M	457	389	414	350	mm
Effective Stiffness	$K_{M,min}$	37.3	35.7	42.1	40.2	kN/mm
Effective Period	T_M	2.38	2.45	2.24	2.31	sec
Effective Damping	β_M	0.09	0.17	0.11	0.19	
Damping Factor	B_M	1.17	1.41	1.22	1.49	
Required Rubber Layer Thickness						
Structural Base Shear	$V_{b\ LB}$	17033	13890	17436	13977	kN
Ratio of Seismic Weight	V_b	0.32	0.26	0.33	0.26	
Dead Load	P_D	912	912	912	912	kN
Live Load	P_L	289	289	289	289	kN
Horizontal EQ (Overturning)	Q_E	3,741	3,489	3,921	3,641	kN
Vertical Effects ($0.2S_{MS}D$)	0.3D	274	274	274	274	kN
$(1.2 + 0.2S_{MS})D + Q_E + L$	P_u	5,399	5,147	5,579	5,299	kN
Drift x 1.2 factor	D_{TM}	549	466	497	418	mm
Delta	δ	1.80	1.90	1.89	2.04	
Nominal Shear Modulus	G_{nom}	0.45	0.45	0.40	0.40	MPa
Rubber thickness for stability	**t**	**7.75**	**6.07**	**7.16**	**6.9**	**mm**

Note 1: Multiply the nominal properties by a 0.85 factor for the lower bound properties

Table B-3 Preliminary Design Iterations, Imperial Units

Property	Symbol	Iteration 1	Iteration 2	Iteration 3	Iteration 4	Units
Nominal Properties[1]						
Effective Lead Yield Stress	$\sigma_{L,nom}$	1.45	1.45	1.682	1.682	ksi
LRB Rubber Shear Modulus	$G_{nom, LR}$	65	65	58	58	psi
NRB Rubber Shear Modulus	$G_{nom, NR}$	65	65	71	71	psi
Isolator Dimensions						
LR Bonded Rubber Diameter	$D_{B, LR}$	34.64	31.5	33.5	31.5	in
Lead Core Diameter	D_L	8.66	8.66	8.66	8.66	in
NR Bonded Rubber	$D_{B, NR}$	34.64	31.5	33.5	29.5	in
NR Mandrel/Hole Diameter	D_{hole}	8.66	8.66	2.756	2.756	
Total Rubber Thickness	T_r	8.66	8.66	8	8	in
Total Post-elastic Stiffness	$K_{d,total\ LB}$	180	147	200	155	kip/in
Total Characteristic Strength	$Q_{d,total\ LB}$	581	871	674	1011	kip
Isolation System Details						
Number of LR Isolators	LRB #	8	12	8	12	
Number of NR Isolators	NR #	24	20	24	20	
ELF Procedure						
MCE Displacement	D_M	18	15.3	16.3	13.7	in
Effective Stiffness	$K_{M,min}$	213	204	241	229	kip/in
Effective Period	T_M	2.38	2.45	2.24	2.31	sec
Effective Damping	β_M	0.09	0.17	0.11	0.20	
Damping Factor	B_M	1.17	1.41	1.22	1.49	
Required Rubber Layer Thickness						
Structural Base Shear	$V_{b\ LB}$	3828	3121	3918	3141	kip
Ratio of Seismic Weight	$V_{b\ LB}/W$	0.32	0.26	0.33	0.26	
Dead Load	P_D	205	205	205	205	kip
Live Load	P_L	65	65	65	65	kip
Horizontal EQ (Overturning)	Q_E	841	784	881	818	kip
Vertical Effects ($0.2S_{MS}D$)	0.3D	62	62	62	62	kip
$(1.2 + 0.2S_{MS})D + Q_E + L$	P_u	1213	1157	1254	1191	kip
Drift x 1.2 factor	D_{TM}	21.6	18.4	19.6	16.4	in
Delta	δ	1.80	1.90	1.89	2.04	
Nominal Shear Modulus	G_{nom}	0.065	0.065	0.058	0.058	ksi
Rubber thickness for stability	**t**	**0.305**	**0.239**	**0.282**	**0.272**	**inch**

Note 1: Multiply the nominal properties by a 0.85 factor for the lower bound properties

APPENDIX C

PRELIMINARY DESIGN OF SLIDING ISOLATION SYSTEM

C.1 Introduction

A different method to that in the SEAOC Design Manual is illustrated for preliminary design. The preliminary design is based on the approach presented in the Constantinou et al. (2011) Appendix C example. The method does not require NLRHA, instead it utilizes simplified calculations based on the equivalent lateral force (ELF) procedure to obtain a reasonable estimate of global response. A *special* type of triple Friction Pendulum (FP) is adopted for design (it is defined in Section 2.3). This reduces the parameters defining the force-displacement behavior from 16 to 8 (6 geometric and 2 friction parameters).

Optimization of the 8 parameters of a triple friction pendulum (FP) isolator is impractical. Although parametric studies will give a theoretical understanding of the tradeoff between forces and displacements, "optimized" isolator configurations that have not been previously manufactured are likely to be much more expensive and would require longer time to manufacture, test and deliver. Furthermore, without testing there will be more uncertainty in performance. The best strategy, as stated in Constantinou et al (2011), is to contact the manufacturer of triple FP isolators and request proposals for isolator configurations that are most suitable for the application (i.e. trial designs) that can then be evaluated by the registered design professional (RDP). The preference is to use standard isolator components and configurations and prototype test data, so that there is a direct development of the isolator systems properties.

It is assumed that the manufacturer recommends the isolator shown in Figure 7-1. The dimensions of this recommended isolator, along with prototype test data can be used directly to check if it satisfies the design requirements, as shown in Section C.3 below. The preliminary design also explores a number other scenarios. In Section C.2 there is discussion on the scope for altering the recommended isolator's geometric parameters (i.e. the isolator's post-elastic stiffness parameter R_1 and displacement capacity d_1). Section C.4 then follows the procedure by Constantinou et al, (2011) and shows how to calculate the friction coefficients based on qualification test data, say in the case where the preliminary design is performed without having prototype test data or the available test data are for isolators that do not meet the similarity requirements of ASCE 7-2016. Calculating friction coefficients is an involved process and does not necessary lead to improved accuracy. However Section C.4 gives insight into how the friction coefficient varies due to isolator pressure, velocity and frictional heating. In practice it is more common for the RDP to simply specify a friction coefficient, within a range, and then the manufacturer will use

their proprietary manufacturing methods and/or change the isolator dimensions to actually achieve this value for the project specific loading conditions.

C.2 Isolator Geometric Parameters

As discussed earlier, contact should be made with a manufacturer to obtain a list of standard isolator dimensions. The radius of curvature of the outer concave plate R_1 (=R_4), along with the friction coefficient on the outer surfaces μ_1 (=μ_4), are critical parameters governing the overall isolator response during significant earthquake excitation. It is sensible for the RDP to only consider the optimization of these parameters at the preliminary design stage, with input from the manufacturer on the selection of other geometric parameters.

In addition to the 6 dimensions that define the force-displacement behavior of the *special* FP isolator, the RDP may also require the diameter of the rigid D_R and articulated sliders D_S (see Figure C-1). This is to calculate the isolator pressure on the inner and outer surfaces and, as shown in SectionC.4, the friction coefficient. Manufacturing constraints for the isolator dictates the useful range of some of the dimensions and are normally determined by the manufacturer.
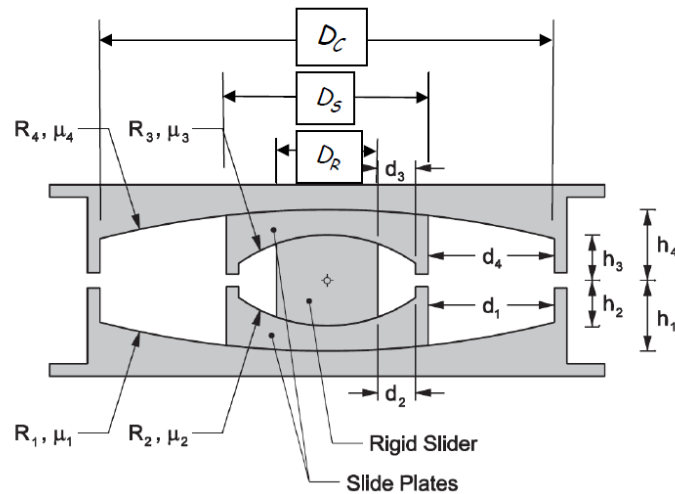
Figure C-1: Special Triple Friction Pendulum Isolator Details

A partial list of the previously manufactured concave plates is given in Table 4-2 of Constantinou et al (2011), with radii of curvatures of 1555mm (61 inch), 2235mm (88 inch), 3048 (120 inch), 3962mm (156 inch) and 6045mm (238 inch). The larger the radius of curvature, the lower the post-elastic stiffness is. This typically results in a lower structural shear at the cost of a larger maximum displacement. In the instance where displacements may not be a governing design criterion, the RDP must still consider the isolation systems lateral restoring force capability, which places a practical limit on the size of R_1. ASCE 7-2016 §17.2.4.4 requires that the force at maximum displacement is at least 0.025W greater than the

force at 50% of the corresponding maximum displacement. By requiring a strong restoring force, cumulative permanent displacements are avoided and the prediction of displacement demand is accomplished with less uncertainty.

The trial designs received from the manufacture may be based on previously manufactured isolators with similar design conditions, or perhaps the manufacturer has already produced and tested the isolators. In this case the manufacturer is able to provide details of an isolator used on a previous project which was tested under similar axial loads (and displacements) to that calculated in the preliminary design. The geometry of the isolator is provided in Figure 7-1.

Here the radius of the outer concave plate R_1 (=R_4) of 2235mm (88inch) and the displacement d_1 (=d_4) of 406mm (16inch), shown in Figure C-1 or 7-1, can be altered with minor effects of the validity of previous test data. The displacement d_1 can be altered based on the required calculated displacement demand. The only geometric parameter which is sensible to vary during preliminary design is the outer radius R_1 with all other dimensions (as per Figure 7-1) held constant. The outer concave plates radius should be altered based on the partial list of previously produced radii listed above. The concave plates with a larger radius than 2235mm (88inch) may have a slightly lower friction. However since the radii changes are small this effect is considered minor. The preliminary design presented herein does not consider variations in the outer surfaces radius and adopts the recommended dimensions in Figure 7-1.

C.3 Design Based on Recommended Isolator Data

The ELF procedure is implemented to get an initial estimate of the maximum displacement and structural shear. The method assumes a rigid superstructure and adopts a rigid-linear hysteretic model (i.e. as per Figure 2-2).

The nominal friction coefficient is calculated from the prototype test data and is the average over three cycles of motion from Test 1 as this is a lower bound value (i.e. greater isolator pressure and velocity hence greater heating effects). The friction value μ_A is the unprocessed value as it is simply related to the distance travelled and the energy dissipated per cycle. From Table 7-1, the nominal values were 0.041 and 0.054 with an average of 0.048 for the two isolators. This is then multiplied by a factor of 0.85 for production tolerance (i.e. the specification lambda) to get a lower bound value of 0.040. Based on the dimensions specified in Figure 7-1 and using an effective yield displacement Y of zero, the parameters for the analysis are:

$$K_d = \frac{W}{2R_{eff,1}} = \frac{W}{2(R_1 - h_1)}$$

$$= \frac{53,090}{2(2235 - 114)} = 12.5\,kN/mm\,(71.4\,kip/in)$$

$$Q_d = \mu_A W$$

$$= 0.040 \times 53,090 = 2124\,kN\,(477\,kip)$$

The equations for the ELF method are given in Appendix B. The ELF method gives a maximum (MCE) displacement of 627mm (24.7inch) which is then multiplied by a 1.2 factor for bi-directional and torsional effects, to give a total maximum displacement D_{TM}=752mm (29.6inch) . Even though the isolator's center of stiffness and center of mass coincide, ASCE 7-2016 sets a limit on the total maximum displacement of 1.15 times the maximum displacement. The isolators displacement capacity is 828mm (32.6inch) with stiffening (i.e. force-displacement response enters regime III) at around 762mm (30 inch), therefore the prototype isolator is adequate and the tri-linear model in Figure 2-4 is applicable.

For an upper bound analysis, the nominal value can be simply doubled. Using the ELF method the upper bound structural base shear is 18% of the seismic weight for an elastic superstructure. This structural shear plus the effects of torsion can then be used to assess the potential for uplift. One approach to do this is discussed in Appendix B since uplift is a more significant issue for elastomeric isolators. If uplift is a concern, then the analysis models must allow for this uplift (i.e. gap elements with zero tension strength). Triple FP have been tested and used on past projects (Sarkisian et al, 2012) with an important check being the uplift displacement and ensuring that it is not greater than the height of the ring of the isolator.

C.4 Design Based on Qualification Data

The preliminary design reported in Section 5.3 is from Section C.3: Design Based on Recommended Isolator Data, and not from this section. The purpose of this section is to illustrate how friction coefficients may be calculated based on qualification test data, say in the case where test data from isolators do not meet the similarity requirements of ASCE 7-2016.

The coefficient of friction is affected by a number of factors, with the more important being the sliding velocity, temperature and isolator pressure. Also, the size of the contact area has an effect even when the apparent isolator pressure is the same due to differences in the true isolator pressure.

Constantinou et al, (2011) have suggested a methodology to estimate the frictional properties based on available qualification data. This approach is described below. The nominal value of the coefficient of friction is defined as the average coefficient of friction during the first three cycles of motion, μ_{3c}, at the design ambient temperatures for a fresh isolator (that is, without any effects of aging, contamination, etc.). If test data from similar isolator units as per ASCE 7-2016 §17.8.2.7 do not exist (i.e. the actual isolators have a greater vertical stress) then one approach is to use qualification test data from the manufacturer to determine a preliminary friction value. Constantinou et al, (2011) proposed that the nominal value μ_{3c} for PTFE composite-stainless steel interfaces typically used in FP isolators may be roughly calculated based on the isolator pressure, p, using:

$$\mu_{3c} = 0.122 - 0.01\text{p } (\text{ksi})\qquad\qquad (\text{C - 1})$$

It is important to note the applicability of equation (C-1). This equation is limited to isolator pressures between 13.8 to 55.2MPa (2 to 8ksi) and is based on experimental data from FP isolators with a contact diameter of 279mm (11 inch), and tested to amplitudes of 300 to 700 mm (12 to 28 inches). Note that the size of the slider does have a small influence the friction coefficient. For example, a larger slider typically has a lower friction coefficient than a smaller slider even though they have the same apparent bearing pressure. Furthermore the experimental testing was carried out at a moderate velocity, where frictional heating has less effect on the friction coefficient. Thus the values predicted by equation (C-1) need to be adjusted for a higher design velocity of the outer surfaces and for the lower velocity in the inner surfaces. Since the inner surface experiences lower velocities, and therefore lower frictional heating, it needs to be adjusted by a smaller amount. However, if the velocity of the inner surfaces is too low, friction may be substantially less even without heating effects and a much larger adjustment is needed. Constantinou et al, (2011) recommends that the value of μ_{3c} calculated from C-1 should be reduced by 0.01 to 0.02 for velocities of around 1000mm/s (39in/s).

Using a structural model in the program SAP2000, the seismic weight (DL plus partition LL) gives an axial load on the interior and exterior isolators of roughly 2140kN (480kip) and 1180kN (265kip), respectively. Based on the geometry of the isolator in Figure 7-1, the isolator pressure for outer surfaces of the building's interior isolators is 29.3MPa (4.2ksi), and the isolator pressure for the outer surfaces of the building's exterior isolators is 16.2MPa (2.3ksi). These pressures are used in equation (C-1) to estimate the friction of the important outer surfaces and then adjust for the high velocity effects. The less important value of μ_{3c} for the inner surfaces is arbitrarily assumed to be 0.03.

The nominal friction coefficient μ_{3c} for the outer surfaces is calculated as 0.099 for the exterior isolator and as 0.080 for the interior isolators using equation (C-1). These values then need to be adjusted for a higher design velocity of the outer surfaces. Here μ_{3c} is adjusted as $0.099 - 0.015 = 0.084$ for the exterior isolators and as $0.080 - 0.015 = 0.065$ for the interior isolators. Constantinou et al, (2011) recommend that the friction coefficient in the first cycle of motion μ_{1c} (used for upper bound analysis) be taken as $1.2 \times \mu_{3c}$. Also, Constantinou et al, (2011) recommend the use of a factor of 1.1x1.05=1.16 for combined aging and contamination effects.

Note that in preliminary design it is inappropriate to follow the limits on lambda factors in equations 17-2-1 and 17.2-2 in ASCE 7-2016. Preliminary design is meant to be a starting point for the sizing of the isolators. Accordingly, the upper and lower bound values of friction are determined based on the experience of the RDP. Herein, we follow the procedures for preliminary design in Constantinou et al, (2011). The upper bound value of friction is calculated as $1.2 \times 1.16 \times \mu_{3c}$, whereas the lower bound value is assumed equal to μ_{3c}. The RDP may adjust the values by incorporating uncertainty.

Hence the friction coefficients are taken as:
- **Exterior Isolators Lower Bound**
    - Exterior Inner Surfaces $\mu_2 = \mu_3 = 0.030$
    - Exterior Outer Surfaces $\mu_1 = \mu_4 = 0.084$
- **Exterior Isolators Upper Bound**
    - Exterior Inner Surfaces $\mu_2 = \mu_3 = 0.030 \times 1.2 \times 1.16 = 0.042$
    - Exterior Outer Surfaces $\mu_1 = \mu_4 = 0.084 \times 1.2 \times 1.16 = 0.117$

- **Interior Isolator Lower Bound**
    - Interior Inner Surfaces $\mu_2 = \mu_3 = 0.03$
    - Interior Outer Surfaces $\mu_1 = \mu_4 = 0.065$
- **Interior Isolator Upper Bound**
    - Interior Inner Surfaces $\mu_2 = \mu_3 = 0.03 \times 1.2 \times 1.16 = 0.042$
    - Interior Outer Surfaces $\mu_1 = \mu_4 = 0.065 \times 1.2 \times 1.16 = 0.091$

The friction properties for the combined system are then taken as the weighted average friction. For example, in the lower bound analysis:

$$\mu_{2\,lower\,bound} = \frac{16 \times 1180 \times 0.030 + 16 \times 2140 \times 0.030}{16 \times 1180 + 16 \times 2140} = 0.030$$

$$\mu_{1\,lower\,bound} = \frac{16 \times 1180 \times 0.065 + 16 \times 2140 \times 0.042}{16 \times 1180 + 16 \times 2140} = 0.050$$

These values along with the dimensions in Figure 7-1 can be used to plot the tri-linear force-displacement relationship.

Alternatively, the value friction at zero displacement, μ can be calculated and used in a bilinear or rigid-linear model to efficiently carry out the ELF procedure. As an example for the lower bound, the parameters for the bilinear model (see Figure 2-1) would be:

$$\mu = \mu_1 - \left(\mu_1 - \mu_2\right)\frac{R_{2,eff}}{R_{1,eff}}$$

$$= 0.050 - \left(0.050 - 0.030\right)\frac{228.6}{2120.9} = 0.0478$$

$$K_d = \frac{W}{2R_{eff,1}} = \frac{W}{2(R_1 - h_1)}$$

$$= \frac{53,000}{2\left(2235 - 114\right)} = 12.5\,kN\,/\,mm\left(71.4\,kip\,/\,in\right)$$

$$Y = u^* / 2 = \left(\mu_1 - \mu_2\right)R_{eff,2} / 2$$

$$= \left(0.050 - 0.030\right) \times \left(305 - 76\right) / 2 = 2.3\,mm\left(0.09\,inch\right)$$

This Page is Intentionally Left Blank

APPENDIX D

ASCE 7-2016 CHAPTER 17 PROPOSAL WITH CHANGES

PROPOSED BY AUTHORS OF THIS REPORT

This appendix presents Proposal TC-12-CH17-01r04 for changes to ASCE 7-2010 Chapter 17 and changes recommended to this proposal (highlighted in red) by the authors of this report. Note that as of late February 2015, the proposal has not yet been balloted at the main committee.

Chapter 17

SEISMIC DESIGN REQUIREMENTS FOR SEISMICALLY ISOLATED STRUCTURES

17.1 GENERAL

Every seismically isolated structure and every portion thereof shall be designed and constructed in accordance with the requirements of this section and the applicable requirements of this standard.

17.1.2 Definitions

BASE LEVEL: The first level of the isolated structure above the isolation interface.

MAXIMUM DISPLACEMENT: The maximum lateral displacement, excluding additional displacement due to actual and accidental torsion, required for design of the isolation system. The Maximum Displacement is to be computed separately using upper bound and lower bound properties.

TOTAL MAXIMUM DISPLACEMENT: The total maximum lateral displacement, including additional displacement due to actual and accidental torsion, required for verification of the stability of the isolation system or elements thereof, design of structure separations, and vertical load testing of isolator unit prototypes. . The Total Maximum Displacement is to be computed separately using upper bound and lower bound properties.

DISPLACEMENT RESTRAINT SYSTEM: A collection of structural elements that limits lateral displacement of seismically isolated structures due to the maximum considered earthquake.

EFFECTIVE DAMPING: The value of equivalent viscous damping corresponding to energy dissipated during cyclic response of the isolation system.

EFFECTIVE STIFFNESS: The value of the lateral force in the isolation system, or an element thereof, divided by the corresponding lateral displacement.

ISOLATION INTERFACE: The boundary between the upper portion of the structure, which is isolated, and the lower portion of the structure, which moves rigidly with the ground.

ISOLATION SYSTEM: The collection of structural elements that includes all individual isolator units, all structural elements that transfer force between elements of the isolation system, and all connections to other structural elements. The isolation system also includes the wind-restraint system, energy-dissipation devices, and/or the displacement restraint system if such systems and devices are used to meet the design requirements of this chapter.

ISOLATOR UNIT: A horizontally flexible and vertically stiff structural element of the isolation system that permits large lateral deformations under design seismic load. An isolator unit is permitted to be used either as part of, or in addition to, the weight-supporting system of the structure.

SCRAGGING: Cyclic loading or working of rubber products, including elastomeric isolators, to effect a reduction in stiffness properties, a portion of which will be recovered over time.

WIND-RESTRAINT SYSTEM: The collection of structural elements that provides restraint of the seismic-isolated structure for wind loads. The wind-restraint system is permitted to be either an integral part of isolator units or a separate device.

17.1.3 Notation

B_M = numerical coefficient as set forth in Table 17.5-1 for effective damping equal to β_M

b = shortest plan dimension of the structure, in ft (mm) measured perpendicular to d

C_{vx} = vertical distribution factor

D_M = maximum displacement, in in. (mm), at the center of rigidity of the isolation system in the direction under consideration, as prescribed by Eq. 17.5-1

D'_M = maximum displacement, in in. (mm), at the center of rigidity of the isolation system in the direction under consideration, as prescribed by Eq. 17.6-1

D_{TM} = total maximum displacement, in in. (mm), of an element of the isolation system including both translational displacement at the center of rigidity and the component of torsional displacement in the direction under consideration, as prescribed by Eq. 17.5-3.

d = longest plan dimension of the structure, in ft (mm) measured perpendicular to b

E_{loop} = energy dissipated in kips-in. (kN-mm), in an isolator unit during a full cycle of reversible load over a test displacement range from Δ^+ to Δ^-, as measured by the area enclosed by the loop of the force-deflection curve

e = actual eccentricity, in ft (mm), measured in plan between the center of mass of the structure above the isolation interface and the center of rigidity of the isolation system, plus accidental eccentricity, in ft. (mm), taken as 5 percent of the maximum building dimension perpendicular to the direction of force under consideration

F^- = minimum negative force in an isolator unit during a single cycle of prototype testing at a displacement amplitude of Δ^-

F^+ = maximum positive force in kips (kN) in an isolator unit during a single cycle of prototype testing at a displacement amplitude of Δ^+

F_x = lateral seismic force, in kips (kN), at Level x as prescribed by Eq. 17.5-9

h_i, h_1, h_x = height above the isolation interface of Level i, 1, or x

h_{sx} = height of story below Level x

k_M = effective stiffness, in kips/in. (kN/mm), of the isolation system in the horizontal direction under consideration, as prescribed by Eq. 17.8-5

k_{eff} = effective stiffness of an isolator unit, as prescribed by Eq. 17.8-1

L = effect of live load in Chapter 17

N = number of isolator units

P_T = ratio of the effective translational period of the isolation system to the effective torsional period of the isolation system, as prescribed by Eq. 17.5-6A, but need not be taken as less than 1.0

r_I　　= radius of gyration of the isolation system in ft (mm), equal to $(b^2 + d^2)^{1/2}/12$ for isolation systems of rectangular plan dimension, b x d

R_I　　= numerical coefficient related to the type of seismic force-resisting system above the isolation system

S_{DS}　　= the MCE_R, 5 percent damped, spectral response acceleration parameter at short periods adjusted for site class effects, as defined in Section 11.4.4

S_{M1}　　= the MCE_R, 5 percent damped, spectral response acceleration parameter at a period of 1s adjusted for site class effects, as defined in Section 11.4.3

S_{MS}　　= the MCE_R, 5 percent damped, spectral response acceleration parameter at short periods adjusted for site class effects, as defined in Section 11.4.3

T_M　　= effective period, in s, of the seismically isolated structure at the displacement D_M in the direction under consideration, as prescribed by Eq. 17.5-2

T_{fb}　　= the fundamental period, in s, of the structure above the isolation interface determined using a modal analysis assuming fixed-base conditions

V_b　　= total lateral seismic design force or shear on elements of the isolation system or elements below isolation system, in kips (kN), as prescribed by Eq. 17.5-7 or Eq. 17.5-7A.

V_s　　= total lateral seismic design force or shear on elements above the base level, in kips (kN), as prescribed by Eq. 17.5-8 and the limits of Section 17.5.4.3

V_{st}　　= total unreduced lateral seismic design force or shear on elements above the base level, in kips (kN), as prescribed by Eq. 17.5-8A

y　　= distance, in ft (mm), between the center of rigidity of the isolation system rigidity and the element of interest measured perpendicular to the direction of seismic loading under consideration

W　　= effective seismic weight, in kips (kN), of the structure above the isolation interface, as defined by Section 12.7.2

W_s　　= effective seismic weight, in kips (kN), of the structure above the isolation interface, as defined by Section 12.7.2, excluding the effective seismic weight, in kips (kN), of the base level

w_i, w_1, w_x　　= portion of W that is located at or assigned to Level i, 1, or x

x_i, y_i　　= horizontal distances in ft (mm) from the center of mass to the ith isolator unit in the two horizontal axes of the isolation system

β_M　　= effective damping of the isolation system at the displacement D_M, as prescribed by Eq. 17.2-4.

β_{eff}　　= effective damping of the isolation system, as prescribed by Eq. 17.8-2

Δ^+　　= maximum positive displacement of an isolator unit during each cycle of prototype testing

Δ^-　　= minimum negative displacement of an isolator unit during each cycle of prototype testing

167

λ_{max} = property modification factor for calculation of the maximum value of the isolator property of interest, used to account for all sources of isolator property variability, as defined in Section 17.2.8.4

λ_{min} = property modification factor for calculation of the minimum value of the isolator property of interest, used to account for all sources of isolator property variability, as defined in Section 17.2.8.4

$\lambda_{(ae, max)}$ = property modification factor for calculation of the maximum value of the isolator property of interest, used to account for aging effects and environmental conditions as defined in Section 17.2.8.4.

$\lambda_{(ae, min)}$ = property modification factor used to calculate the minimum value of the isolator property of interest, used to account for aging effects and environmental conditions as defined in Section 17.2.8.4.

$\lambda_{(test, max)}$ = property modification factor used to calculate the maximum value of the isolator property of interest, used to account for heating, rate of loading, and scragging as defined in Section 17.2.8.4.

$\lambda_{(test, min)}$ = property modification factor used to calculate the minimum value of the isolator property of interest, used to account for heating, rate of loading, and scragging as defined in Section 17.2.8.4.

$\lambda_{(spec, max)}$ = property modification factor used to calculate the maximum value of the isolator property of interest, used to account for permissible manufacturing variation on the average properties of a group of same sized isolators as defined in Section 17.2.8.4.

$\lambda_{(spec, min)}$ = property modification factor used to calculate the minimum value of the isolator property of interest, used to account for permissible manufacturing variation on the average properties of a group of same sized isolators as defined in Section 17.2.8.4.

ΣE_M = total energy dissipated, in kips-in. (kN-mm), in the isolation system during a full cycle of response at displacement D_M

$\sum \left| F_M^+ \right|$ = sum, for all isolator units, of the maximum absolute value of force, in kips (kN), at a positive displacement equal to D_M

$\sum \left| F_M^- \right|$ = sum, for all isolator units, of the maximum absolute value of force, in kips (kN), at a negative displacement equal to D_M

17.2 GENERAL DESIGN REQUIREMENTS

17.2.1 Importance Factor

All portions of the structure, including the structure above the isolation system, shall be assigned a risk category in accordance with Table 1.5-1. The importance factor, I_e, shall be taken as 1.0 for a seismically isolated structure, regardless of its risk category assignment.

17.2.2 Configuration

Each isolated structure shall be designated as having a structural irregularity if the structural configuration above the isolation system has a Type 1b horizontal structural irregularity, as defined in Table 12.3-1, or Type 1a, 1b, 5a, 5b vertical irregularity, as defined in Table 12.3-2.

17.2.3 Redundancy

A redundancy factor, ρ, shall be assigned to the structure above the isolation system based on requirements of Section 12.3.4. The value of redundancy factor, ρ, is permitted to be equal to 1.0 for isolated structures that do not have a structural irregularity, as defined in Section 17.2.2.

17.2.4 Isolation System

17.2.4.1 Environmental Conditions

In addition to the requirements for vertical and lateral loads induced by wind and earthquake, the isolation system shall provide for other environmental conditions including aging effects, creep, fatigue, operating temperature, and exposure to moisture or damaging substances.

17.2.4.2 Wind Forces

Isolated structures shall resist design wind loads at all levels above the isolation interface. At the isolation interface, a wind-restraint system shall be provided to limit lateral displacement in the isolation system to a value equal to that required between floors of the structure above the isolation interface in accordance with Section 17.5.6.

17.2.4.3 Fire Resistance

Fire resistance for the isolation system shall provide at least the same degree of protection as the fire resistance required for the columns, walls, or other such gravity-bearing elements in the same region of the structure.

17.2.4.4 Lateral Restoring Force

The isolation system shall be configured, for both upper bound and lower bound isolation system properties, to produce a restoring force such that the lateral force at the corresponding maximum displacement is at least $0.025W$ greater than the lateral force at 50 percent of the corresponding maximum displacement.

17.2.4.5 Displacement Restraint

The isolation system shall not be configured to include a displacement restraint that limits lateral displacement due to MCE_R ground motions to less than the total maximum displacement, D_{TM}, unless the seismically isolated structure is designed in accordance with all of the following criteria:

1. MCE_R response is calculated in accordance with the dynamic analysis requirements of Section 17.6, explicitly considering the nonlinear characteristics of the isolation system and the structure above the isolation system.

2. The ultimate capacity of the isolation system and structural elements below the isolation system shall exceed the strength and displacement demands of the MCE_R response.

3. The structure above the isolation system is checked for stability and ductility demand of the MCE_R response.

4. The displacement restraint does not become effective at a displacement less than 0.6 times the total maximum displacement.

17.2.4.6 Vertical-Load Stability

Each element of the isolation system shall be designed to be stable under the design vertical load where subjected to a horizontal displacement equal to the total maximum displacement. The design

vertical load shall be computed using load combination (2) of Section 17.2.7.1 for the maximum vertical load and load combination (3) of Section 17.2.7.1 for the minimum vertical load.

17.2.4.7 Overturning

The factor of safety against global structural overturning at the isolation interface shall not be less than 1.0 for required load combinations. All gravity and seismic loading conditions shall be investigated. Seismic forces for overturning calculations shall be based on MCE_R ground motions, and W shall be used for the vertical restoring force.

Local uplift of individual elements shall not be allowed unless the resulting deflections do not cause overstress or instability of the isolator units or other structure elements.

17.2.4.8 Inspection and Replacement

All of the following items shall be addressed as part of the long term inspection and replacement program:

1. Access for inspection and replacement of all components of the isolation system shall be provided.

2. A registered design professional shall complete a final series of observations of structure separation areas and components that cross the isolation interface prior to the issuance of the certificate of occupancy for the seismically isolated structure. Such observations shall verify that conditions allow free and unhindered displacement of the structure up to the total maximum displacement, and that components that cross the isolation interface have been constructed to accommodate the total maximum displacement.

3. Seismically isolated structures shall have a monitoring, inspection, and maintenance plan for the isolation system established by the registered design professional responsible for the design of the isolation system.

4. Remodeling, repair, or retrofitting at the isolation system interface, including that of components that cross the isolation interface, shall be performed under the direction of a registered design professional.

17.2.4.9 Quality Control

A quality control testing program for isolator units shall be established by the registered design professional responsible for the structural design, incorporating the production testing requirements of Section 17.8.6

17.2.5 Structural System

17.2.5.1 Horizontal Distribution of Force

A horizontal diaphragm or other structural elements shall provide continuity above the isolation interface and shall have adequate strength and ductility to transmit forces from one part of the structure to another.

17.2.5.2 Minimum Building Separations

Minimum separations between the isolated structure and surrounding retaining walls or other fixed obstructions shall not be less than the total maximum displacement.

17.2.5.3 Non-building Structures

Non-building structures shall be designed and constructed in accordance with the requirements of Chapter 15 using design displacements and forces calculated in accordance with Sections 17.5 or 17.6.

17.2.5.4 Steel Ordinary Concentrically Braced Frames

Steel Ordinary Concentrically Braced Frames are permitted as the Seismic Force Resisting System in seismically isolated structures assigned to SDC D, E and F and are permitted to a height of 160 feet or less provided that all of the following design requirements are satisfied.

1. The value of R_I as defined in Section 17.5.4. is 1.0

2. The total maximum displacement (D_{TM}) as defined in Equation 17.5-6 shall be increased by a factor of 1.2.

17.2.5.5 Isolation System Connections

Moment –resisting connections of structural steel elements of the seismic isolation system below the base level are permitted to conform to the requirements for Ordinary Steel Moment Frames of AISC 341 E1.6a and E1.6b.

17.2.6 Elements of Structures and Nonstructural Components

Parts or portions of an isolated structure, permanent nonstructural components and the attachments to them, and the attachments for permanent equipment supported by a structure shall be designed to resist seismic forces and displacements as prescribed by this section and the applicable requirements of Chapter 13.

17.2.6.1 Components at or above the Isolation Interface

Elements of seismically isolated structures and nonstructural components, or portions thereof that are at or above the isolation interface shall be designed to resist a total lateral seismic force equal to the maximum dynamic response of the element or component under consideration determined using a response history analysis.

EXCEPTION: Elements of seismically isolated structures and nonstructural components or portions designed to resist seismic forces and displacements as prescribed in Chapter 12 or 13 as appropriate are not required to meet this provision.

17.2.6.2 Components Crossing the Isolation Interface

Elements of seismically isolated structures and nonstructural components, or portions thereof, that cross the isolation interface shall be designed to withstand the total maximum displacement and to accommodate on a long term basis any permanent residual displacement.

17.2.6.3 Components below the Isolation Interface

Elements of seismically isolated structures and nonstructural components, or portions thereof, that are below the isolation interface shall be designed and constructed in accordance with the requirements of Section 12.1 and Chapter 13.

17.2.7 Seismic Load Effects and Load Combinations

All members of the isolated structure, including those not part of the seismic force-resisting system, shall be designed using the seismic load effects of Section 12.4 and the additional load combinations of Section 17.2.7.1 for design of the isolation system and for testing of prototype isolator units.

17.2.7.1 Isolator Unit Vertical Load Combinations

The average, minimum and maximum vertical load on each isolator unit type shall be computed from application of horizontal seismic forces, Q_E, due to MCE$_R$ ground motions and the following applicable vertical load combinations:

1. Average vertical load: load corresponding to 1.0 dead load plus 0.5 live load.

2. Maximum vertical load: load combination 5 of Section 2.3.2, where E is given by Eq. 12.4-1 and S_{DS} is replaced by S_{MS} in Eq. (12.4-4).

3. Minimum vertical load: load combination 7 of Section 2.3.2, where E is given by Eq. 12.4-2 and S_{DS} is replaced by S_{MS} .in Eq. (12.4-4).

17.2.8 Isolation System Properties

17.2.8.1 Isolation System Component Types

All components of the isolation system shall be categorized and grouped in terms of common type and size of isolator unit and common type and size of supplementary damping device, if such devices are also components of the isolation system.

17.2.8.2 Isolator Unit Nominal Properties

Isolator unit type nominal design properties shall be based on average properties over the three cycles of prototype testing, specified by Items 2 and 3 of Section 17.8.2.2. Variation in isolator unit properties with vertical load are permitted to be established based on a single representative deformation cycle by averaging the properties determined using the three vertical load combinations specified in Section 17.2.7.1, at each displacement level, where required to be considered by Section 17.8.2.2.

EXCEPTION: If the measured values of isolator unit effective stiffness and effective damping for vertical load 1 of Section 17.2.7.1 differ by less than 15% from those based on the average of measured values for the three vertical load combinations of Section 17.2.7.1, then nominal design properties are permitted to be computed only for load combination 1 of Section 17.2.7.1.

17.2.8.3 Bounding Properties of Isolation System Components

Bounding properties of isolation system components shall be developed for each isolation system component type. Bounding properties shall include variation in all of the following component properties:

1. measured by prototype testing, Items 2 and 3 of Section 17.8.2.2, considering variation in prototype isolator unit properties due to required variation in vertical test load, rate of test loading or velocity effects, effects of heating during cyclic motion, history of loading, scragging (temporary degradation of mechanical properties with repeated cycling) and other potential sources of variation measured by prototype testing,

2. permitted by manufacturing specification tolerances used to determine acceptability of production isolator units, as required by Section 17.8.6, and

3. due to aging and environmental effects including creep, fatigue, contamination, operating temperature and duration of exposure to that temperature, and wear over the life of the structure.

17.2.8.4 Property Modification Factors

Maximum and minimum property modification (λ) factors shall be used to account for variation of the nominal design parameters of each isolator unit type for the effects of heating due to cyclic dynamic motion, loading rate, scragging and recovery, variability in production bearing properties, temperature, aging, environmental exposure and contamination. When manufacturer-specific qualification test data in accordance with 17.8.1.2 has been approved by the registered design professional, these data are permitted to be used to develop the property modification factors and the maximum and minimum limits of Eqs. 17.2-1 and 17.2-2 need not apply. When qualification test data in accordance with 17.8.1.2 has not been approved by the registered design professional, the maximum and minimum limits of Eqs. 17.2-1 and 17.2-2 shall apply.

Property modification factors (λ) shall be developed for each isolator unit type and when applied to the nominal design parameters shall envelope the hysteretic response for the range of demands from $\pm 0.5D_M$ up to and including the maximum displacement, $\pm D_M$. Property modification factors for environmental conditions are permitted to be developed from data that need not satisfy the similarity requirements of Section 17.8.2.7.

For each isolator unit type, the maximum property modification factor, λ_{max}, and the minimum property modification factor, λ_{min}, shall be established from contributing property modification factors in accordance with Eq. 17.2-1 and Eq. 17.2-2, respectively:

$$\lambda_{max} = (1 + (0.75 * (\lambda_{(ae, max)} - 1))) * \lambda_{(test, max)} * \lambda_{(spec, max)} \geq 1.8 \qquad (17.2\text{-}1)$$

$$\lambda_{min} = (1 - (0.75 * (1 - \lambda_{(ae, min)}))) * \lambda_{(test, min)} * \lambda_{(spec, min)} \leq 0.60 \qquad (17.2\text{-}2)$$

where

$\lambda_{(ae, max)} =$ property modification factor for calculation of the maximum value of the isolator property of interest, used to account for aging effects and environmental conditions.

$\lambda_{(ae, min)} =$ property modification factor used to calculate the minimum value of the isolator property of interest, used to account for aging effects and environmental conditions.

$\lambda_{(test, max)} =$ property modification factor used to calculate the maximum value of the isolator property of interest, used to account for heating, rate of loading, and scragging. $\lambda_{(test, max)}$ shall be determined as the ratio of the first cycle property value obtained in the prototype testing, Items 2 and 3 of Section 17.8.2.2 to the nominal property value.

$\lambda_{(test, min)} =$ property modification factor used to calculate the minimum value of the isolator property of interest, used to account for heating, rate of loading, and scragging. $\lambda_{(test, min)}$ shall be determined as the ratio of the property value at a representative cycle determined by the RDP as obtained in the prototype testing, Items 2 and 3 of Section 17.8.2.2 to the nominal property value. The default cycle is the third cycle.

$\lambda_{(spec, max)} =$ property modification factor used to calculate the maximum value of the isolator property of interest, used to account for permissible manufacturing variation on the average properties of a group of same sized isolators.

$\lambda_{(spec, min)} =$ property modification factor used to calculate the minimum value of the isolator property of interest, used to account for permissible manufacturing variation on the average properties of a group of same sized isolators.

EXCEPTION: If the prototype isolator testing is conducted on full-scale specimen that satisfies the dynamic test data of Sec. 17.8.2.3, then the values of the property modification factors shall be based on the test data and the upper and lower limits of Equations 17.2-1 and 17.2-2 need not apply.

17.2.8.5 Upper-Bound and Lower-Bound Force-Deflection Behavior of Isolation System Components

A mathematical model of upper-bound force-deflection (loop) behavior of each type of isolation system component shall be developed. Upper-bound force-deflection behavior of isolation system components that are essentially hysteretic devices (e.g., isolator units) shall be modeled using the maximum values of isolator properties calculated using the property modification factors of Section 17.2.8.4. Upper-bound force-deflection behavior of isolation system components that are essentially viscous devices (e.g., supplementary viscous dampers), shall be modeled in accordance with the requirements of Chapter 18 for such devices.

A mathematical model of lower-bound force-deflection (loop) behavior of each type of isolation system component shall be developed. Lower-bound force-deflection behavior of isolation system components that are essentially hysteretic devices (e.g., isolator units) shall be modeled using the minimum values of isolator properties calculated using the property modification factors of Section 17.2.8.4. Lower-bound force-deflection behavior of isolation system components that are essentially viscous devices (e.g., supplementary viscous dampers), shall be modeled in accordance with the requirements of Chapter 18 for such devices.

17.2.8.6 Isolation System Properties at Maximum Displacements

The effective stiffness, k_M, of the isolation system at the maximum displacement, D_M, shall be computed using both upper-bound and lower-bound force-deflection behavior of individual isolator units, in accordance with Eq. 17.2-3:

$$k_M = \frac{\sum \left| F_M^+ \right| + \sum \left| F_M^- \right|}{2 D_M}$$

(17.2-3)

The effective damping, β_M, of the isolation system at the maximum displacement, D_M, in inches (mm) shall be computed using both upper-bound and lower-bound force-deflection behavior of individual isolator units, in accordance with Eq. 17.2-4:

$$\beta_M = \frac{\sum E_M}{2\pi k_M D_M^2}$$

(17.2-4)

where

$\sum E_M$ = total energy dissipated, in kips-in. (kN-mm), in the isolation system during a full cycle of response at the displacement D_M.

$\sum F_M^+$ = sum, for all isolator units, of the absolute value of force, in kips (kN), at a positive displacement equal to D_M.

$\sum F_M^-$ = sum, for all isolator units, of the absolute value of force, in kips (kN), at a negative displacement equal to D_M.

17.2.8.7 Upper-Bound and Lower-Bound Isolation System Properties at Maximum Displacement

The analysis of the isolation system and structure shall be performed separately for upper-bound and lower-bound properties, and the governing case for each response parameter of interest shall be used for design. In addition the analysis shall comply with all of the following:

For the equivalent linear force procedure, and for the purposes of establishing minimum forces and displacements for dynamic analysis, the following variables shall be calculated independently for upper-bound and lower-bound isolation system properties: k_M and D_M per Section 17.2.8.6 (Eq.17.2-3 and Eq. 17.2-4), D_M per Section 17.5.3.1 (Eq. 17.5-1), T_M per Section 17.5.3.2 (Eq. 17.5-2), D_{TM} per Section 17.5.3.3 (Eq. 17.5-3), V_b per Section 17.5.4.1 (Eq. 17.5-5), and V_s and V_{st} per Section 17.5.4.2 (Eq. 17.5-5 and Eq. 17.5-6).

The limitations on V_s established Section 17.5.4.3 shall be evaluated independently for both upper-bound and lower-bound isolation system properties and the most adverse requirement shall govern.

For the equivalent linear force procedure, and for the purposes of establishing minimum story shear forces for response spectrum analysis, the vertical force distribution from Section 17.5.4.3 shall be determined separately for upper-bound and lower-bound isolation system properties. This will require independent calculation of F_1, F_x, C_{vx}, and k, per Eqs. 17.5-8 through 17.5-11 respectively.

17.3 SEISMIC GROUND MOTION CRITERIA

17.3.1 Site-Specific Seismic Hazard

The MCE$_R$ response spectrum requirements of Section 11.4.5 and 11.4.6 are permitted to be used to determine the MCE$_R$ response spectrum for the site of interest. The site-specific ground motion procedures set forth in Chapter 21 are also permitted to be used to determine ground motions for any isolated structure. For isolated structures on Site Class F sites, site response analysis shall be performed in accordance with Section 21.1.

17.3.2 MCE$_R$ Response Spectra and Spectral Response Acceleration Parameters, S_{MS}, S_{M1}

The MCE$_R$ response spectrum shall be the MCE$_R$ response spectrum of 11.4.5, 11.4.6 or 11.4.7. The MCE$_R$ response spectral acceleration parameters S_{MS} and S_{M1} shall be determined in accordance with Section 11.4.3, 11.4.5, 11.4.6, or 11.4.7.

17.3.4 MCE$_R$ Ground Motion Records

Where response history analysis procedures are used, MCE$_R$ ground motions shall consist of not less than seven pairs of horizontal acceleration components selected and scaled from individual recorded events having magnitudes, fault distance and source mechanisms that are consistent with those that control the maximum considered earthquake (MCE$_R$). Amplitude or spectral matching is permitted to scale the ground motions. Where the required number of recorded ground motion pairs is not available, simulated ground motion pairs are permitted to make up the total number required.

For each pair of horizontal ground motion components, a square root of the sum of the squares (SRSS) spectrum shall be constructed by taking the SRSS of the 5 percent-damped response spectra for the scaled components (when amplitude scaling is used an identical scale factor is applied to both components of a pair). Each pair of motions shall be scaled such that in the period range from 0.75 T_M, determined using upper bound isolation system properties, to $1.25T_M$, determined using lower bound isolation system properties, the average of the SRSS spectral from all horizontal component pairs does not fall below the corresponding ordinate of the response spectrum used in the design (MCE$_R$), determined in accordance with Section 11.4.6 or 11.4.7.

For records that are spectrally matched each pair of motions shall be scaled such that in the period range from $0.2T_M$, determined using upper bound properties, to $1.25T_M$, determined using lower bound

properties, the response spectrum of one component of the pair is at least 90% of the corresponding ordinate of the response spectrum used in the design determined in accordance with Section 11.4.6 or 11.4.7.

For sites within 3 miles (5 km) of the active fault that controls the hazard, spectral matching shall not be utilized unless the pulse characteristics of the near field ground motions are included in the site specific response spectra, and pulse characteristics when present in individual ground motions are retained after the matching process has been completed.

At sites within 3 miles (5 km) of the active fault that controls the hazard, each pair of components shall be rotated to the fault-normal and fault-parallel directions of the causative fault and shall be scaled so that the average spectrum of the fault normal components is not less than the MCE_R spectrum and the average spectrum of the fault-parallel components is not less than 50% of the MCE_R response spectrum for the period range $0.2T_M$, determined using upper bound properties, to $1.25T_M$, determined using lower bound properties.

17.4 ANALYSIS PROCEDURE SELECTION

Seismically isolated structures except those defined in Section 17.4.1 shall be designed using the dynamic procedures of Section 17.6. Where supplementary viscous dampers are used the response history analysis procedures of Section 17.4.2.2 shall be used.

17.4.1 Equivalent Lateral Force Procedure

The equivalent lateral force procedure of Section 17.5 is permitted to be used for design of a seismically isolated structure provided all of the following items are satisfied. These requirements shall be evaluated separately for upper-bound and lower-bound isolation system properties and the more restrictive requirement shall govern.

1. The structure is located on a Site Class A, B, C and D.

2. The effective period of the isolated structure at the maximum displacement, D_M, is less than or equal to 5.0s.

3. The structure above the isolation interface is less than or equal to 4 stories or 65 ft (19.8m) in structural height measured from the base level. Exception: These limits are permitted to be exceeded if there is no tension/uplift on the isolators.

4. The effective damping of the isolation system at the maximum displacement, DM, is less than or equal to 30%.

5. The effective period of the isolated structure T_M is greater than three times the elastic, fixed-base period of the structure above the isolation system determined using a rational modal analysis.

6. The structure above the isolation system does not have a structural irregularity, as defined in Section 17.2.2.

7. The isolation system meets all of the following criteria:

   a. The effective stiffness of the isolation system at the maximum displacement is greater than one-third of the effective stiffness at 20 percent of the maximum displacement.

   b. The isolation system is capable of producing a restoring force as specified in Section 17.2.4.4.

   c. The isolation system does not limit maximum earthquake displacement to less than the total maximum displacement, D_{TM}.

17.4.2 Dynamic Procedures

The dynamic procedures of Section 17.6 are permitted to be used as specified in this section.

17.4.2.1 Response Spectrum Analysis Procedure

Response spectrum analysis procedure shall not be used for design of a seismically isolated structure unless the structure and isolation system meet the criteria of Section 17.4.1 Items 1, 2, 3, 4 and 6.

17.4.2.2 Response History Analysis Procedure

The response history analysis procedure is permitted to be used for design of any seismically isolated structure and shall be used for design of all seismically isolated structures not meeting the criteria of Section 17.4.2.1.

17.5 EQUIVALENT LATERAL FORCE PROCEDURE

17.5.1 General

Where the equivalent lateral force procedure is used to design seismically isolated structures, the requirements of this section shall apply.

17.5.2 Deformation Characteristics of the Isolation System

Minimum lateral earthquake design displacements and forces on seismically isolated structures shall be based on the deformation characteristics of the isolation system. The deformation characteristics of the isolation system include the effects of the wind-restraint system if such a system is used to meet the design requirements of this standard. The deformation characteristics of the isolation system shall be based on properly substantiated prototype tests performed in accordance with Section 17.8 and incorporate property modification factors in accordance with Section 17.2.8.

The analysis of the isolation system and structure shall be performed separately for upper-bound and lower-bound properties, and the governing case for each response parameter of interest shall be used for design.

17.5.3 Minimum Lateral Displacements Required for Design

17.5.3.1 Maximum Displacement

The isolation system shall be designed and constructed to withstand, as a minimum, the maximum displacement, D_M, determined using upper-bound and lower-bound properties, in the most critical direction of horizontal response, calculated using Eq. 17.5-1:

$$D_M = \frac{g S_{M1} T_M}{4\pi^2 B_M}$$

(17.5-1)

where

g = acceleration due to gravity, in units of in./s^2 (mm/s^2) if the units of the displacement D_M are in in. (mm)

S_{M1} = MCE$_R$ 5 -percent damped spectral acceleration parameter at 1-s period in units of *g-sec.*, as determined in Section 11.4.5

T_M = effective period of the seismically isolated structure in seconds at the displacement D_M in the direction under consideration, as prescribed by Eq. 17.5-2

B_M = numerical coefficient as set forth in Table 17.5-1 for the effective damping of the isolation system β_M, at the displacement D_M

TABLE 17.5-1 Damping Coefficient, B_M

Effective Damping, β_M (percentage of critical)[a,b]	B_M factor
≤ 2	0.8
5	1.0
10	1.2
20	1.5
30	1.7
40	1.9
≥ 50	2.0

[a]The damping coefficient shall be based on the effective damping of the isolation system determined in accordance with the requirements of Section 17.2.8.6.

[b]The damping coefficient shall be based on linear interpolation for effective damping values other than those given.

17.5.3.2 Effective Period at the Maximum Displacement

The effective period of the isolated structure, T_M, at the maximum displacement, D_M, shall be determined using upper-bound and lower-bound deformational characteristics of the isolation system and Eq. 17.5-2:

$$T_M = 2\pi\sqrt{\frac{W}{k_M g}}$$

(17.5-2)

where

W = effective seismic weight of the structure above the isolation interface as defined in Section 12.7.2

k_M = effective stiffness in kips/in. (kN/mm) of the isolation system at the maximum displacement, D_M, as prescribed by Eq. 17.2-3

g = acceleration due to gravity, in units of in./s^2 (mm/s^2) if the units of k_M are in kips/in. (kN/mm).

17.5.3.3 Total Maximum Displacement

The total maximum displacement, D_{TM}, of elements of the isolation system shall include additional displacement due to actual and accidental torsion calculated from the spatial distribution of the lateral stiffness of the isolation system and the most disadvantageous location of eccentric mass. The total maximum displacement, D_{TM}, of elements of an isolation system shall not be taken as less than that prescribed by Eq. 17.5-3:

$$D_{TM} = D_M \left[1 + \left(\frac{y}{\mathrm{P}_T^2} \right) \frac{12e}{b^2 + d^2} \right]$$

<div align="right">(17.5-3)</div>

where

D_M = displacement at the center of rigidity of the isolation system in the direction under consideration as prescribed by Eq. 17.5-1

y = the distance in in. (mm) between the centers of rigidity of the isolation system and the element of interest measured perpendicular to the direction of seismic loading under consideration

e = the actual eccentricity measured in plan between the center of mass of the structure above the isolation interface and the center of rigidity of the isolation system, plus accidental eccentricity, in ft (mm), taken as 5 percent of the longest plan dimension of the structure perpendicular to the direction of force under consideration

b = the shortest plan dimension of the structure in ft (mm) measured perpendicular to d

d = the longest plan dimension of the structure in ft (mm)

P_T = ratio of the effective translational period of the isolation system to the effective torsional period of the isolation system, as calculated by dynamic analysis or as prescribed by Eq. 17.5-3, but need not be taken as less than 1.0.

$$\mathrm{P}_T = \frac{1}{r_I} \sqrt{\frac{\sum_{i=1}^{N} \left(x_i^2 + y_i^2 \right)}{N}}$$

<div align="right">(17.5-3)</div>

where:

x_i, y_i = horizontal distances in ft (mm) from the center of mass to the ith isolator unit in the two horizontal axes of the isolation system

N = number of isolator units

r_I = radius of gyration of the isolation system in ft (mm), which is equal to $((b^2 + d^2)/12)^{1/2}$ for isolation systems of rectangular plan dimensions, $b \times d$

b = the shortest plan dimension of the structure in ft (mm) measured perpendicular to d

d = the longest plan dimension of the structure in ft (mm) measured perpendicular to b

The total maximum displacement, D_{TM}, shall not be taken as less than 1.15 times D_M.

17.5.4 Minimum Lateral Forces Required for Design

17.5.4.1 Isolation System and Structural Elements below the Base Level

The isolation system, the foundation, and all structural elements below the base level shall be designed and constructed to withstand a minimum lateral seismic force, Vb, using all of the applicable requirements for a non-isolated structure and as prescribed by the value of Eq. 17.5-5, determined using both upper-bound and lower-bound isolation system properties:

$$V_b = k_M D_M \tag{17.5-5}$$

where

k_M = effective stiffness, in kips/in. (kN/mm), of the isolation system at the displacement D_M, as prescribed by Eq. 17.2-3

D_M = maximum displacement, in in. (mm), at the center of rigidity of the isolation system in the direction under consideration, as prescribed by Eq. 17.5-3

V_b shall not be taken as less than the maximum force in the isolation system at any displacement up to and including the maximum displacement D_M, as defined in Section 17.5.3.

Overturning loads on elements of the isolation system, the foundation, and structural elements below the base level due to lateral seismic force V_b shall be based on the vertical distribution of force of Section 17.5.5, except that the unreduced lateral seismic design force V_{st} shall be used in lieu of V_s in Eq. 17.5-9.

17.5.4.2 Structural Elements above the Base Level

The structure above the base level shall be designed and constructed using all of the applicable requirements for a non-isolated structure for a minimum shear force, Vs, determined using upper-bound and lower-bound isolation system properties, as prescribed by Eq. 17.5-6:

$$V_s = \frac{V_{st}}{R_I} \tag{17.5-6}$$

where

R_I = numerical coefficient related to the type of seismic force-resisting system above the isolation system

V_{st} = total unreduced lateral seismic design force or shear on elements above the base level, as prescribed by Eq. 17.5-7.

The R_I factor shall be based on the type of seismic force-resisting system used for the structure above the base level in the direction of interest and shall be three-eighths of the value of R given in Table 12.2-1, with a maximum value not greater than 2.0 and a minimum value not less than 1.0.

EXCEPTION: The value of R_I is permitted to be taken greater than 2.0, provided the strength of structure above the base level in the direction of interest, as determined by nonlinear static analysis at a roof displacement corresponding to a maximum story drift the lesser of the MCE design drift or 0.015 h_{sx} is not less than 1.1 times V_b.

The total unreduced lateral seismic force or shear on elements above the base level shall be determined using upper-bound and lower-bound isolation system properties, as prescribed by Eq. 17.5-7:

$$V_{st} = V_b \left(\frac{W_s}{W} \right)^{(1-2.5\beta_M)} \tag{17.5-7}$$

where

W = effective seismic weight, in kips (kN) of the structure above the isolation interface as defined in Section 12.7.2, in kip (kN)

W_s = effective seismic weight, in kips (kN) of the structure above the isolation interface as defined in Section 12.7.2, in kips (kN), excluding the effective seismic weight, in kips (kN), of the base level

The effective seismic weight W_s in Equation 17.5.7 shall be taken as equal to W when the average distance from top of isolator to the underside of base level floor framing above the isolators exceeds 3 feet.

EXCEPTION: For isolation systems whose hysteretic behavior is characterized by an abrupt transition from pre-yield to post-yield or pre-slip to post-slip behavior, the exponent term $(1–2.5\beta_M)$ in equation (17.5-7) shall be replaced by $(1–3.5\beta_M)$.

17.5.4.3 Limits on V_s

The value of V_s shall not be taken as less than each of the following:

1.   The lateral seismic force required by Section 12.8 for a fixed-base structure of the same effective seismic weight, W_S, and a period equal to the period of the isolation system using the upper bound properties T_M.

2.   The base shear corresponding to the factored design wind load.

3.   The lateral seismic force, V_{st}, calculated using Eq. 17.5-7, and with V_b set equal to the force required to fully activate the isolation system utilizing the greater of the upper bound properties, or

1.5 times the nominal properties, for the yield level of a softening system,

the ultimate capacity of a sacrificial wind-restraint system,

the break-away friction force of a sliding system, or

the force at zero displacement of a sliding system following a complete dynamic cycle of motion at D_M.

17.5.5 Vertical Distribution of Force

The lateral seismic force V_s shall be distributed over the height of the structure above the base level, using upper-bound and lower-bound isolation system properties, using the following equations:

$$F_1 = (V_b - V_{st})/R_I$$
(17.5-8)

and

$$F_x = C_{vx}V_s$$
(17.5-9)

and

$$C_{vx} = \frac{w_x h_x^k}{\sum_{i=2}^{n} w_i h_i^k}$$
(17.5-10)

and

$$k = 14\beta_M T_{fb}$$
(17.5-11)

where

F_1 = lateral seismic force, in kips (or kN) induced at Level 1, the base level

F_x = lateral seismic force, in kips (or kN) induced at Level x, $x>1$

C_{vx} = vertical distribution factor

V_s = total lateral seismic design force or shear on elements above the base level as prescribed by Eq. 17.5-6 and the limits of Section 17.5.4.3

w_x = portion of W_s that is located at or assigned to Level i or x

h_x = height above the isolation interface of Level i or x

T_{fb} = the fundamental period, in s, of the structure above the isolation interface determined using a rational modal analysis assuming fixed-base conditions.

EXCEPTION: In lieu of Equation 17.5-7 and 17.5-9, the lateral seismic force F_x is permitted to be calculated as the average value of the force at Level x in the direction of interest using the results of a simplified stick model of the building and a lumped representation of the isolation system using response history analysis scaled to V_b/R_I at the base level.

17.5.6 Drift Limits

The maximum story drift of the structure above the isolation system shall not exceed $0.015h_{sx}$. The drift shall be calculated by Eq. 12.8-15 with C_d for the isolated structure equal to R_I as defined in Section 17.5.4.2.

17.6 DYNAMIC ANALYSIS PROCEDURES

17.6.1 General

Where dynamic analysis is used to design seismically isolated structures, the requirements of this section shall apply.

17.6.2 Modeling

The mathematical models of the isolated structure including the isolation system, the seismic force-resisting system, and other structural elements shall conform to Section 12.7.3 and to the requirements of Sections 17.6.2.1 and 17.6.2.2.

17.6.2.1 Isolation System

The isolation system shall be modeled using deformational characteristics developed in accordance with Section 17.2.8. The lateral displacements and forces shall be computed separately for upper-bound and lower-bound isolation system properties as defined in Section 17.2.8.5. The isolation system shall be modeled with sufficient detail to capture all of the following:

1. Spatial distribution of isolator units.

2. Translation, in both horizontal directions, and torsion of the structure above the isolation interface considering the most disadvantageous location of eccentric mass.

3. Overturning/uplift forces on individual isolator units.

4. Effects of vertical load, bilateral load, and/or the rate of loading if the force-deflection properties of the isolation system are dependent on one or more of these attributes.

The total maximum displacement, D_{TM}, across the isolation system shall be calculated using a model of the isolated structure that incorporates the force-deflection characteristics of nonlinear elements of the isolation system and the seismic force-resisting system.

17.6.2.2 Isolated Structure

The maximum displacement of each floor and design forces and displacements in elements of the seismic force-resisting system are permitted to be calculated using a linear elastic model of the isolated structure provided that all elements of the seismic force-resisting system of the structure above the isolation system remain essentially elastic.

Seismic force-resisting systems with essentially elastic elements include, but are not limited to, regular structural systems designed for a lateral force not less than 100 percent of V_s determined in accordance with Sections 17.5.4.2 and 17.5.4.3.

The analysis of the isolation system and structure shall be performed separately for upper-bound and lower-bound properties, and the governing case for each response parameter of interest shall be used for design.

17.6.3 Description of Procedures

17.6.3.1 General

Response-spectrum analysis shall be performed in accordance with Section 12.9 and the requirements of Section 17.6.3.3. Response history analysis shall be performed in accordance with the requirements of Section 17.6.3.4.

17.6.3.2 MCE_R Ground Motions

The MCE_R ground motions of Section 17.3 shall be used to calculate the lateral forces and displacements in the isolated structure, the total maximum displacement of the isolation system, and the forces in the isolator units, isolator unit connections, and supporting framing immediately above and below the isolators used to resist isolator P-Δ demands.

17.6.3.3 Response-Spectrum Analysis Procedure

Response-spectrum analysis shall be performed using a modal damping value for the fundamental mode in the direction of interest not greater than the effective damping of the isolation system or 30 percent of critical, whichever is less. Modal damping values for higher modes shall be selected consistent with those that would be appropriate for response-spectrum analysis of the structure above the isolation system assuming a fixed base.

Response-spectrum analysis used to determine the total maximum displacement shall include simultaneous excitation of the model by 100 percent of the ground motion in the critical direction and 30 percent of the ground motion in the perpendicular, horizontal direction. The maximum displacement of the isolation system shall be calculated as the vector sum of the two orthogonal displacements.

17.6.3.4 Response-History Analysis Procedure

Response-history analysis shall be performed for a set of ground motion pairs selected and scaled in accordance with Section 17.3.2. Each pair of ground motion components shall be applied simultaneously to the model considering the most disadvantageous location of eccentric mass. The maximum displacement of the isolation system shall be calculated from the vectorial sum of the two orthogonal displacements at each time step.

The parameters of interest shall be calculated for each ground motion used for the response-history analysis and the average value of the response parameter of interest shall be used for design.

For sites identified as near fault each pair of horizontal ground motion components shall be rotated to the fault-normal and fault-parallel directions of the causative faults and applied to the building in such orientation.

For all other sites, individual pairs of horizontal ground motion components need not be applied in multiple orientations.

17.6.3.4.1 Accidental Mass Eccentricity

Torsional response resulting from lack of symmetry in mass and stiffness shall be accounted for in the analysis. In addition, accidental eccentricity consisting of displacement of the center-of-mass from the computed location by an amount equal to 5% of the diaphragm dimension, separately in each of two orthogonal directions at the level under consideration.

The effects of accidental eccentricity are permitted to be accounted for by amplifying forces, drifts and deformations determined from an analysis using only the computed center-of-mass, provided that factors used to amplify forces, drifts and deformations of the center-of-mass analysis are shown to produce results that bound all the mass-eccentric cases.

17.6.4 Minimum Lateral Displacements and Forces

17.6.4.1 Isolation System and Structural Elements below the Base Level

The isolation system, foundation, and all structural elements below the base level shall be designed using all of the applicable requirements for a non-isolated structure and the forces obtained from the dynamic analysis without reduction, but the design lateral force shall not be taken as less than 90 percent of V_b determined by Eq. 17.5-5.

The total maximum displacement of the isolation system shall not be taken as less than 80 percent of D_{TM} as prescribed by Section 17.5.3.3 except that D'_M is permitted to be used in lieu of D_M where:

$$D'_M = \frac{D_M}{\sqrt{1 + (T/T_M)^2}}$$

(17.6-1)

and

D_M = maximum displacement in in. (mm), at the center of rigidity of the isolation system in the direction under consideration, as prescribed by Eq. 17.5-1

T = elastic, fixed-base period, in s, of the structure above the isolation system as determined by Section 12.8.2, and including the coefficient C_u, if the approximate period formulas are used to calculate the fundamental period

T_M = effective period, in s, of the seismically isolated structure, at the displacement D_M in the direction under consideration, as prescribed by Eq. 17.5-2

17.6.4.2 Structural Elements above the Base Level

Subject to the procedure-specific limits of this section, structural elements above the base level shall be designed using the applicable requirements for a non-isolated structure and the forces obtained from the dynamic analysis reduced by a factor of R_I as determined in accordance with Section 17.5.4.2.

For response spectrum analysis, the design shear at any story shall not be less than the story shear resulting from application of the forces calculated using Eq. 17.5-9 and a value of V_b equal to the base shear obtained from the response-spectrum analysis in the direction of interest.

For response history analysis of regular structures, the value of V_b shall not be taken as less than 80 percent of that determined in accordance with 17.5.4.1, and the value V_s shall not be taken as less than 100 percent of the limits specified by Section 17.5.4.3.

For response history analysis of irregular structures, the value of V_b shall not be taken as less than 100 percent of that determined in accordance with 17.5.4.1, and the value V_s shall not be taken as less than 100 percent of the limits specified by Section 17.5.4.3.

17.6.4.3 Scaling of Results

Where the factored lateral shear force on structural elements, determined using either response-spectrum or response-history procedure, is less than the minimum values prescribed by Sections 17.6.4.1 and 17.6.4.2, all design parameters shall be adjusted upward proportionally.

17.6.4.4 Drift Limits

Maximum story drift corresponding to the design lateral force including displacement due to vertical deformation of the isolation system shall comply with either of the following limits:

1. Where response spectra analysis is used the maximum story drift of the structure above the isolation system shall not exceed $0.015h_{sx}$.

2. Where response history analysis based on the force-deflection characteristics of nonlinear elements of the seismic force-resisting system is used the maximum story drift of the structure above the isolation system shall not exceed $0.020h_{sx}$.

Drift shall be calculated using Eq. 12.8-15 with the C_d of the isolated structure equal to R_I as defined in Section 17.5.4.2.

The secondary effects of the maximum lateral displacement of the structure above the isolation system combined with gravity forces shall be investigated if the story drift ratio exceeds $0.010/R_I$.

17.7 DESIGN REVIEW

An independent design review of the isolation system and related test programs shall be performed by one or more individuals possessing knowledge of the following items with a minimum of one reviewer being a RDP. Isolation system design review shall include, but not be limited to, all of the following:

1. Project design criteria including site-specific spectra and ground motion histories.

2. Preliminary design including the selection of the devices, determination of the total design displacement, the total maximum displacement, and the lateral force level.

3. Review of qualification data and appropriate property modification factors for the manufacturer and device selected.

4. Prototype testing program (Section 17.8).

5. Final design of the entire structural system and all supporting analyses including modelling of isolators for response history analysis if performed.

6. Isolator production testing program (Section 17.8.5).

7.

17.8 TESTING

17.8.1 General

The deformation characteristics and damping values of the isolation system used in the design and analysis of seismically isolated structures shall be based on tests of a selected sample of the components prior to construction as described in this section. The isolation system components to be tested shall include the wind-restraint system if such a system is used in the design.

The tests specified in this section are for establishing and validating the isolator unit and isolation system test properties which are used to determine design properties of the isolation system in accordance Section 17.2.8.

17.8.1.1 Qualification Tests

Isolation device manufacturers shall submit for approval by the registered design professional the results of qualification tests, analysis of test data and supporting scientific studies that are permitted to be used to quantify the effects of heating due to cyclic dynamic motion, loading rate, scragging, variability and uncertainty in production bearing properties, temperature, aging, environmental exposure, and contamination. The qualification testing shall be applicable to the component types, models, materials and sizes to be used in the construction. The qualification testing shall have been performed on components manufactured by the same manufacturer supplying the components to be used in the construction. When scaled specimens are used in the qualification testing, principles of scaling and similarity shall be used in the interpretation of the data.

17.8.2 Prototype Tests

Prototype tests shall be performed separately on two full-size specimens (or sets of specimens, as appropriate) of each predominant type and size of isolator unit of the isolation system. The test specimens shall include the wind-restraint system if such a system is used in the design. Specimens tested shall not be used for construction unless accepted by the registered design professional responsible for the design of the structure.

17.8.2.1 Record

For each cycle of each test, the force-deflection behavior of the test specimen shall be recorded.

17.8.2.2 Sequence and Cycles

Each of the following sequence of tests shall be performed for the prescribed number of cycles at a vertical load equal to the average dead load plus one-half the effects due to live load on all isolator units of a common type and size. Prior to these tests being performed the production set of tests specified is Section 17.8.5 shall be performed on each isolator:

1. Twenty fully reversed cycles of loading at a lateral force corresponding to the wind design force.

2. The sequence of either item (a) or item (b) below shall be performed:

   a. Three fully reversed cycles of quasi-static loading at each of the following increments of the displacement — $0.25D_M$, $0.5D_M$, $0.67D_M$, and $1.0D_M$ where D_M is determined in Section 17.5.3.1 or Section 17.6, as appropriate.

   b. The following sequence, performed dynamically at the effective period, T_M: continuous loading of one fully-reversed cycle at each of the following increments of the total maximum displacement 1.0 D_M, 0.67 D_M, 0.5 D_M and 0.25 D_M followed by

continuous loading of one fully-reversed cycle at 0.25 D_M, 0.5 D_M, 0.67 D_M, and 1.0 D_M. A rest interval is permitted between these two sequences.

3. Three fully reversed cycles of <mark>quasi-static or dynamic (at the effective period T_M)</mark> loading at the maximum displacement, $1.0D_M$.

4. The sequence of either item (a) or item (b) below shall be performed:

   a. $30S_{M1}/(S_{MS}B_M)$, but not less than 10, continuous fully reversed cycles of <mark>quasi-static</mark> loading at 0.75 times the total maximum displacement, $0.75D_M$.

   b. The test of 17.8.2.2.4.(a), performed dynamically at the effective period, T_M. This test may comprise separate sets of multiple cycles of loading, with each set consisting of not less than five continuous cycles.

If an isolator unit is also a vertical-load-carrying element, then item 2 of the sequence of cyclic tests specified in the preceding text shall be performed for two additional vertical load cases specified in Section 17.2.7.1. The load increment due to earthquake overturning, Q_E, shall be equal to or greater than the peak earthquake vertical force response corresponding to the test displacement being evaluated. In these tests, the combined vertical load shall be taken as the typical or average downward force on all isolator units of a common type and size. Axial load and displacement values for each test shall be the greater of those determined by analysis using upper-bound and lower-bound values of isolation system properties determined in accordance with Section 17.2.8.5. The effective period T_M shall be the lower of those determined by analysis using upper-bound and lower-bound values.

17.8.2.3 Dynamic Testing

Tests specified in Section 17.8.2.2 shall be performed <mark>either quasi-statically or</mark> dynamically at the lower of the effective periods, T_M, determined using upper-bound and lower-bound properties. <mark>The RDP shall specify whether testing shall be performed quasi-statically or dynamically. When testing is performed quasi-statically, the dynamic effects shall be accounted for in analysis and design using appropriate property modification factors.</mark>

Dynamic testing shall not be required if the prototype testing has been performed dynamically on similar sized isolators meeting the requirements of Section 17.8.2.7, and the testing was conducted at similar loads and accounted for the effects of velocity, amplitude of displacement, and heating affects. The prior dynamic prototype test data shall be used to establish factors that adjust three-cycle average values of k_d and E_{loop} to account for the difference in test velocity and heating effects and to establish $\lambda_{(test, min)}$ and $\lambda_{(test, max)}$.

Only if full scale testing is not possible reduced-scale prototype specimens can be used to quantify rate-dependent properties of isolators. The reduced-scale prototype specimens shall be of the same type and material and be manufactured with the same processes and quality as full-scale prototypes and shall be tested at a frequency that represents full-scale prototype loading rates.

If the force-deflection properties of the isolator units exhibit bilateral load dependence, the tests specified in Sections 17.8.2.2 and 17.8.2.3 shall be augmented to include bilateral load at the following increments of the total design displacement, D_M: 0.25 and 1.0, 0.5 and 1.0, 0.67 and 1.0, and 1.0 and 1.0.

 If reduced-scale specimens are used to quantify bilateral-load-dependent properties they shall meet the requirements of Section 17.8.2.7., the reduced-scale specimens shall be of the same type and material and manufactured with the same processes and quality as full-scale prototypes.

The force-deflection properties of an isolator unit shall be considered to be dependent on bilateral load if the effective stiffness where subjected to bilateral loading is different from the effective stiffness where subjected to unilateral loading, by more than 15 percent.

17.8.2.5 Maximum and Minimum Vertical Load

Isolator units that carry vertical load shall be subjected to one fully reversed cycle of loading at the total maximum displacement, D_{TM}, and at each of the vertical loads corresponding to the maximum and minimum downward vertical loads as specified in Section 17.2.7.1 on any one isolator of a common type and size. Axial load and displacement values for each test shall be the greater of those determined by analysis using the upper-bound and lower-bound values of isolation system properties determined in accordance with Section 17.2.8.5.

EXCEPTION: In lieu of envelope values for a single test, it shall be acceptable to perform two tests, one each for the combination of vertical load and horizontal displacement obtained from analysis using the upper-bound and lower-bound values of isolation system properties, respectively, determined in accordance with Section 17.2.8.5.

17.8.2.6 Sacrificial Wind-Restraint Systems

If a sacrificial wind-restraint system is to be utilized, its ultimate capacity shall be established by test.

17.8.2.7 Testing Similar Units

Prototype tests need not be performed if an isolator unit when compared to another tested unit, complies with all of the following criteria:

1. The isolator design is not more than 15% larger nor more than 30% smaller than the previously tested prototype, in terms of governing device dimensions; and

2. Is of the same type and materials; and

3. Has an energy dissipated per cycle, E_{loop}, that is not less than 85% of the previously tested unit, and

4. Is fabricated by the same manufacturer using the same or more stringent documented manufacturing and quality control procedures.

5. For elastomeric type isolators, the design shall not be subject to a greater shear strain nor greater vertical stress than that of the previously tested prototype.

6. For sliding type isolators, the design shall not be subject to a greater vertical stress or sliding velocity than that of the previously tested prototype using the same sliding material.

The prototype testing exemption above shall be approved by independent design review, as specified in Section 17.7.

When the results of tests of similar isolator units are used to establish dynamic properties in accordance with Section 17.8.2.3, in addition to items 2 to 4 above, the following criteria shall be satisfied:

7. The similar unit shall be tested at a frequency that represents design full-scale loading rates in accordance with principles of scaling and similarity.

8. The length scale of reduced-scale specimens shall not be greater than two.

17.8.3 Determination of Force-Deflection Characteristics

The force-deflection characteristics of an isolator unit shall be based on the cyclic load tests of prototype isolators specified in Section 17.8.2.

As required, the effective stiffness of an isolator unit, k_{eff}, shall be calculated for each cycle of loading as prescribed by Eq. 17.8-1:

$$k_{eff} = \frac{|F^+| + |F^-|}{|\Delta^+| + |\Delta^-|}$$

(17.8-1)

where F^+ and F^- are the positive and negative forces, at the maximum positive and minimum negative displacements Δ^+ and Δ^-, respectively.

As required, the effective damping, β_{eff}, of an isolator unit shall be calculated for each cycle of loading by Eq. 17.8-2:

$$\beta_{eff} = \frac{2}{\pi} \frac{E_{loop}}{k_{eff} \left(|\Delta^+| + |\Delta^-| \right)^2}$$

(17.8-2)

where the energy dissipated per cycle of loading, E_{loop}, and the effective stiffness, k_{eff}, shall be based on peak test displacements of Δ^+ and Δ^-.

As required, the post-yield stiffness, k_d, of each isolator unit shall be calculated for each cycle of loading using the following assumptions:

1. A test loop shall be assumed to have a bilinear hysteretic characteristics with values of k_1, k_d, F_o, F_y, k_{eff}, and E_{loop} as shown in Figure 17.8.3-1

2. The computed loop shall have the same values of effective stiffness, k_{eff}, and energy dissipated per cycle of loading, E_{loop}, as the test loop.

3. The assumed value of k_1 shall be a visual fit to the elastic stiffness of the isolator unit during unloading immediately after D_M.
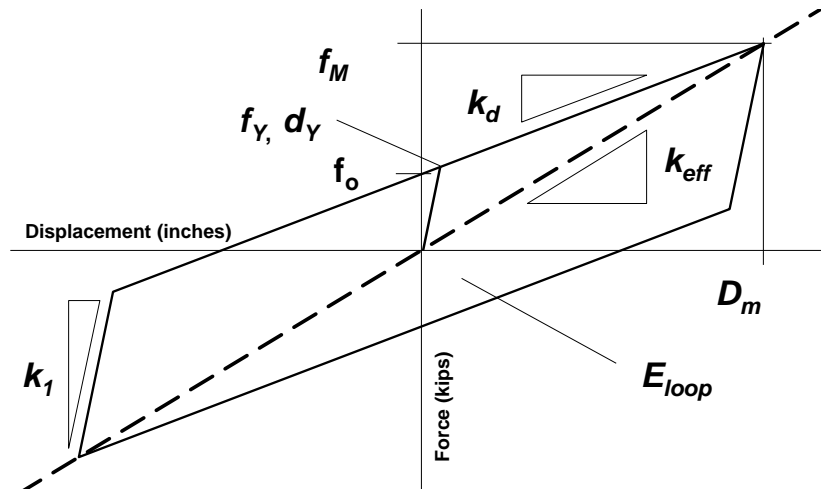
Figure 17.8.3-1 Nominal Properties of the Isolator Bilinear Force-Deflection Model

It is permitted to use different methods for fitting the loop, such as a straight-line fit of k_d directly to the hysteresis curve and then determining k_1 to match E_{loop}, or defining D_y and F_y by visual fit and then determining k_d to match E_{loop}.

189

17.8.4 Test Specimen Adequacy

The performance of the test specimens shall be deemed adequate if all of the following conditions are satisfied:

1. The force-deflection plots for all tests specified in Section 17.8.2 have a positive incremental force-resisting capacity.

2. The average post-yield stiffness, k_d, and energy dissipated per cycle, E_{loop}, for the three cycles of test specified in Section 17.8.2.2(3) for the vertical load equal to the average dead load plus one-half the effects due to live load, including the effects of heating and rate of loading in accordance with Section 17.2.8.3, shall fall within the range of the nominal design values defined by the permissible individual isolator range which are typically +/-5% greater than the $\lambda_{(spec, min)}$ and $\lambda_{(spec, max)}$ range for the average of all isolators.

3. For each increment of test displacement specified in item 2 and item 3 of Section 17.8.2.2 and for each vertical load case specified in Section 17.8.2.2,

   a. For each test specimen the value of the post-yield stiffness, k_d, at each of the cycles of test at a common displacement shall fall within the range defined by $\lambda_{(test, min)}$ and $\lambda_{(test, max)}$ multiplied by the nominal value of post-yield stiffness.

   b. For each cycle of test, the difference between post-yield stiffness, k_d, effective stiffness of the two test specimens of a common type and size of the isolator unit and the average effective stiffness is no greater than 15 percent.

4. ~~For each specimen there is no greater than a 20 percent change in the initial effective stiffness over the cycles of test specified in item 4 of Section 17.8.2.2.~~

4~~5~~. For each test specimen the value of the post-yield stiffness, k_d, and energy dissipated per cycle, E_{loop}, for any number of cycle~~s of each set of five cycles~~ of test 17.8.2.2.4, as determined by the RDP and approved by the reviewer(s), shall fall within the range of the nominal design values defined by $\lambda_{(test, min)}$ and $\lambda_{(test, max)}$. The number of cycles specified by the RDP shall be consistent with the number of equivalent number of cycles at $0.75D_M$ which is representative of the expected performance of the isolation system for the local seismic hazard conditions. When not specified by the RDP, the number of cycles shall be four.

6. ~~For each specimen there is no greater than a 20 percent decrease in the initial effective damping over the cycles of test specified in item 4 of Section 17.8.2.2.~~

5~~7~~. All specimens of vertical-load-carrying elements of the isolation system remain stable where tested in accordance with Section 17.8.2.5.

EXCEPTION: The registered design professional is permitted to adjust the limits of items ~~3 and 4~~ 2 and 3 to account for the property variation factors of Section 17.2.8 used for design of the isolation system.

17.8.5 Production Tests

A test program for the isolator units used in the construction shall be established by the registered design professional. The test program shall evaluate the consistency of measured values of nominal isolator unit properties by testing 100% of the isolators in combined compression and shear at not less than two-thirds of the maximum displacement, D_M, determined using lower bound properties.

The mean results of all tests shall fall within the range of values defined by the $\lambda_{(spec, max)}$ and $\lambda_{(spec, min)}$ values established in Section 17.2.8.4. A different range of values is permitted to be used for individual

isolator units and for the average value across all isolators of a given unit type provided that differences in the ranges of values are accounted for in the design of the each element of the isolation system, as prescribed in Section 17.2.8.4.

This Page is Intentionally Left Blank

APPENDIX E

ASCE 7-2016 COMMENTARY- DEFAULT LAMBDA FACTORS

Variable	Unlubricated Interfaces	Lubricated (liquid) Interfaces	Plain Low Damping Elastomeric	LRB	LRB	HDR	HDR
Symbol	μ or Q_d	μ or Q_d	K	K_d	Q_d	K_d	Q_d
Example - Aging and Environmental Factors							
Aging - λa	1.3	1.8	1.3	1.3	1	1.4	1.3
Contamination - λc	1.2	1.4	1	1	1	1	1
Example Upper Bound - $\lambda(ae,max)$	1.56	2.52	1.3	1.3	1	1.4	1.3
Example Lower Bound - $\lambda(ae,min)$	1	1	1	1	1	1	1
Example - Testing Factors							
All cyclic effects, Upper	1.3	1.3	1.3	1.3	1.6	1.5	1.3
All cyclic effects, Lower	0.7	0.7	0.9	0.9	0.9	0.9	0.9
Example Upper Bound - $\lambda(test,max)$	1.3	1.3	1.3	1.3	1.6	1.5	1.3
Example Lower Bound - $\lambda(test,min)$	0.7	0.7	0.9	0.9	0.9	0.9	0.9
$\lambda_{(PM, max.)} = (1+ (0.75*(\lambda_{(ae, max.)} -1)) * \lambda_{(test, max.)}$	1.85	2.78	1.59	1.59	1.6	1.95	1.59
$\lambda_{(PM, min.)} = (1- (0.75*(1- \lambda_{(ae, min.)})) * \lambda_{(test, min.)}$	0.7	0.7	0.9	0.9	0.9	0.9	0.9
Example – Specification Factors							
Lambda factor for Spec. Tolerance - $\lambda(spec, max)$	1.15	1.15	1.15	1.15	1.15	1.15	1.15
Lambda factor for Spec. Tolerance - $\lambda(spec, min)$	0.85	0.85	0.85	0.85	0.85	0.85	0.85
Upper Bound Design Property Multiplier	2.12	3.2	1.83	1.83	1.84	2.24	1.83
Lower Bound Design Property Multiplier	0.6	0.6	0.77	0.77	0.77	0.77	0.77
Default UB Design Property Multiplier	**2.1**	**3.2**	**1.8**	**1.8**	**1.8**	**2.2**	**1.8**
Default LB Design Property Multiplier	**0.6**	**0.6**	**0.8**	**0.8**	**0.8**	**0.8**	**0.8**

MCEER Technical Reports

MCEER publishes technical reports on a variety of subjects written by authors funded through MCEER. These reports are available from both MCEER Publications and the National Technical Information Service (NTIS). Requests for reports should be directed to MCEER Publications, MCEER, University at Buffalo, State University of New York, 133A Ketter Hall, Buffalo, New York 14260. Reports can also be requested through NTIS, P.O. Box 1425, Springfield, Virginia 22151. NTIS accession numbers are shown in parenthesis, if available.

NCEER-87-0001 "First-Year Program in Research, Education and Technology Transfer," 3/5/87, (PB88-134275, A04, MF-A01).

NCEER-87-0002 "Experimental Evaluation of Instantaneous Optimal Algorithms for Structural Control," by R.C. Lin, T.T. Soong and A.M. Reinhorn, 4/20/87, (PB88-134341, A04, MF-A01).

NCEER-87-0003 "Experimentation Using the Earthquake Simulation Facilities at University at Buffalo," by A.M. Reinhorn and R.L. Ketter, not available.

NCEER-87-0004 "The System Characteristics and Performance of a Shaking Table," by J.S. Hwang, K.C. Chang and G.C. Lee, 6/1/87, (PB88-134259, A03, MF-A01). This report is available only through NTIS (see address given above).

NCEER-87-0005 "A Finite Element Formulation for Nonlinear Viscoplastic Material Using a Q Model," by O. Gyebi and G. Dasgupta, 11/2/87, (PB88-213764, A08, MF-A01).

NCEER-87-0006 "Symbolic Manipulation Program (SMP) - Algebraic Codes for Two and Three Dimensional Finite Element Formulations," by X. Lee and G. Dasgupta, 11/9/87, (PB88-218522, A05, MF-A01).

NCEER-87-0007 "Instantaneous Optimal Control Laws for Tall Buildings Under Seismic Excitations," by J.N. Yang, A. Akbarpour and P. Ghaemmaghami, 6/10/87, (PB88-134333, A06, MF-A01). This report is only available through NTIS (see address given above).

NCEER-87-0008 "IDARC: Inelastic Damage Analysis of Reinforced Concrete Frame - Shear-Wall Structures," by Y.J. Park, A.M. Reinhorn and S.K. Kunnath, 7/20/87, (PB88-134325, A09, MF-A01). This report is only available through NTIS (see address given above).

NCEER-87-0009 "Liquefaction Potential for New York State: A Preliminary Report on Sites in Manhattan and Buffalo," by M. Budhu, V. Vijayakumar, R.F. Giese and L. Baumgras, 8/31/87, (PB88-163704, A03, MF-A01). This report is available only through NTIS (see address given above).

NCEER-87-0010 "Vertical and Torsional Vibration of Foundations in Inhomogeneous Media," by A.S. Veletsos and K.W. Dotson, 6/1/87, (PB88-134291, A03, MF-A01). This report is only available through NTIS (see address given above).

NCEER-87-0011 "Seismic Probabilistic Risk Assessment and Seismic Margins Studies for Nuclear Power Plants," by Howard H.M. Hwang, 6/15/87, (PB88-134267, A03, MF-A01). This report is only available through NTIS (see address given above).

NCEER-87-0012 "Parametric Studies of Frequency Response of Secondary Systems Under Ground-Acceleration Excitations," by Y. Yong and Y.K. Lin, 6/10/87, (PB88-134309, A03, MF-A01). This report is only available through NTIS (see address given above).

NCEER-87-0013 "Frequency Response of Secondary Systems Under Seismic Excitation," by J.A. HoLung, J. Cai and Y.K. Lin, 7/31/87, (PB88-134317, A05, MF-A01). This report is only available through NTIS (see address given above).

NCEER-87-0014 "Modelling Earthquake Ground Motions in Seismically Active Regions Using Parametric Time Series Methods," by G.W. Ellis and A.S. Cakmak, 8/25/87, (PB88-134283, A08, MF-A01). This report is only available through NTIS (see address given above).

NCEER-87-0015 "Detection and Assessment of Seismic Structural Damage," by E. DiPasquale and A.S. Cakmak, 8/25/87, (PB88-163712, A05, MF-A01). This report is only available through NTIS (see address given above).

NCEER-87-0016 "Pipeline Experiment at Parkfield, California," by J. Isenberg and E. Richardson, 9/15/87, (PB88-163720, A03, MF-A01). This report is available only through NTIS (see address given above).

NCEER-87-0017 "Digital Simulation of Seismic Ground Motion," by M. Shinozuka, G. Deodatis and T. Harada, 8/31/87, (PB88-155197, A04, MF-A01). This report is available only through NTIS (see address given above).

NCEER-87-0018 "Practical Considerations for Structural Control: System Uncertainty, System Time Delay and Truncation of Small Control Forces," J.N. Yang and A. Akbarpour, 8/10/87, (PB88-163738, A08, MF-A01). This report is only available through NTIS (see address given above).

NCEER-87-0019 "Modal Analysis of Nonclassically Damped Structural Systems Using Canonical Transformation," by J.N. Yang, S. Sarkani and F.X. Long, 9/27/87, (PB88-187851, A04, MF-A01).

NCEER-87-0020 "A Nonstationary Solution in Random Vibration Theory," by J.R. Red-Horse and P.D. Spanos, 11/3/87, (PB88-163746, A03, MF-A01).

NCEER-87-0021 "Horizontal Impedances for Radially Inhomogeneous Viscoelastic Soil Layers," by A.S. Veletsos and K.W. Dotson, 10/15/87, (PB88-150859, A04, MF-A01).

NCEER-87-0022 "Seismic Damage Assessment of Reinforced Concrete Members," by Y.S. Chung, C. Meyer and M. Shinozuka, 10/9/87, (PB88-150867, A05, MF-A01). This report is available only through NTIS (see address given above).

NCEER-87-0023 "Active Structural Control in Civil Engineering," by T.T. Soong, 11/11/87, (PB88-187778, A03, MF-A01).

NCEER-87-0024 "Vertical and Torsional Impedances for Radially Inhomogeneous Viscoelastic Soil Layers," by K.W. Dotson and A.S. Veletsos, 12/87, (PB88-187786, A03, MF-A01).

NCEER-87-0025 "Proceedings from the Symposium on Seismic Hazards, Ground Motions, Soil-Liquefaction and Engineering Practice in Eastern North America," October 20-22, 1987, edited by K.H. Jacob, 12/87, (PB88-188115, A23, MF-A01). This report is available only through NTIS (see address given above).

NCEER-87-0026 "Report on the Whittier-Narrows, California, Earthquake of October 1, 1987," by J. Pantelic and A. Reinhorn, 11/87, (PB88-187752, A03, MF-A01). This report is available only through NTIS (see address given above).

NCEER-87-0027 "Design of a Modular Program for Transient Nonlinear Analysis of Large 3-D Building Structures," by S. Srivastav and J.F. Abel, 12/30/87, (PB88-187950, A05, MF-A01). This report is only available through NTIS (see address given above).

NCEER-87-0028 "Second-Year Program in Research, Education and Technology Transfer," 3/8/88, (PB88-219480, A04, MF-A01).

NCEER-88-0001 "Workshop on Seismic Computer Analysis and Design of Buildings With Interactive Graphics," by W. McGuire, J.F. Abel and C.H. Conley, 1/18/88, (PB88-187760, A03, MF-A01). This report is only available through NTIS (see address given above).

NCEER-88-0002 "Optimal Control of Nonlinear Flexible Structures," by J.N. Yang, F.X. Long and D. Wong, 1/22/88, (PB88-213772, A06, MF-A01).

NCEER-88-0003 "Substructuring Techniques in the Time Domain for Primary-Secondary Structural Systems," by G.D. Manolis and G. Juhn, 2/10/88, (PB88-213780, A04, MF-A01).

NCEER-88-0004 "Iterative Seismic Analysis of Primary-Secondary Systems," by A. Singhal, L.D. Lutes and P.D. Spanos, 2/23/88, (PB88-213798, A04, MF-A01).

NCEER-88-0005 "Stochastic Finite Element Expansion for Random Media," by P.D. Spanos and R. Ghanem, 3/14/88, (PB88-213806, A03, MF-A01).

NCEER-88-0006   "Combining Structural Optimization and Structural Control," by F.Y. Cheng and C.P. Pantelides, 1/10/88, (PB88-213814, A05, MF-A01).

NCEER-88-0007   "Seismic Performance Assessment of Code-Designed Structures," by H.H-M. Hwang, J-W. Jaw and H-J. Shau, 3/20/88, (PB88-219423, A04, MF-A01). This report is only available through NTIS (see address given above).

NCEER-88-0008   "Reliability Analysis of Code-Designed Structures Under Natural Hazards," by H.H-M. Hwang, H. Ushiba and M. Shinozuka, 2/29/88, (PB88-229471, A07, MF-A01). This report is only available through NTIS (see address given above).

NCEER-88-0009   "Seismic Fragility Analysis of Shear Wall Structures," by J-W Jaw and H.H-M. Hwang, 4/30/88, (PB89-102867, A04, MF-A01).

NCEER-88-0010   "Base Isolation of a Multi-Story Building Under a Harmonic Ground Motion - A Comparison of Performances of Various Systems," by F-G Fan, G. Ahmadi and I.G. Tadjbakhsh, 5/18/88, (PB89-122238, A06, MF-A01). This report is only available through NTIS (see address given above).

NCEER-88-0011   "Seismic Floor Response Spectra for a Combined System by Green's Functions," by F.M. Lavelle, L.A. Bergman and P.D. Spanos, 5/1/88, (PB89-102875, A03, MF-A01).

NCEER-88-0012   "A New Solution Technique for Randomly Excited Hysteretic Structures," by G.Q. Cai and Y.K. Lin, 5/16/88, (PB89-102883, A03, MF-A01).

NCEER-88-0013   "A Study of Radiation Damping and Soil-Structure Interaction Effects in the Centrifuge," by K. Weissman, supervised by J.H. Prevost, 5/24/88, (PB89-144703, A06, MF-A01).

NCEER-88-0014   "Parameter Identification and Implementation of a Kinematic Plasticity Model for Frictional Soils," by J.H. Prevost and D.V. Griffiths, not available.

NCEER-88-0015   "Two- and Three- Dimensional Dynamic Finite Element Analyses of the Long Valley Dam," by D.V. Griffiths and J.H. Prevost, 6/17/88, (PB89-144711, A04, MF-A01).

NCEER-88-0016   "Damage Assessment of Reinforced Concrete Structures in Eastern United States," by A.M. Reinhorn, M.J. Seidel, S.K. Kunnath and Y.J. Park, 6/15/88, (PB89-122220, A04, MF-A01). This report is only available through NTIS (see address given above).

NCEER-88-0017   "Dynamic Compliance of Vertically Loaded Strip Foundations in Multilayered Viscoelastic Soils," by S. Ahmad and A.S.M. Israil, 6/17/88, (PB89-102891, A04, MF-A01).

NCEER-88-0018   "An Experimental Study of Seismic Structural Response With Added Viscoelastic Dampers," by R.C. Lin, Z. Liang, T.T. Soong and R.H. Zhang, 6/30/88, (PB89-122212, A05, MF-A01). This report is available only through NTIS (see address given above).

NCEER-88-0019   "Experimental Investigation of Primary - Secondary System Interaction," by G.D. Manolis, G. Juhn and A.M. Reinhorn, 5/27/88, (PB89-122204, A04, MF-A01).

NCEER-88-0020   "A Response Spectrum Approach For Analysis of Nonclassically Damped Structures," by J.N. Yang, S. Sarkani and F.X. Long, 4/22/88, (PB89-102909, A04, MF-A01).

NCEER-88-0021   "Seismic Interaction of Structures and Soils: Stochastic Approach," by A.S. Veletsos and A.M. Prasad, 7/21/88, (PB89-122196, A04, MF-A01). This report is only available through NTIS (see address given above).

NCEER-88-0022   "Identification of the Serviceability Limit State and Detection of Seismic Structural Damage," by E. DiPasquale and A.S. Cakmak, 6/15/88, (PB89-122188, A05, MF-A01). This report is available only through NTIS (see address given above).

NCEER-88-0023   "Multi-Hazard Risk Analysis: Case of a Simple Offshore Structure," by B.K. Bhartia and E.H. Vanmarcke, 7/21/88, (PB89-145213, A05, MF-A01).

NCEER-88-0024   "Automated Seismic Design of Reinforced Concrete Buildings," by Y.S. Chung, C. Meyer and M. Shinozuka, 7/5/88, (PB89-122170, A06, MF-A01). This report is available only through NTIS (see address given above).

NCEER-88-0025   "Experimental Study of Active Control of MDOF Structures Under Seismic Excitations," by L.L. Chung, R.C. Lin, T.T. Soong and A.M. Reinhorn, 7/10/88, (PB89-122600, A04, MF-A01).

NCEER-88-0026   "Earthquake Simulation Tests of a Low-Rise Metal Structure," by J.S. Hwang, K.C. Chang, G.C. Lee and R.L. Ketter, 8/1/88, (PB89-102917, A04, MF-A01).

NCEER-88-0027   "Systems Study of Urban Response and Reconstruction Due to Catastrophic Earthquakes," by F. Kozin and H.K. Zhou, 9/22/88, (PB90-162348, A04, MF-A01).

NCEER-88-0028   "Seismic Fragility Analysis of Plane Frame Structures," by H.H-M. Hwang and Y.K. Low, 7/31/88, (PB89-131445, A06, MF-A01).

NCEER-88-0029   "Response Analysis of Stochastic Structures," by A. Kardara, C. Bucher and M. Shinozuka, 9/22/88, (PB89-174429, A04, MF-A01).

NCEER-88-0030   "Nonnormal Accelerations Due to Yielding in a Primary Structure," by D.C.K. Chen and L.D. Lutes, 9/19/88, (PB89-131437, A04, MF-A01).

NCEER-88-0031   "Design Approaches for Soil-Structure Interaction," by A.S. Veletsos, A.M. Prasad and Y. Tang, 12/30/88, (PB89-174437, A03, MF-A01). This report is available only through NTIS (see address given above).

NCEER-88-0032   "A Re-evaluation of Design Spectra for Seismic Damage Control," by C.J. Turkstra and A.G. Tallin, 11/7/88, (PB89-145221, A05, MF-A01).

NCEER-88-0033   "The Behavior and Design of Noncontact Lap Splices Subjected to Repeated Inelastic Tensile Loading," by V.E. Sagan, P. Gergely and R.N. White, 12/8/88, (PB89-163737, A08, MF-A01).

NCEER-88-0034   "Seismic Response of Pile Foundations," by S.M. Mamoon, P.K. Banerjee and S. Ahmad, 11/1/88, (PB89-145239, A04, MF-A01).

NCEER-88-0035   "Modeling of R/C Building Structures With Flexible Floor Diaphragms (IDARC2)," by A.M. Reinhorn, S.K. Kunnath and N. Panahshahi, 9/7/88, (PB89-207153, A07, MF-A01).

NCEER-88-0036   "Solution of the Dam-Reservoir Interaction Problem Using a Combination of FEM, BEM with Particular Integrals, Modal Analysis, and Substructuring," by C-S. Tsai, G.C. Lee and R.L. Ketter, 12/31/88, (PB89-207146, A04, MF-A01).

NCEER-88-0037   "Optimal Placement of Actuators for Structural Control," by F.Y. Cheng and C.P. Pantelides, 8/15/88, (PB89-162846, A05, MF-A01).

NCEER-88-0038   "Teflon Bearings in Aseismic Base Isolation: Experimental Studies and Mathematical Modeling," by A. Mokha, M.C. Constantinou and A.M. Reinhorn, 12/5/88, (PB89-218457, A10, MF-A01). This report is available only through NTIS (see address given above).

NCEER-88-0039   "Seismic Behavior of Flat Slab High-Rise Buildings in the New York City Area," by P. Weidlinger and M. Ettouney, 10/15/88, (PB90-145681, A04, MF-A01).

NCEER-88-0040   "Evaluation of the Earthquake Resistance of Existing Buildings in New York City," by P. Weidlinger and M. Ettouney, 10/15/88, not available.

NCEER-88-0041   "Small-Scale Modeling Techniques for Reinforced Concrete Structures Subjected to Seismic Loads," by W. Kim, A. El-Attar and R.N. White, 11/22/88, (PB89-189625, A05, MF-A01).

NCEER-88-0042   "Modeling Strong Ground Motion from Multiple Event Earthquakes," by G.W. Ellis and A.S. Cakmak, 10/15/88, (PB89-174445, A03, MF-A01).

NCEER-88-0043   "Nonstationary Models of Seismic Ground Acceleration," by M. Grigoriu, S.E. Ruiz and E. Rosenblueth, 7/15/88, (PB89-189617, A04, MF-A01).

NCEER-88-0044   "SARCF User's Guide: Seismic Analysis of Reinforced Concrete Frames," by Y.S. Chung, C. Meyer and M. Shinozuka, 11/9/88, (PB89-174452, A08, MF-A01).

NCEER-88-0045   "First Expert Panel Meeting on Disaster Research and Planning," edited by J. Pantelic and J. Stoyle, 9/15/88, (PB89-174460, A05, MF-A01).

NCEER-88-0046   "Preliminary Studies of the Effect of Degrading Infill Walls on the Nonlinear Seismic Response of Steel Frames," by C.Z. Chrysostomou, P. Gergely and J.F. Abel, 12/19/88, (PB89-208383, A05, MF-A01).

NCEER-88-0047   "Reinforced Concrete Frame Component Testing Facility - Design, Construction, Instrumentation and Operation," by S.P. Pessiki, C. Conley, T. Bond, P. Gergely and R.N. White, 12/16/88, (PB89-174478, A04, MF-A01).

NCEER-89-0001   "Effects of Protective Cushion and Soil Compliancy on the Response of Equipment Within a Seismically Excited Building," by J.A. HoLung, 2/16/89, (PB89-207179, A04, MF-A01).

NCEER-89-0002   "Statistical Evaluation of Response Modification Factors for Reinforced Concrete Structures," by H.H-M. Hwang and J-W. Jaw, 2/17/89, (PB89-207187, A05, MF-A01).

NCEER-89-0003   "Hysteretic Columns Under Random Excitation," by G-Q. Cai and Y.K. Lin, 1/9/89, (PB89-196513, A03, MF-A01).

NCEER-89-0004   "Experimental Study of `Elephant Foot Bulge' Instability of Thin-Walled Metal Tanks," by Z-H. Jia and R.L. Ketter, 2/22/89, (PB89-207195, A03, MF-A01).

NCEER-89-0005   "Experiment on Performance of Buried Pipelines Across San Andreas Fault," by J. Isenberg, E. Richardson and T.D. O'Rourke, 3/10/89, (PB89-218440, A04, MF-A01). This report is available only through NTIS (see address given above).

NCEER-89-0006   "A Knowledge-Based Approach to Structural Design of Earthquake-Resistant Buildings," by M. Subramani, P. Gergely, C.H. Conley, J.F. Abel and A.H. Zaghw, 1/15/89, (PB89-218465, A06, MF-A01).

NCEER-89-0007   "Liquefaction Hazards and Their Effects on Buried Pipelines," by T.D. O'Rourke and P.A. Lane, 2/1/89, (PB89-218481, A09, MF-A01).

NCEER-89-0008   "Fundamentals of System Identification in Structural Dynamics," by H. Imai, C-B. Yun, O. Maruyama and M. Shinozuka, 1/26/89, (PB89-207211, A04, MF-A01).

NCEER-89-0009   "Effects of the 1985 Michoacan Earthquake on Water Systems and Other Buried Lifelines in Mexico," by A.G. Ayala and M.J. O'Rourke, 3/8/89, (PB89-207229, A06, MF-A01).

NCEER-89-R010   "NCEER Bibliography of Earthquake Education Materials," by K.E.K. Ross, Second Revision, 9/1/89, (PB90-125352, A05, MF-A01). This report is replaced by NCEER-92-0018.

NCEER-89-0011   "Inelastic Three-Dimensional Response Analysis of Reinforced Concrete Building Structures (IDARC-3D), Part I - Modeling," by S.K. Kunnath and A.M. Reinhorn, 4/17/89, (PB90-114612, A07, MF-A01). This report is available only through NTIS (see address given above).

NCEER-89-0012   "Recommended Modifications to ATC-14," by C.D. Poland and J.O. Malley, 4/12/89, (PB90-108648, A15, MF-A01).

NCEER-89-0013   "Repair and Strengthening of Beam-to-Column Connections Subjected to Earthquake Loading," by M. Corazao and A.J. Durrani, 2/28/89, (PB90-109885, A06, MF-A01).

NCEER-89-0014   "Program EXKAL2 for Identification of Structural Dynamic Systems," by O. Maruyama, C-B. Yun, M. Hoshiya and M. Shinozuka, 5/19/89, (PB90-109877, A09, MF-A01).

NCEER-89-0015   "Response of Frames With Bolted Semi-Rigid Connections, Part I - Experimental Study and Analytical Predictions," by P.J. DiCorso, A.M. Reinhorn, J.R. Dickerson, J.B. Radziminski and W.L. Harper, 6/1/89, not available.

NCEER-89-0016   "ARMA Monte Carlo Simulation in Probabilistic Structural Analysis," by P.D. Spanos and M.P. Mignolet, 7/10/89, (PB90-109893, A03, MF-A01).

NCEER-89-P017   "Preliminary Proceedings from the Conference on Disaster Preparedness - The Place of Earthquake Education in Our Schools," Edited by K.E.K. Ross, 6/23/89, (PB90-108606, A03, MF-A01).

NCEER-89-0017   "Proceedings from the Conference on Disaster Preparedness - The Place of Earthquake Education in Our Schools," Edited by K.E.K. Ross, 12/31/89, (PB90-207895, A012, MF-A02). This report is available only through NTIS (see address given above).

NCEER-89-0018   "Multidimensional Models of Hysteretic Material Behavior for Vibration Analysis of Shape Memory Energy Absorbing Devices, by E.J. Graesser and F.A. Cozzarelli, 6/7/89, (PB90-164146, A04, MF-A01).

NCEER-89-0019   "Nonlinear Dynamic Analysis of Three-Dimensional Base Isolated Structures (3D-BASIS)," by S. Nagarajaiah, A.M. Reinhorn and M.C. Constantinou, 8/3/89, (PB90-161936, A06, MF-A01). This report has been replaced by NCEER-93-0011.

NCEER-89-0020   "Structural Control Considering Time-Rate of Control Forces and Control Rate Constraints," by F.Y. Cheng and C.P. Pantelides, 8/3/89, (PB90-120445, A04, MF-A01).

NCEER-89-0021   "Subsurface Conditions of Memphis and Shelby County," by K.W. Ng, T-S. Chang and H-H.M. Hwang, 7/26/89, (PB90-120437, A03, MF-A01).

NCEER-89-0022   "Seismic Wave Propagation Effects on Straight Jointed Buried Pipelines," by K. Elhmadi and M.J. O'Rourke, 8/24/89, (PB90-162322, A10, MF-A02).

NCEER-89-0023   "Workshop on Serviceability Analysis of Water Delivery Systems," edited by M. Grigoriu, 3/6/89, (PB90-127424, A03, MF-A01).

NCEER-89-0024   "Shaking Table Study of a 1/5 Scale Steel Frame Composed of Tapered Members," by K.C. Chang, J.S. Hwang and G.C. Lee, 9/18/89, (PB90-160169, A04, MF-A01).

NCEER-89-0025   "DYNA1D: A Computer Program for Nonlinear Seismic Site Response Analysis - Technical Documentation," by Jean H. Prevost, 9/14/89, (PB90-161944, A07, MF-A01). This report is available only through NTIS (see address given above).

NCEER-89-0026   "1:4 Scale Model Studies of Active Tendon Systems and Active Mass Dampers for Aseismic Protection," by A.M. Reinhorn, T.T. Soong, R.C. Lin, Y.P. Yang, Y. Fukao, H. Abe and M. Nakai, 9/15/89, (PB90-173246, A10, MF-A02). This report is available only through NTIS (see address given above).

NCEER-89-0027   "Scattering of Waves by Inclusions in a Nonhomogeneous Elastic Half Space Solved by Boundary Element Methods," by P.K. Hadley, A. Askar and A.S. Cakmak, 6/15/89, (PB90-145699, A07, MF-A01).

NCEER-89-0028   "Statistical Evaluation of Deflection Amplification Factors for Reinforced Concrete Structures," by H.H.M. Hwang, J-W. Jaw and A.L. Ch'ng, 8/31/89, (PB90-164633, A05, MF-A01).

NCEER-89-0029   "Bedrock Accelerations in Memphis Area Due to Large New Madrid Earthquakes," by H.H.M. Hwang, C.H.S. Chen and G. Yu, 11/7/89, (PB90-162330, A04, MF-A01).

NCEER-89-0030   "Seismic Behavior and Response Sensitivity of Secondary Structural Systems," by Y.Q. Chen and T.T. Soong, 10/23/89, (PB90-164658, A08, MF-A01).

NCEER-89-0031   "Random Vibration and Reliability Analysis of Primary-Secondary Structural Systems," by Y. Ibrahim, M. Grigoriu and T.T. Soong, 11/10/89, (PB90-161951, A04, MF-A01).

NCEER-89-0032   "Proceedings from the Second U.S. - Japan Workshop on Liquefaction, Large Ground Deformation and Their Effects on Lifelines, September 26-29, 1989," Edited by T.D. O'Rourke and M. Hamada, 12/1/89, (PB90-209388, A22, MF-A03).

NCEER-89-0033   "Deterministic Model for Seismic Damage Evaluation of Reinforced Concrete Structures," by J.M. Bracci, A.M. Reinhorn, J.B. Mander and S.K. Kunnath, 9/27/89, (PB91-108803, A06, MF-A01).

NCEER-89-0034   "On the Relation Between Local and Global Damage Indices," by E. DiPasquale and A.S. Cakmak, 8/15/89, (PB90-173865, A05, MF-A01).

NCEER-89-0035   "Cyclic Undrained Behavior of Nonplastic and Low Plasticity Silts," by A.J. Walker and H.E. Stewart, 7/26/89, (PB90-183518, A10, MF-A01).

NCEER-89-0036   "Liquefaction Potential of Surficial Deposits in the City of Buffalo, New York," by M. Budhu, R. Giese and L. Baumgrass, 1/17/89, (PB90-208455, A04, MF-A01).

NCEER-89-0037   "A Deterministic Assessment of Effects of Ground Motion Incoherence," by A.S. Veletsos and Y. Tang, 7/15/89, (PB90-164294, A03, MF-A01).

NCEER-89-0038   "Workshop on Ground Motion Parameters for Seismic Hazard Mapping," July 17-18, 1989, edited by R.V. Whitman, 12/1/89, (PB90-173923, A04, MF-A01).

NCEER-89-0039   "Seismic Effects on Elevated Transit Lines of the New York City Transit Authority," by C.J. Costantino, C.A. Miller and E. Heymsfield, 12/26/89, (PB90-207887, A06, MF-A01).

NCEER-89-0040   "Centrifugal Modeling of Dynamic Soil-Structure Interaction," by K. Weissman, Supervised by J.H. Prevost, 5/10/89, (PB90-207879, A07, MF-A01).

NCEER-89-0041   "Linearized Identification of Buildings With Cores for Seismic Vulnerability Assessment," by I-K. Ho and A.E. Aktan, 11/1/89, (PB90-251943, A07, MF-A01).

NCEER-90-0001   "Geotechnical and Lifeline Aspects of the October 17, 1989 Loma Prieta Earthquake in San Francisco," by T.D. O'Rourke, H.E. Stewart, F.T. Blackburn and T.S. Dickerman, 1/90, (PB90-208596, A05, MF-A01).

NCEER-90-0002   "Nonnormal Secondary Response Due to Yielding in a Primary Structure," by D.C.K. Chen and L.D. Lutes, 2/28/90, (PB90-251976, A07, MF-A01).

NCEER-90-0003   "Earthquake Education Materials for Grades K-12," by K.E.K. Ross, 4/16/90, (PB91-251984, A05, MF-A05). This report has been replaced by NCEER-92-0018.

NCEER-90-0004   "Catalog of Strong Motion Stations in Eastern North America," by R.W. Busby, 4/3/90, (PB90-251984, A05, MF-A01).

NCEER-90-0005   "NCEER Strong-Motion Data Base: A User Manual for the GeoBase Release (Version 1.0 for the Sun3)," by P. Friberg and K. Jacob, 3/31/90 (PB90-258062, A04, MF-A01).

NCEER-90-0006   "Seismic Hazard Along a Crude Oil Pipeline in the Event of an 1811-1812 Type New Madrid Earthquake," by H.H.M. Hwang and C-H.S. Chen, 4/16/90, (PB90-258054, A04, MF-A01).

NCEER-90-0007   "Site-Specific Response Spectra for Memphis Sheahan Pumping Station," by H.H.M. Hwang and C.S. Lee, 5/15/90, (PB91-108811, A05, MF-A01).

NCEER-90-0008   "Pilot Study on Seismic Vulnerability of Crude Oil Transmission Systems," by T. Ariman, R. Dobry, M. Grigoriu, F. Kozin, M. O'Rourke, T. O'Rourke and M. Shinozuka, 5/25/90, (PB91-108837, A06, MF-A01).

NCEER-90-0009   "A Program to Generate Site Dependent Time Histories: EQGEN," by G.W. Ellis, M. Srinivasan and A.S. Cakmak, 1/30/90, (PB91-108829, A04, MF-A01).

NCEER-90-0010   "Active Isolation for Seismic Protection of Operating Rooms," by M.E. Talbott, Supervised by M. Shinozuka, 6/8/9, (PB91-110205, A05, MF-A01).

NCEER-90-0011   "Program LINEARID for Identification of Linear Structural Dynamic Systems," by C-B. Yun and M. Shinozuka, 6/25/90, (PB91-110312, A08, MF-A01).

NCEER-90-0012   "Two-Dimensional Two-Phase Elasto-Plastic Seismic Response of Earth Dams," by A.N. Yiagos, Supervised by J.H. Prevost, 6/20/90, (PB91-110197, A13, MF-A02).

NCEER-90-0013   "Secondary Systems in Base-Isolated Structures: Experimental Investigation, Stochastic Response and Stochastic Sensitivity," by G.D. Manolis, G. Juhn, M.C. Constantinou and A.M. Reinhorn, 7/1/90, (PB91-110320, A08, MF-A01).

NCEER-90-0014   "Seismic Behavior of Lightly-Reinforced Concrete Column and Beam-Column Joint Details," by S.P. Pessiki, C.H. Conley, P. Gergely and R.N. White, 8/22/90, (PB91-108795, A11, MF-A02).

NCEER-90-0015   "Two Hybrid Control Systems for Building Structures Under Strong Earthquakes," by J.N. Yang and A. Danielians, 6/29/90, (PB91-125393, A04, MF-A01).

NCEER-90-0016   "Instantaneous Optimal Control with Acceleration and Velocity Feedback," by J.N. Yang and Z. Li, 6/29/90, (PB91-125401, A03, MF-A01).

NCEER-90-0017   "Reconnaissance Report on the Northern Iran Earthquake of June 21, 1990," by M. Mehrain, 10/4/90, (PB91-125377, A03, MF-A01).

NCEER-90-0018   "Evaluation of Liquefaction Potential in Memphis and Shelby County," by T.S. Chang, P.S. Tang, C.S. Lee and H. Hwang, 8/10/90, (PB91-125427, A09, MF-A01).

NCEER-90-0019   "Experimental and Analytical Study of a Combined Sliding Disc Bearing and Helical Steel Spring Isolation System," by M.C. Constantinou, A.S. Mokha and A.M. Reinhorn, 10/4/90, (PB91-125385, A06, MF-A01). This report is available only through NTIS (see address given above).

NCEER-90-0020   "Experimental Study and Analytical Prediction of Earthquake Response of a Sliding Isolation System with a Spherical Surface," by A.S. Mokha, M.C. Constantinou and A.M. Reinhorn, 10/11/90, (PB91-125419, A05, MF-A01).

NCEER-90-0021   "Dynamic Interaction Factors for Floating Pile Groups," by G. Gazetas, K. Fan, A. Kaynia and E. Kausel, 9/10/90, (PB91-170381, A05, MF-A01).

NCEER-90-0022   "Evaluation of Seismic Damage Indices for Reinforced Concrete Structures," by S. Rodriguez-Gomez and A.S. Cakmak, 9/30/90, PB91-171322, A06, MF-A01).

NCEER-90-0023   "Study of Site Response at a Selected Memphis Site," by H. Desai, S. Ahmad, E.S. Gazetas and M.R. Oh, 10/11/90, (PB91-196857, A03, MF-A01).

NCEER-90-0024   "A User's Guide to Strongmo: Version 1.0 of NCEER's Strong-Motion Data Access Tool for PCs and Terminals," by P.A. Friberg and C.A.T. Susch, 11/15/90, (PB91-171272, A03, MF-A01).

NCEER-90-0025   "A Three-Dimensional Analytical Study of Spatial Variability of Seismic Ground Motions," by L-L. Hong and A.H.-S. Ang, 10/30/90, (PB91-170399, A09, MF-A01).

NCEER-90-0026   "MUMOID User's Guide - A Program for the Identification of Modal Parameters," by S. Rodriguez-Gomez and E. DiPasquale, 9/30/90, (PB91-171298, A04, MF-A01).

NCEER-90-0027   "SARCF-II User's Guide - Seismic Analysis of Reinforced Concrete Frames," by S. Rodriguez-Gomez, Y.S. Chung and C. Meyer, 9/30/90, (PB91-171280, A05, MF-A01).

NCEER-90-0028   "Viscous Dampers: Testing, Modeling and Application in Vibration and Seismic Isolation," by N. Makris and M.C. Constantinou, 12/20/90 (PB91-190561, A06, MF-A01).

NCEER-90-0029   "Soil Effects on Earthquake Ground Motions in the Memphis Area," by H. Hwang, C.S. Lee, K.W. Ng and T.S. Chang, 8/2/90, (PB91-190751, A05, MF-A01).

NCEER-91-0001   "Proceedings from the Third Japan-U.S. Workshop on Earthquake Resistant Design of Lifeline Facilities and Countermeasures for Soil Liquefaction, December 17-19, 1990," edited by T.D. O'Rourke and M. Hamada, 2/1/91, (PB91-179259, A99, MF-A04).

NCEER-91-0002   "Physical Space Solutions of Non-Proportionally Damped Systems," by M. Tong, Z. Liang and G.C. Lee, 1/15/91, (PB91-179242, A04, MF-A01).

NCEER-91-0003   "Seismic Response of Single Piles and Pile Groups," by K. Fan and G. Gazetas, 1/10/91, (PB92-174994, A04, MF-A01).

NCEER-91-0004   "Damping of Structures: Part 1 - Theory of Complex Damping," by Z. Liang and G. Lee, 10/10/91, (PB92-197235, A12, MF-A03).

NCEER-91-0005   "3D-BASIS - Nonlinear Dynamic Analysis of Three Dimensional Base Isolated Structures: Part II," by S. Nagarajaiah, A.M. Reinhorn and M.C. Constantinou, 2/28/91, (PB91-190553, A07, MF-A01). This report has been replaced by NCEER-93-0011.

NCEER-91-0006   "A Multidimensional Hysteretic Model for Plasticity Deforming Metals in Energy Absorbing Devices," by E.J. Graesser and F.A. Cozzarelli, 4/9/91, (PB92-108364, A04, MF-A01).

NCEER-91-0007   "A Framework for Customizable Knowledge-Based Expert Systems with an Application to a KBES for Evaluating the Seismic Resistance of Existing Buildings," by E.G. Ibarra-Anaya and S.J. Fenves, 4/9/91, (PB91-210930, A08, MF-A01).

NCEER-91-0008   "Nonlinear Analysis of Steel Frames with Semi-Rigid Connections Using the Capacity Spectrum Method," by G.G. Deierlein, S-H. Hsieh, Y-J. Shen and J.F. Abel, 7/2/91, (PB92-113828, A05, MF-A01).

NCEER-91-0009   "Earthquake Education Materials for Grades K-12," by K.E.K. Ross, 4/30/91, (PB91-212142, A06, MF-A01). This report has been replaced by NCEER-92-0018.

NCEER-91-0010   "Phase Wave Velocities and Displacement Phase Differences in a Harmonically Oscillating Pile," by N. Makris and G. Gazetas, 7/8/91, (PB92-108356, A04, MF-A01).

NCEER-91-0011   "Dynamic Characteristics of a Full-Size Five-Story Steel Structure and a 2/5 Scale Model," by K.C. Chang, G.C. Yao, G.C. Lee, D.S. Hao and Y.C. Yeh," 7/2/91, (PB93-116648, A06, MF-A02).

NCEER-91-0012   "Seismic Response of a 2/5 Scale Steel Structure with Added Viscoelastic Dampers," by K.C. Chang, T.T. Soong, S-T. Oh and M.L. Lai, 5/17/91, (PB92-110816, A05, MF-A01).

NCEER-91-0013   "Earthquake Response of Retaining Walls; Full-Scale Testing and Computational Modeling," by S. Alampalli and A-W.M. Elgamal, 6/20/91, not available.

NCEER-91-0014   "3D-BASIS-M: Nonlinear Dynamic Analysis of Multiple Building Base Isolated Structures," by P.C. Tsopelas, S. Nagarajaiah, M.C. Constantinou and A.M. Reinhorn, 5/28/91, (PB92-113885, A09, MF-A02).

NCEER-91-0015   "Evaluation of SEAOC Design Requirements for Sliding Isolated Structures," by D. Theodossiou and M.C. Constantinou, 6/10/91, (PB92-114602, A11, MF-A03).

NCEER-91-0016   "Closed-Loop Modal Testing of a 27-Story Reinforced Concrete Flat Plate-Core Building," by H.R. Somaprasad, T. Toksoy, H. Yoshiyuki and A.E. Aktan, 7/15/91, (PB92-129980, A07, MF-A02).

NCEER-91-0017   "Shake Table Test of a 1/6 Scale Two-Story Lightly Reinforced Concrete Building," by A.G. El-Attar, R.N. White and P. Gergely, 2/28/91, (PB92-222447, A06, MF-A02).

NCEER-91-0018   "Shake Table Test of a 1/8 Scale Three-Story Lightly Reinforced Concrete Building," by A.G. El-Attar, R.N. White and P. Gergely, 2/28/91, (PB93-116630, A08, MF-A02).

NCEER-91-0019   "Transfer Functions for Rigid Rectangular Foundations," by A.S. Veletsos, A.M. Prasad and W.H. Wu, 7/31/91, not available.

NCEER-91-0020   "Hybrid Control of Seismic-Excited Nonlinear and Inelastic Structural Systems," by J.N. Yang, Z. Li and A. Danielians, 8/1/91, (PB92-143171, A06, MF-A02).

NCEER-91-0021   "The NCEER-91 Earthquake Catalog: Improved Intensity-Based Magnitudes and Recurrence Relations for U.S. Earthquakes East of New Madrid," by L. Seeber and J.G. Armbruster, 8/28/91, (PB92-176742, A06, MF-A02).

NCEER-91-0022   "Proceedings from the Implementation of Earthquake Planning and Education in Schools: The Need for Change - The Roles of the Changemakers," by K.E.K. Ross and F. Winslow, 7/23/91, (PB92-129998, A12, MF-A03).

NCEER-91-0023   "A Study of Reliability-Based Criteria for Seismic Design of Reinforced Concrete Frame Buildings," by H.H.M. Hwang and H-M. Hsu, 8/10/91, (PB92-140235, A09, MF-A02).

NCEER-91-0024   "Experimental Verification of a Number of Structural System Identification Algorithms," by R.G. Ghanem, H. Gavin and M. Shinozuka, 9/18/91, (PB92-176577, A18, MF-A04).

NCEER-91-0025   "Probabilistic Evaluation of Liquefaction Potential," by H.H.M. Hwang and C.S. Lee," 11/25/91, (PB92-143429, A05, MF-A01).

NCEER-91-0026   "Instantaneous Optimal Control for Linear, Nonlinear and Hysteretic Structures - Stable Controllers," by J.N. Yang and Z. Li, 11/15/91, (PB92-163807, A04, MF-A01).

NCEER-91-0027   "Experimental and Theoretical Study of a Sliding Isolation System for Bridges," by M.C. Constantinou, A. Kartoum, A.M. Reinhorn and P. Bradford, 11/15/91, (PB92-176973, A10, MF-A03).

NCEER-92-0001   "Case Studies of Liquefaction and Lifeline Performance During Past Earthquakes, Volume 1: Japanese Case Studies," Edited by M. Hamada and T. O'Rourke, 2/17/92, (PB92-197243, A18, MF-A04).

NCEER-92-0002   "Case Studies of Liquefaction and Lifeline Performance During Past Earthquakes, Volume 2: United States Case Studies," Edited by T. O'Rourke and M. Hamada, 2/17/92, (PB92-197250, A20, MF-A04).

NCEER-92-0003   "Issues in Earthquake Education," Edited by K. Ross, 2/3/92, (PB92-222389, A07, MF-A02).

NCEER-92-0004   "Proceedings from the First U.S. - Japan Workshop on Earthquake Protective Systems for Bridges," Edited by I.G. Buckle, 2/4/92, (PB94-142239, A99, MF-A06).

NCEER-92-0005   "Seismic Ground Motion from a Haskell-Type Source in a Multiple-Layered Half-Space," A.P. Theoharis, G. Deodatis and M. Shinozuka, 1/2/92, not available.

NCEER-92-0006   "Proceedings from the Site Effects Workshop," Edited by R. Whitman, 2/29/92, (PB92-197201, A04, MF-A01).

NCEER-92-0007   "Engineering Evaluation of Permanent Ground Deformations Due to Seismically-Induced Liquefaction," by M.H. Baziar, R. Dobry and A-W.M. Elgamal, 3/24/92, (PB92-222421, A13, MF-A03).

NCEER-92-0008   "A Procedure for the Seismic Evaluation of Buildings in the Central and Eastern United States," by C.D. Poland and J.O. Malley, 4/2/92, (PB92-222439, A20, MF-A04).

NCEER-92-0009   "Experimental and Analytical Study of a Hybrid Isolation System Using Friction Controllable Sliding Bearings," by M.Q. Feng, S. Fujii and M. Shinozuka, 5/15/92, (PB93-150282, A06, MF-A02).

NCEER-92-0010   "Seismic Resistance of Slab-Column Connections in Existing Non-Ductile Flat-Plate Buildings," by A.J. Durrani and Y. Du, 5/18/92, (PB93-116812, A06, MF-A02).

NCEER-92-0011   "The Hysteretic and Dynamic Behavior of Brick Masonry Walls Upgraded by Ferrocement Coatings Under Cyclic Loading and Strong Simulated Ground Motion," by H. Lee and S.P. Prawel, 5/11/92, not available.

NCEER-92-0012   "Study of Wire Rope Systems for Seismic Protection of Equipment in Buildings," by G.F. Demetriades, M.C. Constantinou and A.M. Reinhorn, 5/20/92, (PB93-116655, A08, MF-A02).

NCEER-92-0013   "Shape Memory Structural Dampers: Material Properties, Design and Seismic Testing," by P.R. Witting and F.A. Cozzarelli, 5/26/92, (PB93-116663, A05, MF-A01).

NCEER-92-0014   "Longitudinal Permanent Ground Deformation Effects on Buried Continuous Pipelines," by M.J. O'Rourke, and C. Nordberg, 6/15/92, (PB93-116671, A08, MF-A02).

NCEER-92-0015   "A Simulation Method for Stationary Gaussian Random Functions Based on the Sampling Theorem," by M. Grigoriu and S. Balopoulou, 6/11/92, (PB93-127496, A05, MF-A01).

NCEER-92-0016   "Gravity-Load-Designed Reinforced Concrete Buildings: Seismic Evaluation of Existing Construction and Detailing Strategies for Improved Seismic Resistance," by G.W. Hoffmann, S.K. Kunnath, A.M. Reinhorn and J.B. Mander, 7/15/92, (PB94-142007, A08, MF-A02).

NCEER-92-0017   "Observations on Water System and Pipeline Performance in the Limón Area of Costa Rica Due to the April 22, 1991 Earthquake," by M. O'Rourke and D. Ballantyne, 6/30/92, (PB93-126811, A06, MF-A02).

NCEER-92-0018   "Fourth Edition of Earthquake Education Materials for Grades K-12," Edited by K.E.K. Ross, 8/10/92, (PB93-114023, A07, MF-A02).

NCEER-92-0019   "Proceedings from the Fourth Japan-U.S. Workshop on Earthquake Resistant Design of Lifeline Facilities and Countermeasures for Soil Liquefaction," Edited by M. Hamada and T.D. O'Rourke, 8/12/92, (PB93-163939, A99, MF-E11).

NCEER-92-0020   "Active Bracing System: A Full Scale Implementation of Active Control," by A.M. Reinhorn, T.T. Soong, R.C. Lin, M.A. Riley, Y.P. Wang, S. Aizawa and M. Higashino, 8/14/92, (PB93-127512, A06, MF-A02).

NCEER-92-0021   "Empirical Analysis of Horizontal Ground Displacement Generated by Liquefaction-Induced Lateral Spreads," by S.F. Bartlett and T.L. Youd, 8/17/92, (PB93-188241, A06, MF-A02).

NCEER-92-0022   "IDARC Version 3.0: Inelastic Damage Analysis of Reinforced Concrete Structures," by S.K. Kunnath, A.M. Reinhorn and R.F. Lobo, 8/31/92, (PB93-227502, A07, MF-A02).

NCEER-92-0023   "A Semi-Empirical Analysis of Strong-Motion Peaks in Terms of Seismic Source, Propagation Path and Local Site Conditions, by M. Kamiyama, M.J. O'Rourke and R. Flores-Berrones, 9/9/92, (PB93-150266, A08, MF-A02).

NCEER-92-0024   "Seismic Behavior of Reinforced Concrete Frame Structures with Nonductile Details, Part I: Summary of Experimental Findings of Full Scale Beam-Column Joint Tests," by A. Beres, R.N. White and P. Gergely, 9/30/92, (PB93-227783, A05, MF-A01).

NCEER-92-0025   "Experimental Results of Repaired and Retrofitted Beam-Column Joint Tests in Lightly Reinforced Concrete Frame Buildings," by A. Beres, S. El-Borgi, R.N. White and P. Gergely, 10/29/92, (PB93-227791, A05, MF-A01).

NCEER-92-0026   "A Generalization of Optimal Control Theory: Linear and Nonlinear Structures," by J.N. Yang, Z. Li and S. Vongchavalitkul, 11/2/92, (PB93-188621, A05, MF-A01).

NCEER-92-0027   "Seismic Resistance of Reinforced Concrete Frame Structures Designed Only for Gravity Loads: Part I - Design and Properties of a One-Third Scale Model Structure," by J.M. Bracci, A.M. Reinhorn and J.B. Mander, 12/1/92, (PB94-104502, A08, MF-A02).

NCEER-92-0028   "Seismic Resistance of Reinforced Concrete Frame Structures Designed Only for Gravity Loads: Part II - Experimental Performance of Subassemblages," by L.E. Aycardi, J.B. Mander and A.M. Reinhorn, 12/1/92, (PB94-104510, A08, MF-A02).

NCEER-92-0029   "Seismic Resistance of Reinforced Concrete Frame Structures Designed Only for Gravity Loads: Part III - Experimental Performance and Analytical Study of a Structural Model," by J.M. Bracci, A.M. Reinhorn and J.B. Mander, 12/1/92, (PB93-227528, A09, MF-A01).

NCEER-92-0030   "Evaluation of Seismic Retrofit of Reinforced Concrete Frame Structures: Part I - Experimental Performance of Retrofitted Subassemblages," by D. Choudhuri, J.B. Mander and A.M. Reinhorn, 12/8/92, (PB93-198307, A07, MF-A02).

NCEER-92-0031   "Evaluation of Seismic Retrofit of Reinforced Concrete Frame Structures: Part II - Experimental Performance and Analytical Study of a Retrofitted Structural Model," by J.M. Bracci, A.M. Reinhorn and J.B. Mander, 12/8/92, (PB93-198315, A09, MF-A03).

NCEER-92-0032   "Experimental and Analytical Investigation of Seismic Response of Structures with Supplemental Fluid Viscous Dampers," by M.C. Constantinou and M.D. Symans, 12/21/92, (PB93-191435, A10, MF-A03). This report is available only through NTIS (see address given above).

NCEER-92-0033   "Reconnaissance Report on the Cairo, Egypt Earthquake of October 12, 1992," by M. Khater, 12/23/92, (PB93-188621, A03, MF-A01).

NCEER-92-0034   "Low-Level Dynamic Characteristics of Four Tall Flat-Plate Buildings in New York City," by H. Gavin, S. Yuan, J. Grossman, E. Pekelis and K. Jacob, 12/28/92, (PB93-188217, A07, MF-A02).

NCEER-93-0001   "An Experimental Study on the Seismic Performance of Brick-Infilled Steel Frames With and Without Retrofit," by J.B. Mander, B. Nair, K. Wojtkowski and J. Ma, 1/29/93, (PB93-227510, A07, MF-A02).

NCEER-93-0002   "Social Accounting for Disaster Preparedness and Recovery Planning," by S. Cole, E. Pantoja and V. Razak, 2/22/93, (PB94-142114, A12, MF-A03).

NCEER-93-0003   "Assessment of 1991 NEHRP Provisions for Nonstructural Components and Recommended Revisions," by T.T. Soong, G. Chen, Z. Wu, R-H. Zhang and M. Grigoriu, 3/1/93, (PB93-188639, A06, MF-A02).

NCEER-93-0004   "Evaluation of Static and Response Spectrum Analysis Procedures of SEAOC/UBC for Seismic Isolated Structures," by C.W. Winters and M.C. Constantinou, 3/23/93, (PB93-198299, A10, MF-A03).

NCEER-93-0005   "Earthquakes in the Northeast - Are We Ignoring the Hazard? A Workshop on Earthquake Science and Safety for Educators," edited by K.E.K. Ross, 4/2/93, (PB94-103066, A09, MF-A02).

NCEER-93-0006   "Inelastic Response of Reinforced Concrete Structures with Viscoelastic Braces," by R.F. Lobo, J.M. Bracci, K.L. Shen, A.M. Reinhorn and T.T. Soong, 4/5/93, (PB93-227486, A05, MF-A02).

NCEER-93-0007   "Seismic Testing of Installation Methods for Computers and Data Processing Equipment," by K. Kosar, T.T. Soong, K.L. Shen, J.A. HoLung and Y.K. Lin, 4/12/93, (PB93-198299, A07, MF-A02).

NCEER-93-0008   "Retrofit of Reinforced Concrete Frames Using Added Dampers," by A. Reinhorn, M. Constantinou and C. Li, not available.

NCEER-93-0009   "Seismic Behavior and Design Guidelines for Steel Frame Structures with Added Viscoelastic Dampers," by K.C. Chang, M.L. Lai, T.T. Soong, D.S. Hao and Y.C. Yeh, 5/1/93, (PB94-141959, A07, MF-A02).

NCEER-93-0010   "Seismic Performance of Shear-Critical Reinforced Concrete Bridge Piers," by J.B. Mander, S.M. Waheed, M.T.A. Chaudhary and S.S. Chen, 5/12/93, (PB93-227494, A08, MF-A02).

NCEER-93-0011   "3D-BASIS-TABS: Computer Program for Nonlinear Dynamic Analysis of Three Dimensional Base Isolated Structures," by S. Nagarajaiah, C. Li, A.M. Reinhorn and M.C. Constantinou, 8/2/93, (PB94-141819, A09, MF-A02).

NCEER-93-0012   "Effects of Hydrocarbon Spills from an Oil Pipeline Break on Ground Water," by O.J. Helweg and H.H.M. Hwang, 8/3/93, (PB94-141942, A06, MF-A02).

NCEER-93-0013   "Simplified Procedures for Seismic Design of Nonstructural Components and Assessment of Current Code Provisions," by M.P. Singh, L.E. Suarez, E.E. Matheu and G.O. Maldonado, 8/4/93, (PB94-141827, A09, MF-A02).

NCEER-93-0014   "An Energy Approach to Seismic Analysis and Design of Secondary Systems," by G. Chen and T.T. Soong, 8/6/93, (PB94-142767, A11, MF-A03).

NCEER-93-0015   "Proceedings from School Sites: Becoming Prepared for Earthquakes - Commemorating the Third Anniversary of the Loma Prieta Earthquake," Edited by F.E. Winslow and K.E.K. Ross, 8/16/93, (PB94-154275, A16, MF-A02).

NCEER-93-0016   "Reconnaissance Report of Damage to Historic Monuments in Cairo, Egypt Following the October 12, 1992 Dahshur Earthquake," by D. Sykora, D. Look, G. Croci, E. Karaesmen and E. Karaesmen, 8/19/93, (PB94-142221, A08, MF-A02).

NCEER-93-0017   "The Island of Guam Earthquake of August 8, 1993," by S.W. Swan and S.K. Harris, 9/30/93, (PB94-141843, A04, MF-A01).

NCEER-93-0018   "Engineering Aspects of the October 12, 1992 Egyptian Earthquake," by A.W. Elgamal, M. Amer, K. Adalier and A. Abul-Fadl, 10/7/93, (PB94-141983, A05, MF-A01).

NCEER-93-0019   "Development of an Earthquake Motion Simulator and its Application in Dynamic Centrifuge Testing," by I. Krstelj, Supervised by J.H. Prevost, 10/23/93, (PB94-181773, A-10, MF-A03).

NCEER-93-0020   "NCEER-Taisei Corporation Research Program on Sliding Seismic Isolation Systems for Bridges: Experimental and Analytical Study of a Friction Pendulum System (FPS)," by M.C. Constantinou, P. Tsopelas, Y-S. Kim and S. Okamoto, 11/1/93, (PB94-142775, A08, MF-A02).

NCEER-93-0021   "Finite Element Modeling of Elastomeric Seismic Isolation Bearings," by L.J. Billings, Supervised by R. Shepherd, 11/8/93, not available.

NCEER-93-0022   "Seismic Vulnerability of Equipment in Critical Facilities: Life-Safety and Operational Consequences," by K. Porter, G.S. Johnson, M.M. Zadeh, C. Scawthorn and S. Eder, 11/24/93, (PB94-181765, A16, MF-A03).

NCEER-93-0023   "Hokkaido Nansei-oki, Japan Earthquake of July 12, 1993, by P.I. Yanev and C.R. Scawthorn, 12/23/93, (PB94-181500, A07, MF-A01).

NCEER-94-0001   "An Evaluation of Seismic Serviceability of Water Supply Networks with Application to the San Francisco Auxiliary Water Supply System," by I. Markov, Supervised by M. Grigoriu and T. O'Rourke, 1/21/94, (PB94-204013, A07, MF-A02).

NCEER-94-0002   "NCEER-Taisei Corporation Research Program on Sliding Seismic Isolation Systems for Bridges: Experimental and Analytical Study of Systems Consisting of Sliding Bearings, Rubber Restoring Force Devices and Fluid Dampers," Volumes I and II, by P. Tsopelas, S. Okamoto, M.C. Constantinou, D. Ozaki and S. Fujii, 2/4/94, (PB94-181740, A09, MF-A02 and PB94-181757, A12, MF-A03).

NCEER-94-0003   "A Markov Model for Local and Global Damage Indices in Seismic Analysis," by S. Rahman and M. Grigoriu, 2/18/94, (PB94-206000, A12, MF-A03).

NCEER-94-0004   "Proceedings from the NCEER Workshop on Seismic Response of Masonry Infills," edited by D.P. Abrams, 3/1/94, (PB94-180783, A07, MF-A02).

NCEER-94-0005   "The Northridge, California Earthquake of January 17, 1994: General Reconnaissance Report," edited by J.D. Goltz, 3/11/94, (PB94-193943, A10, MF-A03).

NCEER-94-0006   "Seismic Energy Based Fatigue Damage Analysis of Bridge Columns: Part I - Evaluation of Seismic Capacity," by G.A. Chang and J.B. Mander, 3/14/94, (PB94-219185, A11, MF-A03).

NCEER-94-0007   "Seismic Isolation of Multi-Story Frame Structures Using Spherical Sliding Isolation Systems," by T.M. Al-Hussaini, V.A. Zayas and M.C. Constantinou, 3/17/94, (PB94-193745, A09, MF-A02).

NCEER-94-0008   "The Northridge, California Earthquake of January 17, 1994: Performance of Highway Bridges," edited by I.G. Buckle, 3/24/94, (PB94-193851, A06, MF-A02).

NCEER-94-0009   "Proceedings of the Third U.S.-Japan Workshop on Earthquake Protective Systems for Bridges," edited by I.G. Buckle and I. Friedland, 3/31/94, (PB94-195815, A99, MF-A06).

NCEER-94-0010   "3D-BASIS-ME: Computer Program for Nonlinear Dynamic Analysis of Seismically Isolated Single and Multiple Structures and Liquid Storage Tanks," by P.C. Tsopelas, M.C. Constantinou and A.M. Reinhorn, 4/12/94, (PB94-204922, A09, MF-A02).

NCEER-94-0011   "The Northridge, California Earthquake of January 17, 1994: Performance of Gas Transmission Pipelines," by T.D. O'Rourke and M.C. Palmer, 5/16/94, (PB94-204989, A05, MF-A01).

NCEER-94-0012   "Feasibility Study of Replacement Procedures and Earthquake Performance Related to Gas Transmission Pipelines," by T.D. O'Rourke and M.C. Palmer, 5/25/94, (PB94-206638, A09, MF-A02).

NCEER-94-0013   "Seismic Energy Based Fatigue Damage Analysis of Bridge Columns: Part II - Evaluation of Seismic Demand," by G.A. Chang and J.B. Mander, 6/1/94, (PB95-18106, A08, MF-A02).

NCEER-94-0014   "NCEER-Taisei Corporation Research Program on Sliding Seismic Isolation Systems for Bridges: Experimental and Analytical Study of a System Consisting of Sliding Bearings and Fluid Restoring Force/Damping Devices," by P. Tsopelas and M.C. Constantinou, 6/13/94, (PB94-219144, A10, MF-A03).

NCEER-94-0015   "Generation of Hazard-Consistent Fragility Curves for Seismic Loss Estimation Studies," by H. Hwang and J-R. Huo, 6/14/94, (PB95-181996, A09, MF-A02).

NCEER-94-0016   "Seismic Study of Building Frames with Added Energy-Absorbing Devices," by W.S. Pong, C.S. Tsai and G.C. Lee, 6/20/94, (PB94-219136, A10, A03).

NCEER-94-0017   "Sliding Mode Control for Seismic-Excited Linear and Nonlinear Civil Engineering Structures," by J. Yang, J. Wu, A. Agrawal and Z. Li, 6/21/94, (PB95-138483, A06, MF-A02).

NCEER-94-0018   "3D-BASIS-TABS Version 2.0: Computer Program for Nonlinear Dynamic Analysis of Three Dimensional Base Isolated Structures," by A.M. Reinhorn, S. Nagarajaiah, M.C. Constantinou, P. Tsopelas and R. Li, 6/22/94, (PB95-182176, A08, MF-A02).

NCEER-94-0019   "Proceedings of the International Workshop on Civil Infrastructure Systems: Application of Intelligent Systems and Advanced Materials on Bridge Systems," Edited by G.C. Lee and K.C. Chang, 7/18/94, (PB95-252474, A20, MF-A04).

NCEER-94-0020   "Study of Seismic Isolation Systems for Computer Floors," by V. Lambrou and M.C. Constantinou, 7/19/94, (PB95-138533, A10, MF-A03).

NCEER-94-0021   "Proceedings of the U.S.-Italian Workshop on Guidelines for Seismic Evaluation and Rehabilitation of Unreinforced Masonry Buildings," Edited by D.P. Abrams and G.M. Calvi, 7/20/94, (PB95-138749, A13, MF-A03).

NCEER-94-0022   "NCEER-Taisei Corporation Research Program on Sliding Seismic Isolation Systems for Bridges: Experimental and Analytical Study of a System Consisting of Lubricated PTFE Sliding Bearings and Mild Steel Dampers," by P. Tsopelas and M.C. Constantinou, 7/22/94, (PB95-182184, A08, MF-A02).

NCEER-94-0023   "Development of Reliability-Based Design Criteria for Buildings Under Seismic Load," by Y.K. Wen, H. Hwang and M. Shinozuka, 8/1/94, (PB95-211934, A08, MF-A02).

NCEER-94-0024   "Experimental Verification of Acceleration Feedback Control Strategies for an Active Tendon System," by S.J. Dyke, B.F. Spencer, Jr., P. Quast, M.K. Sain, D.C. Kaspari, Jr. and T.T. Soong, 8/29/94, (PB95-212320, A05, MF-A01).

NCEER-94-0025   "Seismic Retrofitting Manual for Highway Bridges," Edited by I.G. Buckle and I.F. Friedland, published by the Federal Highway Administration (PB95-212676, A15, MF-A03).

NCEER-94-0026   "Proceedings from the Fifth U.S.-Japan Workshop on Earthquake Resistant Design of Lifeline Facilities and Countermeasures Against Soil Liquefaction," Edited by T.D. O'Rourke and M. Hamada, 11/7/94, (PB95-220802, A99, MF-E08).

NCEER-95-0001 "Experimental and Analytical Investigation of Seismic Retrofit of Structures with Supplemental Damping: Part 1 - Fluid Viscous Damping Devices," by A.M. Reinhorn, C. Li and M.C. Constantinou, 1/3/95, (PB95-266599, A09, MF-A02).

NCEER-95-0002 "Experimental and Analytical Study of Low-Cycle Fatigue Behavior of Semi-Rigid Top-And-Seat Angle Connections," by G. Pekcan, J.B. Mander and S.S. Chen, 1/5/95, (PB95-220042, A07, MF-A02).

NCEER-95-0003 "NCEER-ATC Joint Study on Fragility of Buildings," by T. Anagnos, C. Rojahn and A.S. Kiremidjian, 1/20/95, (PB95-220026, A06, MF-A02).

NCEER-95-0004 "Nonlinear Control Algorithms for Peak Response Reduction," by Z. Wu, T.T. Soong, V. Gattulli and R.C. Lin, 2/16/95, (PB95-220349, A05, MF-A01).

NCEER-95-0005 "Pipeline Replacement Feasibility Study: A Methodology for Minimizing Seismic and Corrosion Risks to Underground Natural Gas Pipelines," by R.T. Eguchi, H.A. Seligson and D.G. Honegger, 3/2/95, (PB95-252326, A06, MF-A02).

NCEER-95-0006 "Evaluation of Seismic Performance of an 11-Story Frame Building During the 1994 Northridge Earthquake," by F. Naeim, R. DiSulio, K. Benuska, A. Reinhorn and C. Li, not available.

NCEER-95-0007 "Prioritization of Bridges for Seismic Retrofitting," by N. Basöz and A.S. Kiremidjian, 4/24/95, (PB95-252300, A08, MF-A02).

NCEER-95-0008 "Method for Developing Motion Damage Relationships for Reinforced Concrete Frames," by A. Singhal and A.S. Kiremidjian, 5/11/95, (PB95-266607, A06, MF-A02).

NCEER-95-0009 "Experimental and Analytical Investigation of Seismic Retrofit of Structures with Supplemental Damping: Part II - Friction Devices," by C. Li and A.M. Reinhorn, 7/6/95, (PB96-128087, A11, MF-A03).

NCEER-95-0010 "Experimental Performance and Analytical Study of a Non-Ductile Reinforced Concrete Frame Structure Retrofitted with Elastomeric Spring Dampers," by G. Pekcan, J.B. Mander and S.S. Chen, 7/14/95, (PB96-137161, A08, MF-A02).

NCEER-95-0011 "Development and Experimental Study of Semi-Active Fluid Damping Devices for Seismic Protection of Structures," by M.D. Symans and M.C. Constantinou, 8/3/95, (PB96-136940, A23, MF-A04).

NCEER-95-0012 "Real-Time Structural Parameter Modification (RSPM): Development of Innervated Structures," by Z. Liang, M. Tong and G.C. Lee, 4/11/95, (PB96-137153, A06, MF-A01).

NCEER-95-0013 "Experimental and Analytical Investigation of Seismic Retrofit of Structures with Supplemental Damping: Part III - Viscous Damping Walls," by A.M. Reinhorn and C. Li, 10/1/95, (PB96-176409, A11, MF-A03).

NCEER-95-0014 "Seismic Fragility Analysis of Equipment and Structures in a Memphis Electric Substation," by J-R. Huo and H.H.M. Hwang, 8/10/95, (PB96-128087, A09, MF-A02).

NCEER-95-0015 "The Hanshin-Awaji Earthquake of January 17, 1995: Performance of Lifelines," Edited by M. Shinozuka, 11/3/95, (PB96-176383, A15, MF-A03).

NCEER-95-0016 "Highway Culvert Performance During Earthquakes," by T.L. Youd and C.J. Beckman, available as NCEER-96-0015.

NCEER-95-0017 "The Hanshin-Awaji Earthquake of January 17, 1995: Performance of Highway Bridges," Edited by I.G. Buckle, 12/1/95, not available.

NCEER-95-0018 "Modeling of Masonry Infill Panels for Structural Analysis," by A.M. Reinhorn, A. Madan, R.E. Valles, Y. Reichmann and J.B. Mander, 12/8/95, (PB97-110886, MF-A01, A06).

NCEER-95-0019 "Optimal Polynomial Control for Linear and Nonlinear Structures," by A.K. Agrawal and J.N. Yang, 12/11/95, (PB96-168737, A07, MF-A02).

NCEER-95-0020 "Retrofit of Non-Ductile Reinforced Concrete Frames Using Friction Dampers," by R.S. Rao, P. Gergely and R.N. White, 12/22/95, (PB97-133508, A10, MF-A02).

NCEER-95-0021 "Parametric Results for Seismic Response of Pile-Supported Bridge Bents," by G. Mylonakis, A. Nikolaou and G. Gazetas, 12/22/95, (PB97-100242, A12, MF-A03).

NCEER-95-0022 "Kinematic Bending Moments in Seismically Stressed Piles," by A. Nikolaou, G. Mylonakis and G. Gazetas, 12/23/95, (PB97-113914, MF-A03, A13).

NCEER-96-0001 "Dynamic Response of Unreinforced Masonry Buildings with Flexible Diaphragms," by A.C. Costley and D.P. Abrams," 10/10/96, (PB97-133573, MF-A03, A15).

NCEER-96-0002 "State of the Art Review: Foundations and Retaining Structures," by I. Po Lam, not available.

NCEER-96-0003 "Ductility of Rectangular Reinforced Concrete Bridge Columns with Moderate Confinement," by N. Wehbe, M. Saiidi, D. Sanders and B. Douglas, 11/7/96, (PB97-133557, A06, MF-A02).

NCEER-96-0004 "Proceedings of the Long-Span Bridge Seismic Research Workshop," edited by I.G. Buckle and I.M. Friedland, not available.

NCEER-96-0005 "Establish Representative Pier Types for Comprehensive Study: Eastern United States," by J. Kulicki and Z. Prucz, 5/28/96, (PB98-119217, A07, MF-A02).

NCEER-96-0006 "Establish Representative Pier Types for Comprehensive Study: Western United States," by R. Imbsen, R.A. Schamber and T.A. Osterkamp, 5/28/96, (PB98-118607, A07, MF-A02).

NCEER-96-0007 "Nonlinear Control Techniques for Dynamical Systems with Uncertain Parameters," by R.G. Ghanem and M.I. Bujakov, 5/27/96, (PB97-100259, A17, MF-A03).

NCEER-96-0008 "Seismic Evaluation of a 30-Year Old Non-Ductile Highway Bridge Pier and Its Retrofit," by J.B. Mander, B. Mahmoodzadegan, S. Bhadra and S.S. Chen, 5/31/96, (PB97-110902, MF-A03, A10).

NCEER-96-0009 "Seismic Performance of a Model Reinforced Concrete Bridge Pier Before and After Retrofit," by J.B. Mander, J.H. Kim and C.A. Ligozio, 5/31/96, (PB97-110910, MF-A02, A10).

NCEER-96-0010 "IDARC2D Version 4.0: A Computer Program for the Inelastic Damage Analysis of Buildings," by R.E. Valles, A.M. Reinhorn, S.K. Kunnath, C. Li and A. Madan, 6/3/96, (PB97-100234, A17, MF-A03).

NCEER-96-0011 "Estimation of the Economic Impact of Multiple Lifeline Disruption: Memphis Light, Gas and Water Division Case Study," by S.E. Chang, H.A. Seligson and R.T. Eguchi, 8/16/96, (PB97-133490, A11, MF-A03).

NCEER-96-0012 "Proceedings from the Sixth Japan-U.S. Workshop on Earthquake Resistant Design of Lifeline Facilities and Countermeasures Against Soil Liquefaction, Edited by M. Hamada and T. O'Rourke, 9/11/96, (PB97-133581, A99, MF-A06).

NCEER-96-0013 "Chemical Hazards, Mitigation and Preparedness in Areas of High Seismic Risk: A Methodology for Estimating the Risk of Post-Earthquake Hazardous Materials Release," by H.A. Seligson, R.T. Eguchi, K.J. Tierney and K. Richmond, 11/7/96, (PB97-133565, MF-A02, A08).

NCEER-96-0014 "Response of Steel Bridge Bearings to Reversed Cyclic Loading," by J.B. Mander, D-K. Kim, S.S. Chen and G.J. Premus, 11/13/96, (PB97-140735, A12, MF-A03).

NCEER-96-0015 "Highway Culvert Performance During Past Earthquakes," by T.L. Youd and C.J. Beckman, 11/25/96, (PB97-133532, A06, MF-A01).

NCEER-97-0001 "Evaluation, Prevention and Mitigation of Pounding Effects in Building Structures," by R.E. Valles and A.M. Reinhorn, 2/20/97, (PB97-159552, A14, MF-A03).

NCEER-97-0002 "Seismic Design Criteria for Bridges and Other Highway Structures," by C. Rojahn, R. Mayes, D.G. Anderson, J. Clark, J.H. Hom, R.V. Nutt and M.J. O'Rourke, 4/30/97, (PB97-194658, A06, MF-A03).

NCEER-97-0003   "Proceedings of the U.S.-Italian Workshop on Seismic Evaluation and Retrofit," Edited by D.P. Abrams and G.M. Calvi, 3/19/97, (PB97-194666, A13, MF-A03).

NCEER-97-0004   "Investigation of Seismic Response of Buildings with Linear and Nonlinear Fluid Viscous Dampers," by A.A. Seleemah and M.C. Constantinou, 5/21/97, (PB98-109002, A15, MF-A03).

NCEER-97-0005   "Proceedings of the Workshop on Earthquake Engineering Frontiers in Transportation Facilities," edited by G.C. Lee and I.M. Friedland, 8/29/97, (PB98-128911, A25, MR-A04).

NCEER-97-0006   "Cumulative Seismic Damage of Reinforced Concrete Bridge Piers," by S.K. Kunnath, A. El-Bahy, A. Taylor and W. Stone, 9/2/97, (PB98-108814, A11, MF-A03).

NCEER-97-0007   "Structural Details to Accommodate Seismic Movements of Highway Bridges and Retaining Walls," by R.A. Imbsen, R.A. Schamber, E. Thorkildsen, A. Kartoum, B.T. Martin, T.N. Rosser and J.M. Kulicki, 9/3/97, (PB98-108996, A09, MF-A02).

NCEER-97-0008   "A Method for Earthquake Motion-Damage Relationships with Application to Reinforced Concrete Frames," by A. Singhal and A.S. Kiremidjian, 9/10/97, (PB98-108988, A13, MF-A03).

NCEER-97-0009   "Seismic Analysis and Design of Bridge Abutments Considering Sliding and Rotation," by K. Fishman and R. Richards, Jr., 9/15/97, (PB98-108897, A06, MF-A02).

NCEER-97-0010   "Proceedings of the FHWA/NCEER Workshop on the National Representation of Seismic Ground Motion for New and Existing Highway Facilities," edited by I.M. Friedland, M.S. Power and R.L. Mayes, 9/22/97, (PB98-128903, A21, MF-A04).

NCEER-97-0011   "Seismic Analysis for Design or Retrofit of Gravity Bridge Abutments," by K.L. Fishman, R. Richards, Jr. and R.C. Divito, 10/2/97, (PB98-128937, A08, MF-A02).

NCEER-97-0012   "Evaluation of Simplified Methods of Analysis for Yielding Structures," by P. Tsopelas, M.C. Constantinou, C.A. Kircher and A.S. Whittaker, 10/31/97, (PB98-128929, A10, MF-A03).

NCEER-97-0013   "Seismic Design of Bridge Columns Based on Control and Repairability of Damage," by C-T. Cheng and J.B. Mander, 12/8/97, (PB98-144249, A11, MF-A03).

NCEER-97-0014   "Seismic Resistance of Bridge Piers Based on Damage Avoidance Design," by J.B. Mander and C-T. Cheng, 12/10/97, (PB98-144223, A09, MF-A02).

NCEER-97-0015   "Seismic Response of Nominally Symmetric Systems with Strength Uncertainty," by S. Balopoulou and M. Grigoriu, 12/23/97, (PB98-153422, A11, MF-A03).

NCEER-97-0016   "Evaluation of Seismic Retrofit Methods for Reinforced Concrete Bridge Columns," by T.J. Wipf, F.W. Klaiber and F.M. Russo, 12/28/97, (PB98-144215, A12, MF-A03).

NCEER-97-0017   "Seismic Fragility of Existing Conventional Reinforced Concrete Highway Bridges," by C.L. Mullen and A.S. Cakmak, 12/30/97, (PB98-153406, A08, MF-A02).

NCEER-97-0018   "Loss Asssessment of Memphis Buildings," edited by D.P. Abrams and M. Shinozuka, 12/31/97, (PB98-144231, A13, MF-A03).

NCEER-97-0019   "Seismic Evaluation of Frames with Infill Walls Using Quasi-static Experiments," by K.M. Mosalam, R.N. White and P. Gergely, 12/31/97, (PB98-153455, A07, MF-A02).

NCEER-97-0020   "Seismic Evaluation of Frames with Infill Walls Using Pseudo-dynamic Experiments," by K.M. Mosalam, R.N. White and P. Gergely, 12/31/97, (PB98-153430, A07, MF-A02).

NCEER-97-0021   "Computational Strategies for Frames with Infill Walls: Discrete and Smeared Crack Analyses and Seismic Fragility," by K.M. Mosalam, R.N. White and P. Gergely, 12/31/97, (PB98-153414, A10, MF-A02).

NCEER-97-0022   "Proceedings of the NCEER Workshop on Evaluation of Liquefaction Resistance of Soils," edited by T.L. Youd and I.M. Idriss, 12/31/97, (PB98-155617, A15, MF-A03).

MCEER-98-0001   "Extraction of Nonlinear Hysteretic Properties of Seismically Isolated Bridges from Quick-Release Field Tests," by Q. Chen, B.M. Douglas, E.M. Maragakis and I.G. Buckle, 5/26/98, (PB99-118838, A06, MF-A01).

MCEER-98-0002   "Methodologies for Evaluating the Importance of Highway Bridges," by A. Thomas, S. Eshenaur and J. Kulicki, 5/29/98, (PB99-118846, A10, MF-A02).

MCEER-98-0003   "Capacity Design of Bridge Piers and the Analysis of Overstrength," by J.B. Mander, A. Dutta and P. Goel, 6/1/98, (PB99-118853, A09, MF-A02).

MCEER-98-0004   "Evaluation of Bridge Damage Data from the Loma Prieta and Northridge, California Earthquakes," by N. Basoz and A. Kiremidjian, 6/2/98, (PB99-118861, A15, MF-A03).

MCEER-98-0005   "Screening Guide for Rapid Assessment of Liquefaction Hazard at Highway Bridge Sites," by T. L. Youd, 6/16/98, (PB99-118879, A06, not available on microfiche).

MCEER-98-0006   "Structural Steel and Steel/Concrete Interface Details for Bridges," by P. Ritchie, N. Kauhl and J. Kulicki, 7/13/98, (PB99-118945, A06, MF-A01).

MCEER-98-0007   "Capacity Design and Fatigue Analysis of Confined Concrete Columns," by A. Dutta and J.B. Mander, 7/14/98, (PB99-118960, A14, MF-A03).

MCEER-98-0008   "Proceedings of the Workshop on Performance Criteria for Telecommunication Services Under Earthquake Conditions," edited by A.J. Schiff, 7/15/98, (PB99-118952, A08, MF-A02).

MCEER-98-0009   "Fatigue Analysis of Unconfined Concrete Columns," by J.B. Mander, A. Dutta and J.H. Kim, 9/12/98, (PB99-123655, A10, MF-A02).

MCEER-98-0010   "Centrifuge Modeling of Cyclic Lateral Response of Pile-Cap Systems and Seat-Type Abutments in Dry Sands," by A.D. Gadre and R. Dobry, 10/2/98, (PB99-123606, A13, MF-A03).

MCEER-98-0011   "IDARC-BRIDGE: A Computational Platform for Seismic Damage Assessment of Bridge Structures," by A.M. Reinhorn, V. Simeonov, G. Mylonakis and Y. Reichman, 10/2/98, (PB99-162919, A15, MF-A03).

MCEER-98-0012   "Experimental Investigation of the Dynamic Response of Two Bridges Before and After Retrofitting with Elastomeric Bearings," by D.A. Wendichansky, S.S. Chen and J.B. Mander, 10/2/98, (PB99-162927, A15, MF-A03).

MCEER-98-0013   "Design Procedures for Hinge Restrainers and Hinge Sear Width for Multiple-Frame Bridges," by R. Des Roches and G.L. Fenves, 11/3/98, (PB99-140477, A13, MF-A03).

MCEER-98-0014   "Response Modification Factors for Seismically Isolated Bridges," by M.C. Constantinou and J.K. Quarshie, 11/3/98, (PB99-140485, A14, MF-A03).

MCEER-98-0015   "Proceedings of the U.S.-Italy Workshop on Seismic Protective Systems for Bridges," edited by I.M. Friedland and M.C. Constantinou, 11/3/98, (PB2000-101711, A22, MF-A04).

MCEER-98-0016   "Appropriate Seismic Reliability for Critical Equipment Systems: Recommendations Based on Regional Analysis of Financial and Life Loss," by K. Porter, C. Scawthorn, C. Taylor and N. Blais, 11/10/98, (PB99-157265, A08, MF-A02).

MCEER-98-0017   "Proceedings of the U.S. Japan Joint Seminar on Civil Infrastructure Systems Research," edited by M. Shinozuka and A. Rose, 11/12/98, (PB99-156713, A16, MF-A03).

MCEER-98-0018   "Modeling of Pile Footings and Drilled Shafts for Seismic Design," by I. PoLam, M. Kapuskar and D. Chaudhuri, 12/21/98, (PB99-157257, A09, MF-A02).

MCEER-99-0001   "Seismic Evaluation of a Masonry Infilled Reinforced Concrete Frame by Pseudodynamic Testing," by S.G. Buonopane and R.N. White, 2/16/99, (PB99-162851, A09, MF-A02).

MCEER-99-0002   "Response History Analysis of Structures with Seismic Isolation and Energy Dissipation Systems: Verification Examples for Program SAP2000," by J. Scheller and M.C. Constantinou, 2/22/99, (PB99-162869, A08, MF-A02).

MCEER-99-0003   "Experimental Study on the Seismic Design and Retrofit of Bridge Columns Including Axial Load Effects," by A. Dutta, T. Kokorina and J.B. Mander, 2/22/99, (PB99-162877, A09, MF-A02).

MCEER-99-0004   "Experimental Study of Bridge Elastomeric and Other Isolation and Energy Dissipation Systems with Emphasis on Uplift Prevention and High Velocity Near-source Seismic Excitation," by A. Kasalanati and M. C. Constantinou, 2/26/99, (PB99-162885, A12, MF-A03).

MCEER-99-0005   "Truss Modeling of Reinforced Concrete Shear-flexure Behavior," by J.H. Kim and J.B. Mander, 3/8/99, (PB99-163693, A12, MF-A03).

MCEER-99-0006   "Experimental Investigation and Computational Modeling of Seismic Response of a 1:4 Scale Model Steel Structure with a Load Balancing Supplemental Damping System," by G. Pekcan, J.B. Mander and S.S. Chen, 4/2/99, (PB99-162893, A11, MF-A03).

MCEER-99-0007   "Effect of Vertical Ground Motions on the Structural Response of Highway Bridges," by M.R. Button, C.J. Cronin and R.L. Mayes, 4/10/99, (PB2000-101411, A10, MF-A03).

MCEER-99-0008   "Seismic Reliability Assessment of Critical Facilities: A Handbook, Supporting Documentation, and Model Code Provisions," by G.S. Johnson, R.E. Sheppard, M.D. Quilici, S.J. Eder and C.R. Scawthorn, 4/12/99, (PB2000-101701, A18, MF-A04).

MCEER-99-0009   "Impact Assessment of Selected MCEER Highway Project Research on the Seismic Design of Highway Structures," by C. Rojahn, R. Mayes, D.G. Anderson, J.H. Clark, D'Appolonia Engineering, S. Gloyd and R.V. Nutt, 4/14/99, (PB99-162901, A10, MF-A02).

MCEER-99-0010   "Site Factors and Site Categories in Seismic Codes," by R. Dobry, R. Ramos and M.S. Power, 7/19/99, (PB2000-101705, A08, MF-A02).

MCEER-99-0011   "Restrainer Design Procedures for Multi-Span Simply-Supported Bridges," by M.J. Randall, M. Saiidi, E. Maragakis and T. Isakovic, 7/20/99, (PB2000-101702, A10, MF-A02).

MCEER-99-0012   "Property Modification Factors for Seismic Isolation Bearings," by M.C. Constantinou, P. Tsopelas, A. Kasalanati and E. Wolff, 7/20/99, (PB2000-103387, A11, MF-A03).

MCEER-99-0013   "Critical Seismic Issues for Existing Steel Bridges," by P. Ritchie, N. Kauhl and J. Kulicki, 7/20/99, (PB2000-101697, A09, MF-A02).

MCEER-99-0014   "Nonstructural Damage Database," by A. Kao, T.T. Soong and A. Vender, 7/24/99, (PB2000-101407, A06, MF-A01).

MCEER-99-0015   "Guide to Remedial Measures for Liquefaction Mitigation at Existing Highway Bridge Sites," by H.G. Cooke and J. K. Mitchell, 7/26/99, (PB2000-101703, A11, MF-A03).

MCEER-99-0016   "Proceedings of the MCEER Workshop on Ground Motion Methodologies for the Eastern United States," edited by N. Abrahamson and A. Becker, 8/11/99, (PB2000-103385, A07, MF-A02).

MCEER-99-0017   "Quindío, Colombia Earthquake of January 25, 1999: Reconnaissance Report," by A.P. Asfura and P.J. Flores, 10/4/99, (PB2000-106893, A06, MF-A01).

MCEER-99-0018   "Hysteretic Models for Cyclic Behavior of Deteriorating Inelastic Structures," by M.V. Sivaselvan and A.M. Reinhorn, 11/5/99, (PB2000-103386, A08, MF-A02).

MCEER-99-0019   "Proceedings of the 7th U.S.- Japan Workshop on Earthquake Resistant Design of Lifeline Facilities and Countermeasures Against Soil Liquefaction," edited by T.D. O'Rourke, J.P. Bardet and M. Hamada, 11/19/99, (PB2000-103354, A99, MF-A06).

MCEER-99-0020   "Development of Measurement Capability for Micro-Vibration Evaluations with Application to Chip Fabrication Facilities," by G.C. Lee, Z. Liang, J.W. Song, J.D. Shen and W.C. Liu, 12/1/99, (PB2000-105993, A08, MF-A02).

MCEER-99-0021   "Design and Retrofit Methodology for Building Structures with Supplemental Energy Dissipating Systems," by G. Pekcan, J.B. Mander and S.S. Chen, 12/31/99, (PB2000-105994, A11, MF-A03).

MCEER-00-0001   "The Marmara, Turkey Earthquake of August 17, 1999: Reconnaissance Report," edited by C. Scawthorn; with major contributions by M. Bruneau, R. Eguchi, T. Holzer, G. Johnson, J. Mander, J. Mitchell, W. Mitchell, A. Papageorgiou, C. Scaethorn, and G. Webb, 3/23/00, (PB2000-106200, A11, MF-A03).

MCEER-00-0002   "Proceedings of the MCEER Workshop for Seismic Hazard Mitigation of Health Care Facilities," edited by G.C. Lee, M. Ettouney, M. Grigoriu, J. Hauer and J. Nigg, 3/29/00, (PB2000-106892, A08, MF-A02).

MCEER-00-0003   "The Chi-Chi, Taiwan Earthquake of September 21, 1999: Reconnaissance Report," edited by G.C. Lee and C.H. Loh, with major contributions by G.C. Lee, M. Bruneau, I.G. Buckle, S.E. Chang, P.J. Flores, T.D. O'Rourke, M. Shinozuka, T.T. Soong, C-H. Loh, K-C. Chang, Z-J. Chen, J-S. Hwang, M-L. Lin, G-Y. Liu, K-C. Tsai, G.C. Yao and C-L. Yen, 4/30/00, (PB2001-100980, A10, MF-A02).

MCEER-00-0004   "Seismic Retrofit of End-Sway Frames of Steel Deck-Truss Bridges with a Supplemental Tendon System: Experimental and Analytical Investigation," by G. Pekcan, J.B. Mander and S.S. Chen, 7/1/00, (PB2001-100982, A10, MF-A02).

MCEER-00-0005   "Sliding Fragility of Unrestrained Equipment in Critical Facilities," by W.H. Chong and T.T. Soong, 7/5/00, (PB2001-100983, A08, MF-A02).

MCEER-00-0006   "Seismic Response of Reinforced Concrete Bridge Pier Walls in the Weak Direction," by N. Abo-Shadi, M. Saiidi and D. Sanders, 7/17/00, (PB2001-100981, A17, MF-A03).

MCEER-00-0007   "Low-Cycle Fatigue Behavior of Longitudinal Reinforcement in Reinforced Concrete Bridge Columns," by J. Brown and S.K. Kunnath, 7/23/00, (PB2001-104392, A08, MF-A02).

MCEER-00-0008   "Soil Structure Interaction of Bridges for Seismic Analysis," I. PoLam and H. Law, 9/25/00, (PB2001-105397, A08, MF-A02).

MCEER-00-0009   "Proceedings of the First MCEER Workshop on Mitigation of Earthquake Disaster by Advanced Technologies (MEDAT-1), edited by M. Shinozuka, D.J. Inman and T.D. O'Rourke, 11/10/00, (PB2001-105399, A14, MF-A03).

MCEER-00-0010   "Development and Evaluation of Simplified Procedures for Analysis and Design of Buildings with Passive Energy Dissipation Systems, Revision 01," by O.M. Ramirez, M.C. Constantinou, C.A. Kircher, A.S. Whittaker, M.W. Johnson, J.D. Gomez and C. Chrysostomou, 11/16/01, (PB2001-105523, A23, MF-A04).

MCEER-00-0011   "Dynamic Soil-Foundation-Structure Interaction Analyses of Large Caissons," by C-Y. Chang, C-M. Mok, Z-L. Wang, R. Settgast, F. Waggoner, M.A. Ketchum, H.M. Gonnermann and C-C. Chin, 12/30/00, (PB2001-104373, A07, MF-A02).

MCEER-00-0012   "Experimental Evaluation of Seismic Performance of Bridge Restrainers," by A.G. Vlassis, E.M. Maragakis and M. Saiid Saiidi, 12/30/00, (PB2001-104354, A09, MF-A02).

MCEER-00-0013   "Effect of Spatial Variation of Ground Motion on Highway Structures," by M. Shinozuka, V. Saxena and G. Deodatis, 12/31/00, (PB2001-108755, A13, MF-A03).

MCEER-00-0014   "A Risk-Based Methodology for Assessing the Seismic Performance of Highway Systems," by S.D. Werner, C.E. Taylor, J.E. Moore, II, J.S. Walton and S. Cho, 12/31/00, (PB2001-108756, A14, MF-A03).

214

MCEER-01-0001 "Experimental Investigation of P-Delta Effects to Collapse During Earthquakes," by D. Vian and M. Bruneau, 6/25/01, (PB2002-100534, A17, MF-A03).

MCEER-01-0002 "Proceedings of the Second MCEER Workshop on Mitigation of Earthquake Disaster by Advanced Technologies (MEDAT-2)," edited by M. Bruneau and D.J. Inman, 7/23/01, (PB2002-100434, A16, MF-A03).

MCEER-01-0003 "Sensitivity Analysis of Dynamic Systems Subjected to Seismic Loads," by C. Roth and M. Grigoriu, 9/18/01, (PB2003-100884, A12, MF-A03).

MCEER-01-0004 "Overcoming Obstacles to Implementing Earthquake Hazard Mitigation Policies: Stage 1 Report," by D.J. Alesch and W.J. Petak, 12/17/01, (PB2002-107949, A07, MF-A02).

MCEER-01-0005 "Updating Real-Time Earthquake Loss Estimates: Methods, Problems and Insights," by C.E. Taylor, S.E. Chang and R.T. Eguchi, 12/17/01, (PB2002-107948, A05, MF-A01).

MCEER-01-0006 "Experimental Investigation and Retrofit of Steel Pile Foundations and Pile Bents Under Cyclic Lateral Loadings," by A. Shama, J. Mander, B. Blabac and S. Chen, 12/31/01, (PB2002-107950, A13, MF-A03).

MCEER-02-0001 "Assessment of Performance of Bolu Viaduct in the 1999 Duzce Earthquake in Turkey" by P.C. Roussis, M.C. Constantinou, M. Erdik, E. Durukal and M. Dicleli, 5/8/02, (PB2003-100883, A08, MF-A02).

MCEER-02-0002 "Seismic Behavior of Rail Counterweight Systems of Elevators in Buildings," by M.P. Singh, Rildova and L.E. Suarez, 5/27/02. (PB2003-100882, A11, MF-A03).

MCEER-02-0003 "Development of Analysis and Design Procedures for Spread Footings," by G. Mylonakis, G. Gazetas, S. Nikolaou and A. Chauncey, 10/02/02, (PB2004-101636, A13, MF-A03, CD-A13).

MCEER-02-0004 "Bare-Earth Algorithms for Use with SAR and LIDAR Digital Elevation Models," by C.K. Huyck, R.T. Eguchi and B. Houshmand, 10/16/02, (PB2004-101637, A07, CD-A07).

MCEER-02-0005 "Review of Energy Dissipation of Compression Members in Concentrically Braced Frames," by K.Lee and M. Bruneau, 10/18/02, (PB2004-101638, A10, CD-A10).

MCEER-03-0001 "Experimental Investigation of Light-Gauge Steel Plate Shear Walls for the Seismic Retrofit of Buildings" by J. Berman and M. Bruneau, 5/2/03, (PB2004-101622, A10, MF-A03, CD-A10).

MCEER-03-0002 "Statistical Analysis of Fragility Curves," by M. Shinozuka, M.Q. Feng, H. Kim, T. Uzawa and T. Ueda, 6/16/03, (PB2004-101849, A09, CD-A09).

MCEER-03-0003 "Proceedings of the Eighth U.S.-Japan Workshop on Earthquake Resistant Design f Lifeline Facilities and Countermeasures Against Liquefaction," edited by M. Hamada, J.P. Bardet and T.D. O'Rourke, 6/30/03, (PB2004-104386, A99, CD-A99).

MCEER-03-0004 "Proceedings of the PRC-US Workshop on Seismic Analysis and Design of Special Bridges," edited by L.C. Fan and G.C. Lee, 7/15/03, (PB2004-104387, A14, CD-A14).

MCEER-03-0005 "Urban Disaster Recovery: A Framework and Simulation Model," by S.B. Miles and S.E. Chang, 7/25/03, (PB2004-104388, A07, CD-A07).

MCEER-03-0006 "Behavior of Underground Piping Joints Due to Static and Dynamic Loading," by R.D. Meis, M. Maragakis and R. Siddharthan, 11/17/03, (PB2005-102194, A13, MF-A03, CD-A00).

MCEER-04-0001 "Experimental Study of Seismic Isolation Systems with Emphasis on Secondary System Response and Verification of Accuracy of Dynamic Response History Analysis Methods," by E. Wolff and M. Constantinou, 1/16/04 (PB2005-102195, A99, MF-E08, CD-A00).

MCEER-04-0002 "Tension, Compression and Cyclic Testing of Engineered Cementitious Composite Materials," by K. Kesner and S.L. Billington, 3/1/04, (PB2005-102196, A08, CD-A08).

MCEER-04-0003 "Cyclic Testing of Braces Laterally Restrained by Steel Studs to Enhance Performance During Earthquakes," by O.C. Celik, J.W. Berman and M. Bruneau, 3/16/04, (PB2005-102197, A13, MF-A03, CD-A00).

MCEER-04-0004 "Methodologies for Post Earthquake Building Damage Detection Using SAR and Optical Remote Sensing: Application to the August 17, 1999 Marmara, Turkey Earthquake," by C.K. Huyck, B.J. Adams, S. Cho, R.T. Eguchi, B. Mansouri and B. Houshmand, 6/15/04, (PB2005-104888, A10, CD-A00).

MCEER-04-0005 "Nonlinear Structural Analysis Towards Collapse Simulation: A Dynamical Systems Approach," by M.V. Sivaselvan and A.M. Reinhorn, 6/16/04, (PB2005-104889, A11, MF-A03, CD-A00).

MCEER-04-0006 "Proceedings of the Second PRC-US Workshop on Seismic Analysis and Design of Special Bridges," edited by G.C. Lee and L.C. Fan, 6/25/04, (PB2005-104890, A16, CD-A00).

MCEER-04-0007 "Seismic Vulnerability Evaluation of Axially Loaded Steel Built-up Laced Members," by K. Lee and M. Bruneau, 6/30/04, (PB2005-104891, A16, CD-A00).

MCEER-04-0008 "Evaluation of Accuracy of Simplified Methods of Analysis and Design of Buildings with Damping Systems for Near-Fault and for Soft-Soil Seismic Motions," by E.A. Pavlou and M.C. Constantinou, 8/16/04, (PB2005-104892, A08, MF-A02, CD-A00).

MCEER-04-0009 "Assessment of Geotechnical Issues in Acute Care Facilities in California," by M. Lew, T.D. O'Rourke, R. Dobry and M. Koch, 9/15/04, (PB2005-104893, A08, CD-A00).

MCEER-04-0010 "Scissor-Jack-Damper Energy Dissipation System," by A.N. Sigaher-Boyle and M.C. Constantinou, 12/1/04 (PB2005-108221).

MCEER-04-0011 "Seismic Retrofit of Bridge Steel Truss Piers Using a Controlled Rocking Approach," by M. Pollino and M. Bruneau, 12/20/04 (PB2006-105795).

MCEER-05-0001 "Experimental and Analytical Studies of Structures Seismically Isolated with an Uplift-Restraint Isolation System," by P.C. Roussis and M.C. Constantinou, 1/10/05 (PB2005-108222).

MCEER-05-0002 "A Versatile Experimentation Model for Study of Structures Near Collapse Applied to Seismic Evaluation of Irregular Structures," by D. Kusumastuti, A.M. Reinhorn and A. Rutenberg, 3/31/05 (PB2006-101523).

MCEER-05-0003 "Proceedings of the Third PRC-US Workshop on Seismic Analysis and Design of Special Bridges," edited by L.C. Fan and G.C. Lee, 4/20/05, (PB2006-105796).

MCEER-05-0004 "Approaches for the Seismic Retrofit of Braced Steel Bridge Piers and Proof-of-Concept Testing of an Eccentrically Braced Frame with Tubular Link," by J.W. Berman and M. Bruneau, 4/21/05 (PB2006-101524).

MCEER-05-0005 "Simulation of Strong Ground Motions for Seismic Fragility Evaluation of Nonstructural Components in Hospitals," by A. Wanitkorkul and A. Filiatrault, 5/26/05 (PB2006-500027).

MCEER-05-0006 "Seismic Safety in California Hospitals: Assessing an Attempt to Accelerate the Replacement or Seismic Retrofit of Older Hospital Facilities," by D.J. Alesch, L.A. Arendt and W.J. Petak, 6/6/05 (PB2006-105794).

MCEER-05-0007 "Development of Seismic Strengthening and Retrofit Strategies for Critical Facilities Using Engineered Cementitious Composite Materials," by K. Kesner and S.L. Billington, 8/29/05 (PB2006-111701).

MCEER-05-0008 "Experimental and Analytical Studies of Base Isolation Systems for Seismic Protection of Power Transformers," by N. Murota, M.Q. Feng and G-Y. Liu, 9/30/05 (PB2006-111702).

MCEER-05-0009 "3D-BASIS-ME-MB: Computer Program for Nonlinear Dynamic Analysis of Seismically Isolated Structures," by P.C. Tsopelas, P.C. Roussis, M.C. Constantinou, R. Buchanan and A.M. Reinhorn, 10/3/05 (PB2006-111703).

MCEER-05-0010 "Steel Plate Shear Walls for Seismic Design and Retrofit of Building Structures," by D. Vian and M. Bruneau, 12/15/05 (PB2006-111704).

MCEER-05-0011 "The Performance-Based Design Paradigm," by M.J. Astrella and A. Whittaker, 12/15/05 (PB2006-111705).

MCEER-06-0001 "Seismic Fragility of Suspended Ceiling Systems," H. Badillo-Almaraz, A.S. Whittaker, A.M. Reinhorn and G.P. Cimellaro, 2/4/06 (PB2006-111706).

MCEER-06-0002 "Multi-Dimensional Fragility of Structures," by G.P. Cimellaro, A.M. Reinhorn and M. Bruneau, 3/1/06 (PB2007-106974, A09, MF-A02, CD A00).

MCEER-06-0003 "Built-Up Shear Links as Energy Dissipators for Seismic Protection of Bridges," by P. Dusicka, A.M. Itani and I.G. Buckle, 3/15/06 (PB2006-111708).

MCEER-06-0004 "Analytical Investigation of the Structural Fuse Concept," by R.E. Vargas and M. Bruneau, 3/16/06 (PB2006-111709).

MCEER-06-0005 "Experimental Investigation of the Structural Fuse Concept," by R.E. Vargas and M. Bruneau, 3/17/06 (PB2006-111710).

MCEER-06-0006 "Further Development of Tubular Eccentrically Braced Frame Links for the Seismic Retrofit of Braced Steel Truss Bridge Piers," by J.W. Berman and M. Bruneau, 3/27/06 (PB2007-105147).

MCEER-06-0007 "REDARS Validation Report," by S. Cho, C.K. Huyck, S. Ghosh and R.T. Eguchi, 8/8/06 (PB2007-106983).

MCEER-06-0008 "Review of Current NDE Technologies for Post-Earthquake Assessment of Retrofitted Bridge Columns," by J.W. Song, Z. Liang and G.C. Lee, 8/21/06 (PB2007-106984).

MCEER-06-0009 "Liquefaction Remediation in Silty Soils Using Dynamic Compaction and Stone Columns," by S. Thevanayagam, G.R. Martin, R. Nashed, T. Shenthan, T. Kanagalingam and N. Ecemis, 8/28/06 (PB2007-106985).

MCEER-06-0010 "Conceptual Design and Experimental Investigation of Polymer Matrix Composite Infill Panels for Seismic Retrofitting," by W. Jung, M. Chiewanichakorn and A.J. Aref, 9/21/06 (PB2007-106986).

MCEER-06-0011 "A Study of the Coupled Horizontal-Vertical Behavior of Elastomeric and Lead-Rubber Seismic Isolation Bearings," by G.P. Warn and A.S. Whittaker, 9/22/06 (PB2007-108679).

MCEER-06-0012 "Proceedings of the Fourth PRC-US Workshop on Seismic Analysis and Design of Special Bridges: Advancing Bridge Technologies in Research, Design, Construction and Preservation," Edited by L.C. Fan, G.C. Lee and L. Ziang, 10/12/06 (PB2007-109042).

MCEER-06-0013 "Cyclic Response and Low Cycle Fatigue Characteristics of Plate Steels," by P. Dusicka, A.M. Itani and I.G. Buckle, 11/1/06 06 (PB2007-106987).

MCEER-06-0014 "Proceedings of the Second US-Taiwan Bridge Engineering Workshop," edited by W.P. Yen, J. Shen, J-Y. Chen and M. Wang, 11/15/06 (PB2008-500041).

MCEER-06-0015 "User Manual and Technical Documentation for the REDARS^{TM} Import Wizard," by S. Cho, S. Ghosh, C.K. Huyck and S.D. Werner, 11/30/06 (PB2007-114766).

MCEER-06-0016 "Hazard Mitigation Strategy and Monitoring Technologies for Urban and Infrastructure Public Buildings: Proceedings of the China-US Workshops," edited by X.Y. Zhou, A.L. Zhang, G.C. Lee and M. Tong, 12/12/06 (PB2008-500018).

MCEER-07-0001 "Static and Kinetic Coefficients of Friction for Rigid Blocks," by C. Kafali, S. Fathali, M. Grigoriu and A.S. Whittaker, 3/20/07 (PB2007-114767).

MCEER-07-0002 "Hazard Mitigation Investment Decision Making: Organizational Response to Legislative Mandate," by L.A. Arendt, D.J. Alesch and W.J. Petak, 4/9/07 (PB2007-114768).

MCEER-07-0003 "Seismic Behavior of Bidirectional-Resistant Ductile End Diaphragms with Unbonded Braces in Straight or Skewed Steel Bridges," by O. Celik and M. Bruneau, 4/11/07 (PB2008-105141).

MCEER-07-0004   "Modeling Pile Behavior in Large Pile Groups Under Lateral Loading," by A.M. Dodds and G.R. Martin, 4/16/07(PB2008-105142).

MCEER-07-0005   "Experimental Investigation of Blast Performance of Seismically Resistant Concrete-Filled Steel Tube Bridge Piers," by S. Fujikura, M. Bruneau and D. Lopez-Garcia, 4/20/07 (PB2008-105143).

MCEER-07-0006   "Seismic Analysis of Conventional and Isolated Liquefied Natural Gas Tanks Using Mechanical Analogs," by I.P. Christovasilis and A.S. Whittaker, 5/1/07, not available.

MCEER-07-0007   "Experimental Seismic Performance Evaluation of Isolation/Restraint Systems for Mechanical Equipment – Part 1: Heavy Equipment Study," by S. Fathali and A. Filiatrault, 6/6/07 (PB2008-105144).

MCEER-07-0008   "Seismic Vulnerability of Timber Bridges and Timber Substructures," by A.A. Sharma, J.B. Mander, I.M. Friedland and D.R. Allicock, 6/7/07 (PB2008-105145).

MCEER-07-0009   "Experimental and Analytical Study of the XY-Friction Pendulum (XY-FP) Bearing for Bridge Applications," by C.C. Marin-Artieda, A.S. Whittaker and M.C. Constantinou, 6/7/07 (PB2008-105191).

MCEER-07-0010   "Proceedings of the PRC-US Earthquake Engineering Forum for Young Researchers," Edited by G.C. Lee and X.Z. Qi, 6/8/07 (PB2008-500058).

MCEER-07-0011   "Design Recommendations for Perforated Steel Plate Shear Walls," by R. Purba and M. Bruneau, 6/18/07, (PB2008-105192).

MCEER-07-0012   "Performance of Seismic Isolation Hardware Under Service and Seismic Loading," by M.C. Constantinou, A.S. Whittaker, Y. Kalpakidis, D.M. Fenz and G.P. Warn, 8/27/07, (PB2008-105193).

MCEER-07-0013   "Experimental Evaluation of the Seismic Performance of Hospital Piping Subassemblies," by E.R. Goodwin, E. Maragakis and A.M. Itani, 9/4/07, (PB2008-105194).

MCEER-07-0014   "A Simulation Model of Urban Disaster Recovery and Resilience: Implementation for the 1994 Northridge Earthquake," by S. Miles and S.E. Chang, 9/7/07, (PB2008-106426).

MCEER-07-0015   "Statistical and Mechanistic Fragility Analysis of Concrete Bridges," by M. Shinozuka, S. Banerjee and S-H. Kim, 9/10/07, (PB2008-106427).

MCEER-07-0016   "Three-Dimensional Modeling of Inelastic Buckling in Frame Structures," by M. Schachter and AM. Reinhorn, 9/13/07, (PB2008-108125).

MCEER-07-0017   "Modeling of Seismic Wave Scattering on Pile Groups and Caissons," by I. Po Lam, H. Law and C.T. Yang, 9/17/07 (PB2008-108150).

MCEER-07-0018   "Bridge Foundations: Modeling Large Pile Groups and Caissons for Seismic Design," by I. Po Lam, H. Law and G.R. Martin (Coordinating Author), 12/1/07 (PB2008-111190).

MCEER-07-0019   "Principles and Performance of Roller Seismic Isolation Bearings for Highway Bridges," by G.C. Lee, Y.C. Ou, Z. Liang, T.C. Niu and J. Song, 12/10/07 (PB2009-110466).

MCEER-07-0020   "Centrifuge Modeling of Permeability and Pinning Reinforcement Effects on Pile Response to Lateral Spreading," by L.L Gonzalez-Lagos, T. Abdoun and R. Dobry, 12/10/07 (PB2008-111191).

MCEER-07-0021   "Damage to the Highway System from the Pisco, Perú Earthquake of August 15, 2007," by J.S. O'Connor, L. Mesa and M. Nykamp, 12/10/07, (PB2008-108126).

MCEER-07-0022   "Experimental Seismic Performance Evaluation of Isolation/Restraint Systems for Mechanical Equipment – Part 2: Light Equipment Study," by S. Fathali and A. Filiatrault, 12/13/07 (PB2008-111192).

MCEER-07-0023   "Fragility Considerations in Highway Bridge Design," by M. Shinozuka, S. Banerjee and S.H. Kim, 12/14/07 (PB2008-111193).

MCEER-07-0024 "Performance Estimates for Seismically Isolated Bridges," by G.P. Warn and A.S. Whittaker, 12/30/07 (PB2008-112230).

MCEER-08-0001 "Seismic Performance of Steel Girder Bridge Superstructures with Conventional Cross Frames," by L.P. Carden, A.M. Itani and I.G. Buckle, 1/7/08, (PB2008-112231).

MCEER-08-0002 "Seismic Performance of Steel Girder Bridge Superstructures with Ductile End Cross Frames with Seismic Isolators," by L.P. Carden, A.M. Itani and I.G. Buckle, 1/7/08 (PB2008-112232).

MCEER-08-0003 "Analytical and Experimental Investigation of a Controlled Rocking Approach for Seismic Protection of Bridge Steel Truss Piers," by M. Pollino and M. Bruneau, 1/21/08 (PB2008-112233).

MCEER-08-0004 "Linking Lifeline Infrastructure Performance and Community Disaster Resilience: Models and Multi-Stakeholder Processes," by S.E. Chang, C. Pasion, K. Tatebe and R. Ahmad, 3/3/08 (PB2008-112234).

MCEER-08-0005 "Modal Analysis of Generally Damped Linear Structures Subjected to Seismic Excitations," by J. Song, Y-L. Chu, Z. Liang and G.C. Lee, 3/4/08 (PB2009-102311).

MCEER-08-0006 "System Performance Under Multi-Hazard Environments," by C. Kafali and M. Grigoriu, 3/4/08 (PB2008-112235).

MCEER-08-0007 "Mechanical Behavior of Multi-Spherical Sliding Bearings," by D.M. Fenz and M.C. Constantinou, 3/6/08 (PB2008-112236).

MCEER-08-0008 "Post-Earthquake Restoration of the Los Angeles Water Supply System," by T.H.P. Tabucchi and R.A. Davidson, 3/7/08 (PB2008-112237).

MCEER-08-0009 "Fragility Analysis of Water Supply Systems," by A. Jacobson and M. Grigoriu, 3/10/08 (PB2009-105545).

MCEER-08-0010 "Experimental Investigation of Full-Scale Two-Story Steel Plate Shear Walls with Reduced Beam Section Connections," by B. Qu, M. Bruneau, C-H. Lin and K-C. Tsai, 3/17/08 (PB2009-106368).

MCEER-08-0011 "Seismic Evaluation and Rehabilitation of Critical Components of Electrical Power Systems," S. Ersoy, B. Feizi, A. Ashrafi and M. Ala Saadeghvaziri, 3/17/08 (PB2009-105546).

MCEER-08-0012 "Seismic Behavior and Design of Boundary Frame Members of Steel Plate Shear Walls," by B. Qu and M. Bruneau, 4/26/08 . (PB2009-106744).

MCEER-08-0013 "Development and Appraisal of a Numerical Cyclic Loading Protocol for Quantifying Building System Performance," by A. Filiatrault, A. Wanitkorkul and M. Constantinou, 4/27/08 (PB2009-107906).

MCEER-08-0014 "Structural and Nonstructural Earthquake Design: The Challenge of Integrating Specialty Areas in Designing Complex, Critical Facilities," by W.J. Petak and D.J. Alesch, 4/30/08 (PB2009-107907).

MCEER-08-0015 "Seismic Performance Evaluation of Water Systems," by Y. Wang and T.D. O'Rourke, 5/5/08 (PB2009-107908).

MCEER-08-0016 "Seismic Response Modeling of Water Supply Systems," by P. Shi and T.D. O'Rourke, 5/5/08 (PB2009-107910).

MCEER-08-0017 "Numerical and Experimental Studies of Self-Centering Post-Tensioned Steel Frames," by D. Wang and A. Filiatrault, 5/12/08 (PB2009-110479).

MCEER-08-0018 "Development, Implementation and Verification of Dynamic Analysis Models for Multi-Spherical Sliding Bearings," by D.M. Fenz and M.C. Constantinou, 8/15/08 (PB2009-107911).

MCEER-08-0019 "Performance Assessment of Conventional and Base Isolated Nuclear Power Plants for Earthquake Blast Loadings," by Y.N. Huang, A.S. Whittaker and N. Luco, 10/28/08 (PB2009-107912).

MCEER-08-0020   "Remote Sensing for Resilient Multi-Hazard Disaster Response – Volume I: Introduction to Damage Assessment Methodologies," by B.J. Adams and R.T. Eguchi, 11/17/08 (PB2010-102695).

MCEER-08-0021   "Remote Sensing for Resilient Multi-Hazard Disaster Response – Volume II: Counting the Number of Collapsed Buildings Using an Object-Oriented Analysis: Case Study of the 2003 Bam Earthquake," by L. Gusella, C.K. Huyck and B.J. Adams, 11/17/08 (PB2010-100925).

MCEER-08-0022   "Remote Sensing for Resilient Multi-Hazard Disaster Response – Volume III: Multi-Sensor Image Fusion Techniques for Robust Neighborhood-Scale Urban Damage Assessment," by B.J. Adams and A. McMillan, 11/17/08 (PB2010-100926).

MCEER-08-0023   "Remote Sensing for Resilient Multi-Hazard Disaster Response – Volume IV: A Study of Multi-Temporal and Multi-Resolution SAR Imagery for Post-Katrina Flood Monitoring in New Orleans," by A. McMillan, J.G. Morley, B.J. Adams and S. Chesworth, 11/17/08 (PB2010-100927).

MCEER-08-0024   "Remote Sensing for Resilient Multi-Hazard Disaster Response – Volume V: Integration of Remote Sensing Imagery and VIEWS^{TM} Field Data for Post-Hurricane Charley Building Damage Assessment," by J.A. Womble, K. Mehta and B.J. Adams, 11/17/08 (PB2009-115532).

MCEER-08-0025   "Building Inventory Compilation for Disaster Management: Application of Remote Sensing and Statistical Modeling," by P. Sarabandi, A.S. Kiremidjian, R.T. Eguchi and B. J. Adams, 11/20/08 (PB2009-110484).

MCEER-08-0026   "New Experimental Capabilities and Loading Protocols for Seismic Qualification and Fragility Assessment of Nonstructural Systems," by R. Retamales, G. Mosqueda, A. Filiatrault and A. Reinhorn, 11/24/08 (PB2009-110485).

MCEER-08-0027   "Effects of Heating and Load History on the Behavior of Lead-Rubber Bearings," by I.V. Kalpakidis and M.C. Constantinou, 12/1/08 (PB2009-115533).

MCEER-08-0028   "Experimental and Analytical Investigation of Blast Performance of Seismically Resistant Bridge Piers," by S.Fujikura and M. Bruneau, 12/8/08 (PB2009-115534).

MCEER-08-0029   "Evolutionary Methodology for Aseismic Decision Support," by Y. Hu and G. Dargush, 12/15/08.

MCEER-08-0030   "Development of a Steel Plate Shear Wall Bridge Pier System Conceived from a Multi-Hazard Perspective," by D. Keller and M. Bruneau, 12/19/08 (PB2010-102696).

MCEER-09-0001   "Modal Analysis of Arbitrarily Damped Three-Dimensional Linear Structures Subjected to Seismic Excitations," by Y.L. Chu, J. Song and G.C. Lee, 1/31/09 (PB2010-100922).

MCEER-09-0002   "Air-Blast Effects on Structural Shapes," by G. Ballantyne, A.S. Whittaker, A.J. Aref and G.F. Dargush, 2/2/09 (PB2010-102697).

MCEER-09-0003   "Water Supply Performance During Earthquakes and Extreme Events," by A.L. Bonneau and T.D. O'Rourke, 2/16/09 (PB2010-100923).

MCEER-09-0004   "Generalized Linear (Mixed) Models of Post-Earthquake Ignitions," by R.A. Davidson, 7/20/09 (PB2010-102698).

MCEER-09-0005   "Seismic Testing of a Full-Scale Two-Story Light-Frame Wood Building: NEESWood Benchmark Test," by I.P. Christovasilis, A. Filiatrault and A. Wanitkorkul, 7/22/09 (PB2012-102401).

MCEER-09-0006   "IDARC2D Version 7.0: A Program for the Inelastic Damage Analysis of Structures," by A.M. Reinhorn, H. Roh, M. Sivaselvan, S.K. Kunnath, R.E. Valles, A. Madan, C. Li, R. Lobo and Y.J. Park, 7/28/09 (PB2010-103199).

MCEER-09-0007   "Enhancements to Hospital Resiliency: Improving Emergency Planning for and Response to Hurricanes," by D.B. Hess and L.A. Arendt, 7/30/09 (PB2010-100924).

MCEER-09-0008 "Assessment of Base-Isolated Nuclear Structures for Design and Beyond-Design Basis Earthquake Shaking," by Y.N. Huang, A.S. Whittaker, R.P. Kennedy and R.L. Mayes, 8/20/09 (PB2010-102699).

MCEER-09-0009 "Quantification of Disaster Resilience of Health Care Facilities," by G.P. Cimellaro, C. Fumo, A.M Reinhorn and M. Bruneau, 9/14/09 (PB2010-105384).

MCEER-09-0010 "Performance-Based Assessment and Design of Squat Reinforced Concrete Shear Walls," by C.K. Gulec and A.S. Whittaker, 9/15/09 (PB2010-102700).

MCEER-09-0011 "Proceedings of the Fourth US-Taiwan Bridge Engineering Workshop," edited by W.P. Yen, J.J. Shen, T.M. Lee and R.B. Zheng, 10/27/09 (PB2010-500009).

MCEER-09-0012 "Proceedings of the Special International Workshop on Seismic Connection Details for Segmental Bridge Construction," edited by W. Phillip Yen and George C. Lee, 12/21/09 (PB2012-102402).

MCEER-10-0001 "Direct Displacement Procedure for Performance-Based Seismic Design of Multistory Woodframe Structures," by W. Pang and D. Rosowsky, 4/26/10 (PB2012-102403).

MCEER-10-0002 "Simplified Direct Displacement Design of Six-Story NEESWood Capstone Building and Pre-Test Seismic Performance Assessment," by W. Pang, D. Rosowsky, J. van de Lindt and S. Pei, 5/28/10 (PB2012-102404).

MCEER-10-0003 "Integration of Seismic Protection Systems in Performance-Based Seismic Design of Woodframed Structures," by J.K. Shinde and M.D. Symans, 6/18/10 (PB2012-102405).

MCEER-10-0004 "Modeling and Seismic Evaluation of Nonstructural Components: Testing Frame for Experimental Evaluation of Suspended Ceiling Systems," by A.M. Reinhorn, K.P. Ryu and G. Maddaloni, 6/30/10 (PB2012-102406).

MCEER-10-0005 "Analytical Development and Experimental Validation of a Structural-Fuse Bridge Pier Concept," by S. El-Bahey and M. Bruneau, 10/1/10 (PB2012-102407).

MCEER-10-0006 "A Framework for Defining and Measuring Resilience at the Community Scale: The PEOPLES Resilience Framework," by C.S. Renschler, A.E. Frazier, L.A. Arendt, G.P. Cimellaro, A.M. Reinhorn and M. Bruneau, 10/8/10 (PB2012-102408).

MCEER-10-0007 "Impact of Horizontal Boundary Elements Design on Seismic Behavior of Steel Plate Shear Walls," by R. Purba and M. Bruneau, 11/14/10 (PB2012-102409).

MCEER-10-0008 "Seismic Testing of a Full-Scale Mid-Rise Building: The NEESWood Capstone Test," by S. Pei, J.W. van de Lindt, S.E. Pryor, H. Shimizu, H. Isoda and D.R. Rammer, 12/1/10 (PB2012-102410).

MCEER-10-0009 "Modeling the Effects of Detonations of High Explosives to Inform Blast-Resistant Design," by P. Sherkar, A.S. Whittaker and A.J. Aref, 12/1/10 (PB2012-102411).

MCEER-10-0010 "L'Aquila Earthquake of April 6, 2009 in Italy: Rebuilding a Resilient City to Withstand Multiple Hazards," by G.P. Cimellaro, I.P. Christovasilis, A.M. Reinhorn, A. De Stefano and T. Kirova, 12/29/10.

MCEER-11-0001 "Numerical and Experimental Investigation of the Seismic Response of Light-Frame Wood Structures," by I.P. Christovasilis and A. Filiatrault, 8/8/11 (PB2012-102412).

MCEER-11-0002 "Seismic Design and Analysis of a Precast Segmental Concrete Bridge Model," by M. Anagnostopoulou, A. Filiatrault and A. Aref, 9/15/11.

MCEER-11-0003 'Proceedings of the Workshop on Improving Earthquake Response of Substation Equipment," Edited by A.M. Reinhorn, 9/19/11 (PB2012-102413).

MCEER-11-0004 "LRFD-Based Analysis and Design Procedures for Bridge Bearings and Seismic Isolators," by M.C. Constantinou, I. Kalpakidis, A. Filiatrault and R.A. Ecker Lay, 9/26/11.

MCEER-11-0005   "Experimental Seismic Evaluation, Model Parameterization, and Effects of Cold-Formed Steel-Framed Gypsum Partition Walls on the Seismic Performance of an Essential Facility," by R. Davies, R. Retamales, G. Mosqueda and A. Filiatrault, 10/12/11.

MCEER-11-0006   "Modeling and Seismic Performance Evaluation of High Voltage Transformers and Bushings," by A.M. Reinhorn, K. Oikonomou, H. Roh, A. Schiff and L. Kempner, Jr., 10/3/11.

MCEER-11-0007   "Extreme Load Combinations: A Survey of State Bridge Engineers," by G.C. Lee, Z. Liang, J.J. Shen and J.S. O'Connor, 10/14/11.

MCEER-12-0001   "Simplified Analysis Procedures in Support of Performance Based Seismic Design," by Y.N. Huang and A.S. Whittaker.

MCEER-12-0002   "Seismic Protection of Electrical Transformer Bushing Systems by Stiffening Techniques," by M. Koliou, A. Filiatrault, A.M. Reinhorn and N. Oliveto, 6/1/12.

MCEER-12-0003   "Post-Earthquake Bridge Inspection Guidelines," by J.S. O'Connor and S. Alampalli, 6/8/12.

MCEER-12-0004   "Integrated Design Methodology for Isolated Floor Systems in Single-Degree-of-Freedom Structural Fuse Systems," by S. Cui, M. Bruneau and M.C. Constantinou, 6/13/12.

MCEER-12-0005   "Characterizing the Rotational Components of Earthquake Ground Motion," by D. Basu, A.S. Whittaker and M.C. Constantinou, 6/15/12.

MCEER-12-0006   "Bayesian Fragility for Nonstructural Systems," by C.H. Lee and M.D. Grigoriu, 9/12/12.

MCEER-12-0007   "A Numerical Model for Capturing the In-Plane Seismic Response of Interior Metal Stud Partition Walls," by R.L. Wood and T.C. Hutchinson, 9/12/12.

MCEER-12-0008   "Assessment of Floor Accelerations in Yielding Buildings," by J.D. Wieser, G. Pekcan, A.E. Zaghi, A.M. Itani and E. Maragakis, 10/5/12.

MCEER-13-0001   "Experimental Seismic Study of Pressurized Fire Sprinkler Piping Systems," by Y. Tian, A. Filiatrault and G. Mosqueda, 4/8/13.

MCEER-13-0002   "Enhancing Resource Coordination for Multi-Modal Evacuation Planning," by D.B. Hess, B.W. Conley and C.M. Farrell, 2/8/13.

MCEER-13-0003   "Seismic Response of Base Isolated Buildings Considering Pounding to Moat Walls," by A. Masroor and G. Mosqueda, 2/26/13.

MCEER-13-0004   "Seismic Response Control of Structures Using a Novel Adaptive Passive Negative Stiffness Device," by D.T.R. Pasala, A.A. Sarlis, S. Nagarajaiah, A.M. Reinhorn, M.C. Constantinou and D.P. Taylor, 6/10/13.

MCEER-13-0005   "Negative Stiffness Device for Seismic Protection of Structures," by A.A. Sarlis, D.T.R. Pasala, M.C. Constantinou, A.M. Reinhorn, S. Nagarajaiah and D.P. Taylor, 6/12/13.

MCEER-13-0006   "Emilia Earthquake of May 20, 2012 in Northern Italy: Rebuilding a Resilient Community to Withstand Multiple Hazards," by G.P. Cimellaro, M. Chiriatti, A.M. Reinhorn and L. Tirca, June 30, 2013.

MCEER-13-0007   "Precast Concrete Segmental Components and Systems for Accelerated Bridge Construction in Seismic Regions," by A.J. Aref, G.C. Lee, Y.C. Ou and P. Sideris, with contributions from K.C. Chang, S. Chen, A. Filiatrault and Y. Zhou, June 13, 2013.

MCEER-13-0008   "A Study of U.S. Bridge Failures (1980-2012)," by G.C. Lee, S.B. Mohan, C. Huang and B.N. Fard, June 15, 2013.

MCEER-13-0009   "Development of a Database Framework for Modeling Damaged Bridges," by G.C. Lee, J.C. Qi and C. Huang, June 16, 2013.

MCEER-13-0010   "Model of Triple Friction Pendulum Bearing for General Geometric and Frictional Parameters and for Uplift Conditions," by A.A. Sarlis and M.C. Constantinou, July 1, 2013.

MCEER-13-0011   "Shake Table Testing of Triple Friction Pendulum Isolators under Extreme Conditions," by A.A. Sarlis, M.C. Constantinou and A.M. Reinhorn, July 2, 2013.

MCEER-13-0012   "Theoretical Framework for the Development of MH-LRFD," by G.C. Lee (coordinating author), H.A Capers, Jr., C. Huang, J.M. Kulicki, Z. Liang, T. Murphy, J.J.D. Shen, M. Shinozuka and P.W.H. Yen, July 31, 2013.

MCEER-13-0013   "Seismic Protection of Highway Bridges with Negative Stiffness Devices," by N.K.A. Attary, M.D. Symans, S. Nagarajaiah, A.M. Reinhorn, M.C. Constantinou, A.A. Sarlis, D.T.R. Pasala, and D.P. Taylor, September 3, 2014.

MCEER-14-0001   "Simplified Seismic Collapse Capacity-Based Evaluation and Design of Frame Buildings with and without Supplemental Damping Systems," by M. Hamidia, A. Filiatrault, and A. Aref, May 19, 2014.

MCEER-14-0002   "Comprehensive Analytical Seismic Fragility of Fire Sprinkler Piping Systems," by Siavash Soroushian, Emmanuel "Manos" Maragakis, Arash E. Zaghi, Alicia Echevarria, Yuan Tian and Andre Filiatrault, August 26, 2014.

MCEER-14-0003   "Hybrid Simulation of the Seismic Response of a Steel Moment Frame Building Structure through Collapse," by M. Del Carpio Ramos, G. Mosqueda and D.G. Lignos, October 30, 2014.

MCEER-14-0004   "Blast and Seismic Resistant Concrete-Filled Double Skin Tubes and Modified Steel Jacketed Bridge Columns," by P.P. Fouche and M. Bruneau, June 30, 2015.

MCEER-14-0005   "Seismic Performance of Steel Plate Shear Walls Considering Various Design Approaches," by R. Purba and M. Bruneau, October 31, 2014.

MCEER-14-0006   "Air-Blast Effects on Civil Structures," by Jinwon Shin, Andrew S. Whittaker, Amjad J. Aref and David Cormie, October 30, 2014.

MCEER-14-0007   "Seismic Performance Evaluation of Precast Girders with Field-Cast Ultra High Performance Concrete (UHPC) Connections," by G.C. Lee, C. Huang, J. Song, and J. S. O'Connor, July 31, 2014.

MCEER-14-0008   "Post-Earthquake Fire Resistance of Ductile Concrete-Filled Double-Skin Tube Columns," by Reza Imani, Gilberto Mosqueda and Michel Bruneau, December 1, 2014.

MCEER-14-0009   "Cyclic Inelastic Behavior of Concrete Filled Sandwich Panel Walls Subjected to In-Plane Flexure," by Y. Alzeni and M. Bruneau, December 19, 2014.

MCEER-14-0010   "Analytical and Experimental Investigation of Self-Centering Steel Plate Shear Walls," by D.M. Dowden and M. Bruneau, December 19, 2014.

MCEER-15-0001   "Seismic Analysis of Multi-story Unreinforced Masonry Buildings with Flexible Diaphragms," by J. Aleman, G. Mosqueda and A.S. Whittaker, June 12, 2015.

MCEER-15-0002   "Site Response, Soil-Structure Interaction and Structure-Soil-Structure Interaction for Performance Assessment of Buildings and Nuclear Structures," by C. Bolisetti and A.S. Whittaker, June 15, 2015.

MCEER-15-0003   "Stress Wave Attenuation in Solids for Mitigating Impulsive Loadings," by R. Rafiee-Dehkharghani, A.J. Aref and G. Dargush, to be published.

MCEER-15-0004   "Computational, Analytical, and Experimental Modeling of Masonry Structures," by K.M. Dolatshahi and A.J. Aref, to be published.

MCEER-15-0005   "Property Modification Factors for Seismic Isolators: Design Guidance for Buildings," by W.J. McVitty and M.C. Constantinou, June 30, 2015.